



TOXICOLOGICAL REVIEW

OF

TRICHLOROETHYLENE

CHAPTER 3

(CAS No. 79-01-6)

**In Support of Summary Information on the
Integrated Risk Information System (IRIS)**

September 2011

3. TOXICOKINETICS

TCE is a lipophilic compound that readily crosses biological membranes. Exposures may occur via the oral, dermal, and inhalation routes, with evidence for systemic availability from each route. TCE is rapidly and nearly completely absorbed from the gut following oral administration, and studies with animals indicate that exposure vehicle may impact the time-course of absorption: oily vehicles may delay absorption, whereas aqueous vehicles result in a more rapid increase in blood concentrations.

Following absorption to the systemic circulation, TCE distributes from blood to solid tissues by each organ's solubility. This process is mainly determined by the blood:tissue partition coefficients, which are largely established by tissue lipid content. Adipose partitioning is high, adipose tissue may serve as a reservoir for TCE, and accumulation into adipose tissue may prolong internal exposures. TCE attains high concentrations relative to blood in the brain, kidney, and liver—all of which are important target organs of toxicity. TCE is cleared via metabolism mainly in three organs: the kidney, liver, and lungs.

The metabolism of TCE is an important determinant of its toxicity. Metabolites are generally thought to be responsible for toxicity—especially for the liver and kidney. Initially, TCE may be oxidized via cytochrome P450 (CYP) xenobiotic metabolizing isozymes or conjugated with glutathione (GSH) by glutathione-S-transferase (GST) enzymes. While CYP2E1 is generally accepted to be the CYP form most responsible for TCE oxidation at low concentrations, other forms may also contribute, though their contributions may be more important at higher, rather than lower, environmentally-relevant exposures.

Once absorbed, TCE is excreted primarily either in breath as unchanged TCE or carbon dioxide (CO₂), or in urine as metabolites. Minor routes of elimination include excretion of metabolites in saliva, sweat, and feces. Following oral administration or upon cessation of inhalation exposure, exhalation of unmetabolized TCE is a major elimination pathway. Initially, elimination of TCE upon cessation of inhalation exposure demonstrates a steep concentration-time profile: TCE is rapidly eliminated in the minutes and hours postexposure, and then the rate of elimination via exhalation decreases. Following oral or inhalation exposure, urinary elimination of parent TCE is minimal, with urinary elimination of the metabolites TCA and TCOH accounting for the bulk of the absorbed dose of TCE.

Sections 3.1–3.4 below describe the absorption, distribution, metabolism, and excretion (ADME) of TCE and its metabolites in greater detail. Section 3.5 then discusses PBPK modeling of TCE and its metabolites.

3.1. ABSORPTION

TCE is a low-molecular-weight lipophilic solvent; these properties explain its rapid transfer from environmental media into the systemic circulation after exposure. As discussed below, it is readily absorbed into the bloodstream following exposure via oral ingestion and inhalation, with more limited data indicating dermal penetration.

3.1.1. Oral

Available reports on human exposure to TCE via the oral route are largely restricted to case reports of occupational or intentional (suicidal) ingestions and suggest significant gastric absorption (e.g., [Brüning et al., 1998](#); [Yoshida et al., 1996](#); [Perbellini et al., 1991](#)). Clinical symptoms attributable to TCE or metabolites were observed in these individuals within a few hours of ingestion (such as lack of consciousness), indicating absorption of TCE. In addition, TCE and metabolites were measured in blood or urine at the earliest times possible after ingestion, typically upon hospital admission, while urinary excretion of TCE metabolites was followed for several days following exposure. Therefore, based on these reports, it is likely that TCE is readily absorbed in the gastrointestinal (GI) tract; however, the degree of absorption cannot be confidently quantified because the ingested amounts are not known.

Experimental evidence in mice and rats supports rapid and extensive absorption of TCE, although variables such as stomach contents, vehicle, and dose may affect the degree of gastric absorption. D'Souza et al. ([1985](#)) reported on bioavailability and blood kinetics in fasted and nonfasted male Sprague-Dawley rats following intragastric administration of TCE at 5–25 mg/kg in 50% polyethylene glycol (PEG 400) in water. TCE rapidly appeared in peripheral blood (at the initial 0.5 minutes sampling) of fasted and nonfasted rats with peak levels being attained shortly thereafter (6–10 minutes), suggesting that absorption is not diffusion limited, especially in fasted animals. The presence of food in the GI tract, however, seems to influence TCE absorption based on findings in the nonfasted animals of lesser bioavailability (60–80 vs. 90% in fasted rats), smaller peak blood levels (two- to threefold lower than nonfasted animals), and a somewhat longer terminal half-life ($t_{1/2}$) (174 vs. 112 minutes in fasted rats).

Studies by Prout et al. ([1985](#)) and Dekant et al. ([1986b](#)) have shown that up to 98% of administered radiolabel was found in expired air and urine of rats and mice following gavage administration of [^{14}C]-radiolabeled TCE ([^{14}C]-TCE). Prout et al. ([1985](#)) and Green and Prout ([1985](#)) compared the degree of absorption, metabolites, and routes of elimination among two strains each of male rats (Osborne-Mendel and Park Wistar) and male mice (B6C3F₁ and Swiss-Webster) following a single oral administration of 10, 500, or 1,000 [^{14}C]-TCE. Additional dose groups of Osborne-Mendel male rats and B6C3F₁ male mice also received a single oral dose of 2,000 mg/kg [^{14}C]-TCE. At the lowest dose of 10 mg/kg, there were no major differences between rats and mice in routes of excretion, with most of the administered radiolabel (nearly 60–70%) being in the urine. At this dose, the expired air from all groups

contained 1–4% of unchanged TCE and 9–14% CO₂. Fecal elimination of the radiolabel ranged from 8.3% in Osborne-Mendel rats to 24.1% in Park Wistar rats. However, at doses between 500 and 2,000 mg/kg, the rat progressively excreted a higher proportion of the radiolabel as unchanged TCE in expired air, such that 78% of the administered high dose was found in expired air (as unchanged TCE) while only 13% was excreted in the urine.

Following exposure to a chemical by the oral route, distribution is determined by delivery to the first organ encountered in the circulatory pathway—the liver (i.e., the first-pass effect), where metabolism and elimination may limit the proportion that may reach extrahepatic organs. Lee et al. ([1996](#)) evaluated the efficiency and dose-dependency of presystemic elimination of TCE in male Sprague-Dawley rats following administration into the carotid artery, jugular vein, hepatic portal vein, or the stomach of TCE (0.17, 0.33, 0.71, 2, 8, 16, or 64 mg/kg) in a 5% aqueous Alkamus emulsion (polyethoxylated vegetable oil) in 0.9% saline. The first-pass elimination, decreased from 57.5 to <1% with increasing dose (0.17–16 mg/kg), which implied that hepatic TCE metabolism may be saturated at doses >16 mg/kg in the male rat. At doses of ≥16 mg/kg, hepatic first-pass elimination was almost nonexistent indicating that, at relatively large doses, virtually all of TCE passes through the liver without being extracted ([Lee et al., 1996](#)). In addition to the hepatic first-pass elimination findings, pulmonary extraction, which was relatively constant (at nearly 5–8% of dose) over the dose range, also played a role in eliminating TCE.

In addition, oral absorption appears to be affected by both dose and vehicle used. The majority of oral TCE studies have used either aqueous solution or corn oil as the dosing vehicle. Most studies that relied on an aqueous vehicle delivered TCE as an emulsified suspension in Tween 80[®] or PEG 400 in order to circumvent the water solubility problems. Lee et al. ([2000a](#); [2000b](#)) used Alkamus (a polyethoxylated vegetable oil emulsion) to prepare a 5% aqueous emulsion of TCE that was administered by gavage to male Sprague-Dawley rats. The findings confirmed rapid TCE absorption, but reported decreasing absorption rate constants (i.e., slower absorption) with increasing gavage dose (2–432 mg/kg). The time to reach blood peak concentrations increased with dose and ranged between 2 and 26 minutes postdosing. Other pharmacokinetics data, including area under the blood concentration time curve (AUC) and prolonged elevation of blood TCE levels at the high doses, indicated prolonged GI absorption and delayed elimination due to metabolic saturation occurring at the higher TCE doses.

A study by Withey et al. ([1983](#)) evaluated the effect of dosing TCE with corn oil vs. pure water as a vehicle by administering four VOCs separately in each dosing vehicle to male Wistar rats. Based on its limited solubility in pure water, the dose for TCE was selected at 18 mg/kg (administered in 5 mL/kg). Times to peak in blood reported for TCE averaged 5.6 minutes when water was used. In comparison, the time to peak in blood was much longer (approximately 100 minutes) when the oil vehicle was used and the peaks were smaller, below the level of detection, and not reportable.

Time-course studies reporting times to peak in blood or other tissues have been performed using both vehicles ([Larson and Bull, 1992a, b](#); [D'Souza et al., 1985](#); [Green and Prout, 1985](#); [Dekant et al., 1984](#); [Withey et al., 1983](#)). Related data for other solvents ([Dix et al., 1997](#); [Lilly et al., 1994](#); [Kim et al., 1990a](#); [Kim et al., 1990b](#); [Chieco et al., 1981](#)) confirmed differences in TCE absorption and peak height between the two administered vehicles. One study has also evaluated the absorption of TCE from soil in rats ([Kadry et al., 1991](#)) and reported absorption within 16 hours for clay and 24 hours for sandy soil. In summary, these studies confirm that TCE is relatively quickly absorbed from the stomach, and that absorption is dependent on the vehicle used.

3.1.2. Inhalation

TCE is a lipophilic volatile compound that is readily absorbed from inspired air. Uptake from inhalation is rapid and the absorbed dose is proportional to exposure concentration and duration, and pulmonary ventilation rate. Distribution into the body via arterial blood leaving the lungs is determined by the net dose absorbed and eliminated by metabolism in the lungs. Metabolic clearance in the lungs will be further discussed in Section 3.3, below. In addition to metabolism, solubility in blood is the major determinant of the TCE concentration in blood entering the heart and being distributed to the each body organ via the arterial blood. The measure of TCE solubility in each organ is the partition coefficient, or the concentration ratio between both organ phases of interest. The blood-to-air partition coefficient quantifies the resulting concentration in blood leaving the lungs at equilibrium with alveolar air. The value of the blood-to-air partition coefficient is used in PBPK modeling (see Section 3.5). The blood-to-air partition has been measured in vitro using the same principles in different studies and found to range between 8.1 and 11.7 in humans with somewhat higher values in mice and rats (13.3–25.8) (see Tables 3-1–3-2, and references therein).

Table 3-1. Blood:air partition coefficient values for humans

Blood:air partition coefficient	Reference/notes
8.1 ± 1.8	Fiserova-Bergerova et al. (1984); mean ± SD (SD converted from SE based on n = 5)
8.11	Gargas et al. (1989); (n = 3–15)
9.13 ± 1.73 [6.47–11]	Fisher et al. (1998); mean ± SD [range] of females (n = 6)
9.5	Sato and Nakajima (1979); (n = 1)
9.77	Koizumi (1989)
9.92	Sato et al. (1977); (n = 1)
11.15 ± 0.74 [10.1–12.1]	Fisher et al. (1998); mean ± SD [range] of males (n = 7)
11.2 ± 1.8 [7.9–15]	Mahle et al. (2007); mean ± SD; 20 male pediatric patients aged 3–7 yrs (range; USAF, 2004)
11.0 ± 1.6 [6.6–13.5]	Mahle et al. (2007); mean ± SD; 18 female pediatric patients aged 3–17 yrs (range; USAF, 2004)
11.7 ± 1.9 [6.7–16.8]	Mahle et al. (2007); mean ± SD; 32 male patients aged 23–82 yrs (range; USAF, 2004)
10.6 ± 2.3 [3–14.4]	Mahle et al. (2007); mean ± SD; 27 female patients aged 23–82 yrs (range; USAF, 2004)

SE = standard error

Table 3-2. Blood:air partition coefficient values for rats and mice

Blood:air partition coefficient	Reference/notes
Rat	
15 ± 0.5	Fisher et al. (1998); mean ± SD (SD converted from SE based on n = 3)
17.5	Rodriguez et al. (2007)
20.5 ± 2.4	Barton et al. (1995); mean ± SD (SD converted from SE based on n = 4)
20.69 ± 3.3	Simmons et al. (2002); mean ± SD (n = 7–10)
21.9	Gargas et al. (1989) (n = 3–15)
25.8	Koizumi (1989) (pooled n = 3)
25.82 ± 1.7	Sato et al. (1977); mean ± SD (n = 5)
13.3 ± 0.8 [11.6–15]	Mahle et al. (2007); mean ± SD; 10 PND 10 male rat pups (range; USAF, 2004)
13.4 ± 1.8 [11.8–17.2]	Mahle et al. (2007); mean ± SD; 10 PND 10 female rat pups (range; USAF, 2004)
17.5 ± 3.6 [11.7–23.1]	Mahle et al. (2007); mean ± SD; 9 adult male rats (range; USAF, 2004)
21.8 ± 1.9 [16.9–23.5]	Mahle et al. (2007); mean ± SD; 11 aged male rats (range; USAF, 2004)
Mouse	
13.4	Fisher et al. (1991); male
14.3	Fisher et al. (1991); female
15.91	Abbas and Fisher (1997)

PND = postnatal day

TCE enters the human body quickly by inhalation, and, at high concentrations, it may lead to death (Coopman et al., 2003), narcosis, unconsciousness, and acute kidney damage (Carrieri et al., 2007). Controlled exposure studies in humans have shown absorption of TCE to approach a steady state within a few hours after the start of inhalation exposure (Fernandez et al., 1977; Monster et al., 1976; Vesterberg and Astrand, 1976; Vesterberg et al., 1976). Several studies have calculated the net dose absorbed by measuring the difference between the inhaled concentration and the exhaled air concentration. Soucek and Vlachova (1960) reported 58–70% absorption of the amount inhaled for 5-hour exposures of 93–158 ppm. Bartonicek (1962) obtained an average retention value of 58% after 5 hours of exposure to 186 ppm. Monster et al. (1976) also took into account minute ventilation measured for each exposure, and calculated of 37–49% absorption in subjects exposed to 70 and 140 ppm. The impact of exercise, the increase in workload, and its effect on breathing has also been measured in controlled inhalation exposures. Astrand and Ovrum (1976) reported 50–58% uptake at rest and 25–46% uptake during exercise from exposure to 100 or 200 ppm (540 or 1,080 mg/m³, respectively) of TCE for 30 minutes (see Table 3-3). These authors also monitored heart rate and pulmonary ventilation. In contrast, Jakubowski and Wieczorek (1988) calculated about 40% retention in volunteers exposed to TCE at 9 ppm (mean inspired concentration of 48–49 mg/m³) for 2 hours at rest, with no change in retention during increased workload due to exercise (see Table 3-4).

Table 3-3. Air and blood concentrations during exposure to TCE in humans

TCE concentration (mg/m ³)	Work load (watt)	Exposure series ^a	TCE concentration in			Uptake as % of amount available	Amount taken up (mg)
			Alveolar air (mg/m ³)	Arterial blood (mg/kg)	Venous blood (mg/kg)		
540	0	I	124 ± 9	1.1 ± 0.1	0.6 ± 0.1	53 ± 2	79 ± 4
540	0	II	127 ± 11	1.3 ± 0.1	0.5 ± 0.1	52 ± 2	81 ± 7
540	50	I	245 ± 12	2.7 ± 0.2	1.7 ± 0.4	40 ± 2	160 ± 5
540	50	II	218 ± 7	2.8 ± 0.1	1.8 ± 0.3	46 ± 1	179 ± 2
540	50	II	234 ± 12	3.1 ± 0.3	2.2 ± 0.4	39 ± 2	157 ± 2
540	50	II	244 ± 16	3.3 ± 0.3	2.2 ± 0.4	37 ± 2	147 ± 9
1,080	0	I	280 ± 18	2.6 ± 0.0	1.4 ± 0.3	50 ± 2	156 ± 9
1,080	0	III	212 ± 7	2.1 ± 0.2	1.2 ± 0.1	58 ± 2	186 ± 7
1,080	50	I	459 ± 44	6.0 ± 0.2	3.3 ± 0.8	45 ± 2	702 ± 31
1,080	50	III	407 ± 30	5.2 ± 0.5	2.9 ± 0.7	51 ± 3	378 ± 18
1,080	100	III	542 ± 33	7.5 ± 0.7	4.8 ± 1.1	36 ± 3	418 ± 39
1,080	150	III	651 ± 53	9.0 ± 1.0	7.4 ± 1.1	25 ± 5	419 ± 84

^aSeries I consisted of 30-minute exposure periods of rest, rest, 50 watts, and 50 watts; Series II consisted of 30-minute exposure periods of rest, 50 watts, 50 watts, 50 watts; and Series III consisted of 30-minute exposure periods of rest, 50 watts, 100 watts, 150 watts.

Source: Astrand and Ovrum (1976)

Table 3-4. Retention of inhaled TCE vapor in humans

Workload	Inspired concentration (mg/m ³)	Pulmonary ventilation (m ³ /hr)	Retention	Uptake (mg/hr)
Rest	48 ± 3 ^a	0.65 ± 0.07	0.40 ± 0.05	12 ± 1.1
25 Watts	49 ± 1.3	1.30 ± 0.14	0.40 ± 0.05	25 ± 2.9
50 Watts	49 ± 1.6	1.53 ± 0.13	0.42 ± 0.06	31 ± 2.8
75 Watts	48 ± 1.9	1.87 ± 0.14	0.41 ± 0.06	37 ± 4.8

^aMean ± SD, n = 6 adult males.

Source: Jakubowski and Wieczorek (1988)

Environmental or occupational settings may result from a pattern of repeated exposure to TCE. Monster et al. (1979a) reported 70-ppm TCE exposures in volunteers for 4 hours for 5 consecutive days, averaging a total uptake of 450 mg per 4 hours of exposure (see Table 3-5). In dry-cleaning workers, Skender et al. (1991) reported initial blood concentrations of 0.38 µmol/L, increasing to 3.4 µmol/L 2 days after. Results of these studies support rapid absorption of TCE via inhalation.

Table 3-5. Uptake of TCE in volunteers following 4 hour exposure to 70 ppm

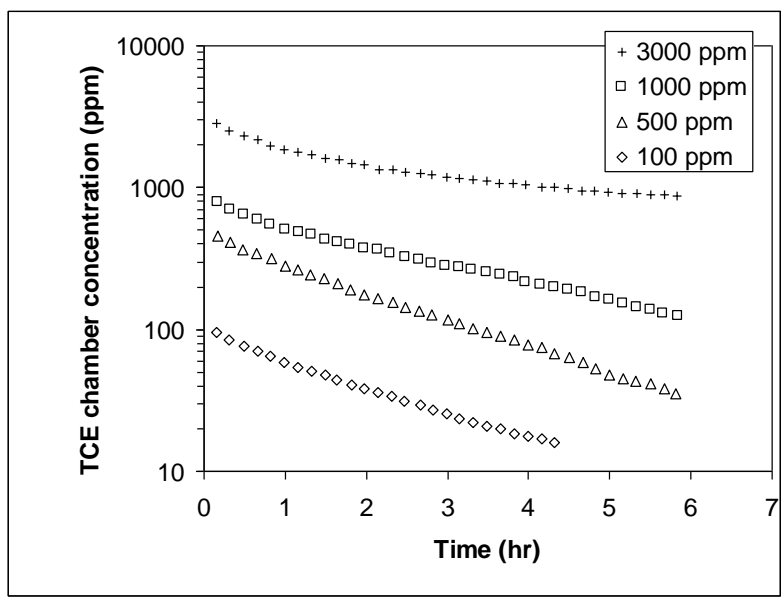
	Body weight (kg)	Minute-volume (L/min)	Percentage retained	Uptake (mg/d)	Uptake (mg/kg-d)
A	80	9.8 ± 0.4	45 ± 0.8	404 ± 23	5.1
B	82	12.0 ± 0.7	44 ± 0.9	485 ± 35	5.9
C	82	10.9 ± 0.8	49 ± 1.2	493 ± 28	6.0
D	67	11.8 ± 0.8	35 ± 2.6	385 ± 38	5.7
E	90	11.0 ± 0.7	46 ± 1.1	481 ± 25	5.3
Mean					5.6 ± 0.4

Source: Monster et al. ([1979b](#)).

Direct measurement of retention after inhalation exposure in rodents is more difficult because exhaled breath concentrations are challenging to obtain. The only available data are from Dallas et al. ([1991](#)), who designed a nose-only exposure system for rats using a facemask equipped with one-way breathing valves to obtain measurements of TCE in inspired and exhaled air. In addition, indwelling carotid artery cannulae were surgically implanted to facilitate the simultaneous collection of blood. After a 1-hour acclimatization period, rats were exposed to 50 or 500 ppm TCE for 2 hours, and the time course of TCE in blood and expired air was measured during and for 3 hours following exposure. When air concentration data were analyzed to reveal absorbed dose (minute volume multiplied by the concentration difference between inspired and exhaled breath), it was demonstrated that the fractional absorption of either concentration was >90% during the initial 5 minutes of exposure. Fractional absorption then decreased to 69 and 71% at 50 and 500 ppm during the second hour of exposure. Cumulative uptake appeared linear with respect to time over the 2-hour exposure, resulting in absorbed doses of 8.4 and 73.3 mg/kg in rats exposed to 50 and 500 ppm, respectively. Given the 10-fold difference in inspired concentration and the 8.7-fold difference in uptake, the authors interpreted this information to indicate that metabolic saturation occurred at some concentration <500 ppm. In comparing the absorbed doses to those developed for the 70-ppm-exposed human [see Monster et al. ([1979a](#))], Dallas et al. ([1991](#)) concluded that on a systemic dose (mg/kg) basis, rats receive a much higher TCE dose from a given inhalation exposure than do humans. In particular, using the results cited above, the absorption per ppm-hour was 0.084 and 0.073 mg/kg-ppm-hour at 50 and 500 ppm in rats ([Dallas et al., 1991](#)) and 0.019 mg/kg-ppm-hour at 70 ppm in humans ([Monster et al., 1979a](#))—a difference of around fourfold. However, rats have about a 10-fold higher alveolar ventilation rate per unit body weight than humans ([Brown et al., 1997](#)), which more than accounts for the observed increase in absorption.

Other experiments, such as closed-chamber gas uptake experiments or blood concentration measurements following open-chamber (fixed concentration) experiments, measure absorption indirectly but are consistent with significant retention. Closed-chamber gas-

uptake methods ([Gargas et al., 1988](#)) place laboratory animals or in vitro preparations into sealed systems in which a known amount of TCE is injected to produce a predetermined chamber concentration. As the animal retains a quantity of TCE inside its body, due to metabolism, the closed-chamber concentration decreases with time when compared to the start of exposure. Many different studies have made use of this technique in both rats and mice to calculate total TCE metabolism (i.e., [Simmons et al., 2002](#); [Fisher et al., 1991](#); [Andersen et al., 1987a](#)). This inhalation technique is combined with PBPK modeling to calculate metabolic parameters, and the results of these studies are consistent with rapid absorption of TCE via the respiratory tract. Figure 3-1 shows an example from Simmons et al. ([2002](#)), in Long-Evans rats, that demonstrates an immediate decline in chamber concentrations of TCE indicating absorption, with multiple initial concentrations needed for each metabolic calculation. At concentrations below metabolic saturation, a secondary phase of uptake appears, after 1 hour from starting the exposure, indicative of metabolism. At concentrations >1,000 ppm, metabolism appears saturated, with time-course curves having a flat phase after absorption. At intermediate concentrations, between 100 and 1,000 ppm, the secondary phase of uptake appears after distribution as continued decreases in chamber concentration as metabolism proceeds. Using a combination of experiments that include both metabolic linear decline and saturation obtained by using different initial concentrations, both components of metabolism can be estimated from the gas uptake curves, as shown in Figure 3-1.



Symbols represent measured chamber concentrations. Source: Simmons et al. ([2002](#)).

Figure 3-1. Gas uptake data from closed-chamber exposure of rats to TCE.

Several other studies in humans and rodents have measured blood concentrations of TCE or metabolites and urinary excretion of metabolites during and after inhalation exposure (e.g., [Fisher et al., 1998](#); [1991](#); [1990](#); [Filser and Bolt, 1979](#)). While qualitatively indicative of absorption, blood concentrations are also determined by metabolism, distribution, and excretion; thus, comparisons between species may reflect similarities or differences in any of the absorption, distribution, metabolism, and excretion processes.

3.1.3. Dermal

Skin membrane is believed to present a diffusional barrier for entrance of the chemical into the body, and TCE absorption can be quantified using a permeability rate or permeability constant, though not all studies performed such a calculation. Absorption through the skin has been shown to be rapid by both vapor and liquid TCE contact with the skin. Human dermal absorption of TCE vapors was investigated by Kezic et al. ([2000](#)). Volunteers were exposed to 3.18×10^4 ppm around each enclosed arm for 20 minutes. Adsorption was found to be rapid (within 5 minutes), reaching a peak in exhaled breath around 30 minutes, with a calculated dermal penetration rate averaging 0.049 cm/hour for TCE vapors.

With respect to dermal penetration of liquid TCE, Nakai et al. ([1999](#)) used surgically removed skin samples exposed to TCE in aqueous solution in a chamber designed to measure the difference between incoming and outgoing [^{14}C]-TCE. The in vitro permeability constant calculated by these researchers averaged 0.12 cm/hour. In vivo, Sato and Nakajima ([1978](#)) exposed adult male volunteers dermally to liquid TCE for 30 minutes, with exhaled TCE appearing at the initial sampling time of 5 minutes after start of exposure, with a maximum observed at 15 minutes. In Kezic et al. ([2001](#)), volunteers were exposed dermally for 3 minutes to neat liquid TCE, with TCE detected in exhaled breath at the first sampling point of 3 minutes, and maximal concentrations observed at 5 minutes. Skin irritancy was reported in all subjects, which may have increased absorption. A dermal flux of 430 ± 295 (mean \pm standard error [SE]) nmol/cm²/minute was reported in these subjects, suggesting high interindividual variability.

Another species where dermal absorption for TCE has been reported is in guinea pigs. Jakobson et al. ([1982](#)) applied liquid TCE to the shaved backs of guinea pigs and reported peak blood TCE levels at 20 minutes after initiation of exposure. Bogen et al. ([1992](#)) estimated permeability constants for dermal absorption of TCE in hairless guinea pigs of 0.16–0.47 mL/cm²/hour across a range of concentrations (19–100,000 ppm).

3.2. DISTRIBUTION AND BODY BURDEN

TCE crosses biological membranes and quickly results in rapid systemic distribution to tissues—regardless of the route of exposure. In humans, in vivo studies of tissue distribution are limited to tissues taken from autopsies following accidental poisonings or from surgical patients exposed environmentally, so the level of exposure is typically unknown. Tissue levels reported

after autopsy show wide systemic distribution across all tested tissues, including the brain, muscle, heart, kidney, lung, and liver ([Coopman et al., 2003](#); [Dehon et al., 2000](#); [De Baere et al., 1997](#); [Ford et al., 1995](#)). However, the reported levels themselves are difficult to interpret because of the high exposures and differences in sampling protocols. In addition, human populations exposed environmentally show detectable levels of TCE across different tissues, including the liver, brain, kidney, and adipose tissues ([Kroneld, 1989](#); [Pellizzari et al., 1982](#); [McConnell et al., 1975](#)).

In addition, TCE vapors have been shown to cross the human placenta during childbirth ([Laham, 1970](#)), with experiments in rats confirming this finding ([Withey and Karpinski, 1985](#)). In particular, Laham ([1970](#)) reported determinations of TCE concentrations in maternal and fetal blood following administration of TCE vapors (concentration unreported) intermittently and at birth (see Table 3-6). TCE was present in all samples of fetal blood, with ratios of concentrations in fetal:maternal blood ranging from approximately 0.5 to approximately 2. The concentration ratio was <1.0 in six pairs, >1 in three pairs, and approximately 1 in one pair; in general, higher ratios were observed at maternal concentrations <2.25 mg/100 mL. Because no details of exposure concentration, duration, or time postexposure were given for samples taken, these results are not suitable for use in PBPK modeling, but they do demonstrate the placental transfer of TCE in humans. Withey and Karpinski ([1985](#)) exposed pregnant rats to TCE vapors (302, 1,040, 1,559, or 2,088 ppm for 5 hours) on gestation day (GD) 17 and concentrations of TCE in maternal and fetal blood were determined. At all concentrations, TCE concentration in fetal blood was approximately one-third of the concentration in corresponding maternal blood. Maternal blood concentrations approximated 15, 60, 80, and 110 µg/g blood. When the position along the uterine horn was examined, TCE concentrations in fetal blood decreased toward the tip of the uterine horn. TCE appears to also distribute to mammary tissues and is excreted in milk. Pellizzari et al. ([1982](#)) conducted a survey of environmental contaminants in human milk using samples from cities in the northeastern region of the United States and one in the southern region. No details of times postpartum, milk lipid content, or TCE concentration in milk or blood were reported, but TCE was detected in 8 milk samples taken from 42 lactating women. Fisher et al. ([1990](#)) exposed lactating rats to 600 ppm TCE for 4 hours and collected milk immediately following the cessation of exposure. TCE was clearly detectable in milk, and, from a visual interpretation of the graphic display of their results, concentrations of TCE in milk approximated 110 µg/mL milk.

Table 3-6. Concentrations of TCE in maternal and fetal blood at birth

TCE concentration in blood (mg/100 mL)		Ratio of concentrations fetal:maternal
Maternal	Fetal	
4.6	2.4	0.52
3.8	2.2	0.58
8	5	0.63
5.4	3.6	0.67
7.6	5.2	0.68
3.8	3.3	0.87
2	1.9	0.95
2.25	3	1.33
0.67	1	1.49
1.05	2	1.90

Source: Laham (1970).

In rodents, detailed tissue distribution experiments have been performed using different routes of administration ([Keys et al., 2003](#); [Simmons et al., 2002](#); [Greenberg et al., 1999](#); [Abbas and Fisher, 1997](#); [Pfaffenberger et al., 1980](#); [Savolainen et al., 1977](#)). Savolainen et al. (1977) exposed adult male rats to 200 ppm TCE for 6 hours/day for a total of 5 days. Concentrations of TCE in the blood, brain, liver, lung, and perirenal fat were measured 17 hours after cessation of exposure on the fourth day and after 2, 3, 4, and 6 hours of exposure on the fifth day (see Table 3-7). TCE appeared to be rapidly absorbed into blood and distributed to brain, liver, lungs, and perirenal fat. TCE concentrations in these tissues reached near-maximal values within 2 hours of initiation of exposure on the fifth day. Pfaffenberger et al. (1980) dosed rats by gavage with 1 or 10 mg TCE/kg/day in corn oil for 25 days to evaluate the distribution from serum to adipose tissue. During the exposure period, concentrations of TCE in serum were below the limit of detection (1 µg/L) and were 280 and 20,000 ng/g fat in the 1 and 10 mg/day dose groups, respectively. Abbas and Fisher (1997) and Greenberg et al. (1999) measured tissue concentrations in the liver, lung, kidney, and fat of mice administered TCE by gavage (300–2,000 mg/kg) and by inhalation exposure (100 or 600 ppm for 4 hours). In a study to investigate the effects of TCE on neurological function, Simmons et al. (2002) conducted pharmacokinetic experiments in rats exposed to 200, 2,000, or 4,000 ppm TCE vapors for 1 hour. Time-course data were collected on blood, liver, brain, and fat. The data were used to develop a PBPK model to explore the relationship between internal dose and neurological effect. Keys et al. (2003), exposed groups of rats to TCE vapors of 50 or 500 ppm for 2 hours and sacrificed at different time points during exposure. In addition to inhalation, this study also includes gavage and intra-arterial (i.a.) dosing, with the following time course measured: liver, fat, muscle, blood, GI, brain, kidney, heart, lung, and spleen. These pharmacokinetic data were presented with an updated PBPK model for all routes.

Table 3-7. Distribution of TCE to rat tissues^a following inhalation exposure

Exposure on 5 th d	Tissue (concentration in nmol/g tissue)					
	Cerebrum	Cerebellum	Lung	Liver	Perirenal fat	Blood
0 ^b	0	0	0.08	0.04	0.23 ± 0.09	0.35 ± 0.1
2	9.9 ± 2.7	11.7 ± 4.2	4.9 ± 0.3	3.6	65.9 ± 1.2	7.5 ± 1.6
3	7.3 ± 2.2	8.8 ± 2.1	5.5 ± 1.4	5.5 ± 1.7	69.3 ± 3.3	6.6 ± 0.9
4	7.2 ± 1.7	7.6 ± 0.5	5.8 ± 1.1	2.5 ± 1.4	69.5 ± 6.3	6.0 ± 0.2
6	7.4 ± 2.1	9.5 ± 2.5	5.6 ± 0.5	2.4 ± 0.2	75.4 ± 14.9	6.8 ± 1.2

^aData presented as mean of two determinations ± range.

^bSample taken 17 hours following cessation of exposure on day 4.

Source: Savolainen et al. (1977).

Besides the route of administration, another important factor contributing to body distribution is the individual solubility of the chemical in each organ, as measured by a partition coefficient. For volatile compounds, partition coefficients are measured in vitro using the vial equilibration technique to determine the ratio of concentrations between organ and air at equilibrium. Table 3-8 reports values developed by several investigators from mouse, rat, and human tissues. In humans, partition coefficients in the following tissues have been measured: brain, fat, kidney, liver, lung, and muscle; the organ having the highest TCE partition coefficient is fat (63–70), while the lowest is the lung (0.5–1.7). The adipose tissue also has the highest measured value in rodents, and is one of the considerations needed to be accounted for when extrapolating across species. However, the rat adipose partition coefficient value is smaller (23–36), when compared to humans (i.e., TCE is less lipophilic in rats than humans). For the mouse, the measured fat partition coefficient averages 36, ranging between rats and humans. The value of the partition coefficient plays a role in distribution for each organ and is computationally described in computer simulations using a PBPK model. Due to its high lipophilicity in fat, as compared to blood, the adipose tissue behaves as a storage compartment for this chemical, affecting the slower component of the chemical's distribution. For example Monster et al. (1979a) reported that, following repeated inhalation exposures to TCE, TCE concentrations in expired breath postexposure were highest for the subject with the greatest amount of adipose tissue (adipose tissue mass ranged 3.5-fold among subjects). The intersubject range in TCE concentration in exhaled breath increased from approximately 2-fold at 20 hours to approximately 10-fold 140 hours postexposure. Notably, they reported that this difference was not due to differences in uptake, as body weight and lean body mass were most closely associated with TCE retention. Thus, adipose tissue may play an important role in postexposure distribution, but does not affect its rapid absorption.

Table 3-8. Tissue:blood partition coefficient values for TCE

Species/ tissue	TCE partition coefficient		References
	Tissue:blood	Tissue:air	
Human			
Brain	2.62	21.2	Fiserova-Bergerova et al. (1984)
Fat	63.8–70.2	583–674.4	Sato et al. (1977); Fiserova-Bergerova et al. (1984); Fisher et al. (1998)
Kidney	1.3–1.8	12–14.7	Fiserova-Bergerova et al. (1984); Fisher et al. (1998)
Liver	3.6–5.9	29.4–54	Fiserova-Bergerova et al. (1984); Fisher et al. (1998)
Lung	0.48–1.7	4.4–13.6	Fiserova-Bergerova et al. (1984); Fisher et al. (1998)
Muscle	1.7–2.4	15.3–19.2	Fiserova-Bergerova et al. (1984); Fisher et al. (1998)
Rat			
Brain	0.71–1.29	14.6–33.3	Sato et al. (1977); Simmons et al. (2002); Rodriguez et al. (2007)
Fat	22.7–36.1	447–661	Gargas et al. (1989); Sato et al. (1977); Simmons et al. (2002); Rodriguez et al. (2007); Fisher et al. (1989); Koizumi (1989); Barton et al. (1995)
Heart	1.1	28.4	Sato et al. (1977)
Kidney	1.0–1.55	17.7–40	Sato et al., (1977); Barton et al., (1995); Rodriguez et al., (2007)
Liver	1.03–2.43	20.5–62.7	Gargas et al. (1989); Sato et al. (1977); Simmons et al. (2002); Rodriguez et al. (2007); Fisher et al. (1989); Koizumi, (1989); Barton et al. (1995)
Lung	1.03	26.6	Sato et al. (1977)
Muscle	0.46–0.84	6.9–21.6	Gargas et al. (1989); Sato et al. (1977); Simmons et al. (2002); Rodriguez et al. (2007); Fisher et al. (1989); Koizumi, (1989); Barton et al. (1995)
Spleen	1.15	29.7	Sato et al. (1977)
Testis	0.71	18.3	Sato et al. (1977)
Milk	7.10	Not reported	Fisher et al. (1990)
Mouse			
Fat	36.4	578.8	Abbas and Fisher (1997)
Kidney	2.1	32.9	Abbas and Fisher (1997)
Liver	1.62	23.2	Fisher et al. (1991)
Lung	2.6	41.5	Abbas and Fisher (1997)
Muscle	2.36	37.5	Abbas and Fisher (1997)

Mahle et al. (2007) reported age-dependent differences in partition coefficients in rats, (see Table 3-9) that can have implications as to life-stage-dependent differences in tissue TCE distribution. To investigate the potential impact of these differences, Rodriguez et al. (2007) developed models for the postnatal day (PND) 10 rat pup; the adult and the aged rat, including age-specific tissue volumes and blood flows; and age-scaled metabolic constants. The models predict similar uptake profiles for the adult and the aged rat during a 6-hour exposure to 500 ppm; uptake by the PND 10 rat was higher (see Table 3-10). The effect was heavily dependent on age-dependent changes in anatomical and physiological parameters (alveolar

ventilation rates and metabolic rates); age-dependent differences in partition coefficient values had minimal impact on predicted differences in uptake.

Table 3-9. Age-dependence of tissue:air partition coefficients in rats

Age ^a	Liver	Kidney	Fat	Muscle	Brain
PND 10 male	22.1 ± 2.3 ^b	15.2 ± 1.3	398.7 ± 89.2	43.9 ± 11.0	11.0 ± 0.6
PND 10 female	21.2 ± 1.7	15.0 ± 1.1	424.5 ± 67.5	48.6 ± 17.3	11.6 ± 1.2
Adult male	20.5 ± 4.0	17.6 ± 3.9 ^c	631.4 ± 43.1 ^c	12.6 ± 4.3	17.4 ± 2.6
Aged male	34.8 ± 8.7 ^{c,d}	19.9 ± 3.4 ^c	757.5 ± 48.3 ^{c,d}	26.4 ± 10.3 ^{c,d}	25.0 ± 2.0 ^{c,d}

^an = 10, adult male and pooled male and female litters; n = 11, aged males.

^bData are mean ± SD.

^cStatistically significant ($p \leq 0.05$) difference between either the adult or aged partition coefficient and the PND 10 male partition coefficient.

^dStatistically significant ($p \leq 0.05$) difference between aged and adult partition coefficient.

Source: Mahle et al. (2007).

Table 3-10. Predicted maximal concentrations of TCE in rat blood following a 6-hour inhalation exposure

Age	Exposure concentration					
	50 ppm			500 ppm		
	Predicted peak concentration (mg/L) in: ^a		Predicted time to reach 90% of steady state (hr) ^b	Predicted peak concentration (mg/L) in: ^a		Predicted time to reach 90% of steady state (hr) ^b
	Venous blood	Brain		Venous blood	Brain	
PND 10	3.0	2.6	4.1	33	28	4.2
Adult	0.8	1.0	3.5	22	23	11.9
Aged	0.8	1.2	6.7	21	26	23.3

^aDuring a 6-hour exposure.

^bUnder continuous exposure.

Source: Rodriguez et al. (2007).

Finally, TCE binding to tissues or cellular components within tissues can affect overall pharmacokinetics. The binding of a chemical to plasma proteins, for example, affects the availability of the chemical to other organs and the calculation of the total half-life. However, most studies have evaluated binding using [¹⁴C]-TCE, from which one cannot distinguish covalent binding of TCE from that of TCE metabolites. Nonetheless, several studies have demonstrated binding of TCE-derived radiolabel to cellular components (Mazzullo et al., 1992; Moslen et al., 1977). Bolt and Filser (1977) examined the total amount irreversibly bound to tissues following 9-, 100-, and 1,000-ppm exposures via inhalation in closed-chambers. The largest percent of in vivo radioactivity taken up occurred in the liver; albumin is the protein

favored for binding (see Table 3-11). Banerjee and van Duuren (1978) evaluated the in vitro binding of TCE to microsomal proteins from the liver, lung, kidney, and stomachs in rats and mice. In both rats and mice, radioactivity was similar in stomach and lung, but about 30% lower in kidney and liver.

Table 3-11. Tissue distribution of TCE metabolites following inhalation exposure

Tissue ^a	Percent of radioactivity taken up/g tissue					
	TCE = 9 ppm, n = 4 ^b		TCE = 100 ppm, n = 4		TCE = 1,000 ppm, n = 3	
	Total metabolites	Irreversibly bound	Total metabolites	Irreversibly bound	Total metabolites	Irreversibly bound
Lung	0.23 ± 0.026 ^c	0.06 ± 0.002	0.24 ± 0.025	0.06 ± 0.006	0.22 ± 0.055	0.1 ± 0.003
Liver	0.77 ± 0.059	0.28 ± 0.027	0.68 ± 0.073	0.27 ± 0.019	0.88 ± 0.046	0.48 ± 0.020
Spleen	0.14 ± 0.015	0.05 ± 0.002	0.15 ± 0.001	0.05 ± 0.004	0.15 ± 0.006	0.08 ± 0.003
Kidney	0.37 ± 0.005	0.09 ± 0.007	0.40 ± 0.029	0.09 ± 0.007	0.39 ± 0.045	0.14 ± 0.016
Small intestine	0.41 ± 0.058	0.05 ± 0.010	0.38 ± 0.062	0.07 ± 0.008	0.28 ± 0.015	0.09 ± 0.015
Muscle	0.11 ± 0.005	0.014 ± 0.001	0.11 ± 0.013	0.012 ± 0.001	0.10 ± 0.011	0.027 ± 0.003

^aMale Wistar rats, 250 g.

^bn = number of animals.

^cValues shown are means ± SD.

Source: Bolt and Filser (1977).

Based on studies of the effects of metabolizing enzyme induction on binding, there is some evidence that a major contributor to the observed binding is from TCE metabolites rather than from TCE itself. Dekant et al. (1986b) studied the effect of enzyme modulation on the binding of radiolabel from [¹⁴C]-TCE by comparing tissue binding after administration of 200 mg/kg via gavage in corn oil between control (naïve) rats and rats pretreated with phenobarbital (a known inducer of CYP2B family) or Aroclor 1254 (a known inducer of both CYP1A and CYP2B families of isoenzymes) (see Table 3-12). The results indicate that induction of total CYP content by 3–4-fold resulted in nearly 10-fold increase in radioactivity (disintegrations per minute; [DPM]) bound in liver and kidney. By contrast, Mazzullo et al. (1992) reported that phenobarbital pretreatment did not result in consistent or marked alterations of in vivo binding of radiolabel to deoxyribonucleic acid (DNA), ribonucleic acid (RNA), or protein in rats and mice at 22 hours after an intraperitoneal (i.p.) injection of [¹⁴C]-TCE. On the other hand, in vitro experiments by Mazzullo et al. (1992) reported reduction of TCE-radiolabel binding to calf thymus DNA with introduction of a CYP inhibitor into incubations containing rat liver microsomal protein. Moreover, increase/decrease of GSH levels in incubations containing lung cytosolic protein led to a parallel increase/decrease in TCE-radiolabel binding to calf thymus DNA.

Table 3-12. Binding of [¹⁴C] from [¹⁴C]-TCE in rat liver and kidney at 72 hours after oral administration of 200 mg/kg [¹⁴C]-TCE

Tissue	DPM/g tissue		
	Untreated	Phenobarbital	Arochlor 1254
Liver	850 ± 100	9,300 ± 1,100	8,700 ± 1,000
Kidney	680 ± 100	5,700 ± 900	7,300 ± 800

Source: Dekant et al. ([1986b](#)).

3.3. METABOLISM

This section focuses on both in vivo and in vitro studies of the biotransformation of TCE, identifying metabolites that are deemed significant for assessing toxicity and carcinogenicity. In addition, metabolism studies may be used to evaluate the flux of parent compound through the known metabolic pathways. Sex-, species-, and interindividual differences in the metabolism of TCE are discussed, as are factors that possibly contribute to this variability. Additional discussion of variability and susceptibility is presented in Section 4.10.

3.3.1. Introduction

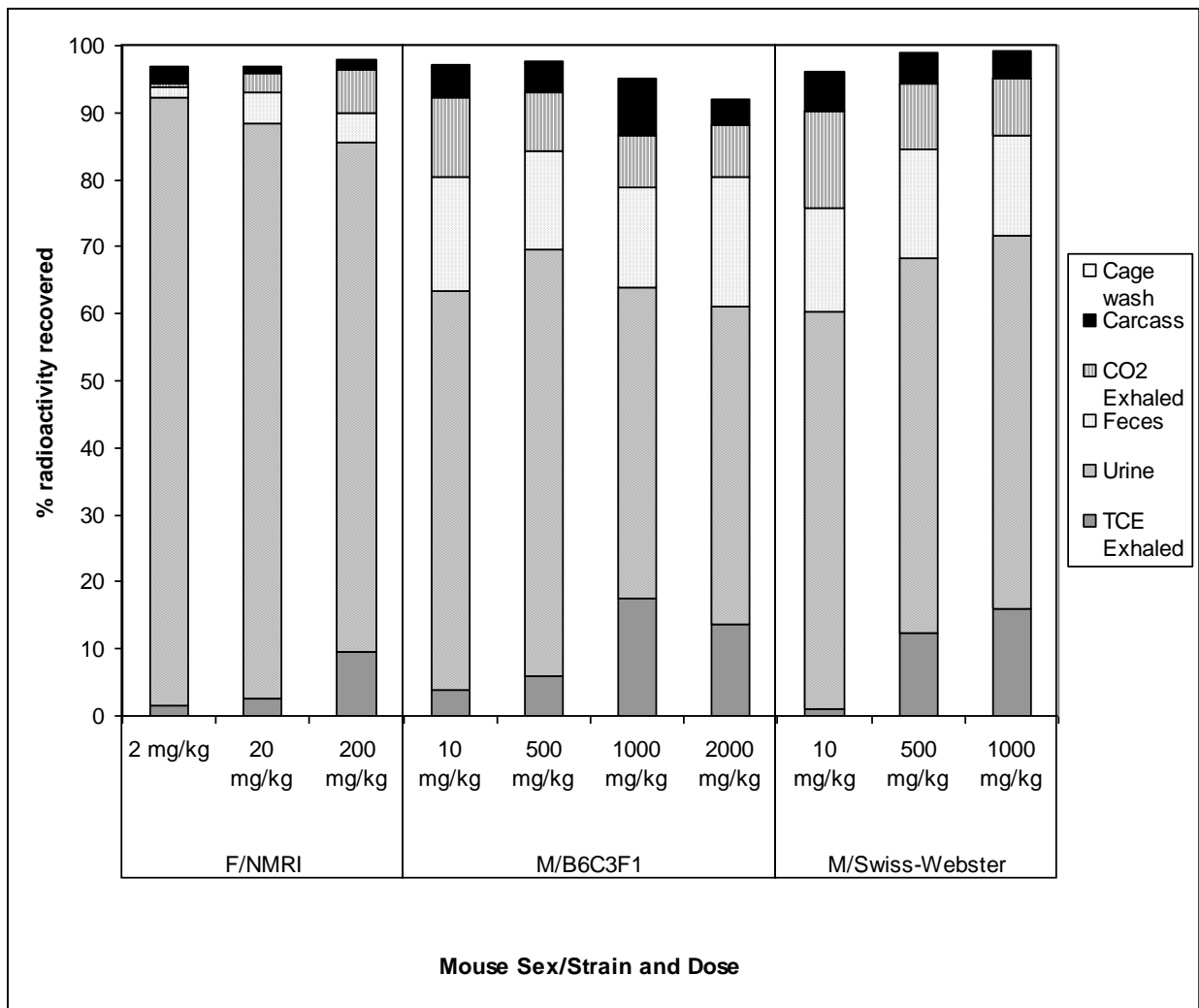
The metabolism of TCE has been studied mostly in mice, rats, and humans and has been extensively reviewed ([Lash et al., 2000a](#); [Lash et al., 2000b](#); [IARC, 1995b](#); [US EPA, 1985](#)). It is now well accepted that TCE is metabolized in laboratory animals and in humans through at least two distinct pathways: (1) oxidative metabolism via the CYP mixed-function oxidase system and (2) GSH conjugation followed by subsequent further biotransformation and processing, either through the cysteine conjugate beta lyase pathway or by other enzymes ([Lash et al., 2000a](#); [Lash et al., 2000b](#)). While the flux through the conjugative pathway is less, quantitatively, than the flux through oxidation ([Bloemen et al., 2001](#)), GSH conjugation is an important route toxicologically, giving rise to relatively potent toxic biotransformation products ([Elfarrar et al., 1987](#); [Elfarrar et al., 1986](#)).

Information about metabolism is important because, as discussed extensively in Chapter 4, certain metabolites are thought to cause one or more of the same acute and chronic toxic effects, including carcinogenicity, as TCE. Thus, in many of these cases, the toxicity of TCE is generally considered to reside primarily in its metabolites rather than in the parent compound itself.

3.3.2. Extent of Metabolism

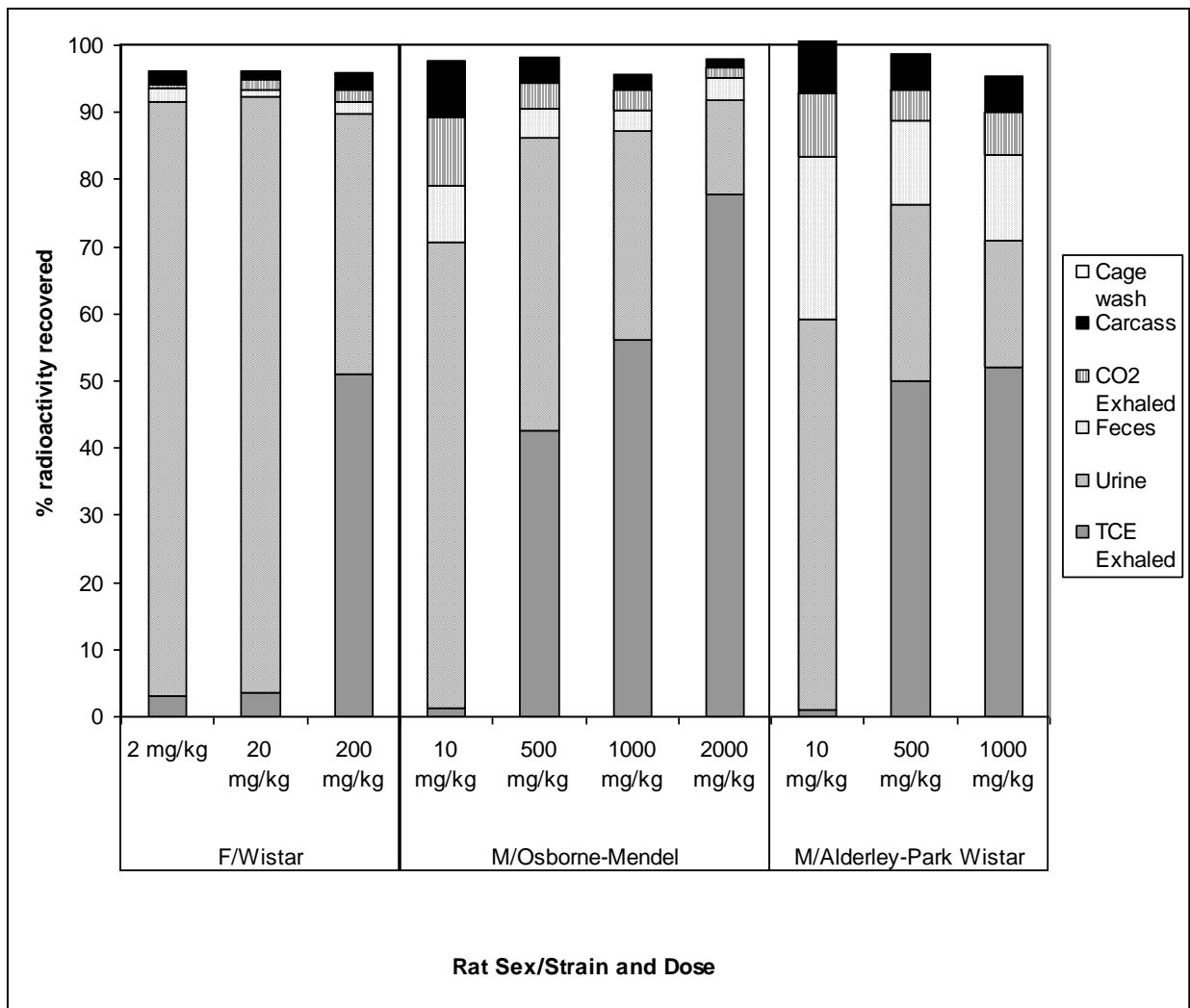
TCE is extensively metabolized in animals and humans. The most comprehensive mass-balance studies are in mice and rats ([Dekant et al., 1986a](#); [Dekant et al., 1986b](#); [Green and Prout, 1985](#); [Prout et al., 1985](#); [Dekant et al., 1984](#)) in which [¹⁴C]-TCE is administered by gavage at

doses of 2–2,000 mg/kg, the data from which are summarized in Figures 3-2 and 3-3. In both mice and rats, regardless of sex and strain, there is a general trend of increasing exhalation of unchanged TCE with dose, suggesting saturation of a metabolic pathway. The increase is smaller in mice (from 1–6 to 10–18%) than in rats (from 1–3 to 43–78%), suggesting greater overall metabolic capacity in mice. The dose at which apparent saturation occurs appears to be more sex- or strain-dependent in mice than in rats. In particular, the marked increase in exhaled TCE occurred between 20 and 200 mg/kg in female NMRI mice, between 500 and 1,000 mg/kg in B6C3F₁ mice, and between 10 and 500 mg/kg in male Swiss-Webster mice. However, because only one study is available in each strain, interlot or interindividual variability might also contribute to the observed differences. In rats, all three strains tested showed marked increase in unchanged TCE exhaled between 20 and 200 mg/kg or between 10 and 500 mg/kg. Recovered urine, the other major source of excretion, had mainly TCA, TCOH, and trichloroethanol-glucuronide conjugate (TCOG), but revealed no detectable TCE. The source of radioactivity in feces was not analyzed, but it is presumed not to include substantial TCE given the complete absorption expected from the corn oil vehicle. Therefore, at all doses tested in mice, and at doses <200 mg/kg in rats, the majority of orally administered TCE is metabolized. Pretreatment of rats with P450 inducers prior to a 200 mg/kg dose did not change the pattern of recovery, but it did increase the amount recovered in urine by 10–15%, with a corresponding decrease in the amount of exhaled unchanged TCE ([Dekant et al., 1986b](#)).



Sources: Dekant et al. (1986b; 1984); Green and Prout (1985); Prout et al. (1985).

Figure 3-2. Disposition of [¹⁴C]-TCE administered by gavage in mice.



Sources: Dekant et al. (1986b; 1984); Green and Prout (1985); Prout et al. (1985).

Figure 3-3. Disposition of [¹⁴C]-TCE administered by gavage in rats.

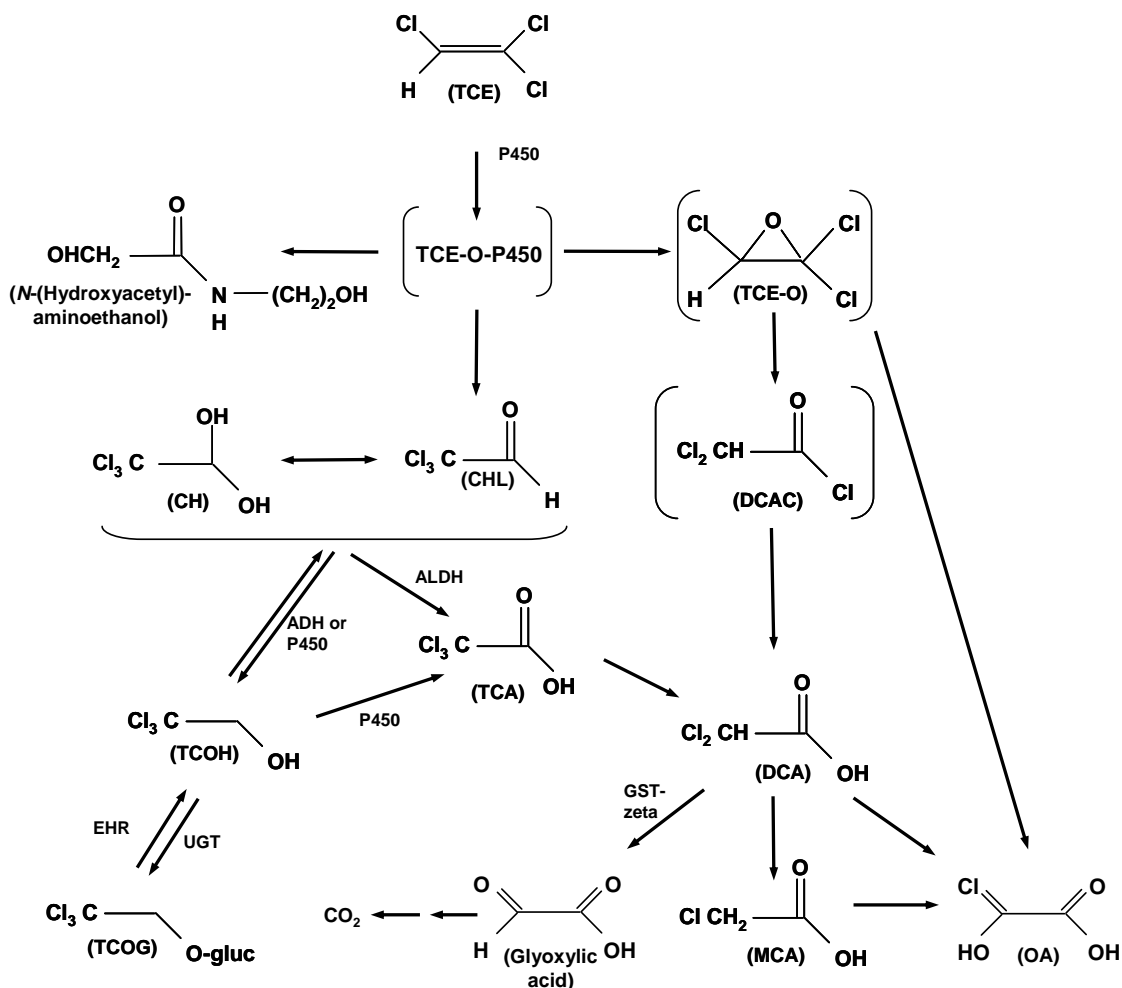
The differences among these studies may reflect a combination of interindividual variability and errors due to the difficulty in precisely estimating dose in inhalation studies, but in all cases, <20% of the retained dose was exhaled unchanged and >50% was excreted in urine as TCA and TCOH. Therefore, it is clear that TCE is extensively metabolized in humans. No saturation was evident in any of these human recovery studies at the exposure levels tested.

3.3.3. Pathways of Metabolism

As mentioned in Section 3.3.1, TCE metabolism in animals and humans has been observed to occur via two major pathways: P450-mediated oxidation and GSH conjugation. Products of the initial oxidation or conjugation step are further metabolized to a number of other metabolites. For P450 oxidation, all steps of metabolism occur primarily in the liver, although limited oxidation of TCE has been observed in the lungs of mice, as discussed below. The GSH conjugation pathway also begins predominantly in the liver, but toxicologically significant metabolic steps occur extrahepatically—particularly in the kidney ([Lash et al., 2006](#); [Lash et al., 1999a](#); [Lash et al., 1998b](#); [Lash et al., 1995](#)). The mass-balance studies cited above found that at exposures below the onset of saturation, >50% of TCE intake is excreted in urine as oxidative metabolites (primarily as TCA and TCOH), so TCE oxidation is generally greater than TCE conjugation. This is discussed in detail in Section 3.3.3.3.

3.3.3.1. CYP-Dependent Oxidation

Oxidative metabolism by the CYP, or CYP-dependent, pathway is quantitatively the major route of TCE biotransformation ([Lash et al., 2000a](#); [Lash et al., 2000b](#); [US EPA, 1985](#)). The pathway is operative in humans and rodents and leads to several metabolic products, some of which are known to cause toxicity and carcinogenicity ([IARC, 1995c](#); [US EPA, 1985](#)). Although several of the metabolites in this pathway have been clearly identified, others are speculative or questionable. Figure 3-4 depicts the overall scheme of TCE P450 metabolism.



Adapted from: Clewell et al. (2000); Cummings et al. (2001); Forkert et al. (2006); Lash et al. (2000a; 2000b); Tong et al. (1998).

Figure 3-4. Scheme for the oxidative metabolism of TCE.

In brief, TCE oxidation via P450, primarily CYP2E1 (Guengerich and Shimada, 1991), yields an oxygenated TCE-P450 intermediate. The TCE-P450 complex is a transition state that goes on to form chloral or TCE oxide. In the presence of water, chloral rapidly equilibrates with chloral hydrate (CH), which undergoes reduction and oxidation by alcohol dehydrogenase and aldehyde dehydrogenase or aldehyde oxidase to form TCOH and TCA, respectively (Dekant et al., 1986b; Green and Prout, 1985; Miller and Guengerich, 1983). TCE oxide can rearrange to DCAC. Table 3-13 summarizes available in vitro measurements of TCE oxidation, as assessed by the formation of CH, TCOH, and TCA. Glucuronidation of TCOH forms TCOG, which is readily excreted in urine. Alternatively, TCOG can be excreted in bile and passed to the small intestine where it is hydrolyzed back to TCOH and reabsorbed (Bull, 2000). TCA is poorly metabolized but may undergo dechlorination to form dichloroacetic acid (DCA). However, TCA is predominantly excreted in urine, albeit at a relatively slow rate as compared to TCOG. Like

the TCE-P450 complex, TCE oxide also seems to be a transient metabolite. Recent data suggest that it is transformed to dichloroacetyl chloride, which subsequently decomposes to form DCA (Cai and Guengerich, 1999). As shown in Figure 3-4, several other metabolites, including oxalic acid and *N*-(hydroxyacetyl) aminoethanol, may form from the TCE oxide or the TCE-O-P450 intermediate and have been detected in the urine of rodents and humans following TCE exposure. Pulmonary excretion of CO₂ has been identified in exhaled breath from rodents exposed to [¹⁴C]-labeled TCE and is thought to arise from metabolism of DCA. The following sections provide details as to pathways of TCE oxidation, including discussion of inter- and intraspecies differences in metabolism.

Table 3-13. In vitro TCE oxidative metabolism in hepatocytes and microsomal fractions

In vitro system	K _M	V _{MAX}	1,000 × V _{MAX} /K _M ^a	Source
	μM in medium	nmol TCE oxidized/min/mg MSP or 10 ⁶ hepatocytes		
Human hepatocytes	210 ± 159 ^b (45–403)	0.268 ± 0.215 (0.101–0.691)	2.45 ± 2.28 (0.46–5.57)	Lipscomb et al. (1998b)
Human liver microsomal protein	16.7 ± 2.45 (13.3–19.7)	1.246 ± 0.805 (0.490–3.309)	74.1 ± 44.1 (38.9–176)	Lipscomb et al. (1997) (low K _M)
	30.9 ± 3.3 (27.0–36.3)	1.442 ± 0.464 (0.890–2.353)	47.0 ± 16.0 (30.1–81.4)	Lipscomb et al. (1997) (mid K _M)
	51.1 ± 3.77 (46.7–55.7)	2.773 ± 0.577 (2.078–3.455)	54.9 ± 14.1 (37.3–69.1)	Lipscomb et al. (1997) (high K _M)
	24.6	1.44	58.5	Lipscomb et al. (1998c) (pooled)
	12 ± 3 (9–14)	0.52 ± 0.17 (0.37–0.79)	48 ± 23 (26–79)	Elfarrar et al. (1998) (males, high affinity)
	26 ± 17 (13–45)	0.33 ± 0.15 (0.19–0.48)	15 ± 10 (11–29)	Elfarrar et al. (1998) (females, high affinity)
Rat liver microsomal protein	55.5	4.826	87.0	Lipscomb et al. (1998c) (pooled)
	72 ± 82	0.96 ± 0.65	24 ± 21	Elfarrar et al. (1998) (males, high affinity)
	42 ± 21	2.91 ± 0.71	80 ± 34	Elfarrar et al. (1998) (females, high affinity)
Rat kidney microsomal protein	940	0.154	0.164	Cummings et al. (2001)
Mouse liver microsomal protein	35.4	5.425	153	Lipscomb et al. (1998c) (pooled)
	378 ± 414	8.6 ± 4.5	42 ± 29	Elfarrar et al. (1998) (males)
	161 ± 29	26.06 ± 7.29	163 ± 37	Elfarrar et al. (1998) (females)

^aK_M for human hepatocytes converted from ppm in headspace to μM in medium using reported hepatocyte:air partition coefficient (Lipscomb et al., 1998b).

^bResults presented as mean ± SD (minimum–maximum).

MSP = Microsomal protein.

3.3.3.1.1. Formation of TCE oxide

In previous studies of halogenated alkene metabolism, the initial step was the generation of a reactive epoxide (Anders and Jakobson, 1985). Early studies in anesthetized human patients

([Powell, 1945](#)), dogs ([Butler, 1949](#)), and later reviews (e.g., [Goeptar et al., 1995](#)) suggest that the TCE epoxide may be the initial reaction product of TCE oxidation.

Epoxides can form acyl chlorides or aldehydes, which can then form aldehydes, carboxylic acids, or alcohols, respectively. Thus, earlier studies suggesting the appearance of CH, TCA, and TCOH as the primary metabolites of TCE were considered consistent with the oxidation of TCE to an epoxide intermediate ([Butler, 1949](#); [Powell, 1945](#)). Following in vivo exposures to 1,1-DCE, a halocarbon very similar in structure to TCE, mouse liver cytosol and microsomes and lung Clara cells exhibited extensive P450-mediated epoxide formation ([Forkert, 1999b](#); [Forkert, 1999a](#); [Forkert et al., 1999](#); [Dowsley et al., 1996](#)). Indeed, TCE oxide inhibits purified CYP2E1 activity ([Cai and Guengerich, 2001b](#)) similarly to TCE inhibition of CYP2E1 in human liver microsomes ([Lipscomb et al., 1997](#)).

Conversely, cases have been made against TCE oxide as an obligate intermediate to the formation of chloral. Using liver microsomes and reconstituted P450 systems ([Miller and Guengerich, 1983, 1982](#)) or isolated rat hepatocytes ([Miller and Guengerich, 1983](#)), it has been suggested that chlorine migration and generation of a TCE-O-P450 complex (via the heme oxygen) would better explain the observed destruction of the P450 heme, an outcome not likely to be epoxide-mediated. Miller and Guengerich ([1982](#)) found CYP2E1 to generate an epoxide but argued that the subsequent production of chloral was not likely related to the epoxide. Green and Prout ([1985](#)) argued against epoxide (free form) formation in vivo in mice and rats, suggesting that the expected predominant metabolites would be carbon monoxide, CO₂, MCA, and DCA, rather than the observed predominant appearance of TCA, TCOH, and TCOG.

It appears likely that both a TCE-O-P450 complex and a TCE oxide are formed, resulting in both CH and DCAC, respectively, though it appears that the former predominates. In particular, it has been shown that DCAC can be generated from TCE oxide, dichloroacetyl chloride can be trapped with lysine ([Cai and Guengerich, 1999](#)), and dichloroacetyl-lysine adducts are formed in vivo ([Forkert et al., 2006](#)). Together, these data strongly suggest TCE oxide as an intermediate metabolite, albeit short-lived, from TCE oxidation in vivo.

3.3.3.1.2. Formation of CH, TCOH and TCA

CH (in equilibrium with chloral) is a major oxidative metabolite produced from TCE as has been shown in numerous in vitro systems, including human liver microsomes and purified P450 CYP2E1 ([Guengerich et al., 1991](#)) as well as recombinant rat, mouse, and human P450s including CYP2E1 ([Forkert et al., 2005](#)). However, in rats and humans, in vivo circulating CH is generally absent from blood following TCE exposure. In mice, CH is detectable in blood and tissues but is rapidly cleared from systemic circulation ([Abbas and Fisher, 1997](#)). The low systemic levels of CH are due to its rapid transformation to other metabolites.

CH is further metabolized predominantly to TCOH ([Shultz and Weiner, 1979](#); [Sellers et al., 1972](#)) and/or CYP2E1 ([Ni et al., 1996](#)). The role for alcohol dehydrogenase was suggested

by the observation that ethanol inhibited CH reduction to TCOH ([Larson and Bull, 1989](#); [Muller et al., 1975](#); [Sellers et al., 1972](#)). For instance, Sellers et al. (1972) reported that co-exposure of humans to ethanol and CH resulted in a higher percentage of urinary TCOH (24% of CH metabolites) compared to TCA (19%). When ethanol was absent, 10 and 11% of CH was metabolized to TCOH and TCA, respectively. However, because ethanol can be oxidized by both alcohol dehydrogenase and CYP2E1, there is some ambiguity as to whether these observations involve competition with one or the other of these enzymes. For instance, Ni et al. (1996) reported that CYP2E1 expression was necessary for metabolism of CH to mutagenic metabolites in a human lymphoblastoid cell line, suggesting a role for CYP2E1. Furthermore, Ni et al. (1996) reported that cotreatment of mice with CH and pyrazole, a specific CYP2E1 inducer, resulted in enhanced liver microsomal lipid peroxidation, while treatment with 2,4-dichloro-6-phenoxyethylamine, an inhibitor of CYP2E1, suppressed lipid peroxidation, suggesting CYP2E1 as a primary enzyme for CH metabolism in this system. Lipscomb et al. (1996) suggested that two enzymes are likely responsible for CH reduction to TCOH based on observation of biphasic metabolism for this pathway in mouse liver microsomes. This behavior has also been observed in mouse liver cytosol, but was not observed in rat or human liver microsomes. Moreover, CH metabolism to TCOH increased significantly both in the presence of nicotinamide adenine dinucleotide (NADH) in the 700 × g supernatant of mouse, rat, and human liver homogenate as well as with the addition of nicotinamide adenine dinucleotide phosphate-oxidase (NADPH) in human samples, suggesting that two enzymes may be involved ([Lipscomb et al., 1996](#)).

TCOH formed from CH is available for oxidation to TCA (see below) or glucuronidation via uridine 5'-diphospho-glucuronyltransferase to TCOG, which is excreted in urine or in bile ([Stenner et al., 1997](#)). Biliary TCOG is hydrolyzed in the gut and available for reabsorption to the liver as TCOH, where it can be glucuronidated again or metabolized to TCA. This enterohepatic circulation appears to play a significant role in the generation of TCA from TCOH and in the observed lengthy residence time of this metabolite, compared to TCE. Using jugular-, duodenal-, and bile duct-cannulated rats, Stenner et al. (1997) showed that enterohepatic circulation of TCOH from the gut back to the liver and subsequent oxidation to TCA was responsible for 76% of TCA measured in the systemic blood.

Oxidation of CH and TCOH to TCA has been demonstrated in vivo in mice ([Larson and Bull, 1992a](#); [Dekant et al., 1986b](#); [Green and Prout, 1985](#)), rats ([Stenner et al., 1997](#); [Pravecsek et al., 1996](#); [Templin et al., 1995b](#); [Larson and Bull, 1992a](#); [Dekant et al., 1986b](#); [Green and Prout, 1985](#)), dogs ([Templin et al., 1995b](#)), and humans ([Sellers et al., 1978](#)). Urinary metabolite data in mice and rats exposed to 200 mg/kg TCE ([Larson and Bull, 1992a](#); [Dekant et al., 1986b](#)); and humans following oral CH exposure ([Sellers et al., 1978](#)) show greater TCOH production relative to TCA production. However, because of the much longer urinary half-life in humans of TCA relative to TCOH, the total amount of TCA excreted may be similar to TCOH ([Fisher et al.,](#)

1998; [Monster et al., 1976](#)). This is thought to be primarily due to conversion of TCOH to TCA, either directly or via “back-conversion” of TCOH to CH, rather than due to the initial formation of TCA from CH ([Owens and Marshall, 1955](#)).

In vitro data are also consistent with CH oxidation to TCA being much less than CH reduction to TCOH. For instance, Lipscomb et al. ([1996](#)) reported 1,832-fold differences in K_M values and 10–195-fold differences in clearance efficiency (V_{MAX}/K_M) for TCOH and TCA in all three species (see Table 3-14). Clearance efficiency of CH to TCA in mice is very similar to humans but is 13-fold higher than rats. Interestingly, Bronley-DeLancey et al. ([2006](#)) recently reported that similar amounts of TCOH and TCA were generated from CH using cryopreserved human hepatocytes. However, the intersample variation was extremely high, with measured V_{MAX} ranging from 8-fold greater TCOH to 5-fold greater TCA and clearance (V_{MAX}/K_M) ranging from 13-fold greater TCOH to 17-fold greater TCA. Moreover, because a comparison with fresh hepatocytes or microsomal protein was not made, it is not clear to what extent these differences are due to population heterogeneity or experimental procedures.

Table 3-14. In vitro kinetics of TCOH and TCA formation from CH in rat, mouse, and human liver homogenates

Species	TCOH			TCA		
	K_M^a	V_{MAX}^b	V_{MAX}/K_M^c	K_M^a	V_{MAX}^b	V_{MAX}/K_M^c
Rat	0.52	24.3	46.7	16.4	4	0.24
Mouse ^d	0.19	11.3	59.5	3.5	10.6	3.0
High affinity	0.12	6.3	52.5	Not applicable	Not applicable	Not applicable
Low affinity	0.51	6.1	12.0	Not applicable	Not applicable	Not applicable
Human	1.34	34.7	25.9	23.9	65.2	2.7

^a K_M presented as mM CH in solution.

^b V_{MAX} presented as nmoles/mg supernatant protein/minute.

^cClearance efficiency represented by V_{MAX}/K_M .

^dMouse kinetic parameters derived for observations over the entire range of CH exposure as well as discrete, bi-phasic regions for CH concentrations below (high affinity) and above (low affinity) 1.0 mM.

Source: Lipscomb et al. ([1996](#)).

The metabolism of CH to TCA and TCOH involves several enzymes including CYP2E1, alcohol dehydrogenase, and aldehyde dehydrogenase enzymes ([Ni et al., 1996](#); [Wang et al., 1993](#); [Guengerich et al., 1991](#); [Miller and Guengerich, 1983](#); [Shultz and Weiner, 1979](#)). Because these enzymes have preferred cofactors (NADPH, NADH, and NAD⁺), cellular cofactor ratio and redox status of the liver may have an impact on the preferred pathway ([Lipscomb et al., 1996](#); [Kawamoto et al., 1988a](#)).

3.3.3.1.3. Formation of DCA and other products

As discussed above, DCA could hypothetically be formed via multiple pathways. The work reviewed by Guengerich (2004) suggested that one source of DCA may be through a TCE oxide intermediary. Miller and Guengerich (1983) reported evidence of formation of the epoxide, and Cai and Guengerich (1999) reported that a significant amount (about 35%) of DCA is formed from aqueous decomposition of TCE oxide via hydrolysis in an almost pH-independent manner. Because this reaction forming DCA from TCE oxide is a chemical process rather than a process mediated by enzymes, and because evidence suggests that some epoxide was formed from TCE oxidation, Guengerich (2004) notes that DCA would be an expected product of TCE oxidation (see also Yoshioka et al., 2002). Alternatively, dechlorination of TCA and oxidation of TCOH have been proposed as sources of DCA (Lash et al., 2000a). Merdink et al. (2000) investigated dechlorination of TCA and reported trapping a DCA radical with the spin-trapping agent phenyl-tert-butyl nitroxide, identified by gas chromatography/mass spectroscopy, in both a chemical Fenton system and rodent microsomal incubations with TCA as substrate. Dose-dependent catalysis of TCA to DCA was observed in cultured microflora from B6C3F₁ mice (Moghaddam et al., 1996). However, while antibiotic-treated mice lost the ability to produce DCA in the gut, plasma DCA levels were unaffected by antibiotic treatment, suggesting that the primary site of murine DCA production is other than the gut (Moghaddam et al., 1997).

However, direct evidence for DCA formation from TCE exposure remains equivocal. In vitro studies in human and animal systems have demonstrated very little DCA production in the liver (James et al., 1997). In vivo, DCA was detected in the blood of mice (Templin et al., 1993; Larson and Bull, 1992a) and humans (Fisher et al., 1998) and in the urine of rats and mice (Larson and Bull, 1992b) exposed to TCE by aqueous gavage. However, the use of strong acids in the analytical methodology produces ex vivo conversion of TCA to DCA in mouse blood (Ketcha et al., 1996). This method may have resulted in the appearance of DCA as an artifact in human plasma (Fisher et al., 1998) and mouse blood in vivo (Templin et al., 1995b). Evidence for the artifact is suggested by DCA AUCs that were larger than would be expected from the available TCA (Templin et al., 1995b). After the discovery of these analytical issues, Merdink et al. (1998) reevaluated the formation of DCA from TCE, TCOH, and TCA in mice, with particular focus on the hypothesis that DCA is formed from dechlorination of TCA. They were unable to detect blood DCA in naive mice after administration of TCE, TCOH, or TCA. Low levels of DCA were detected in the blood of children administered therapeutic doses of CH (Henderson et al., 1997), suggesting TCA or TCOH as the source of DCA. Oral TCE exposure in rats and dogs failed to produce detectable levels of DCA (Templin et al., 1995b).

Another difficulty in assessing the formation of DCA is its rapid metabolism at low exposure levels. Degradation of DCA is mediated by GST-zeta (Saghir and Schultz, 2002; Tong et al., 1998), apparently occurring primarily in the hepatic cytosol. DCA metabolism results in

suicide inhibition of the enzyme, evidenced by decreased DCA metabolism in DCA-treated animals ([Gonzalez-Leon et al., 1999](#)) and humans ([Shroads et al., 2008](#)) and loss of DCA metabolic activity and enzymatic protein in liver samples from treated animals ([Schultz et al., 2002](#)). This effect has been noted in young mice exposed to DCA in drinking water at doses approximating 120 mg/kg-day ([Schultz et al., 2002](#)). The experimental data and pharmacokinetic model simulations of several investigators ([Li et al., 2008](#); [Shroads et al., 2008](#); [Jia et al., 2006](#); [Keys et al., 2004](#); [Merdink et al., 1998](#)) suggest that several factors prevent the accumulation of measurable amounts of DCA: (1) its formation as a short-lived intermediate metabolite and (2) its rapid elimination relative to its formation from TCA. While DCA elimination rates appear approximately one order of magnitude higher in rats and mice than in humans ([James et al., 1997](#)) (see Table 3-15), they still may be rapid enough so that even if DCA were formed in humans, it would be metabolized too quickly to appear in detectable quantities in blood.

Table 3-15. In vitro kinetics of DCA metabolism in hepatic cytosol of mice, rats, and humans

Species	V_{MAX} (nmol/min/mg protein)	K_M (μ M)	V_{MAX}/K_M
Mouse	13.1	350	37.4
Rat	11.6	280	41.4
Human	0.37	71	5.2

Source: James et al. ([1997](#)).

A number of other metabolites, such as oxalic acid, MCA, glycolic acid, and glyoxylic acid, are formed from DCA ([Saghir and Schultz, 2002](#); [Lash et al., 2000a](#)). Unlike other oxidative metabolites of TCE, DCA appears to be metabolized primarily via hepatic cytosolic proteins. Since P450 activity resides almost exclusively in the microsomal and mitochondrial cell fractions, DCA metabolism appears to be independent of P450. Rodent microsomal and mitochondrial metabolism of DCA was measured to be $\leq 10\%$ of cytosolic metabolism ([Lipscomb et al., 1995](#)). DCA in the liver cytosol from rats and humans is transformed to glyoxylic acid via a GSH-dependent pathway ([James et al., 1997](#)). In rats, the K_M for GSH was 0.075 mM with a V_{MAX} for glyoxylic acid formation of 1.7 nmol/mg protein/minute. While this pathway may not involve GST (as evidenced by very low GST activity in this study), Tong et al. ([1998](#)) showed GST-zeta, purified from rat liver, to be involved in metabolizing DCA to glyoxylic acid, with a V_{MAX} of 1,334 nmol/mg protein/minute and K_M of 71.4 μ M for glyoxylic acid formation and a GSH K_M of 59 μ M.

3.3.3.1.4. Tissue distribution of oxidative metabolism and metabolites

Oxidative metabolism of TCE, irrespective of the route of administration, occurs predominantly in the liver, but TCE metabolism via the P450 (CYP) system also occurs at other sites because CYP isoforms are present to some degree in most tissues of the body. For example, both the lung and kidneys exhibit CYP enzyme activities ([Forkert et al., 2005](#); [Cummings et al., 2001](#); [1997a](#); [Green et al., 1997b](#)). Green et al. ([1997b](#)) detected TCE oxidation to chloral in microsomal fractions of whole-lung homogenates from mice, rats, and humans, with the activity in mice the greatest and in humans the least. The rates were slower than in the liver (which also has a higher microsomal protein content as well as greater tissue mass) by 1.8-, 10-, and >10-fold in mice, rats, and humans, respectively. While qualitatively informative, these rates were determined at a single concentration of about 1 mM TCE. A full kinetic analysis was not performed, so clearance and maximal rates of metabolism could not be determined. With the kidney, Cummings et al. ([2001](#)) performed a full kinetic analysis using kidney microsomes and found that clearance rates (V_{MAX}/K_M) for oxidation were >100-fold smaller than average rates found in the liver (see Table 3-13). In human kidney microsomes, Amet et al. ([1997](#)) reported that CYP2E1 activity was weak and near detection limits, with no CYP2E1 detectable using immunoblot analysis. Cummings and Lash ([2000](#)) reported detecting oxidation of TCE in only one of four kidney microsome samples, and only at the highest tested concentration of 2 mM, with a rate of 0.13 nmol/minute/mg protein. This rate contrasts with the V_{MAX} values for human liver microsomal protein of 0.19–3.5 nmol/minute/mg protein reported in various experiments (see Table 3-13). Extrahepatic oxidation of TCE may play an important role for generation of toxic metabolites in situ. The roles of local metabolism in kidney and lung toxicity are discussed in detail in Sections 4.4 and 4.7, respectively.

With respect to further metabolism beyond oxidation of TCE, CH has been shown to be metabolized to TCA and TCOH in lysed whole blood of mice and rats and fractionated human blood ([Lipscomb et al., 1996](#)) (see Table 3-16). TCOH production is similar in mice and rats and is approximately twofold higher in rodents than in human blood. However, TCA formation in human blood is two- or threefold higher than in mouse or rat blood, respectively. In human blood, TCA is formed only in the erythrocytes. TCOH formation occurs in both plasma and erythrocytes, but fourfold more TCOH is found in plasma than in an equal volume of packed erythrocytes. While blood metabolism of CH may contribute further to its low circulating levels in vivo the metabolic capacity of blood (and kidney) may be substantially lower than liver. Regardless, any CH reaching the blood may be rapidly metabolized to TCA and TCOH. DCA and TCA are known to bind to plasma proteins. Schultz et al. ([1999](#)) measured DCA binding in rats at a single concentration of about 100 μ M and found a binding fraction of <10%. However, these data are not greatly informative for TCE exposure in which DCA levels are significantly lower than 100 μ M. In addition, the limitation to a single concentration in this experiment precludes fitting a binding curve, as can be done for TCA with Templin et al. ([1995a](#); [1995b](#);

[1993](#)), Schultz et al. ([1999](#)), Lumpkin et al. ([2003](#)), and Yu et al. ([2003](#)), all of which measured TCA binding in various species and at various concentration ranges. Of these, Templin et al. ([1995a](#); [1995b](#)) and Lumpkin et al. ([2003](#)) measured levels in humans, mice, and rats. Lumpkin et al. ([2003](#)) studied the widest concentration range, spanning reported TCA plasma concentrations from experimental studies. Table 3-17 shows derived binding parameters. However, these data are not entirely consistent among researchers; two- to fivefold differences in B_{MAX} and K_d are noted in some cases, although some differences existed in the rodent strains and experimental protocols used. In general, however, at lower concentrations, the bound fraction appears greater in humans than in rats and mice. Typical human TCE exposures, even in controlled experiments with volunteers, lead to TCA blood concentrations well below the reported K_d (see Table 3-17, below), so the TCA binding fraction should be relatively constant. However, in rats and mice, experimental exposures may lead to peak concentrations similar to, or above, the reported K_d (e.g., [Yu et al., 2000](#); [Templin et al., 1993](#)), meaning that the bound fraction should temporarily decrease following such exposures.

Table 3-16. TCOH and TCA formed from CH in vitro in lysed whole blood of rats and mice or fractionated blood of humans (nmoles formed in 400 μ L samples over 30 minutes)

	Rat	Mouse	Human	
			Erythrocytes	Plasma
TCOH	45.4 \pm 4.9	46.7 \pm 1.0	15.7 \pm 1.4	4.48 \pm 0.2
TCA	0.14 \pm 0.2	0.21 \pm 0.3	0.42 \pm 0.0	Not detected

Source: Lipscomb et al. ([1996](#)).

Table 3-17. Reported TCA plasma binding parameters^a

	A	B_{MAX} (μ M)	K_d (μ M)	A+ B_{MAX}/K_d	Concentration range (μ M bound+free)
Human					
Templin et al. (1995b)	–	1,020	190	5.37	3–1,224
Lumpkin et al. (2003)	–	708.9	174.6	4.06	0.06–3,065
Rat					
Templin et al. (1995b)	–	540	400	1.35	3–1,224
Yu et al. (2000)	0.602	312	136	2.90	3.8–1,530
Lumpkin et al. (2003)	–	283.3	383.6	0.739	0.06–3,065
Mouse					
Templin et al. (1993)	–	310	248	1.25	3–1,224
Lumpkin et al. (2003)	–	28.7	46.1	0.623	0.06–1,226

^aBinding parameters based on the equation $C_{bound} = A \times C_{free} + B_{MAX} \times C_{free}/(K_d + C_{free})$, where C_{bound} is the bound concentration, C_{free} is the free concentration, and $A = 0$ for Templin et al. ([1995b](#); [1993](#)) and Lumpkin et al. ([2003](#)). The quantity $A + B_{MAX}/K_d$ is the ratio of bound-to-free at low concentrations.

Limited data are available on tissue:blood partitioning of the oxidative metabolites CH, TCA, TCOH, and DCA, as shown in Table 3-18. As these chemicals are all water soluble and not lipophilic, it is not surprising that their partition coefficients are close to one (within about twofold). It should be noted that the TCA tissue:blood partition coefficients reported in Table 3-18 were measured at concentrations 1.6–3.3 M, over 1,000-fold higher than the reported K_d . Therefore, these partition coefficients should reflect the equilibrium between tissue and free blood concentrations. In addition, only one in vitro measurement has been reported of blood:plasma concentration ratios for TCA: Schultz et al. (1999) reported a value of 0.76 in rats.

Table 3-18. Partition coefficients for TCE oxidative metabolites

Species/tissue ^a	Tissue:blood partition coefficient			
	CH	TCA	TCOH	DCA
Human^b				
Kidney	–	0.66	2.15	-
Liver	–	0.66	0.59	-
Lung	–	0.47	0.66	-
Muscle	–	0.52	0.91	-
Mouse^c				
Kidney	0.98	0.74	1.02	0.74
Liver	1.42	1.18	1.3	1.08
Lung	1.65	0.54	0.78	1.23
Muscle	1.35	0.88	1.11	0.37

^aTCA and TCOH partition coefficients have not been reported for rats.

^bFisher et al. (1998).

^cAbbas and Fisher (1997).

3.3.3.1.5. Species-, sex-, and age-dependent differences of oxidative metabolism

The ability to describe species- and sex-dependent variations in TCE metabolism is important for species extrapolation of bioassay data and identification of human populations that are particularly susceptible to TCE toxicity. In particular, information on the variation in the initial oxidative step of CH formation from TCE is desirable, because this is the rate-limiting step in the eventual formation and distribution of the putative toxic metabolites TCA and DCA (Lipscomb et al., 1997).

Inter- and intraspecies differences in TCE oxidation have been investigated in vitro using cellular or subcellular fractions, primarily of the liver. The available in vitro metabolism data on TCE oxidation in the liver (see Table 3-13) show substantial inter- and intraspecies variability. Across species, microsomal data show that mice apparently have greater capacity (V_{MAX}) than rat or humans, but the variability within species can be 2–10-fold. Part of the explanation may be related to CYP2E1 content. Although liver P450 content is similar across species, mice and rats exhibit higher levels of CYP2E1 content (0.85 and 0.89 nmol/mg protein, respectively)

([Davis et al., 2002](#); [Nakajima et al., 1993](#)) than humans (approximately 0.25–0.30 nmol/mg protein) ([Davis et al., 2002](#); [Elfarra et al., 1998](#)). Thus, the data suggest that rodents would have a higher capacity than humans to metabolize TCE, but this is difficult to verify in vivo because very high exposure concentrations in humans would be necessary to assess the maximum capacity of TCE oxidation.

With respect to the K_M of liver microsomal TCE oxidative metabolism, where K_M is indicative of affinity (the lower the numerical value of K_M , the higher the affinity), the trend appears to be that mice and rats have higher K_M values (i.e., lower affinity) than humans, but with substantial overlap due to interindividual variability. Note that, as shown in Table 3-13, the ranking of rat and mouse liver microsomal K_M values between the two reports by Lipscomb et al. ([1998c](#)) and Elfarra et al. ([1998](#)) is not consistent. However, both studies clearly show that K_M is the lowest (i.e., affinity is highest) in humans. Because clearance at lower concentrations is determined by the ratio V_{MAX} to K_M , the lower apparent K_M in humans may partially offset the lower human V_{MAX} , and lead to similar oxidative clearances in the liver at environmentally relevant doses. However, differences in activity measured in vitro may not translate into in vivo differences in metabolite production, as the rate of metabolism in vivo depends also on the rate of delivery to the tissue via blood flow ([Lipscomb et al., 2003](#)). The interaction of enzyme activity and blood flow is best investigated using PBPK models and is discussed, along with descriptions of in vivo data, in Section 3.5.

Data on sex- and age-dependence in oxidative TCE metabolism are limited but suggest relatively modest differences in humans and animals. In an extensive evaluation of CYP-dependent activities in human liver microsomal protein and cryopreserved hepatocytes, Parkinson et al. ([2004](#)) identified no age- or gender-related differences in CYP2E1 activity. In liver microsomes from 23 humans, the K_M values for females was lower than males, but V_{MAX} values were very similar ([Lipscomb et al., 1997](#)). Appearance of total trichloro compounds (TTCs) in urine following i.p. dosing with TCE was 28% higher in female rats than in males ([Verma and Rana, 2003](#)). The oxidation of TCE in male and female rat liver microsomes was not significantly different; however, pregnancy resulted in a decrease of 27–39% in the rate of CH production in treated microsomes from females ([Nakajima et al., 1992b](#)). Formation of CH in liver microsomes in the presence of 0.2 or 5.9 mM TCE exhibited some dependency on age of rats, with formation rates in both sexes of 1.1–1.7 nmol/mg protein/minute in 3-week-old animals and 0.5–1.0 nmol/mg protein/minute in 18-week-old animals ([Nakajima et al., 1992b](#)).

Fisher et al. ([1991](#)) reviewed data available at that time on urinary metabolites to characterize species differences in the amount of urinary metabolism accounted for by TCA (see Table 3-19). They concluded that TCA seemed to represent a higher percentage of urinary metabolites in primates than in other mammalian species, indicating a greater proportion of oxidation leading ultimately to TCA relative to TCOG.

Table 3-19. Urinary excretion of TCA by various species exposed to TCE (based on data reviewed in [Fisher et al., 1991](#))

Species ^a	Percentage of urinary excretion of TCA		Dose route	TCE dose (mg TCE/kg)	References
	Male	Female			
Baboon ^{b,c}	16	–	Intramuscular injection	50	Mueller et al. (1982)
Chimpanzee ^b	24	22	Intramuscular injection	50	Mueller et al. (1982)
Monkey, Rhesus ^{b,c}	19	–	Intramuscular injection	50	Mueller et al. (1982)
Mice, NMRI ^d	–	8–20	Oral intubation	2–200	Dekant et al. (1986b)
Mice, B6C3F ₁ ^b	7–12	–	Oral intubation	10–2,000	Green and Prout (1985)
Rabbit, Japanese White ^{b,c}	0.5	–	i.p. injection	200	Nomiyama and Nomiyama (1979)
Rat, Wistar ^d	–	14–17	Oral intubation	2–200	Dekant et al. (1986b)
Rat, Osborne-Mendel ^a	6–7	–	Oral intubation	10–2,000	Green and Prout (1985)
Rat, Holtzman ^a	7	–	i.p. injection	10 mg TCE/rat	Nomiyama and Nomiyama (1979)

^aThe human data tabulated in Fisher et al. ([1991](#)) from Nomiyama and Nomiyama ([1971](#)) were not included here because they were relative to urinary excretion of TTCs—not as fraction of intake as was the case for the other data included here.

^bPercentage urinary excretion determined from accumulated amounts of TCOH and TCA in urine 3–6 days postexposure.

^cSex not specified.

^dPercentage urinary excretion determined from accumulated amounts of TCOH, DCA, oxalic acid, and *N*-(hydroxyacetyl)aminoethanol in urine 3 days postexposure.

3.3.3.1.6. CYP isoforms and genetic polymorphisms

A number of studies have identified multiple P450 isozymes as having a role in the oxidative metabolism of TCE. These isozymes include CYP2E1 ([Nakajima et al., 1992a](#); [Guengerich et al., 1991](#); [Guengerich and Shimada, 1991](#); [Nakajima et al., 1990](#); [Nakajima et al., 1988](#)), CYP3A4 ([Shimada et al., 1994](#)), CYP1A1/2, CYP2C11/6 ([Nakajima et al., 1993](#); [Nakajima et al., 1992a](#)), CYP2F, and CYP2B1 ([Forkert et al., 2005](#)). Recent studies in CYP2E1-knockout mice have shown that in the absence of CYP2E1, mice still have substantial capacity for TCE oxidation ([Forkert et al., 2006](#); [Kim and Ghanayem, 2006](#)). However, CYP2E1 appears to be the predominant (i.e., higher affinity) isoform involved in oxidizing TCE ([Forkert et al., 2005](#); [Nakajima et al., 1992a](#); [Guengerich et al., 1991](#); [Guengerich and Shimada, 1991](#)). In rat liver, CYP2E1 catalyzed TCE oxidation more than CYP2C11/6 ([Nakajima et al., 1992a](#)). In rat recombinant-derived P450s, the CYP2E1 had a lower K_M (higher affinity) and higher V_{MAX}/K_M ratio (intrinsic clearance) than CYP2B1 or CYP2F4 ([Forkert et al., 2005](#)). Interestingly, there was substantial differences in K_M between rat and human CYP2E1s and between rat CYP2F4

and mouse CYP2F2, suggesting that species-specific isoforms have different kinetic behavior (see Table 3-20).

Table 3-20. P450 isoform kinetics for metabolism of TCE to CH in human, rat, and mouse recombinant P450s

Experiment	K_M μM	V_{MAX} pmol/min/pmol P450	V_{MAX}/K_M
Human rCYP2E1	196 ± 40	4 ± 0.2	0.02
Rat rCYP2E1	14 ± 3	11 ± 0.3	0.79
Rat rCYP2B1	131 ± 36	9 ± 0.5	0.07
Rat rCYP2F4	64 ± 9	17 ± 0.5	0.27
Mouse rCYP2F2	114 ± 17	13 ± 0.4	0.11

Source: Forkert et al. (2005).

The presence of multiple P450 isoforms in human populations affects the variability in individuals' ability to metabolize TCE. Studies using microsomes from human liver or from human lymphoblastoid cell lines expressing CYP2E1, CYP1A1, CYP1A2, or CYP3A4 have shown that CYP2E1 is responsible for >60% of oxidative TCE metabolism (Lipscomb et al., 1997). Similarities between metabolism of chlorzoxazone (a CYP2E1 substrate) in liver microsomes from 28 individuals (Peter et al., 1990) and TCE metabolism helped identify CYP2E1 as the predominant (high affinity) isoform for TCE oxidation. Additionally, Lash et al. (2000a) suggested that, at concentrations above the K_M value for CYP2E1, CYP1A2, and CYP2A4 may also metabolize TCE in humans; however, their contribution to the overall TCE metabolism was considered low compared to that of CYP2E1. Given the difference in expression of known TCE-metabolizing P450 isoforms (see Table 3-21) and the variability in P450-mediated TCE oxidation (Lipscomb et al., 1997), significant variability may exist in individual human susceptibility to TCE toxicity.

Table 3-21. P450 isoform activities in human liver microsomes exhibiting different affinities for TCE

Affinity group	CYP isoform activity (pmol/min/mg protein) ^a		
	CYP2E1	CYP1A2	CYP3A4
Low K_M	520 ± 295	241 ± 146	2.7 ± 2.7
Mid K_M	820 ± 372	545 ± 200	2.9 ± 2.8
High K_M	1,317 ± 592	806 ± 442	1.8 ± 1.1

^aActivities of CYP1A2, CYP2E1, and CYP3A4 were measured with phenacetin, chlorzoxazone, and testosterone as substrates, respectively. Data are means ± SD from 10, 9, and 4 samples for the low-, mid-, and high- K_M groups, respectively. Only CYP3A4 activities are not significantly different ($p < 0.05$) from one another by Kruskal-Wallis one-way analysis of variance.

Source: Lash et al. (2000a).

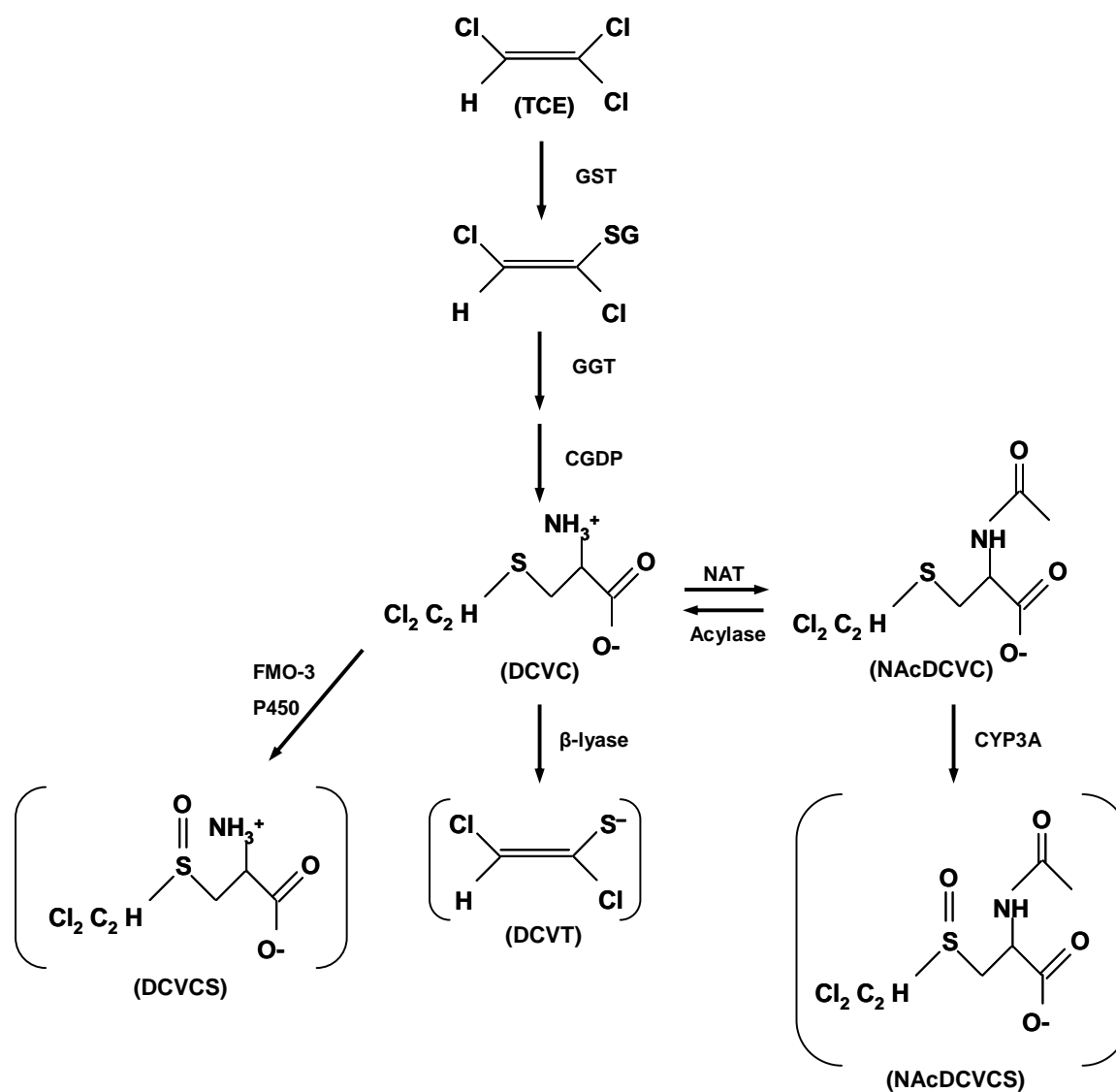
Differences in content and/or intrinsic catalytic properties (K_M , V_{MAX}) of specific enzymes among species, strains, and individuals may play an important role in the observed differences in TCE metabolism and resulting toxicities. Lipscomb et al. (1997) reported observing three statistically distinct groups of K_M values for TCE oxidation using human microsomes. The mean ± standard deviation (SD) (μM TCE) for each of the three groups was 16.7 ± 2.5 ($n = 10$), 30.9 ± 3.3 ($n = 9$), and 51.1 ± 3.8 ($n = 4$). Within each group, there were no significant differences in sex or ethnicity. However, the overall observed K_M values in female microsomes ($21.9 \pm 3.5 \mu\text{M}$, $n = 10$) were significantly lower than males ($33.1 \pm 3.5 \mu\text{M}$, $n = 13$). Interestingly, in human liver microsomes, different groups of individuals with different affinities for TCE oxidation appeared to also have different activities for other substrates not only with respect to CYP2E1 but also CYP1A2 (Lash et al., 2000a) (see Table 3-21). Genetic polymorphisms in humans have been identified in the CYP isozymes thought to be responsible for TCE metabolism (Pastino et al., 2000), but no data exist correlating these polymorphisms with enzyme activity. It is relevant to note that repeat polymorphism (Hu et al., 1999) or polymorphism in the regulatory sequence (McCarver et al., 1998) were not involved in the constitutive expression of human CYP2E1; however, it is unknown if these types of polymorphisms may play a role in the inducibility of the respective gene.

Individual susceptibilities to TCE toxicity may also result from variations in enzyme content, either at baseline or due to enzyme induction/inhibition, which can lead to alterations in the amounts of metabolites formed. Certain physiological and pathological conditions or exposure to other chemicals (e.g., ethanol and acetaminophen) can induce, inhibit, or compete for enzymatic activity. Given the well-established (or well-characterized) role of the liver to oxidatively metabolize TCE (by CYP2E1), increasing the CYP2E1 content or activity (e.g., by enzyme induction) may not result in further increases in TCE oxidation. Indeed, Kaneko et al. (1994) reported that enzyme induction by ethanol consumption in humans increased TCE metabolism only at high concentrations (500 ppm , $2,687 \text{ mg/m}^3$) in inspired air. However, other

interactions between ethanol and the enzymes that oxidatively metabolize TCE metabolites can result in altered metabolic fate of TCE metabolites. In addition, enzyme inhibition or competition can decrease TCE oxidation and subsequently alter the TCE toxic response via, for instance, increasing the proportion undergoing GSH conjugation Lash et al. (2000a). TCE itself is a competitive inhibitor of CYP2E1 activity (Lipscomb et al., 1997), as shown by reduced *p*-nitrophenol hydroxylase activity in human liver microsomes, and may therefore alter the toxicity of other chemicals metabolized through that pathway. On the other hand, suicidal CYP heme destruction by the TCE-oxygenated CYP intermediate has also been shown (Miller and Guengerich, 1983).

3.3.3.2. GSH Conjugation Pathway

Historically, the conjugative metabolic pathways have been associated with xenobiotic detoxification. This is true for GSH conjugation of many compounds. However, several halogenated alkanes and alkenes, including TCE, are bioactivated to cytotoxic metabolites by the GSH conjugate processing pathway (mercapturic acid) pathways (Elfarra et al., 1987; Elfarra et al., 1986). In the case of TCE, production of reactive species several steps downstream from the initial GSH conjugation is believed to cause cytotoxicity and carcinogenicity, particularly in the kidney. Since the GSH conjugation pathway is in competition with the P450 oxidative pathway for TCE biotransformation, it is important to understand the role of various factors in determining the flux of TCE through each pathway. Figure 3-5 depicts the present understanding of TCE metabolism via GSH conjugation.



Adapted from: Lash et al. (2000a); Cummings and Lash (2000); NRC (2006).

Figure 3-5. Scheme for GSH-dependent metabolism of TCE.

3.3.3.2.1. Formation of S-(1,2-dichlorovinyl)glutathione or S-(2,2-dichlorovinyl)glutathione (DCVG)

The conjugation of TCE to GSH produces S-(1,2-dichlorovinyl)glutathione or its isomer S-(2,2-dichlorovinyl)glutathione (collectively, S-dichlorovinyl-glutathione, DCVG). There is some uncertainty as to which GST isoforms mediate TCE conjugation. Lash and colleagues studied TCE conjugation in renal tissue preparations, isolated renal tubule cells from male F344 rats and purified GST alpha-class isoforms 1-1, 1-2, and 2-2 (Cummings and Lash, 2000; Cummings et al., 2000b; Lash et al., 2000b). The results demonstrated high conjugative activity in the renal cortex and proximal tubule cells. Although the isoforms studied had similar V_{MAX}

values, the K_M value for GST 2-2 was significantly lower than the other forms, indicating that this form will catalyze TCE conjugation at lower (more physiologically relevant) substrate concentrations. In contrast, using purified rat and human enzymes, Hissink et al. (2002) reported in vitro activity for DCVG formation only for mu- and pi-class GST isoforms, and none towards alpha-class isoforms; however, the rat mu-class GST 3-3 was several-fold more active than the human mu-class GST M1-1. Although GSTs are present in tissues throughout the body, the majority of TCE GSH conjugation is thought to occur in the liver (Lash et al., 2000a). Using in vitro studies with renal preparations, it has been demonstrated that GST catalyzed conjugation of TCE is increased following the inhibition of CYP-mediated oxidation (Cummings and Lash, 2000).

In F344 rats, following gavage doses of 263–1,971 mg/kg TCE in 2 mL corn oil, DCVG was observed in the liver and kidney of females only, in blood of both sexes (Lash et al., 2006), and in bile of males (Dekant, 1990). The data from Lash et al. (2006) are difficult to interpret because the time courses seem extremely erratic, even for the oxidative metabolites TCOH and TCA. Moreover, a comparison of blood levels of TCA and TCOH with other studies in rats at similar doses reveals differences of over 1,000-fold in reported concentrations. For instance, at the lowest dose of 263 mg/kg, the peak blood levels of TCE and TCA in male F344 rats were 10.5 and 1.6 $\mu\text{g/L}$, respectively (Lash et al., 2006). By contrast, Larson and Bull (1992a) reported peak blood TCE and TCA levels in male Sprague-Dawley rats over 1,000-fold higher—around 10 and 13 mg/L, respectively—following oral doses of 197 mg/kg as a suspension in 1% aqueous Tween 80[®]. The results of Larson and Bull (1992a) are similar to Lee et al. (2000b), who reported peak blood TCE levels of 20–50 mg/L after male Sprague-Dawley rats received oral doses of 144–432 mg/kg in a 5% aqueous Alkamus emulsion (polyethoxylated vegetable oil), and to Stenner et al. (1997), who reported peak blood levels of TCA in male F344 rats of about 5 mg/L at a slightly lower TCE oral dose of 100 mg/kg administered to fasted animals in 2% Tween 80[®]. Thus, while useful qualitatively as an indicator of the presence of DCVG in rats, the quantitative reliability of reported concentrations, for metabolites of either oxidation or GSH conjugation, may be questionable.

In humans, DCVG was readily detected at in human blood following onset of a 4-hour TCE inhalation exposure to 50 or 100 ppm (269 or 537 mg/m³) (Lash et al., 1999b). At 50 ppm, peak blood levels ranged from 2.5 to 30 μM , while at 100 ppm, the mean (\pm SE, n = 8) peak blood levels were 46.1 \pm 14.2 μM in males and 13.4 \pm 6.6 μM in females. Although on average, male subjects had threefold higher peak blood levels of DCVG than females, DCVG blood levels in half of the male subjects were similar to or lower than those of female subjects. This suggests a polymorphism in GSH conjugation of TCE rather than a true gender difference (Lash et al., 1999b) as also has been indicated by Hissink et al. (2002) for the human mu-class GST M1-1 enzyme. Interestingly, as shown in Table 3-22, the peak blood levels of DCVG are similar on a

molar basis to peak levels of TCE, TCA, and TCOH in the same subjects, as reported in Fisher et al. (1998).

Table 3-22. Comparison of peak blood concentrations in humans exposed to 100 ppm (537 mg/m³) TCE for 4 hours

Chemical species	Peak blood concentration (mean ± SD, μM)	
	Males	Females
TCE	23 ± 11	14 ± 4.7
TCA	56 ± 9.8	59 ± 12
TCOH	21 ± 5.0	15 ± 5.6
DCVG	46.1 ± 14.2	13.4 ± 6.6

Sources: Fisher et al. (1998); Lash et al. (1999a).

Tables 3-23–3-25 summarize DCVG formation from TCE conjugation from in vitro studies of liver and kidney cellular and subcellular fractions in mouse, rat, and human (tissue-distribution and species- and gender-differences in DCVG formation are discussed below). As shown by these tables, different investigators have reported considerably different rates for TCE conjugation in human liver and kidney cell fractions. For instance, values in Table 3-23 from Lash et al. (1999b) are between 2 and 5 orders of magnitude higher than those reported by Green et al. (1997a) or Dekant et al. (1990) (see Table 3-25). In addition, Green et al. (1997a) and Dekant et al. (1990) reported a difference in the relative importance of rat liver cytosol and rat liver microsomes for GSH conjugation, with Green et al. (1997a) reporting activity in the cytosol and none in the microsomes and Dekant et al. (1990) reporting the opposite.

Table 3-23. GSH conjugation of TCE (at 1–2 mM) in liver and kidney cellular fractions in humans, male F344 rats, and male B6C3F₁ mice from Lash laboratory

Species and cellular/subcellular fraction (TCE concentration)	DCVG formation (nmol/hr/mg protein or 10 ⁶ cells) ^a	
	Male	Female
Human		
Hepatocytes (0.9 mM) (pooled)	11 ± 3	
Liver cytosol (1 mM) (individual samples)	156 ± 16	174 ± 13
Liver cytosol (2 mM) (pooled)	346	
Liver microsomes (1 mM) (individual samples)	108 ± 24	83 ± 11
Liver microsomes (1 mM) (pooled)	146	
Kidney cytosol (2 mM) (pooled)	42	
Kidney microsomes (1 mM) (pooled)	320	
Rat		
Liver cytosol (2 mM)	7.30 ± 2.8	4.86 ± 0.14
Liver microsomes (2 mM)	10.3 ± 2.8	7.24 ± 0.24
Kidney cortical cells (2 mM)	0.48 ± 0.02	0.65 ± 0.15
Kidney cytosol (2 mM)	0.45 ± 0.22	0.32 ± 0.02
Kidney microsomes (2 mM)	Not detected	0.61 ± 0.06
Mouse		
Liver cytosol (2 mM)	24.5 ± 2.4	21.7 ± 0.9
Liver microsomes (2 mM)	40.0 ± 3.1	25.6 ± 0.8
Kidney cytosol (2 mM)	5.6 ± 0.24	3.7 ± 0.48
Kidney microsomes (2 mM)	5.47 ± 1.41	16.7 ± 4.7

^aMean ± SE.

Sources: Lash et al. ([1999a](#); [1998a](#); [1995](#)); Cummings and Lash ([2000](#)).

Table 3-24. Kinetics of TCE metabolism via GSH conjugation in male F344 rat kidney and human liver and kidney cellular and subcellular fractions from Lash laboratory

Tissue and cellular fraction	K_M (μ M TCE)	V_{MAX} (nmol DCVG/min/mg protein or 10^6 hepatocytes)	$1,000 \times$ V_{MAX}/K_M
Rat			
Kidney proximal tubular cells: low affinity	2,910	0.65	0.22
Kidney proximal tubular cells: high affinity	460	0.47	1.0
Human			
Liver hepatocytes ^a	37~106	0.16~0.26	2.4~4.5
Liver cytosol: low affinity	333	8.77	2.6
Liver cytosol: high affinity	22.7	4.27	190
Liver microsomes: low affinity	250	3.1	12
Liver microsomes: high affinity	29.4	1.42	48
Kidney proximal tubular cells: low affinity	29,400	1.35	0.046
Kidney proximal tubular cells: high affinity	580	0.11	0.19
Kidney cytosol	26.3	0.81	31
Kidney microsomes	167	6.29	38

^aKinetic analyses of first 6–9 (out of 10) data points from Figure 1 from Lash et al. (1999b) using Lineweaver-Burk or Eadie-Hofstee plots and linear regression ($R^2 = 0.50\text{--}0.95$). Regression with best R^2 used first 6 data points and Eadie-Hofstee plot, with resulting K_M and V_{MAX} of 106 and 0.26, respectively.

Sources: Lash et al. (1999b); Cummings and Lash (2000); (Cummings et al., 2000b).

Table 3-25. GSH conjugation of TCE (at 1.4–4 mM) in liver and kidney cellular fractions in humans, male F344 rats, and male B6C3F₁ mice from Green and Dekant laboratories

Species and cellular/subcellular fraction (TCE concentration)	DCVG formation (nmol/hr/mg protein) (substrate concentration in mM) ^a	
	Dekant et al. (1990)	Green et al. (1997a)
Human		
Liver cytosol	-	0.00019 ± 0.00014
Liver microsomes	-	Not determined
Kidney cytosol	-	Not determined
Kidney microsomes	-	Not determined
Rat		
Liver cytosol	<0.002	0.00162 ± 0.00002
Liver microsomes	0.002	Not determined
Kidney cytosol	-	Not determined
Kidney microsomes	-	Not determined
Mouse		
Liver cytosol	-	0.0025
Liver microsomes	-	Not determined
Kidney cytosol	-	Not determined
Kidney microsomes	-	Not determined

^aWhere available, mean ± SD.

Sources: Dekant et al. (1990), Green et al. (1997a).

The reasons for such discrepancies are unclear, but they may be related to different analytical methods (Lash et al., 2000a). In particular, Lash et al. (1999b) employed the “Reed method,” which used ion-exchange high-performance liquid chromatography (HPLC) of derivatized analytes. This HPLC method is characterized by variability and an overall decline in retention times over the life of the HPLC column due to derivatization of amine groups on the column (Lash et al., 1999a). Although data are limited, the GSH pathway metabolite levels reported by methods that utilize [¹⁴C]-TCE and radiochemical detection followed by mass spectrometry (MS) identification of the metabolites are lower. In particular, Green et al. (1997a) and Dekant et al. (1990) both used HPLC with radiochemical detection. Peak identity was confirmed by Green et al. (1997a) using liquid chromatography (LC)/MS and by GC/MS following hydrolysis by Dekant et al. (1990). In addition, studies using HPLC-MS/MS techniques with stable isotope-labeled DCVG and dichlorovinyl cysteine (DCVC) standards have also been used to detect GSH pathway metabolite levels Kim et al. (2009). Based on the in vitro work presented in Table 3-23 using the “Reed method,” one would expect mouse serum DCVG levels to be ~4-6 times lower than humans. However, using the HPLC-MS/MS technique of Kim et al. (2009), the peak DCVG serum levels are ~1,000 times lower in mouse

serum than determined by Lash et al. ([1999b](#)) in human serum. Although advances in LC technology, and differences in exposure routes (inhalation vs. oral, with different first pass), exposure doses, and the degree of competition with TCE oxidation (greater in mouse than in human) should be considered, this much-larger-than-expected difference is consistent with the suggestion that the “Reed method” provides an overestimation of DCVG levels in humans. This could occur if the “Reed method” identifies nonspecific derivatives as DCVG or other GSH pathway metabolites. However, the degree of overestimation is unclear, and differing results in humans may be attributable to true interindividual variation (especially since GSTs are known to be polymorphic). Overall, there remains significant uncertainty in the quantitative estimation of DCVG formation from TCE both in vivo and in vitro.

3.3.3.2.2. Formation of S-(1,2-dichlorovinyl) cysteine or S-(2,2-dichlorovinyl) cysteine (DCVC)

The cysteine conjugate, isomers S-(1,2-dichlorovinyl) cysteine (1,2-DCVC) or S-(2,2-dichlorovinyl) cysteine (2,2-DCVC) (collectively S-dichlorovinyl-cysteine, DCVC), is formed from DCVG in a two-step sequence. DCVG is first converted to the cysteinylglycine conjugate S-(1,2-dichlorovinyl)-L-cysteinylglycine or its isomer S-(2,2-dichlorovinyl)-L-cysteinylglycine by γ -glutamyl transpeptidase (GGT) in the renal brush border ([Lash et al., 1988](#); [Elfarrar and Anders, 1984](#)).

Cysteinylglycine dipeptidases in the renal brush border and basolateral membrane convert DCVG to DCVC via glycine cleavage ([Goepfert et al., 1995](#); [Lash et al., 1995](#)). This reaction can also occur in the bile or gut, as DCVG excreted into the bile is converted to DCVC and reabsorbed into the liver where it may undergo further acetylation.

3.3.3.2.3. Formation of N-Acetyl-S-(1,2-dichlorovinyl)-L-cysteine or N-Acetyl-S-(2,2-dichlorovinyl)-L-cysteine (NAcDCVC)

N-acetylation of DCVC can either occur in the kidney, as demonstrated in rat kidney microsomes ([Duffel and Jakoby, 1982](#)), or in the liver ([Birner et al., 1997](#)). Subsequent release of DCVC from the liver to blood may result in distribution to the kidney resulting in increased internal kidney exposure to the acetylated metabolite over and above what the kidney already is capable of generating. In the kidney, N-Acetyl-S-(1,2-dichlorovinyl)-L-cysteine or N-Acetyl-S-(2,2-dichlorovinyl)-L-cysteine (collectively N-Acetyl-S-dichlorovinyl-L-cysteine, NAcDCVC) may undergo deacetylation, which is considered a rate-limiting-step in the production of proximal tubule damage ([Wolfgang et al., 1989a](#); [Zhang and Stevens, 1989](#)). As a polar mercapturate, NAcDCVC may be excreted in the urine as evidenced by findings in mice ([Birner et al., 1993](#)), rats ([Bernauer et al., 1996](#); [Commandeur and Vermeulen, 1990](#)), and humans who were exposed to TCE ([Bernauer et al., 1996](#); [Birner et al., 1993](#)), suggesting a common GSH-mediated metabolic pathway for DCVC among species.

3.3.3.2.4. Beta lyase metabolism of DCVC

The enzyme cysteine conjugate β -lyase catalyzes the breakdown of 1,2-DCVC to reactive nephrotoxic metabolites ([Goeptar et al., 1995](#)). This reaction involves removal of pyruvate and ammonia and production of S-dichlorovinyl thiol (DCVT), an unstable intermediate, which rearranges to other reactive alkylation metabolites that form covalent bonds with cellular nucleophiles ([Goeptar et al., 1995](#); [Dekant et al., 1988](#)). The rearrangement of DCVT to enethiols and their acetylating agents has been described in trapping experiments ([Dekant et al., 1988](#)) and proposed to be responsible for nucleophilic adduction and toxicity in the kidney. The quantification of acid-labile adducts was proposed as a metric for TCE flux through the GSH pathway. However, the presence of analytical artifacts precluded such analysis. In fact, measurement of acid-labile adduct products resulted in higher values in mice than in rats ([Eyre et al., 1995b, a](#)).

DCVC metabolism to reactive species via a β -lyase pathway has been observed in vitro by Green et al. ([1997a](#)), who reported greater β -lyase activity in rats than in mice or humans. However, in vitro DCVC metabolism by the competing enzyme *N*-acetyl transferase was also reported to be greater in rats than mice and humans. In vivo, β -lyase activity in humans and rats (reaction rates were not reported) was demonstrated using a surrogate substrate, 2-(fluoromethoxy)-1,1,3,3,3-pentafluoro-1-propene ([Iyer et al., 1998](#)). β -lyase-mediated reactive adducts have been described in several extrarenal tissues, including rat and human liver and intestinal microflora ([Larsen and Stevens, 1986](#); [Tomisawa et al., 1986](#); [Stevens, 1985](#); [Tomisawa et al., 1984](#); [Stevens and Jakoby, 1983](#); [Dohn and Anders, 1982](#); [Tateishi et al., 1978](#)) and rat brain ([Alberati-Giani et al., 1995](#); [Malherbe et al., 1995](#)).

In the kidneys, glutamine transaminase K appears to be primarily responsible for β -lyase metabolism of DCVC ([Perry et al., 1993](#); [Lash et al., 1990](#); [Jones et al., 1988](#); [Stevens et al., 1988](#); [Lash et al., 1986](#); [Stevens et al., 1986](#)). β -Lyase transformation of DCVC appears to be regulated by 2-keto acids. DCVC toxicity in isolated rat proximal tubular cells was significantly increased with the addition of α -keto- γ -methiolbutyrate or phenylpyruvate ([Elfarra et al., 1986](#)). The presence of α -keto acid cofactors is necessary to convert the inactive form of the β -lyase enzyme (containing pyridoxamine phosphate) to the active form (containing pyridoxal phosphate) ([Goeptar et al., 1995](#)).

Both low- and high-molecular-weight enzymes with β -lyase activities have been identified in rat kidney cytosol and mitochondria ([Abraham et al., 1995a](#); [Abraham et al., 1995b](#); [Stevens et al., 1988](#); [Lash et al., 1986](#)). While glutamine transaminase K and kynureninase-associated β -lyase activities have been identified in rat liver ([Alberati-Giani et al., 1995](#); [Stevens, 1985](#)), they are quite low compared to renal glutamine transaminase K activity and do not result in hepatotoxicity in DCVG- or DCVC-treated rats ([Elfarra and Anders, 1984](#)). Similar isoforms of β -lyase have also been reported in mitochondrial fractions of brain tissue ([Cooper, 2004](#)).

The kidney enzyme, L- α -hydroxy (L-amino) acid oxidase, is capable of forming an iminium intermediate and keto acid analogues (pyruvate or S-(1,2-dichlorovinyl)-2-oxo-3-mercaptopropionate) of DCVC, which decomposes to dichlorovinylthiol ([Lash et al., 1990](#); [Stevens et al., 1989](#)). In rat kidney homogenates, this enzyme activity resulted in as much as 35% of GSH pathway-mediated bioactivation. However, this enzyme is not present in humans, an important consideration for extrapolation of renal effects across species.

3.3.3.2.5. DCVC and NAcDCVC

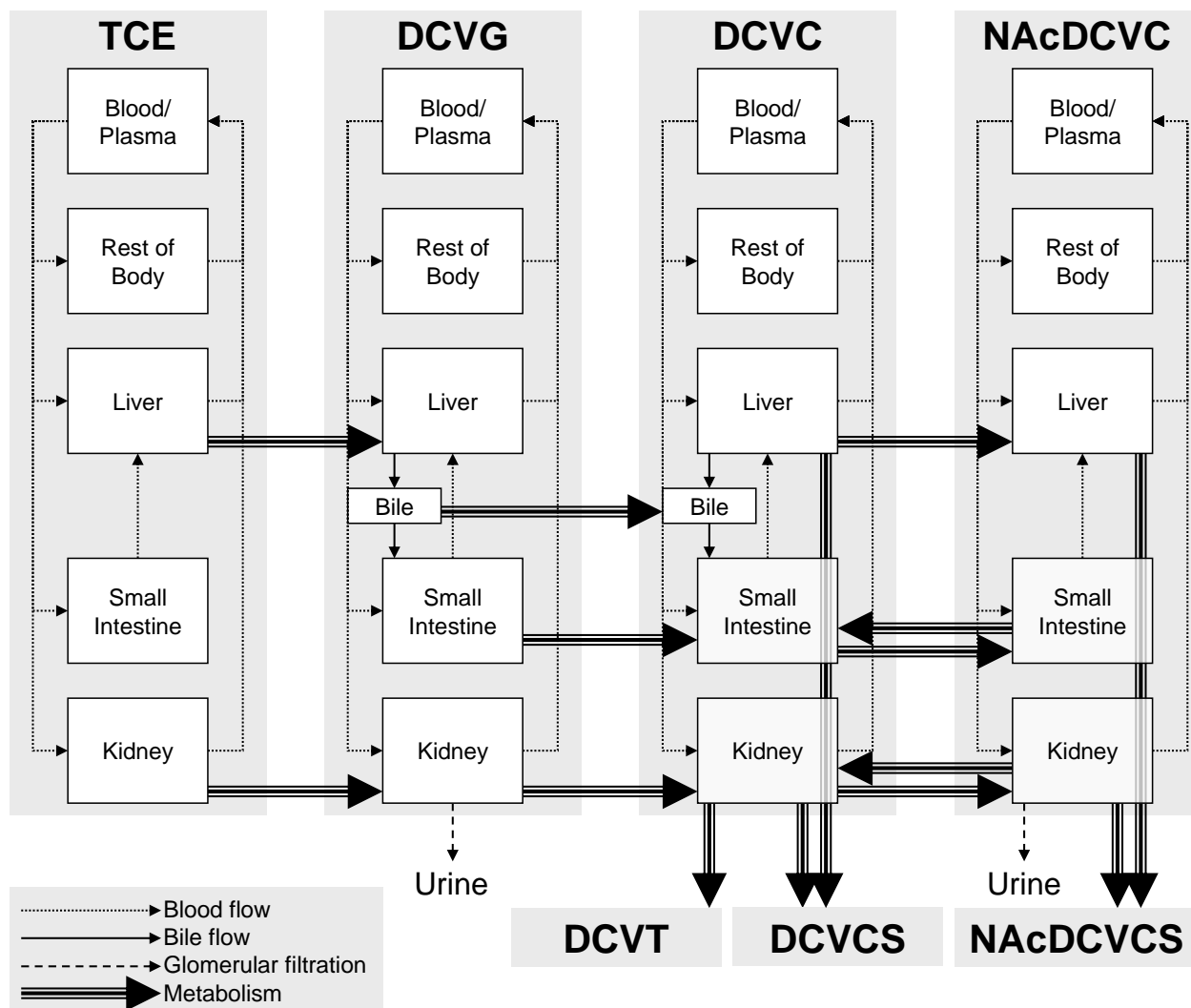
A second pathway for bioactivation of TCE S-conjugates involves sulfoxidation of either the cysteine or mercapturic acid conjugates ([Krause et al., 2003](#); [Lash et al., 2003](#); [Birner et al., 1998](#); [Werner et al., 1996, 1995a](#); [Werner et al., 1995b](#); [Lash et al., 1994](#); [Park et al., 1992](#); [Sausen and Elfarra, 1990](#)). Sulfoxidation of DCVC was mediated mainly by flavin monooxygenase 3 (FMO3), rather than CYP, in rabbit liver microsomes ([Ripp et al., 1997](#)) and human liver microsomes ([Krause et al., 2003](#)). Krause et al. ([2003](#)) also reported DCVC sulfoxidation by human cDNA-expressed FMO3, as well as detection of FMO3 protein in human kidney samples. While Krause et al. ([2003](#)) were not able to detect sulfoxidation in human kidney microsomes, the authors noted FMO3 expression in the kidney was lower and more variable than that in the liver. However, sulfoxidation products in tissues or urine have not been reported *in vivo*.

Sulfoxidation of NAcDCVC, by contrast, was found to be catalyzed predominantly, if not exclusively, by CYP3A enzymes ([Werner et al., 1996](#)), whose expressions are highly polymorphic in humans. Sulfoxidation of other haloalkyl mercapturic acid conjugates has also been shown to be catalyzed by CYP3A ([Altuntas et al., 2004](#); [Werner et al., 1995a](#); [Werner et al., 1995b](#)). While Lash et al. ([2000a](#)) suggested that this pathway would be quantitatively minor because of the relatively low CYP3A levels in the kidney, no direct data exist to establish the relative toxicological importance of this pathway relative to bioactivation of DCVC by β -lyase or FMO3. However, the contribution of CYP3A in S-conjugate sulfoxidation to nephrotoxicity *in vivo* was recently demonstrated by Sheffels et al. ([2004](#)) with fluoromethyl-2,2-difluoro-1-(trifluoromethyl)vinyl ether (FDVE). In particular, *in vivo* production and urinary excretion of FDVE-mercapturic acid sulfoxide metabolites were unambiguously established by mass spectrometry, and CYP inducers/inhibitors increased/decreased nephrotoxicity *in vivo* while having no effect on urinary excretion of metabolites produced through β -lyase ([Sheffels et al., 2004](#)). These data suggest that, by analogy, sulfoxidation of NAcDCVC may be an important bioactivating pathway.

3.3.3.2.6. Tissue distribution of GSH metabolism

The sites of enzymatic metabolism of TCE to the various GSH pathway-mediated metabolites are significant in determining target tissue toxicity along this pathway. Figure 3-6

presents a schematic of interorgan transport and metabolism of TCE along the GSH pathway. TCE is taken up either by the liver or kidney and conjugated to DCVG. The primary factors affecting TCE flux via this pathway include high hepatic GST activity, efficient transport of DCVG from the liver to the plasma or bile, high renal brush border and low hepatic GGT activities, and the capability for GSH conjugate uptake into the renal basolateral membranes with limited or no uptake into liver cell plasma membranes.



See Figure 3-5 for enzymes involved in metabolic steps. Source: Lash et al. (2000a; 2000b); NRC (2006).

Figure 3-6. Interorgan TCE transport and metabolism via the GSH pathway.

As discussed previously, GST activity is present in many different cell types. However, the liver is the major tissue for GSH conjugation. GST activities in rat and mouse cytosolic fractions were measured using 1-chloro-2,4-dinitrobenzene, a GST substrate that is nonspecific

for particular isoforms ([Lash et al., 1998b](#)). Specific activities (normalized for protein content) in whole-kidney cytosol were slightly less than those in the liver (0.64 compared to 0.52 mU/mg protein for males and females). However, the much larger mass of the liver compared to the kidney indicates that far more total GST activity resides in the liver. This is consistent with *in vitro* data on TCE conjugation to DCVG, discussed previously (see Tables 3-23 and 3-24). For instance, in humans, rats, and mice, liver cytosol exhibits greater DCVG production than kidney cytosol. Distinct high- and low-affinity metabolic profiles were observed in the liver but not in the kidney (see Table 3-24). In microsomes, human liver and kidney had similar rates of DCVG production, while for rats and mice, the production in the liver was substantially greater. According to studies by Lash et al. ([1998a](#); [1998b](#)), the activity of GGT, the first step in the conversion of DCVG to DCVC, is much higher in the kidney than the liver of mice, rats, and humans, with most of the activity being concentrated in the microsomal, rather than the cytosolic, fraction of the cell (see Table 3-26). In rats, this activity is quite high in the kidney but is below the level of detection in the liver, while the relative kidney-to-liver levels in humans and mice were higher by 18- and up to 2,300-fold, respectively. Similar qualitative findings were also reported in another study ([Hinchman and Ballatori, 1990](#)) when total organ GGT levels were compared in several species (see Table 3-27). Cysteinylglycine dipeptidase was also preferentially higher in the kidney than the liver of all tested species although the interorgan differences in this activity (one–ninefold) seemed to be less dramatic than for GGT (see Table 3-27). High levels of both GGT and dipeptidases have also been reported in the small intestine of rat ([Kozak and Tate, 1982](#)) and mouse ([Habib et al., 1996](#)), as well as GGT in the human jejunum ([Fairman et al., 1977](#)). No specific human intestinal cysteinylglycine dipeptidase has been identified; however, a related enzyme (EC 3.4.13.11) from human kidney microsomes has been purified and studied ([Adachi et al., 1989](#)), while several human intestinal dipeptidases have been characterized including a membrane dipeptidase (EC 3.4.13.19), which has a wide dipeptide substrate specificity including cysteinylglycine ([Ristoff and Larsson, 2007](#); [Hooper et al., 1994](#)).

Table 3-26. GGT activity in liver and kidney subcellular fractions of mice, rats, and humans

Species	Sex	Tissue	Cellular fraction	Activity (mU/mg)
Mouse	Male	Liver	Cytosol	0.07 ± 0.04
			Microsomes	0.05 ± 0.04
		Kidney	Cytosol	1.63 ± 0.85
			Microsomes	92.6 ± 15.6
	Female	Liver	Cytosol	0.10 ± 0.10
			Microsomes	0.03 ± 0.03
		Kidney	Cytosol	0.79 ± 0.79
			Microsomes	69.3 ± 14.0
Rat	Male	Liver	Cytosol	<0.02
			Microsomes	<0.02
		Kidney	Cytosol	<0.02
			Microsomes	1,570 ± 100
	Female	Liver	Cytosol	<0.02
			Microsomes	<0.02
		Kidney	Cytosol	<0.02
			Microsomes	1,840 ± 40
Human	Male	Liver	Cytosol	8.89 ± 3.58
			Microsomes	29
		Kidney	Cytosol	13.2 ± 1.0
			Microsomes	960 ± 77

Sources: Lash et al. ([1999a](#); [1998a](#))

Table 3-27. Multispecies comparison of whole-organ activity levels of GGT and dipeptidase

Species	Whole organ enzyme activity (μmol substrate/organ)			
	Kidney		Liver	
	GGT	Dipeptidase	GGT	Dipeptidase
Rat	1,010 ± 41	20.2 ± 1.1	7.1 ± 1.4	6.1 ± 0.4
Mouse	60.0 ± 4.2	3.0 ± 0.3	0.47 ± 0.05	1.7 ± 0.2
Rabbit	1,119 ± 186	112 ± 17	71.0 ± 9.1	12.6 ± 1.0
Guinea pig	148 ± 13	77 ± 10	46.5 ± 4.2	13.2 ± 1.5
Pig	3,800 ± 769	2,428 ± 203	1,600 ± 255	2,178 ± 490
Macaque	988	136	181	71

Source: Hinchman and Ballatori ([1990](#)).

3.3.3.2.7. Sex- and species-dependent differences in GSH metabolism

Diverse sex and species differences appear to exist in TCE metabolism via the GSH pathway. In rodents, rates of TCE conjugation to GSH in male rats and mice are higher than

females (see Table 3-23). Verma and Rana (2003) reported twofold higher GST activity values in liver cytosol of female rats, compared to males, given 15 i.p. injections of TCE over 30 days period. This effect may be due to sex-dependent variation in induction, as GST activities in male and female controls were similar. DCVG formation rates by liver and kidney subcellular fractions were much higher in both sexes of mice than in rats and, except for mouse kidney microsomes, the rates were generally higher in males than in females of the same species (see Table 3-23).

In terms of species differences, comparisons at 1–2 mM TCE concentrations (see Table 3-23) suggest that, in liver and kidney cytosol, the greatest DCVG production rate was in humans, followed by mice and then rats. However, different investigators have reported considerably different rates for TCE conjugation in human liver and kidney cell fractions. For instance, values in Table 3-23 from Lash et al. (1999b) are between 2 and 5 orders of magnitude higher than those reported by Green et al. (1997a). The rates of DCVG formation by liver cytosol from male F344 rat, male B6C3F₁ mouse, and human were 1.62, 2.5, and 0.19 pmol/minute/mg protein, respectively, while there was no measurable activity in liver microsomes or subcellular kidney fractions (Green et al., 1997a). The reasons for such discrepancies are unclear but may be related to different analytical methods employed such as detection of radiolabeled substrate vs. derivatized analytes (Lash et al., 2000a).

Expression of GGT activity does not appear to be influenced by sex (see Table 3-26); but species differences in kidney GGT activity are notable with rat subcellular fractions exhibiting the highest levels and mice and humans exhibiting about 4–6 and 50%, respectively, of rat levels (Lash et al., 1999a; Lash et al., 1998a). Table 3-27 shows measures of whole-organ GGT and dipeptidase activities in rats, mice, guinea pigs, rabbits, pigs, and monkeys. These data show that the whole kidney possesses higher activities than liver for these enzymes, despite the relatively larger mass of the liver.

As discussed above, the three potential bioactivating pathways subsequent to the formation of DCVC are catalyzed by β -lyase, FMO3, or CYP3A. Lash et al. (2000a) compared in vitro β -lyase activities and kinetic constants (when available) for kidney of rats, mice, and humans. They reported that variability of these values spans up to two orders of magnitude depending on substrate, analytical method used, and research group. Measurements of rat, mouse, and human β -lyase activities collected by the same researchers following tetrachloroethylene exposure (Green et al., 1990) resulted in higher K_M and lower V_{MAX} values for mice and humans than rats. Further, female rats exhibited higher K_M and lower V_{MAX} values than males.

With respect to FMO3, Ripp et al. (1999) found that this enzyme appeared catalytically similar across multiple species, including humans, rats, dogs, and rabbits, with respect to several substrates, including DCVC, but that there were species differences in expression. Specifically, in male liver microsomes, rabbits had 3-fold higher methionine S-oxidase activity than mice and dogs had 1.5-fold higher activity than humans and rats. Species differences were also noted in

male and female kidney microsomes; rats exhibited two- to sixfold higher methionine S-oxidase activity than the other species. Krause et al. (2003) detected DCVC sulfoxidation in incubations with human liver microsomes but did not in an incubation with a single sample of human kidney microsomes. However, FMO3 expression in the 26 human kidney samples was found to be highly variable, with a range of five- to sixfold (Krause et al., 2003).

No data on species differences in CYP3A-mediated sulfoxidation of NAcDCVC are available. However, Altuntas et al. (2004) examined sulfoxidation of cysteine and mercapturic acid conjugates of fluoromethyl-2,2-difluoro-1-(trifluoromethyl)vinyl ether (FDVE) in rat and human liver and kidney microsomes. They reported that the formation of sulfoxides from the mercapturates *N*-Ac-FFVC and (Z)-*N*-Ac-FFVC (FFVC is (*E,Z*)-S-(1-fluoro-2-fluoromethoxy-2-(trifluoromethyl)vinyl)-L-cysteine) were greatest in rat liver microsomes, and 2–30-fold higher than in human liver microsomes (which had high variability). Sulfoxidation of *N*-Ac-FFVC could not be detected in either rat or human kidney microsomes, but sulfoxidation of (Z)-*N*-Ac-FFVC was detected in both rat and human kidney microsomes at rates comparable to human liver microsomes. Using human- and rat-expressed CYP3A, Altuntas et al. (2004) reported that rates of sulfoxidation of (Z)-*N*-Ac-FFVC were comparable in human CYP3A4 and rat CYP3A1 and CYP3A2, but that only rat CYP3A1 and A2 catalyzed sulfoxidation of *N*-Ac-FFVC. As the presence or absence of the species differences in mercapturate sulfoxidation appears to be highly chemical-specific, no clear inferences can be made as to whether species differences exist for sulfoxidation of NAcDCVC

Also relevant to assess the flux through the various pathways are the rates of *N*-acetylation and de-acetylation of DCVC. This is demonstrated by the results of Elfarra and Hwang (1990) using S-(2-benzothiazolyl)-L-cysteine as a marker for β -lyase metabolism in rats, mice, hamsters, and guinea pigs. Guinea pigs exhibited about twofold greater flux through the β -lyase pathway, but this was not attributable to higher β -lyase activity. Rather, guinea pigs have relatively low *N*-acetylation and high deacetylation activities, leading to a high level of substrate recirculation (Lau et al., 1995). Thus, a high *N*-deacetylase:*N*-acetylase activity ratio may favor DCVC recirculation and subsequent metabolism to reactive species. In human, Wistar rat, Fischer rat, and mouse cytosol, deacetylation rates for NAcDCVC varied less than threefold (0.35, 0.41, 0.61, and 0.94 nmol DCVC formed/minute/mg protein in humans, rats, and mice) (Birner et al., 1993). However, similar experiments have not been carried out for *N*-acetylation of DCVC, so the balance between its *N*-acetylation and de-acetylation has not been established.

3.3.3.2.8. Human variability and susceptibility in GSH conjugation

Knowledge of human variability in metabolizing TCE through the GSH pathway is limited to in vitro comparisons of variance in GST activity rates. Unlike CYP-mediated oxidation, quantitative differences in the polymorphic distribution or activity levels of GST isoforms in humans are not presently known. However, the available data (Lash et al., 1999a;

[Lash et al., 1999b](#)) do suggest that significant variation in GST-mediated conjugation of TCE exists in humans. In particular, at a single substrate concentration of 1 mM, the rate of GSH conjugation of TCE in human liver cytosol from 9 male and 11 females spanned a range of 2.4-fold (34.7–83.6 nmol DCVG formed/20-minute/mg protein) ([Lash et al., 1999a](#)). In liver microsomes from 5 males and 15 females, the variation in activity was 6.5-fold (9.9–64.6 nmol DCVG formed/20 minute/mg protein). No sex-dependent variation was identified. Despite being less pronounced than the known variability in human CYP-mediated oxidation, the impact on risk assessment of the variability in GSH conjugation to TCE is currently unknown especially in the absence of data on variability for *N*-acetylation and bioactivation via β -lyase, FMO3, or CYP3A in the human kidney.

3.3.3.3. Relative roles of the CYP and GSH pathways

In vivo mass balance studies in rats and mice, discussed above, have shown unequivocally that in these species, CYP oxidation of TCE predominates over GSH conjugation. In these species, at doses of 2–2,000 mg/kg of [¹⁴C]-TCE, the sum of radioactivity in exhaled TCE, urine, and exhaled CO₂ constitutes 69–94% of the dose, with the vast majority of the radioactivity in urine (95–99%) attributable to oxidative metabolites ([Dekant et al., 1986b](#); [Green and Prout, 1985](#); [Prout et al., 1985](#); [Dekant et al., 1984](#)). The rest of the radioactivity was found mostly in feces and the carcass. More rigorous quantitative limits on the amount of GSH conjugation based on in vivo data such as these can be obtained using PBPK models, discussed in Section 3.5.

Comprehensive mass-balance studies are unavailable in humans. DCVG and DCVC in urine have not been detected in any species, while the amount of urinary NAcDCVC from human exposures is either below detection limits or very small from a total mass balance point of view ([Bloemen et al., 2001](#); [Lash et al., 1999b](#); [Bernauer et al., 1996](#); [Birner et al., 1993](#)). For instance, the ratio of primary oxidative metabolites (TCA + TCOH) to NAcDCVC in urine of rats and humans exposed to 40–160 ppm (215–860 mg/m³) TCE heavily favored oxidation, resulting in ratios of 986–2,562:1 in rats and 3,292–7,163:1 in humans ([Bernauer et al., 1996](#)). [Bloemen et al. \(2001\)](#) reported that, at most, 0.05% of an inhaled TCE dose would be excreted as NAcDCVC, and concluded that this suggested that TCE metabolism by GSH conjugation was of minor importance. While it is a useful biomarker of exposure and an indicator of GSH conjugation, NAcDCVC may capture only a small fraction of TCE flux through the GSH conjugation pathway due to the dominance of bioactivating pathways ([Lash et al., 2000a](#)).

A number of lines of evidence suggest that the amount of TCE conjugation to GSH in humans, while likely smaller than the amount of oxidation, may be much more substantial than analysis of urinary mercapturates would suggest. In Table 3-28, in vitro estimates of the V_{MAX} , K_M , and clearance (V_{MAX}/K_M) for hepatic oxidation and conjugation of TCE are compared in a manner that accounts for differences in cytosolic and microsomal partitioning and protein

content. Surprisingly, the range of in vitro kinetic estimates for oxidation and conjugation of TCE substantially overlap, suggesting similar flux through each pathway, though with high interindividual variation. The microsomal and cytosolic protein measurements of GSH conjugation should be caveated by the observation by Lash et al. (1999b) that GSH conjugation of TCE was inhibited by ~50% in the presence of oxidation. Note that this comparison cannot be made in rats and mice because in vitro kinetic parameters for GSH conjugation in the liver are not available in those species (only activity at 1 or 2 mM have been measured).

Table 3-28. Comparison of hepatic in vitro oxidation and conjugation of TCE^a

Cellular or subcellular fraction	V_{MAX}^b (nmol TCE metabolized/min/g tissue)		K_M^c (μ M in blood)		V_{MAX}/K_M (mL/min/g tissue)	
	Oxidation	GSH conjugation	Oxidation	GSH conjugation	Oxidation	GSH conjugation
Hepatocytes	10.0–68.4	16~25	22.1–198	16~47	0.087–1.12	0.55~1.0
Liver microsomes	6.1–111	45	2.66–11.1*	5.9*	1.71–28.2*	7.6*
			71.0–297**	157**	0.064–1.06**	0.29**
Liver cytosol	–	380	–	4.5*	–	84*
	–		–	22.7**	–	16.7**

^aWhen biphasic metabolism was reported, only high affinity pathway is shown here.

^bConversion assumptions for V_{MAX} : hepatocellularity of 99 million cells/g liver (Barter et al., 2007); liver microsomal protein content of 32 mg protein/g tissue (Barter et al., 2007); and liver cytosolic protein content of 89 mg protein/g tissue (based on rats: Prasanna et al. (1989); van Bree et al. (1990)).

^cConversion assumptions for K_M :

For hepatocytes, K_M in headspace converted to K_M in blood using blood:air partition coefficient of 9.5 (reported range of measured values 6.5–12.1, Table 3-1);

For microsomal protein, option (*) assumes K_M in medium is equal to K_M in tissue, and converts to K_M in blood by using a liver:blood partition coefficient of 5 (reported ranges of measured values 3.6–5.9, Table 3-8), and option (**) converts K_M in medium to K_M in air using the measured microsomal protein:air partition coefficient of 1.78 (Lipscomb et al., 1997), and then converts to K_M in blood by using the blood:air partition coefficient of 9.5; and For cytosolic protein, option (*) assumes K_M in medium is equal to K_M in tissue, and converts to K_M in blood by using a liver:blood partition coefficient of 5 (reported ranges of measured values 3.6–5.9, Table 3-8), and option (**) assumes K_M in medium is equal to K_M in blood, so no conversion is necessary.

Furthermore, as shown earlier in Table 3-22, the human in vivo data of Lash et al. (1999b) show blood concentrations of DCVG similar, on a molar basis, to those of TCE, TCA, or TCOH, suggesting substantial conjugation of TCE. In addition, these data give a lower limit as to the amount of TCE conjugated. In particular, by multiplying the peak blood concentration of DCVG by the blood volume, a minimum amount of DCVG in the body at that time can be derived (i.e., assuming the minimal empirical distribution volume equal to the blood volume). As shown in Table 3-29, this lower limit amounts to about 0.4–3.7% of the inhaled TCE dose. Since this is the minimum amount of DCVG in the body at a single time point, the total amount of DCVG formed is likely to be substantially greater, owing to possible distribution outside of

the blood as well as the metabolism and/or excretion of DCVG. Lash et al. (1999b) found that levels of urinary mercapturates were near or below the level of detection of 0.19 μM , results that are consistent with those of Bloemen et al. (2001), who reported urinary concentrations below 0.04 μM at two- to fourfold lower cumulative exposures. Taken together, these results confirm the suggestion by Lash et al. (2000a) that NAcDCVC is a poor quantitative marker for the flux through the GSH pathway.

Table 3-29. Estimates of DCVG in blood relative to inhaled TCE dose in humans exposed to 50 and 100 ppm (269 and 537 mg/m^3) (Lash et al., 1999b)

Sex exposure	Estimated inhaled TCE dose (mmol) ^a	Estimated peak amount of DCVG in blood (mmol) ^b
Males		
50 ppm \times 4 hrs	3.53	0.11 \pm 0.08
100 ppm \times 4 hrs	7.07	0.26 \pm 0.08
Females		
50 ppm \times 4 hrs	2.36	0.010 \pm 0
100 ppm \times 4 hrs	4.71	0.055 \pm 0.027

^aInhaled dose estimated by (50 or 100 ppm)/(24,450 ppm/mM) \times (240 minutes) \times Q_p , where alveolar ventilation rate Q_p is 7.2 L/minute for males and 4.8 L/minute for females. Q_p is calculated as $(V_T - V_D) \times f_R$ with the following respiratory parameters: tidal volume V_T (0.75 L for males, 0.46 L for females), dead space V_D (0.15 L for males, 0.12 L for females), and respiration frequency f_R (12 minutes⁻¹ for males, 14 minutes⁻¹ for females) [assumed sitting, awake from The International Commission on Radiological Protection (ICRP, 2003)].

^bPeak amount of DCVG in blood estimated by multiplying the peak blood concentration by the estimated blood volume: 5.6 L in males and 4.1 L in females (ICRP, 2003).

Sources: Fisher et al. (1998); Lash et al. (1999b).

However, as discussed in Section 3.3.3.2.1, data from other laboratories have reported substantially lower amounts of GSH conjugation in vitro. The reasons for such discrepancies are unclear, but they may be related to different analytical methods (Lash et al., 2000a). More recent in vivo data from Kim et al. (2009) in mice reported ~1,000 times lower DCVG in mouse serum as compared to the levels of DCVG reported by Lash et al. (1999b) in human blood. These data are consistent with the suggestion that the “Reed method” employed by Lash et al. (1999b) overestimated DCVG levels in humans. However, the degree of overestimation is unclear, as is the degree to which differences may be attributable to true inter-species or inter-individual variability.

In summary, TCE oxidation is likely to be greater quantitatively than conjugation with GSH in mice, rats, and humans. Some evidence suggests that the flux through the GSH pathway, particularly in humans, may be greater by an order of magnitude or more than the <0.1% typically excreted of NAcDCVC in urine. This is evidenced both by a direct comparison of in vitro rates of oxidation and conjugation, as well as by in vivo data on the amount of DCVG in

blood. PBPK models can be used to more quantitatively synthesize these data and put more rigorous limits on the relative amounts of TCE oxidation and conjugation with GSH. Such analyses are discussed in Section 3.5. However, these data are not consistent with studies in other laboratories using different analytical methods, which report 2–5 orders of magnitude lower estimates of GSH conjugation. Because the reason for these differences have not been fully determined, substantial uncertainty remains in the degree of GSH conjugation, particularly in humans.

3.4. TCE EXCRETION

This section discusses the major routes of excretion of TCE and its metabolites in exhaled air, urine, and feces. Unmetabolized TCE is eliminated primarily via exhaled air. As discussed in Section 3.3, the majority of TCE absorbed into the body is eliminated by metabolism. With the exception of CO₂, which is eliminated solely via exhalation, most TCE metabolites have low volatility and, therefore, are excreted primarily in urine and feces. Although trace amounts of TCE metabolites have also been detected in sweat and saliva ([Bartonicek, 1962](#)), these excretion routes are likely to be relatively minor.

3.4.1. Exhaled Air

In humans, pulmonary elimination of unchanged TCE and other volatile compounds is related to ventilation rate, cardiac output, and the solubility of the compound in blood and tissue, which contribute to final exhaled air concentration of TCE. In their study of the impact of workload on TCE absorption and elimination, Astrand and Ovrum ([1976](#)) characterized the postexposure elimination of TCE in expired breath. TCE exposure (540 or 1,080 mg/m³; 100 or 200 ppm) was for a total of 2 hours, at workloads of 0–150 watts. Elimination profiles were roughly equivalent among groups, demonstrating a rapid decline in TCE concentrations in expired breath postexposure (see Table 3-30).

Table 3-30. Concentrations of TCE in expired breath from inhalation-exposed humans ([Astrand, 1982](#))

Time postexposure	Alveolar air		
	I ^a	II	III
0 min	459 ± 44	244 ± 16	651 ± 53
30 min	70 ± 5	51 ± 3	105 ± 18
60 min	40 ± 4	28 ± 2	69 ± 8
90 min	35 ± 9	21 ± 1	55 ± 2
120 min	31 ± 8	16 ± 1	45 ± 1
300 min	8 ± 1	9 ± 2	14 ± 2
420 min	5 ± 0.5	4 ± 0.5	8 ± 1.3
19 hrs	2 ± 0.3	2 ± 0.2	4 ± 0.5

^aRoman numerals refer to groups assigned different workloads; concentrations are in mg/m³ for expired air.

The lung clearance of TCE represents the volume of air from which all TCE can be removed per unit time, and is a measure of the rate of excretion via the lungs. Monster et al. (1976) reported lung clearances ranging from 3.8 to 4.9 L/minute in four adults exposed at rest to 70 and 140 ppm of TCE for 4 hours. Pulmonary ventilation rates in these individuals at rest ranged from 7.7 to 12.3 L/minute. During exercise, when ventilation rates increased to 29–30 L/minute, lung clearance was correspondingly higher, 7.7–12.3 L/minute. Under single and repeated exposure conditions, Monster et al. (1979; 1976) reported that 7–17% of absorbed TCE was excreted in exhaled breath. Pulmonary elimination of unchanged TCE at the end of exposure is a first-order diffusion process across the lungs from blood into alveolar air, and it can be thought of as the reversed equivalent of its uptake from the lungs. Exhaled pulmonary excretion occurs in several distinct (delayed) phases corresponding to release from different tissue groups, at different times. Sato et al. (1977) detected three first-order phases of pulmonary excretion in the first 10 hours after exposure to 100 ppm for 4 hours, with fitted half-times of pulmonary elimination of 0.04, 0.67, and 5.6 hours, respectively. Opdam (1989) sampled alveolar air up to 20–310 hours after 29–62-minute exposures to 6–38 ppm, and reported terminal half-lives of 8–44 hours at rest. Chiu et al. (2007) sampled alveolar air up to 100 hours after 6-hour exposures to 1 ppm and reported terminal half-lives of 14–23 hours. The long terminal half-time of TCE pulmonary excretion indicates that considerable time is necessary to completely eliminate the compound, primarily due to the high partitioning to adipose tissues (see Section 3.2).

As discussed above, several studies (Green and Prout, 1985; Prout et al., 1985; Dekant et al., 1984) have investigated the disposition of [¹⁴C]-TCE in rats and mice following gavage administrations (see Section 3.3.2). These studies have reported CO₂ as an exhalation excretion product in addition to unchanged TCE. With low doses, the amount of TCE excreted unchanged in exhaled breath is relatively low. With increasing dose in rats, a disproportionately increased amount of radiolabel is expired as unchanged TCE. This may indicate saturation of metabolic activities in rats at doses ≥200 mg/kg, which is perhaps only minimally apparent in the data from mice. In addition, exhaled air TCE concentration has been measured after constant inhalation exposure for 2 hours to 50 or 500 ppm in rats (Dallas et al., 1991), and after dermal exposure in rats and humans (Poet et al., 2000). Exhaled TCE data from rodents and humans have been integrated into the PBPK model presented in Section 3.5.

Finally, TCOH is also excreted in exhaled breath, though at a rate about 10,000-fold lower than unmetabolized TCE (Monster, 1979; Monster et al., 1976).

3.4.2. Urine

Urinary excretion after TCE exposure consists predominantly of the metabolites, TCA and TCOH, with minor contributions from other oxidative metabolites and GSH conjugates.

Measurements of unchanged TCE in urine have been at or below detection limits (e.g., [Chiu et al., 2007](#); [Fisher et al., 1998](#)). The recovery of urinary oxidative metabolites in mice, rats, and humans was addressed earlier (see Section 3.3.2) and will not be discussed here. Because of their relatively long elimination half-life, urinary oxidative metabolites have been used as an occupational biomarker of TCE exposure for many decades ([Carrieri et al., 2007](#); [Ikeda and Imamura, 1973](#)). Ikeda and Imamura ([1973](#)) measured TTCs, TCOH, and TCA in urine over 3 consecutive postexposure days for four exposure groups totaling 24 adult males and one exposure group comprising 6 adult females. The elimination half-lives for TTC were 26.1–48.8 hours in males and 50.7 hours in females. The elimination half-lives for TCOH were 15.3 hours in the only group of males studied and 42.7 hours in females. The elimination half-lives for TCA were 39.7 hours in the only group of males studied and 57.6 hours in females. These authors compared their results to previously published elimination half-lives for TTC, TCOH, and TCA. Following experimental exposures of groups of two–five adults, elimination half-lives were 31–50 hours for TTC, 19–29 hours for TCOH, and 36–55 hours for TCA ([Nomiyama and Nomiyama, 1971](#); [Ogata et al., 1971](#); [Stewart et al., 1970](#); [Bartonicek, 1962](#)). The urinary elimination half-lives of TCE metabolites in a subject who worked with and was addicted to sniffing TCE for 6–8 years approximated 49.7 hours for TCOH, 72.6 hours for TCA, and 72.6 hours for TTC ([Ikeda et al., 1971](#)).

The quantitative relationship between urinary concentrations of oxidative metabolites and exposure in an occupational setting was investigated by Ikeda ([1977](#)). This study examined the urinary elimination of TCE and metabolites in urine of 51 workers from 10 workshops. The concentration of TCA and TCOH in urine demonstrated a marked concentration-dependence, with concentrations of TCOH being approximately twice as high as those for TCA. Urinary half-life values were calculated for six males and six females from five workshops; males were intermittently exposed to 200 ppm and females were intermittently exposed to 50 ppm (269 mg/m³). Urinary elimination half-lives for TTC, TCOH, and TCA were 26.1, 15.3, and 39.7 hours in males, respectively, and 50.7, 42.7 and 57.6 hours in females, respectively, which were similar to the range of values previously reported. These authors estimated that urinary elimination of parent TCE during exposure might account for one-third of the systemically absorbed dose. Importantly, urinary TCA exhibited marked saturation at exposures >50 ppm. Because neither TTC nor urinary TCOH (in the form of the glucuronide TCOG) showed such an effect, this saturation cannot be due to TCE oxidation itself, but must rather be from one of the metabolic processes forming TCA from TCOH. Unfortunately, since biological monitoring programs usually measure only urinary TCA, rather than TTC, urinary TCA levels above around 150 mg/L cannot distinguish between exposures at 50 ppm and at much higher concentrations.

It is interesting to attempt to extrapolate on a cumulative exposure basis the Ikeda ([1977](#)) results for urinary metabolites obtained after occupational exposures at 50 ppm to the controlled exposure study by Chiu et al. ([2007](#)) at 1.2 ppm for 6 hours (the only controlled exposure study

for which urinary concentrations, rather than only cumulative excretion, are available). Ikeda (1977) reported that measurements were made during the second half of the week, so one can postulate a cumulative exposure duration of 20~40 hours. At 50 ppm, Ikeda (1977) report a urinary TCOH concentration of about 290 mg/L, so that per ppm-hour, the expected urinary concentration would be $290/(50 \times 20 \sim 40) = 0.145 \sim 0.29$ mg/L-ppm-hour. The cumulative exposure in Chiu et al. (2007) is $1.2 \times 6 = 7.2$ ppm-hour, so the expected urinary TCOH concentration would be $7.2 \times (0.145 \sim 0.29) = 1.0 \sim 2.1$ mg/L. This estimate is somewhat surprisingly consistent with the actual measurements of Chiu et al. (2007) during the first day postexposure, which ranged from 0.8 to ~1.2 mg/L TCOH in urine.

On the other hand, extrapolation of TCA concentrations was less consistent. At 50 ppm, Ikeda (1977) report a urinary TCA concentration of about 140 mg/L, so that per ppm-hour, the expected urinary concentration would be $140/(50 \times 20 \sim 40) = 0.07 \sim 0.14$ mg/L-ppm-hour. The cumulative exposure in Chiu et al. (2007) is $1.2 \times 6 = 7.2$ ppm-hour, so the expected urinary TCA concentration would be $7.2 \times (0.07 \sim 0.14) = 0.5 \sim 1.0$ mg/L, whereas Chiu et al. (2007) reported urinary TCA concentrations on the first day after exposure of 0.03~0.12 mg/L. However, as noted in Chiu et al. (2007), relative urinary excretion of TCA was 3–10-fold lower in Chiu et al. (2007) than other studies at exposures of 50~140 ppm, which may explain part of the discrepancies. However, this may be due, in part, to saturation of many urinary TCA measurements, and, furthermore, interindividual variance, observed to be substantial in Fisher et al. (1998), cannot be ruled out.

Urinary elimination kinetics have been reported to be much faster in rodents than in humans. For instance, adult rats were exposed to 50, 100, or 250 ppm (269, 537, or 1,344 mg/m³) via inhalation for 8 hours or were administered an i.p. injection (1.47 g/kg) and the urinary elimination of TTCs was followed for several days (Ikeda and Imamura, 1973). These authors calculated urinary elimination half-lives of 14.3–15.6 hours for female rats and 15.5–16.6 hours for male rats; the route of administration did not appear to influence half-life value. In other rodent experiments using orally administered radiolabeled TCE, urinary elimination was complete within 1 or 2 days after exposure (Green and Prout, 1985; Prout et al., 1985; Dekant et al., 1984).

3.4.3. Feces

Fecal elimination accounts for a small percentage of TCE as shown by limited information in the available literature. Bartonicek (1962) exposed seven volunteers to 1.042 mg TCE/L air for 5 hours and examined TCOH and TCA in feces on the 3rd and 7th day following exposure. The mean amount of TCE retained during exposure was 1,107 mg, representing 51–64% (mean 58%) of administered dose. On the 3rd day following TCE exposure, TCOH and TCA in feces demonstrated mean concentrations of 17.1 and 18.5 mg/100 g feces, similar to concentrations in urine. However, because of the 10-fold smaller daily rate of excretion of feces

relative to urine, this indicates fecal excretion of these metabolites is much less significant than urinary excretion. Neither TCOH nor TCA was detected in feces on the 7th day following exposure.

In rats and mice, total radioactivity has been used to measure excretion in feces after gavage TCE administration in corn oil, but since the radiolabel was not characterized, it is not possible to determine whether the radiolabel in feces represented unabsorbed parent compound, excreted parent compound, and/or excreted metabolites. Dekant et al. (1984) reported that mice eliminated 5% of the total administered TCE, while rats eliminated 2% after gavage. Dekant et al. (1986b) reported a dose-response-related increase in fecal elimination with dose, ranging between 0.8 and 1.9% in rats and between 1.6 and 5% in mice after gavage in corn oil. Due to the relevant role of CYP2E1 in the metabolism of TCE (see Section 3.3.3.1.6), Kim and Ghanayem (2006) compared fecal elimination in both wild-type and CYP2E1 knockout mice and reported fecal elimination ranging between 4.1 and 5.2% in wild-type and between 2.1 and 3.8% in knockout mice exposed by gavage in aqueous solution.

3.5. PBPK MODELING OF TCE AND ITS METABOLITES

3.5.1. Introduction

PBPK models are extremely useful tools for quantifying the relationship between external measures of exposure and internal measures of toxicologically relevant dose. In particular, for the purposes of this assessment, PBPK models are evaluated for the following: (1) providing additional quantitative insights into the ADME of TCE and metabolites described in the sections above; (2) cross-species pharmacokinetic extrapolation of rodent studies of both cancer and noncancer effects; (3) exposure-route extrapolation; and (4) characterization of human pharmacokinetic variability. The following sections first describe and evaluate previous and current TCE PBPK modeling efforts, then discuss the insights into ADME (1, above), and finally present conclusions as to the utility of the model to predict internal doses for use in dose-response assessment (2–4, above).

3.5.2. Previous PBPK Modeling of TCE for Risk Assessment Application

TCE has an extensive number of both in vivo pharmacokinetic and PBPK modeling studies [see Chiu et al. (2006b) supplementary material, for a review]. Models previously developed for occupational or industrial hygiene applications are not discussed here but are reviewed briefly in Clewell et al. (2000). Models designed for risk assessment applications have focused on descriptions of TCE and its major oxidative metabolites, TCA, TCOH, and TCOG. Most of these models were extensions of the “first generation” of models developed by Fisher and coworkers (Allen and Fisher, 1993; Fisher et al., 1991) in rats, mice, and humans. These models, in turn, are based on a Ramsey and Andersen (1984) structure with flow-limited tissue compartments and equilibrium gas exchange, saturable Michaelis-Menten kinetics for oxidative

metabolism, and lumped volumes for the major circulating oxidative metabolites TCA and TCOH. Fisher and coworkers updated their models with new in vivo and in vitro experiments performed in mice ([Greenberg et al., 1999](#); [Abbas and Fisher, 1997](#)) and volunteers ([Fisher et al., 1998](#)) and summarized their findings in Fisher ([2000](#)). Clewell et al. ([2000](#)) added enterohepatic recirculation of TCOG and pathways for local oxidative metabolism in the lung and GST metabolism in the liver. While Clewell et al. ([2000](#)) does not include the updated Fisher ([2000](#)) data, they have used a wider set of in vivo and in vitro mouse, rat, and human data than previous models. Finally, Bois ([2000a, b](#)) performed reestimations of PBPK model parameters for the Fisher and Clewell models using a Bayesian population approach [Gelman ([1996](#)), and discussed further below].

As discussed in Rhomberg ([2000](#)), the choice as to whether to use the Fisher, Clewell, and/or Bois models for cross-species extrapolation of rodent cancer bioassays led to quantitative results that differed by as much as an order of magnitude. There are a number of differences in modeling approaches that can explain their differing results. First, the Clewell et al. ([2000](#)) model differed structurally in its use of single-compartment volume-of-distribution models for metabolites as opposed to the Fisher ([Fisher, 2000](#)) models, which use multiple physiologic compartments. Also, the Clewell et al. ([2000](#)) model, but not the Fisher models, includes enterohepatic recirculation of TCOH/TCOG (although reabsorption was set to zero in some cases). In addition to structural differences in the models, the input parameter values for these various models were calibrated using different subsets of the overall in vivo database [see Chiu et al. ([2006b](#)), supplementary material, for a review]. The Clewell et al. ([2000](#)) model is based primarily on a variety of data published before 1995; the Fisher ([2000](#)) models were based primarily on new studies conducted by Fisher and coworkers (after 1997); and the Bois ([2000a, b](#)) reestimations of the parameters for the Clewell et al. ([2000](#)) and Fisher ([2000](#)) models used slightly different data sets than the original authors. The Bois ([2000a, b](#)) reanalyses also led to somewhat different parameter estimates than the original authors, both because of the different data sets used as well as because the methodology used by Bois allowed many more parameters to be estimated simultaneously than were estimated in the original analyses.

Given all of these methodological differences, it is not altogether surprising that the different models led to different quantitative results. Even among the Fisher models themselves, Fisher ([2000](#)) noted some inconsistencies, including differing estimates for metabolic parameters between mouse gavage and inhalation experiments. These authors included possible explanations for these inconsistencies: the impact of corn oil vehicle use during gavage ([Staats et al., 1991](#)) and the impact of a decrease in ventilation rate in mice due to sensory irritation during the inhalation of solvents [e.g., Stadler and Kennedy ([1996](#))].

As discussed in a report by the National Research Council ([NRC, 2006](#)), several additional PBPK models relevant to TCE pharmacokinetics have been published since 2000 and are reviewed briefly here. Poet et al. ([2000](#)) incorporated dermal exposure to TCE in PBPK

models in rats and humans, and published in vivo data in both species from dermal exposure ([Poet et al., 2000](#); [Thrall and Poet, 2000](#)). Albanese et al. ([2002](#)) published a series of models with more complex descriptions of TCE distribution in adipose tissue but did not show comparisons with experimental data. Simmons et al. ([2002](#)) developed a PBPK model for TCE in the Long-Evans rat that focused on neurotoxicity endpoints and compared model predictions with experimentally determined TCE concentrations in several tissues, including the brain. Keys et al. ([2003](#)) investigated the lumping and unlumping of various tissue compartments in a series of PBPK models in the rat and compared model predictions with TCE tissue concentrations in a multitude of tissues. Although none of these TCE models included metabolite descriptions, the experimental data were available for either model or evaluation. Finally, Keys et al. ([2004](#)) developed a model for DCA in the mouse that included a description of suicide inhibition of GST-zeta, but this model was not been linked to TCE.

3.5.3. Development and Evaluation of an Interim “Harmonized” TCE PBPK Model

Throughout 2004, EPA and the U.S. Air Force jointly sponsored an integration of the Fisher, Clewell, and Bois modeling efforts ([Hack et al., 2006](#)). In brief, a single interim PBPK model structure combining features from both the Fisher and Clewell models was developed and used for all three species of interest (mice, rats, and humans). An effort was made to combine structures in as simple a manner as possible; the evaluation of most alternative structures was left for future work. The one level of increased complexity introduced was inclusion of species- and dose-dependent TCA plasma binding, although only a single in vitro study of Lumpkin et al. ([2003](#)) was used as parameter inputs. As part of this joint effort, a hierarchical Bayesian population analysis using Markov chain Monte Carlo (MCMC) sampling [similar to the Bois ([2000a, b](#)) analyses] was performed on the revised model with a cross-section of the combined database of kinetic data to provide estimates of parameter uncertainty and variability ([Hack et al., 2006](#)). Particular attention was given to using data from each of the different efforts, but owing to time and resource constraints, a combined analysis of all data was not performed. The results from this effort suggested that a single model structure could provide reasonable fits to a variety of data evaluated for TCE and its major oxidative metabolites TCA, TCOH, and TCOG. However, in many cases, different parameter values—particularly for metabolism—were required for different studies, indicating significant interindividual or interexperimental variability. In addition, these authors concluded that dosimetry of DCA, conjugative metabolites, and metabolism in the lung remained highly uncertain ([Hack et al., 2006](#)).

Subsequently, EPA conducted a detailed evaluation of the Hack et al. ([2006](#)) model that included: (1) additional model runs to improve convergence; (2) evaluation of posterior distributions for population parameters; and (3) comparison of model predictions both with the data used in the Hack et al. ([2006](#)) analysis as well as with additional data sets identified in the

literature. Appendix A provides the details and conclusions of this evaluation, briefly summarized in Table 3-31, along with their pharmacokinetic implications.

3.5.4. PBPK Model for TCE and Metabolites Used for This Assessment

3.5.4.1. Introduction

Based on the recommendations of the NRC (2006) as well as additional analysis and evaluation of the Hack et al. (2006) PBPK model, an updated PBPK model for TCE and metabolites was developed for use in this risk assessment. The updated model is reported in Evans et al. (2009) and Chiu et al. (2009), and the discussion below provides some details in addition to the information in the published articles.

This updated model included modification of some aspects of the Hack et al. (2006) PBPK model structure, incorporation of additional in vitro and in vivo data for estimating model parameters, and an updated hierarchical Bayesian population analysis of PBPK model uncertainty and variability. In the subsections below, the updated PBPK model and baseline parameter values are described, as well as the approach and results of the analysis of PBPK model uncertainty and variability. Appendix A provides more detailed descriptions of the model and parameters, including background on hierarchical Bayesian analyses, model equations, statistical distributions for parameter uncertainty and variability, data sources for these parameter values, and the PBPK model code. Additional computer codes containing input files to the MCSim program are available electronically.

Table 3-31. Conclusions from evaluation of Hack et al. (2006), and implications for PBPK model development

Conclusion from evaluation of Hack et al. (2006) model	Implications for PBPK model parameters, structure, or data
<p>For some model parameters, posterior distributions were somewhat inconsistent with the prior distributions.</p> <ul style="list-style-type: none"> • For parameters with strongly informative priors (e.g., tissue volumes and flows), this may indicate errors in the model. • For many parameters, the prior distributions were based on visual fits to the same data. If the posteriors are inconsistent, then the priors were “inappropriately” informative, and, thus, the same data were used twice. 	<p>Reevaluation of all prior distributions.</p> <ul style="list-style-type: none"> • Update priors for parameters with independent data (physiological parameters, partition coefficients, in vitro metabolism), looking across all available data sets. • For priors without independent data (e.g., many metabolism parameters), use less informative priors (e.g., log-uniform distributions with wide bounds) to prevent bias. <p>Evaluate modifications to the model structure, as discussed below.</p>
<p>A number of data sets involve TCE (i.a., portal vein), TCA (oral, i.v.), and TCOH (oral, i.v.) dosing routes that are not currently in the model, but could be useful for calibration.</p>	<ul style="list-style-type: none"> • Additional dosing routes can be added easily.
<p>TCE concentrations in blood, air, and tissues well-predicted only in rats, not in mice and humans. Specifically:</p> <ul style="list-style-type: none"> • In mice, the oral uptake model could not account for the time-course of several data sets. Blood TCE concentrations after inhalation were consistently overpredicted. • In rats, tissue concentrations measured in data not used for calibration were accurately predicted. • In humans, blood and air TCE concentrations were consistently overpredicted in the majority of (but not all) data sets. 	<ul style="list-style-type: none"> • In mice, uptake from the stomach compartment (currently zero), but previously included in Abbas and Fisher (1997), may improve the model fit. • In mice and humans, additional extrahepatic metabolism, either presystemic (e.g., in the lung) or postsystemic (e.g., in the kidney) and/or a wash-in/wash-out effect may improve the model fit.
<p>Total metabolism appears well-predicted in rats and mice based on closed-chamber data, but required significantly different V_{MAX} values between dose groups. Total recovery in humans (60–70%) is less than the model would predict. In all three species, the ultimate disposition of metabolism is uncertain. In particular, there are uncertainties in attributing the “missing” metabolism to</p> <ul style="list-style-type: none"> • GSH pathway (e.g., urinary mercapturates may only capture a fraction of the total flux; moreover, in Bernauer et al. (1996), excretion was still on-going at end of collection period; model does not accurately depict time-course of mercapturate excretion). • Other hepatic oxidation (currently attributed to DCA). • Extrahepatic systemic metabolism (e.g., kidney). • Presystemic metabolism in the lung. • Additional metabolism of TCOH or TCA (see below). 	<ul style="list-style-type: none"> • Calibration of GSH pathway may be improved by utilizing in vitro data on liver and kidney GSH metabolism, adding a DCVG compartment to improve the prediction of the time-course for mercapturate excretion, and/or using the Lash et al. (1999b) blood DCVG in humans (necessitating the addition of a DCVG compartment). • Presystemic lung metabolism can only be evaluated if added to the model (in vitro data exist to estimate the V_{MAX} for such metabolism). In addition, a wash-in/wash-out effect (e.g., suggested by Greenberg et al., (1999) can be evaluated using a continuous breathing model that separately tracks inhaled and exhaled air, with adsorption/desorption in the respiratory tract. • Additional elimination pathways for TCOH and TCA can be added for evaluation.

Table 3-31. Conclusions from evaluation of Hack et al. (2006), and implications for PBPK model development (continued)

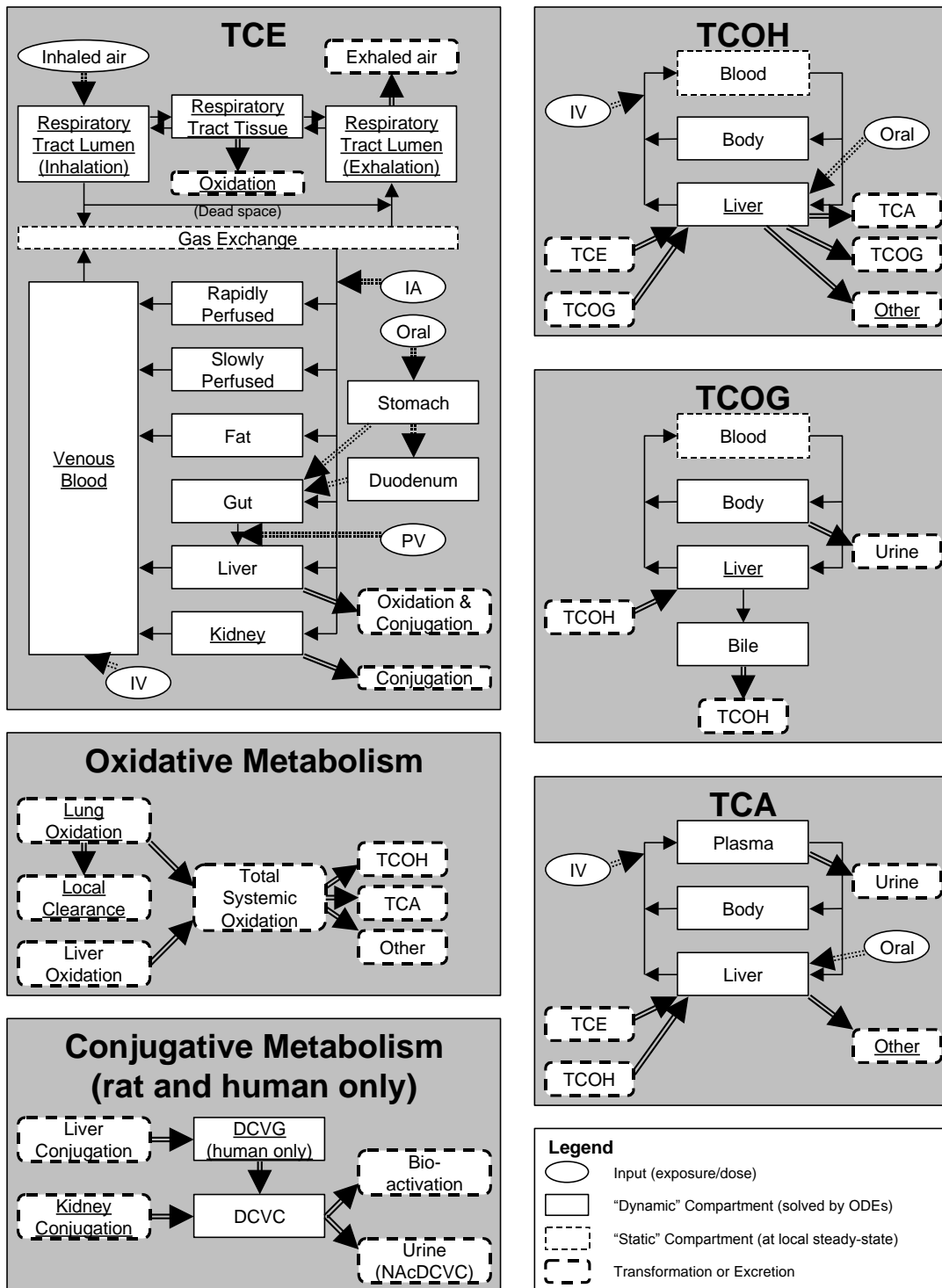
Conclusion from evaluation of Hack et al. (2006) model	Implications for PBPK model parameters, structure, or data
<p>TCA blood/plasma concentrations were well-predicted following TCE exposures in all species. However, there may be inaccuracies in the total flux of TCA production, as well as its disposition.</p> <ul style="list-style-type: none"> • In TCA dosing studies, the majority (>50%), but substantially <100%, was recovered in urine, suggesting significant metabolism of TCA. Although urinary TCA was well-predicted in mice and humans (but not in rats), if TCA metabolism is significant, then the current model underestimates the flux of TCE metabolism to TCA. • An improved TCOH/TCOG model may also provide better estimates of TCA kinetics (see below). <p>TCOH/TCOG concentrations and excretion were inconsistently predicted, particularly after TCOH dosing.</p> <ul style="list-style-type: none"> • In mice and rats, first-order clearance for TCOH glucuronidation was predicted to be greater than hepatic blood flow, which is consistent with a first-pass effect that is not currently accounted for. • In humans, the estimated clearance rate for TCOH glucuronidation was substantially smaller than hepatic blood flow. However, the presence of substantial TCOG in blood (as opposed to free TCOH) in the Chiu et al. (2007) data are consistent with greater glucuronidation than predicted by the model. • In TCOH dosing studies, substantially <100% was recovered in urine as TCOG and TCA, suggesting another metabolism or elimination pathway. 	<ul style="list-style-type: none"> • Additional elimination pathways for TCOH and TCA can be added for evaluation. • The addition of a liver compartment for TCOH and TCOG would permit hepatic first-pass effects to be accounted for, as appears necessary for mice and rats.

i.v. = intravenous

3.5.4.2. Updated PBPK Model Structure

The updated TCE PBPK model is illustrated in Figure 3-7, with detailed descriptions of the model structure, equations, and parameters found in Appendix A (see Section A.4), and the major changes from the Hack et al. (2006) model described here. The TCE submodel was augmented by the addition of kidney and venous blood compartments, and an updated respiratory tract model that included both metabolism and the possibility of local storage in the respiratory tissue. In particular, in the updated lung, separate processes describing inhalation and exhalation allowed for adsorption and desorption from tracheobronchial epithelium (wash-in/wash-out), with the possibility of local metabolism as well. In addition, conjugative metabolism in the kidney was added, motivated by the in vitro data on TCE conjugation described in Sections 3.3.3.2–3.3.3.3. With respect to oxidation, a portion of the lung metabolism was assumed to produce systemically available oxidative metabolites, including TCOH and TCA, with the remaining fraction assumed to be locally cleared. This is clearly a lumping of a multistep process, but the lack of data precludes the development of a more sequential model. TCE oxidation in the kidney was not included because it was not likely to constitute a substantial flux of total TCE oxidation given the much lower CYP activity in the kidney relative to the liver (Cummings and Lash, 2000; Cummings et al., 1999) and the greater tissue mass of the liver.² In addition, liver compartments were added to the TCOH and TCOG submodels to account properly for first-pass hepatic metabolism, which is important for consistency across routes of exposure. Furthermore, additional clearance pathways of TCOH and TCA were added to their respective submodels. With respect to TCE conjugation, in humans, an additional DCVG compartment was added between TCE conjugation and production of DCVC. In addition, it should be noted that the urinary clearance of DCVC represents a lumping of *N*-acetylation of DCVC, deacetylation of NAcDCVC, and urinary excretion NAcDCVC, and that the bioactivation of DCVC represents a lumping of thiol production from DCVC by beta-lyase, sulfoxidation of DCVC by FMO3, and sulfoxidation of NAcDCVC by CYP3A. Such lumping was used because these processes are not individually identifiable given the available data.

²The extraction ratio for kidney oxidation is likely to be very low, as shown by the following calculation in rats and humans. In rats, the in vitro kidney oxidative clearance (V_{MAX}/K_M) rate (see Table 3-13, converting units) is 1.64×10^{-7} L/minutes/mg microsomal protein. Converting units using 16 mg microsomal protein to g tissue (Bong et al., 1985) gives a clearance rate per unit tissue mass of 2.6×10^{-6} L/minutes/g kidney. This is more than 1,000-fold smaller than the kidney specific blood flow rate of 6.3×10^{-3} L/minutes/g kidney (Brown et al., 1997). In humans, an in vitro clearance rate of 6.5×10^{-8} L/minutes/mg microsomal protein is derived from the only detectable in vitro oxidation rate from Cummings and Lash (2000) of 0.13 nmol/minutes/mg protein at 2 mM. Using the same conversion from microsomal protein to tissue mass gives a clearance rate of 1.0×10^{-6} L/minutes/g kidney, more than 1,000-fold smaller than the kidney specific blood flow of 3.25×10^{-3} L/minutes/g kidney (Brown et al., 1997). No data on kidney metabolism are available in mice, but the results are likely to be similar. Therefore, even accounting for uncertainties of up to an order of magnitude in the in-vitro-to-in-vivo conversion, kidney oxidation should contribute negligibly to total metabolism of TCE.



Boxes with underlined labels are additions or modifications of the Hack et al. (2006) model, which are discussed in Table 3-32.

Figure 3-7. Overall structure of PBPK model for TCE and metabolites used in this assessment.

Table 3-32. Discussion of changes to the Hack et al. (2006) PBPK model implemented for this assessment

Change to Hack et al. (2006) PBPK model	Discussion
TCE respiratory tract compartments and metabolism	In vitro data indicate that the lung (at least in the mouse) has a significant capacity for oxidizing TCE. However, in the Hack et al. (2006) model, respiratory metabolism was blood flow-limited. The model structure used was inconsistent with other PBPK models in which the same mechanism for respiratory metabolism is assumed (e.g., styrene, Sarangapani et al. (2003)). In these models, the main source of exposure in the respiratory tract tissue is from the respiratory lumen—not from the tracheobronchial blood flow. In addition, a wash-in/wash-out effect has also been postulated. The current structure, which invokes a “continuous breathing” model with separate “inhaled” and “exhaled” respiratory lumens, can accommodate both respiratory metabolism due to exposure from the respiratory lumen as well as a wash-in/wash-out effect in which there is temporary storage in the respiratory tract tissue. Moreover, preliminary analyses indicated that these changes to the model structure allowed for a substantially better fit to mouse closed-chamber data under the requirement that all of the dose levels are modeled using the same set of parameters.
TCE kidney compartment	In vitro data indicate that the kidney has a significant capacity for conjugating TCE with GSH.
TCE venous blood compartment	Many PBPK models have used a separate blood compartment. It was believed to be potentially important and feasible to implement here because: (1) TCE blood concentrations were often not well-predicted by the Hack et al. (2006) model; (2) the TCA submodel has a plasma compartment, which is a fraction of the blood volume based on the blood volume; (3) adequate independent information on blood volume is available; and (4) the updated model was to include the i.v. route of exposure.
TCOH and TCOG liver compartments	In mice and rats, the Hack et al. (2006) model estimated a rate of TCOH glucuronidation that exceeded hepatic blood flow (all glucuronidation is assumed to occur in the liver), which indicated a significant first-pass effect. Therefore, a separate liver compartment is necessary to account properly for hepatic first-pass.
TCOH and TCA “other” elimination pathways	Mass-balance studies with TCOH and TCA dosing indicated that, although the majority of TCOH and TCA are excreted in urine, the amount is still substantially <100%. Therefore, additional elimination of TCOH and TCA must exist and should be accounted for.
DCVG compartment (human model only)	Blood DCVG data in humans exist as part of the Fisher et al. (1998) experiments, reported in Lash et al. (1999b), and a DCVG compartment is necessary in order to utilize those data.

3.5.4.3. Specification of Baseline PBPK Model Parameter

Point estimates for PBPK model parameters (“baseline values”), used as central estimates in the prior distributions for population mean parameters in the hierarchical Bayesian statistical model (see Appendix A), were developed using standard methodologies to ensure biological plausibility, and were a refinement of those used in Hack et al. (2006). Because the Bayesian parameter estimation methodology utilizes the majority of the useable in vivo data on TCE pharmacokinetics, all baseline parameter estimates were based solely on measurements independent of the in vivo data. This avoids using the same data in both the prior and the likelihood. These parameters were, in turn, given truncated normal or lognormal distributions for the uncertainty in the population mean. If no independent data were available, as is the case for many “downstream” metabolism parameters, then no baseline value was specified, and a

noninformative prior was used. Section 3.5.5.4, below, discusses the updating of these noninformative priors using interspecies scaling.

In keeping with standard practice, many of the PBPK model parameters were “scaled” by body or organ weights, cardiac output, or allometrically by an assumed (fixed) power of body weight. Metabolic capacity and cardiac output were scaled by the $3/4$ power of body weight and rate coefficients were scaled by the $-1/4$ power of body weight, in keeping with general expectations as to the relationship between metabolic rates and body size ([West et al., 2002](#); [U.S. EPA, 1992](#)). So as to ensure a consistent model structure across species as well as improve the performance of the MCMC algorithm, parameters were further scaled to the baseline point-estimates where available, as was done by Hack et al. ([2006](#)). For example, to obtain the actual liver volume (VLivC) in L, a point estimate is first obtained by multiplying the fixed, species-specific baseline point estimate for the fractional liver volume by a fixed body weight (measured or species-specific default) with density of 1 kg/L assumed to convert from kg to L. Then, any deviation from this point estimate is represented by multiplying by a separate “scaled” parameter VLivC that has a value of 1 if there is no deviation from the point estimate. These “scaled” parameters are those estimated by the MCMC algorithm, and for which population means and variances are estimated.

Baseline physiological parameters were reestimated based on the updated tissue lumping (e.g., separate blood and kidney compartments) using the standard references, International Commission on Radiological Protection ([ICRP, 2003](#)) and Brown et al. ([1997](#)). For a few of these parameters, such as hematocrit and respiratory tract volumes in rodents, additional published sources were used as available, but no attempt was made to compile a comprehensive review of available measurements. In addition, a few parameters, such as the slowly perfused volume, were calculated rather than sampled in order to preserve total mass or flow balances.

For chemical-specific distribution and metabolism parameters, in vitro data from various sources were used. Where multiple measurements had been made, as was the case for many partition coefficients, TCA plasma protein binding parameters, and TCE metabolism, different results were pooled together, with their uncertainty reflected appropriately in the prior distribution. Such in vitro measurements were available for most chemical partition coefficients, except for those for TCOG (TCOH used as a proxy) and DCVG. There were also such data to develop baseline values for the oxidative metabolism of TCE in the liver (V_{MAX} and K_M), the relative split in TCE oxidation between formation of TCA and TCOH, and the V_{MAX} for TCE oxidation in the lung. For GSH conjugation, the geometric means of the in vitro data from Lash et al. ([1999a](#)) and Green et al. ([1997a](#)) were used as central estimates, with a wide enough uncertainty range to encompass both (widely disparate) estimates. Thus, the prior distribution for these parameters was only mildly informative, and the results are primarily determined by the available in vivo data. All other metabolism parameters were not given baseline values and needed to be estimated from the in vivo data.

3.5.4.4. Dose-Metric Predictions

The purpose of this PBPK model is to make predictions of internal dose in rodents used in toxicity studies or in humans in the general population, and not in the groups or individuals for which pharmacokinetic data exist. Therefore, to evaluate its predictive utility for risk assessment, a number of dose-metrics were selected for simulation in a “generic” mouse, rat, or human, summarized in Table 3-33. The parent dose-metric was AUC in blood. TCE metabolism dose-metrics (i.e., related to the amount metabolized) included both total metabolism, metabolism splits between oxidation vs. conjugation, oxidation in the liver vs. the lung, the amount of oxidation in the liver to products *other* than TCOH and TCA, and the amount of TCA produced. These metabolism rate dose-metrics are scaled by body weight in the case of TCA produced, by the metabolizing tissue volume and by body weight to the $\frac{3}{4}$ power in the cases of the lung and “other” oxidation in the liver, and by body weight to the $\frac{3}{4}$ power only in other cases. With respect to the oxidative metabolites, liver concentrations of TCA and blood concentrations of free TCOH were used. With respect to conjugative metabolites, the dose-metrics considered were total GSH metabolism scaled by body weight to the $\frac{3}{4}$ power, and the amount of DCVC bioactivated (rather than excreted in urine) per unit body weight to the $\frac{3}{4}$ power and per unit kidney mass.

Table 3-33. PBPK model-based dose-metrics

Abbreviation	Description
ABioactDCVCBW34	Amount of DCVC bioactivated in the kidney (mg) per unit body weight ^{3/4} (kg ^{3/4})
ABioactDCVCKid	Amount of DCVC bioactivated in the kidney (mg) per unit kidney mass (kg)
AMetGSHBW34	Amount of TCE conjugated with GSH (mg) per unit body weight ^{3/4} (kg ^{3/4})
AMetLiv1BW34	Amount of TCE oxidized in the liver per unit body weight ^{3/4} (kg ^{3/4})
AMetLivOtherBW34	Amount of TCE oxidized to metabolites other than TCA and TCOH in the liver (mg) per unit body weight ^{3/4} (kg ^{3/4})
AMetLivOtherLiv	Amount of TCE oxidized to metabolites other than TCA and TCOH in the liver (mg) per unit liver mass (kg)
AMetLngBW34	Amount of TCE oxidized in the respiratory tract (mg) per unit body weight ^{3/4} (kg ^{3/4})
AMetLngResp	Amount of TCE oxidized in the respiratory tract (mg) per unit respiratory tract tissue mass (kg)
AUCCBld	Area under the curve of the venous blood concentration of TCE (mg-hr/L)
AUCCTCOH	Area under the curve of the blood concentration of TCOH (mg-hr/L)
AUCLivTCA	Area under the curve of the liver concentration of TCA (mg-hr/L)
TotMetabBW34	Total amount of TCE metabolized (mg) per unit body weight ^{3/4} (kg ^{3/4})
TotOxMetabBW34	Total amount of TCE oxidized (mg) per unit body weight ^{3/4} (kg ^{3/4})
TotTCAInBW	Total amount of TCA produced (mg) per unit body weight (kg)

All dose-metrics are converted to daily or weekly averages based on simulations lasting 10 weeks for rats and mice and 100 weeks for humans. These simulation times were the shortest

for which additional simulation length did not add substantially to the average (i.e., less than a few percent change with a doubling of simulation time).

3.5.5. Bayesian Estimation of PBPK Model Parameters, and Their Uncertainty and Variability

3.5.5.1. Updated Pharmacokinetic Database

An extensive search was made for data not previously considered in the PBPK modeling of TCE and metabolites, with a few studies identified or published subsequent to the review by Chiu et al. (2006b). The studies considered for analysis are listed in Tables 3-34 and 3-35, along with an indication of whether and how they were used.³

The least amount of data was available for mice, so an effort was made to include as many studies as feasible for use in calibrating the PBPK model parameters. Exceptions include mouse studies with CH or DCA dosing, since those metabolites are not included in the PBPK model. In addition, the Birner et al. (1993) data only reported urine concentrations, not the amount excreted in urine. Because there is uncertainty as to total volume of urine excreted, and over what time period, these data were not used. Moreover, many other studies had urinary excretion data, so this exclusion should have minimal impact. Several data sets not included by Hack et al. (2006) were used here. Of particular importance was the inclusion of TCA and TCOH dosing data from Abbas et al. (1997), Green and Prout (1985), Larson and Bull (1992a), and Templin et al. (1993). A substantial amount of data is available in rats, so some data that appeared to be redundant were excluded from the calibration set and saved for comparison with posterior predictions (a “validation” set). In particular, those used for “validation” are one closed-chamber experiment (Andersen et al., 1987b), several data sets with only TCE blood data (Lee et al., 1996; Jakobson et al., 1986; D'Souza et al., 1985), and selected time courses from Fisher et al. (1991) and Lee et al. (2000a; 2000b), and one unpublished data set (Bruckner et al., unpublished). The Andersen et al. (1987b) data were selected randomly from the available closed-chamber data, while the other data sets were selected because they were unpublished or because they were more limited in scope (e.g., TCE blood only) and so were not as efficient for use in the computationally-intensive calibration stage. As with the mouse analyses, TCA and TCOH dosing data were incorporated to better calibrate those pathways.

³Additional in vivo data on TCE or metabolites published after the PBPK modeling was completed (Kim et al., 2009; Liu et al., 2009; Sweeney et al., 2009) were evaluated separately, and discussed in Appendix A.

Table 3-34. Rodent studies with pharmacokinetic data considered for analysis

Reference	Species (strain)	Sex	TCE exposures	Other exposures	Calibration	Validation	Not used	Comments
Mouse studies								
Abbas et al. (1996)	Mouse (B6C3F ₁)	M	–	CH i.v.			√	CH not in model.
Abbas and Fisher (1997)	Mouse (B6C3F ₁)	M	Oral (corn oil)	–	√ ^a			
Abbas et al. (1997)	Mouse (B6C3F ₁)	M	–	TCOH, TCA i.v.	√			
Barton et al. (1999)	Mouse (B6C3F ₁)	M	–	DCA i.v. and oral (aqueous)			√	DCA not in model.
Birner et al. (1993)	Mouse (NMRI)	M+F	Gavage	–			√	Only urine concentrations available, not amount.
Fisher and Allen, (1993)	Mouse (B6C3F ₁)	M+F	Gavage (corn oil)	–	√			
Fisher et al. (1991)	Mouse (B6C3F ₁)	M+F	Inhalation	–	√ ^a			
Green and Prout (1985)	Mouse (B6C3F ₁)	M	Gavage (corn oil)	TCA i.v.	√			
Greenberg et al. (1999)	Mouse (B6C3F ₁)	M	Inhalation	–	√ ^a			
Larson and Bull (1992b)	Mouse (B6C3F ₁)	M	–	DCA, TCA oral (aqueous)	√			Only data on TCA dosing was used, since DCA is not in the model.
Larson and Bull (1992a)	Mouse (B6C3F ₁)	M	Oral (aqueous)	–	√			
Merdink et al. (1998)	Mouse (B6C3F ₁)	M	i.v.	CH i.v.	√			Only data on TCE dosing was used, since CH is not in the model.

Table 3-34. Rodent studies with pharmacokinetic data considered for analysis (continued)

Reference	Species (strain)	Sex	TCE exposures	Other exposures	Calibration	Validation	Not used	Comments
Prout et al. (1985)	Mouse (B6C3F ₁ , Swiss)	M	Gavage (corn oil)	–	√ ^a			
Templin et al. (1993)	Mouse (B6C3F ₁)	M	Oral (aqueous)	TCA oral	√ ^a			
Rat studies								
Andersen et al. (1997)	Rat (F344)	M	Inhalation	–		√ ^a		
Barton et al. (1995)	Rat (Sprague-Dawley)	M	Inhalation	–			√	Initial chamber concentrations unavailable, so not used.
Bernauer et al. (1996)	Rat (Wistar)	M	Inhalation	–	√ ^a			
Birner et al. (1993)	Rat (Wistar, F344)	M+F	Gavage (ns)	–			√	Only urine concentrations available, not amount.
Birner et al. (1997)	Rat (Wistar)	M+F	–	DCVC i.v.			√	Single dose, route does not recapitulate how DCVC is formed from TCE, excreted NAcDCVC ~100-fold greater than that from relevant TCE exposures (Bernauer et al., 1996).
Bruckner et al. unpublished	Rat (Sprague-Dawley)	M	Inhalation	–		√		Not published, so not used for calibration. Similar to Keys et al. (2003) data.
Dallas et al. (1991)	Rat (Sprague-Dawley)	M	Inhalation	–	√			
D'Souza et al. (1985)	Rat (Sprague-Dawley)	M	i.v., oral (aqueous)	–			√	Only TCE blood measurements, and ≥10-fold greater than other similar studies.
Fisher et al. (1989)	Rat (F344)	F	Inhalation	–	√			
Fisher et al. (1991)	Rat (F344)	M+F	Inhalation	–	√ ^a	√		Experiment with blood only data not used for calibration.

Table 3-34. Rodent studies with pharmacokinetic data considered for analysis (continued)

Reference	Species (strain)	Sex	TCE exposures	Other exposures	Calibration	Validation	Not used	Comments
Green and Prout (1985)	Rat (Osborne-Mendel)	M	Gavage (corn oil)	TCA gavage (aqueous)	√			
Hissink et al. (2002)	Rat (Wistar)	M	Gavage (corn oil), i.v.	–	√			
Jakobson et al. (1986)	Rat (Sprague-Dawley)	F	Inhalation	Various pretreatments (oral)		√		Pretreatments not included. Only blood TCE data available.
Kaneko et al. (1994)	Rat (Wistar)	M	Inhalation	Ethanol pretreatment (oral)	√			Pretreatments not included.
Keys et al. (2003)	Rat (Sprague-Dawley)	M	Inhalation, oral (aqueous), i.a.	–	√			
Kimmerle and Eben (1973b)	Rat (Wistar)	M	Inhalation	–	√			
Larson and Bull (1992b)	Rat (F344)	M	–	DCA, TCA oral (aqueous)	√			Only TCA dosing data used, since DCA is not in the model.
Larson and Bull (1992a)	Rat (Sprague-Dawley)	M	Oral (aqueous)	–	√ ^a			
Lash et al. (2006)	Rat (F344)	M+F	Gavage (corn oil)	–			√	Highly inconsistent with other studies.
Lee et al. (1996)	Rat (Sprague-Dawley)	M	Arterial, venous, portal, stomach injections	–		√		Only blood TCE data available.
Lee et al. (2000a; 2000b)	Rat (Sprague-Dawley)	M	Stomach injection, i.v., p.v.	p-Nitrophenol pretreatment (i.a.)	√	√		Pretreatments not included. Only experiments with blood and liver data used for calibration.
Merdink et al. (1999)	Rat (F344)	M	–	CH, TCOH i.v.	√			TCOH dosing used; CH not in model.
Poet et al. (2000)	Rat (F344)	M	Dermal	–			√	Dermal exposure not in model.
Prout et al. (1985)	Rat (Osborne-Mendel, Wistar)	M	Gavage (corn oil)	–	√ ^a			

Table 3-34. Rodent studies with pharmacokinetic data considered for analysis (continued)

Reference	Species (strain)	Sex	TCE exposures	Other exposures	Calibration	Validation	Not used	Comments
Saghir et al. (2002)	Rat (F344)	M	–	DCA i.v., oral (aqueous)			√	DCA not in model.
Simmons et al. (2002)	Rat (Long-Evans)	M	Inhalation	–	√			
Stenner et al. (1997)	Rat (F344)	M	intraduodenal	TCOH, TCA i.v.	√			
Templin et al. (1995b)	Rat (F344)	M	Oral (aqueous)	–	√ ^a			
Thrall et al. (2000)	Rat (F344)	M	i.v., i.p.	With toluene			√	Only exhaled breath data available from i.v. study; i.p. dosing not in model.
Yu et al. (2000)	Rat (F344)	M	–	TCA i.v.	√			

^aPart or all of the data in the study was used for calibration in Hack et al. ([2006](#)).

p.v. = intraperitoneous

Table 3-35. Human studies with pharmacokinetic data considered for analysis

Reference	Species (number of individuals)	Sex	TCE exposures	Other exposures	Calibration	Validation	Not used	Comments
Bartonicek (1962)	Human (n = 8)	M+F	Inhalation	–		√		Sparse data, so not included for calibration to conserve computational resources.
Bernauer et al. (1996)	Human	M	Inhalation	–	√ ^a			Grouped data, but unique in that includes NAcDCVC urine data.
Bloemen et al. (2001)	Human (n = 4)	M	Inhalation	–		√		Sparse data, so not included for calibration to conserve computational resources.
Chiu et al. (2007)	Human (n = 6)	M	Inhalation	–	√			
Ertle et al. (1972)	Human	M	Inhalation	CH oral			√	Very similar to Muller data.
Fernandez et al. (1977)	Human	M	Inhalation	–		√		
Fisher et al. (1998)	Human (n = 17)	M+F	Inhalation	–	√ ^a			
Kimmerle and Eben (1973a)	Human (n = 12)	M+F	Inhalation	–	√			
Lapare et al. (1995)	Human (n = 4)	M+F	Inhalation	–		√ ^b		Complex exposure patterns, and only grouped data available for urine, so used for validation.
Lash et al. (1999b)	Human	M+F	Inhalation	–	√			Grouped only, but unique in that DCVG blood data available (same individuals as Fisher et al. (1998)).
Monster et al. (1976)	Human (n = 4)	M	Inhalation	–	√ ^b			Experiments with exercise not included.
Monster et al. (1979)	Human	M	Inhalation	–		√ ^a		Grouped data only.
Muller et al. (1972)	Human	ns	Inhalation	–			√	Same data also included in Muller et al. (1975).

Table 3-35. Human studies with pharmacokinetic data considered for analysis (continued)

Reference	Species (number of individuals)	Sex	TCE exposures	Other exposures	Calibration	Validation	Not used	Comments
Muller et al. (1974)	Human	M	Inhalation	CH, TCA, TCOH oral	√	√ ^a		TCA and TCOH dosing data used for calibration, since it is rare to have metabolite dosing data. TCE dosing data used for validation, since only grouped data available. CH not in model.
Muller et al. (1975)	Human	M	Inhalation	Ethanol oral		√ ^a		Grouped data only.
Paykoc et al. (1945)	Human (n = 3)	ns	–	TCA i.v.	√			
Poet et al. (2000)	Human	M+F	Dermal	–				Dermal exposure not in model.
Sato et al. (1977)	Human	M	Inhalation	–		√		
Stewart et al. (1970)	Human	ns	Inhalation	–		√ ^a		
Treibig et al. (1976)	Human	ns	Inhalation	–		√ ^a		
Vesterberg and Astrand (1976)	Human	M	Inhalation	–			√	All experiments included exercise, so were not included.

^aPart or all of the data in the study was used for calibration in Hack et al. (2006).

^bGrouped data from this study was used for calibration in Hack et al. (2006), but individual data were used here.

The human pharmacokinetic database of controlled exposure studies is extensive, but also more complicated. For the majority of the studies, only grouped or aggregated data were available, and most of those data were saved for “validation” since there remained a large number of studies for which individual data were available. However, some data that may be uniquely informative are only available in grouped form, in particular DCVG blood concentrations, NAcDCVC urinary excretion, and data from TCA and TCOH dosing. While there are analytic uncertainties as to the DCVG blood measurements, discussed above in Section 3.3.3.2.1, they were nonetheless included here because they are the only *in vivo* data available on this measurement in humans. The uncertainty associated with their use is discussed below (see Section 3.5.7.3.2).

In addition, several human data sets, while having individual data, involved sparse collection at only one or a few time points per exposure ([Bloemen et al., 2001](#); [Bartoniczek, 1962](#)) and were subsequently excluded to conserve computational resources. Lapare et al. ([1995](#)), which involved multiple, complex exposure patterns over the course of a month and was missing the individual urine data, was also excluded due to the relatively low amount of data given the large computational effort required to simulate the data. Several studies also investigated the effects of exercise during exposure on human TCE toxicokinetics. The additional parameters in a model including exercise would include those for characterizing the changes in cardiac output, alveolar ventilation, and regional blood flow as well as their interindividual variability, and would have further increased the computational burden. Therefore, it was decided that such data would be excluded from this analysis. Even with these exclusions, data on a total of 42 individuals, some involving multiple exposures, were included in the calibration.

3.5.5.2. Updated Hierarchical Population Statistical Model and Prior Distributions

While the individual animals of a common strain and sex within a study are likely to vary to some extent, this variability was not included as part of the hierarchical population model for several reasons. First, generally, only aggregated pharmacokinetic data (arithmetic mean and SD or SE) are available from rodent studies. While methods exist for addressing between-animal variability with aggregated data ([e.g., Chiu and Bois, 2007](#)), they require a higher level of computational intensity. Second, dose-response data are generally also only separated by sex and strain, and otherwise aggregated. Thus, in analyzing dose-response data (see Chapter 5), one usually has no choice but to treat all of the animals in a particular study of a particular strain and sex as identical units. In the Hack et al. ([2006](#)) model, each simulation was treated as a separate observational unit, so different dosing levels within the same study were treated separately and assigned different PBPK model parameters. However, the animals within a study are generally inbred and kept under similarly controlled conditions, whereas animals in different studies—even if of the same strain and sex—likely have differences in genetic lineage, diet, and handling. Thus, animals *within* a study are likely to be much more homogeneous than animals *between*

studies. As a consequence, in the revised model, for rodents, different animals of the same sex and strain in the same study (or series of studies conducted simultaneously) were treated as identical, and grouped together as a single “subject.” Thus, the predictions from the population model in rodents simulate “average” pharmacokinetics for a particular “lot” of rodents of a particular species, strain, and sex. Between-animal variability is not explicitly modeled, but it is incorporated in a “residual” error term as part of the likelihood function (see Appendix A, Section A.4.3.4). Therefore, a high degree of within-study variability would be reflected in a high posterior value in the variance of the residual-error.

In humans, however, interindividual variability is of interest, and, furthermore, substantial individual data are available in humans. However, in some studies, the same individual was exposed more than once, so those data should be grouped together [in the Hack et al. (2006) model, they were treated as different “individuals”]. Because the primary interest here is chronic exposure, and because it would add substantially to the computational burden, interoccasion variability—changes in pharmacokinetic parameters in a single individual over time—is not addressed. Therefore, each individual is considered a single “subject,” and the predictions from the population model in humans are the “average” across different occasions for a particular individual (adult). Between-occasion variability is not explicitly modeled, but it is incorporated in a “residual” error term as part of the likelihood function (see Appendix A, Section A.4.3.4). Therefore, a high degree of between-occasion variability would be reflected in a high posterior value in the variance of the residual-error.

As discussed in Section 3.3.3.1, sex and (in rodents) strain differences in oxidative metabolism were modest or minimal. While some sex-differences have been noted in GSH metabolism (see Sections 3.3.3.2.7 and 3.3.3.2.8), almost all of the available in vivo data are in males, making it more difficult to statistically characterize that difference with PBPK modeling. Therefore, within a species, different sexes and (in rodents) strains were considered to be drawn from a single, species-level population. For humans, each individual was considered to be drawn from a single (adult) human population.

Thus, from here forward, the term “subject” will be used to refer to both a particular “lot” of a particular rodents’ species, strain, and sex for, and a particular human individual. The term “population” will, therefore, refer to the collection of rodent “lots” of the same species and the collection of human individuals.

Figure A-1 in Appendix A illustrates the hierarchical structure. Informative prior distributions reflecting the uncertainty in the population mean and variance, detailed in Appendix A, were updated from those used in Hack et al. (2006) based on an extensive analysis of the available literature. The population variability of the scaling parameter across subjects is assumed to be distributed as a truncated normal distribution, a standard assumption in the absence of specific data suggesting otherwise. Because of the truncation of extreme values, the sensitivity to this choice is expected to be small as long as the true underlying distribution is uni-

modal and symmetric. In addition, most scaling parameters, being strictly positive in their original units, were log-transformed—so these parameters have lognormal distributions in their original units. The uncertainty distribution for the population parameters was assumed to be a truncated normal distribution for population mean parameters and an inverse gamma distribution for population variance parameters—both standard choices in hierarchical models.

Section 3.5.5.3, next, discusses specification of prior distributions in the case where no data independent of the calibration data exist.

3.5.5.3. Use of Interspecies Scaling to Update Prior Distributions in the Absence of Other Data

For many metabolic parameters, little or no in vitro or other prior information is available to develop prior distributions. Initially, for such parameters, noninformative priors in the form of log-uniform distributions with a range spanning at least 10^4 were specified. However, in the time available for analysis (up to about 100,000 iterations), only for the mouse did all of these parameters achieve adequate convergence. This suggests that some of these parameters are poorly identified for the rat and human. Additional preliminary runs indicated replacing the log-uniform priors with lognormal priors and/or requiring more consistency between species could improve identifiability sufficiently for adequate convergence. However, an objective method of “centering” the lognormal distributions that did not rely on the in vivo data (e.g., via visual fitting or limited optimization) being calibrated against was necessary in order to minimize potential bias.

Therefore, the approach taken was to consider three species sequentially, from mouse to rat to human, and to use interspecies scaling to update the prior distributions across species. This sequence was chosen because the models are essentially “nested” in this order, the rat model adds to the mouse model the “downstream” GSH conjugation pathways, and the human model adds to the rat model the intermediary DCVG compartment. Therefore, for those parameters with little or no independent data *only*, the mouse posteriors were used to update the rat priors, and both the mouse and rat posteriors were used to update the human priors. Table 3-36 contains a list of the parameters for which this scaling was used to update prior distributions. The scaling relationship is defined by the “scaled parameters” listed in Appendix A (see Section A.4.1, Table A-4), and generally follows standard practice. For instance, V_{MAX} and clearance rates scale by body weight to the $\frac{3}{4}$ power, whereas K_M values are assumed to not scale, and rate constants (inverse time units) scale by body weight to the $-\frac{1}{4}$ power.

Table 3-36. Parameters for which scaling from mouse to rat, or from mouse and rat to human, was used to update the prior distributions

Parameter with no or highly uncertain a priori data	Mouse → rat	Rat → human	Mouse+ rat → human	Comments
Respiratory lumen→tissue diffusion flow rate	√		√	No a priori information
TCOG body/blood partition coefficient	√		√	Prior centered on TCOH data, but highly uncertain
TCOG liver/body partition coefficient	√		√	Prior centered on TCOH data, but highly uncertain
Fraction of hepatic TCE oxidation not to TCA+TCOH	√		√	No a priori information
V _{MAX} for hepatic TCE GSH conjugation	√			Rat data on at 1 and 2 mM. Human data at more concentrations, so V _{MAX} and K _M can be estimated
K _M for hepatic TCE GSH conjugation	√			
V _{MAX} for renal TCE GSH conjugation	√			Rat data on at 1 and 2 mM. Human data at more concentrations, so V _{MAX} and K _M can be estimated
K _M for renal TCE GSH conjugation	√			
V _{MAX} for Tracheo-bronchial TCE oxidation	√		√	Prior based on activity at a single concentration
K _M for Tracheo-bronchial TCE oxidation	√		√	No a priori information
Fraction of respiratory oxidation entering systemic circulation	√		√	No a priori information
V _{MAX} for hepatic TCOH→TCA	√		√	No a priori information
K _M for hepatic TCOH→TCA	√		√	No a priori information
V _{MAX} for hepatic TCOH→TCOG	√		√	No a priori information
K _M for hepatic TCOH→TCOG	√		√	No a priori information
Rate constant for hepatic TCOH→other	√		√	No a priori information
Rate constant for TCA plasma→urine	√		√	Prior centered at glomerular filtration rate, but highly uncertain
Rate constant for hepatic TCA→other	√		√	No a priori information
Rate constant for TCOG liver→bile	√		√	No a priori information
Lumped rate constant for TCOG bile→TCOH liver	√		√	No a priori information
Rate constant for TCOG→urine	√		√	Prior centered at glomerular filtration rate, but highly uncertain
Lumped rate constant for DCVC→Urinary NAcDCVC		√		Not included in mouse model
Rate constant for DCVC bioactivation		√		Not included in mouse model

^aSee Appendix A, Table A-4 for scaling relationships.

The scaling model is given explicitly as follows. If θ_i are the “scaled” parameters (usually also natural-log-transformed) that are actually estimated, and A is the “universal” (species-independent) parameter, then $\theta_i = A + \varepsilon_i$, where ε_i is the species-specific “departure” from the scaling relationship, assumed to be normally distributed with variance σ_ε^2 . Therefore, the mouse model gives an initial estimate of “A,” which is used to update the prior distribution for $\theta_r = A + \varepsilon_r$ in the rat. The rat and mouse together then give a “better” estimate of A, which is used to update the prior distribution for $\theta_h = A + \varepsilon_h$ in the human, with the assumed distribution for ε_h . The mathematical details are given in Appendix A, but three key points in this model are worth noting here:

- It is known that interspecies scaling is not an exact relationship, and that, therefore, in any *particular* case, it may either over- or underestimate. Therefore, the variance in the new priors reflect a combination of (1) the uncertainty in the “previous” species’ posteriors as well as (2) a “prediction error” that is distributed lognormally with geometric standard deviation (GSD) of 3.16-fold, so that the 95% confidence range about the central estimate spans 100-fold. This choice was dictated partially by practicality, as larger values of the GSD used in preliminary runs did not lead to adequate convergence within the time available for analysis.
- The rat posterior is a product of its prior (which is based on the mouse posterior) and its likelihood. Therefore, using the rat and mouse posteriors together to update the human priors would use the mouse posterior “twice.” Therefore, the rat posterior is disaggregated into its prior and its likelihood using a lognormal approximation (since the prior is lognormal), and only the (approximate) likelihood is used along with the mouse posterior to develop the human prior.
- The model transfers the marginal distributions for each parameter across species, so correlations between parameters are not retained. This is a restriction on the software used for conducting MCMC analyses. However, assuming independence will lead to a “broader” joint distribution, given the same marginal distributions. Therefore, this assumption tends to reduce the weight of the interspecies scaling as compared to the species-specific calibration data.

To summarize, in order to improve rate of the convergence of the MCMC analyses in rats and humans, a sequential approach was used for fitting scaling parameters without strong prior species-specific information. In particular, an additional assumption was made that *across species*, these scaling parameters were, in absence of other information, expected to have a common underlying value. These assumptions are generally based on allometric scaling principles—with partition coefficients and concentrations scaling directly and rate constants scaling by body weight to the $-1/4$ power (so clearances and maximum metabolic capacities would scale by body weight to the $3/4$ power). These assumptions are used consistently throughout the parameter calibration process. Therefore, after running the mouse model, the posterior distribution for these parameters was used, with an additional error term, as priors for the rat

model. Subsequently, after the mouse and rat model were run, their posterior distributions were combined, with an additional error term, to use as priors for the human model. With this methodology for updating the prior distributions, adequate convergence was achieved for the rat and human after 110,000~140,000 iterations (discussed further below).

3.5.5.4. Implementation

The PBPK model was coded in for use in the MCSim software (version 5.0.0), which was developed particularly for implementing MCMC simulations. As a quality control check, results were checked against the original Hack et al. (2006) model, with the original structures restored and parameter values made equivalent, and the results were within the error tolerances of the ordinary differential equation (ODE) solver after correcting an error in the Hack et al. (2006) model for calculating the TCA liver plasma flow. In addition, the model was translated to MatLab (version 7.2.0.232) with simulation results checked and found to be within the error tolerances of the ODE solver used (“ode15s”). Mass balances were also checked using the baseline parameters, as well as parameters from preliminary MCMC simulations, and found to be within the error tolerances of the ODE solver. Appendix A contains the MCSim model code.

3.5.6. Evaluation of Updated PBPK Model

3.5.6.1. Convergence

As in previous similar analyses (David et al., 2006; Hack et al., 2006; Bois, 2000b, a; Gelman et al., 1996), the potential scale reduction factor “*R*” is used to determine whether different independent MCMC chains have converged to a common distribution. The *R* diagnostic is calculated for each parameter in the model, and represents the factor by which the SD or other measure of scale of the posterior distribution (such as a confidence interval [CI]) may potentially be reduced with additional samples (Gelman et al., 2003). This convergence diagnostic declines to 1 as the number of simulation iterations approaches infinity, so values close to 1 indicate approximate convergence, with values of ≤ 1.1 commonly considered adequate (Gelman et al., 2003). However, as an additional diagnostic, the convergence of model dose-metric predictions was also assessed. Specifically, dose-metrics for a number of generic exposure scenarios similar to those used in long-term bioassays were generated, and their natural log (due to their approximate lognormal posterior distributions) was assessed for convergence using the potential scale reduction factor “*R*.” This is akin to the idea of utilizing sensitivity analysis so that effort is concentrated on calibrating the most sensitive parameters for the purpose of interest. In addition, predictions of interest that do not adequately converge can be flagged as such, so that the statistical uncertainty associated with the limited sample size can be considered.

The mouse model had the most rapid reduction in potential scale reduction factors. Initially, four chains of 42,500 iterations each were run, with the first 12,500 discarded as “burn-in” iterations. The initial decision for determining “burn-in” was determined by visual

inspection. At this point, evaluating the 30,000 remaining iterations, all of the population parameters except for the V_{MAX} for DCVG formation had $R < 1.2$, with only the first-order clearance rate for DCVG formation and the V_{MAX} and K_M for TCOH glucuronidation having $R > 1.1$. For the samples used for inference, all of these initial iterations were treated as “burn-in” iterations, and each chain was then restarted and run for an additional 68,700–71,400 iterations (chains were terminated at the same time, so the number of iterations per chains was slightly different). For these iterations, all values of R were < 1.03 . Dose-metric predictions calculated for exposure scenarios of 10–600 ppm either continuously or 7 hours/day, 5 days/week and 10–3,000 mg/kg-day either continuously or by gavage 5 days/week. These predictions were all adequately converged, with all values of $R < 1.03$.

As discussed above, for parameters with little or no a priori information, the posterior distributions from the mouse model were used to update prior distributions for the rat model, accounting for both the uncertainty reflected in the mouse posteriors as well as the uncertainty in interspecies extrapolation. Four chains were run to 111,960–128,000 iterations each (chains were terminated at the same time and run on computers with slightly different processing speeds, so the number of iterations per chains was slightly different). As is standard, about the first “half” of the chains (i.e., the first 64,000 iterations) were discarded as “burn-in” iterations, and the remaining iterations were used for inferences. For these remaining iterations, the diagnostic R was < 1.1 for all population parameters except the fraction of oxidation not producing TCA or TCOH ($R = 1.44$ for population mean, $R = 1.35$ for population variance), the K_M for TCOH \rightarrow TCA ($R = 1.19$ for population mean), the V_{MAX} and K_M for TCOH glucuronidation ($R = 1.23$ and 1.12 , respectively for population mean, and $R = 1.13$ for both population variances), and the rate of “other” metabolism of TCOH ($R = 1.29$ for population mean and $R = 1.18$ for population variance). Due to resource constraints, chains needed to be stopped at this point. However, these are similar to the degree of convergence reported in Hack et al. (2006). Dose-metric predictions calculated for two inhalation exposure scenarios (10–600 ppm continuously or 7 hours/day, 5 days/week) and two oral exposure scenarios (10–3,000 mg/kg-day continuously or by gavage 5 days/week).

All dose-metric predictions had $R < 1.04$, except for the amount of “other” oxidative metabolism (i.e., not producing TCA or TCOH), which had $R = 1.12$ – 1.16 , depending on the exposure scenario. The poorer convergence of this dose-metric is expected given that a key determining parameter, the fraction of oxidation not producing TCA or TCOH, had the poorest convergence among the population parameters.

For the human model, a set of four chains was run for 74,160–84,690 iterations using “preliminary” updated prior distributions based on the mouse posteriors and preliminary runs of the rat model. Once the rat chains were completed, final updated prior distributions were calculated and the last iteration of the preliminary runs were used as starting points for the final runs. The center of the final updated priors shifted by $< 25\%$ of the SD of either the preliminary

or revised priors, so that the revised median was between the 40th and 60th percentile of the preliminary median, and vice versa. The SDs changed by <5%. Therefore, the use of the preliminary chains as a starting point should introduce no bias, as long as an appropriate burn-in period is used for the final runs.

The final chains were run for an additional 59,140–61,780 iterations, at which point, due to resource constraints, chains needed to be stopped. After the first 20,000 iterations, visual inspection revealed the chains were no longer dependent on the starting point. These iterations were therefore discarded as “burn-in” iterations, and for the remaining ~40,000 iterations used for inferences. All population mean parameters had $R < 1.1$ except for the respiratory tract diffusion constant ($R = 1.20$), the liver:blood partition coefficient for TCOG ($R = 1.23$), the rate of TCE clearance in the kidney producing DCVG ($R = 1.20$), and the rate of elimination of TCOG in bile ($R = 1.46$). All population variances also had $R < 1.1$ except for the variance for the fraction of oxidation not producing TCOH or TCA ($R = 1.10$). Dose-metric predictions were assessed for continuous exposure scenarios at 1–60 ppm in air or 1–300 mg/kg-day orally. These predictions were all adequately converged with all values of $R < 1.02$.

3.5.6.2. Evaluation of Posterior Parameter Distributions

Posterior distributions of the population parameters need to be checked as to whether they appear reasonable given the prior distributions. Inconsistency between the prior and posterior distributions may indicate insufficiently broad (i.e., due to overconfidence) or otherwise incorrectly specified priors, a misspecification of the model structure (e.g., leading to pathological parameter estimates), or an error in the data. As was done with the evaluation of Hack et al. (2006) in Appendix A, parameters were flagged if the interquartile regions of their prior and posterior distributions did not overlap.

Appendix A contains detailed tables of the “sampled” parameters, and their prior and posterior distributions. Because these parameters are generally scaled one or more times to obtain a physically meaningful parameter, they are difficult to interpret. Therefore, in Tables 3-37–3-39, the prior and posterior population distributions for the PBPK model parameters obtained *after* scaling are summarized. Since it is desirable to characterize the contributions from both uncertainty in population parameters and variability within the population, the following procedure is adopted. First, 500 sets of population parameters (i.e., population mean and variance for each scaling parameter) are either generated from the prior distributions via Monte Carlo or extracted from the posterior MCMC samples—these represent the uncertainty in the population parameters. To minimize autocorrelation, for the posteriors, the samples were obtained by “thinning” the chains to the appropriate degree. From each of these sets of population parameters, 100 sets of “subject”-level parameters were generated by Monte Carlo—each of these represents the population variability, given a *particular* set of population parameters. Thus, a total of 50,000 subjects, representing 100 (variability) each for 500 different

populations (uncertainty), were generated. For each of the 500 populations, the scaling parameters are converted to PBPK model parameters, and the population median and GSD is calculated—representing the central tendency and variability for that population. Then, the median and the 95% CIs for the population median and GSD are calculated, and presented in the tables that follow. Thus, these tables summarize separately the uncertainty in population distribution as well as the variability in the population, while also accounting for correlations among the population-level parameters. Finally, Table 3-40 shows the change in the CI in the population median for the PBPK model parameters between the prior and posterior distributions, as well as the shift in the central estimate (median) of the population median PBPK model parameter.

The prior and posterior distributions for most physiological parameters were similar. The posterior distribution was substantially narrower (i.e., less uncertainty) than the prior distribution only in the case of the diffusion rate from the respiratory lumen to the respiratory tissue, which also was to be expected given the very wide, noninformative prior for that parameter.

For distribution parameters, there were only relatively minor changes between prior and posterior distributions for TCE and TCOH partition coefficients. The posterior distributions for several TCA partition coefficients and plasma binding parameters were substantially narrower than their corresponding priors, but the central estimates were similar, meaning that values at the high and low extremes were not likely. For TCOG as well, partition coefficient posterior distributions were substantially narrower, which was expected given the greater uncertainty in the prior distributions (TCOH partition coefficients were used as a proxy).

Again, posterior distributions indicated that the high and low extremes were not likely. Finally, posterior distribution for the distribution volume for DCVG was substantially narrower than the prior distribution, which only provided a lower bound given by the blood volume. In this case, the upper bounds were substantially lower in the posterior.

Posterior distributions for oral absorption parameters in mice and rats (there were no oral studies in humans) were also informed by the data, as reflected in their being substantially more narrow than the corresponding priors. Finally, with a few exceptions, TCE and metabolite kinetic parameters showed substantially narrower posterior distributions than prior distributions, indicating that they were fairly well specified by the in vivo data. The exceptions were the V_{MAX} for hepatic oxidation in humans (for which there was substantial in vitro data) and the V_{MAX} for respiratory metabolism in mice and rats (although the posterior distribution for the K_M for this pathway was substantially narrower than the corresponding prior).

Table 3-37. Prior and posterior uncertainty and variability in mouse PBPK model parameters

Parameter description	PBPK parameter	Prior population median: median (2.5%, 97.5%)	Posterior population median: median (2.5%, 97.5%)	Prior population GSD: median (2.5%, 97.5%)	Posterior population GSD: median (2.5%, 97.5%)
Cardiac output (L/hr)	QC	0.84 (0.59, 1.2)	1 (0.79, 1.3)	1.17 (1.1, 1.4)	1.35 (1.15, 1.54)
Alveolar ventilation (L/hr)	QP	2.1 (1.3, 3.5)	2.1 (1.5, 2.7)	1.27 (1.17, 1.54)	1.45 (1.28, 1.66)
Scaled fat blood flow	QFatC	0.07 (0.03, 0.11)	0.072 (0.044, 0.1)	1.65 (1.22, 2.03)	1.64 (1.3, 1.99)
Scaled gut blood flow	QGutC	0.14 (0.11, 0.17)	0.16 (0.14, 0.17)	1.15 (1.09, 1.19)	1.12 (1.07, 1.19)
Scaled liver blood flow	QLivC	0.02 (0.016, 0.024)	0.021 (0.017, 0.024)	1.15 (1.09, 1.19)	1.15 (1.09, 1.19)
Scaled slowly perfused blood flow	QSlwC	0.22 (0.14, 0.29)	0.21 (0.15, 0.28)	1.3 (1.15, 1.38)	1.3 (1.17, 1.39)
Scaled rapidly perfused blood flow	QRapC	0.46 (0.37, 0.56)	0.45 (0.37, 0.52)	1.15 (1.11, 1.2)	1.17 (1.12, 1.2)
Scaled kidney blood flow	QKidC	0.092 (0.054, 0.13)	0.091 (0.064, 0.12)	1.34 (1.14, 1.45)	1.34 (1.18, 1.44)
Respiratory lumen:tissue diffusive clearance rate (L/hr)	DResp	0.017 (0.000032, 15)	2.5 (1.4, 5.1)	1.37 (1.25, 1.62)	1.53 (1.37, 1.73)
Fat fractional compartment volume	VFatC	0.071 (0.032, 0.11)	0.089 (0.061, 0.11)	1.59 (1.19, 1.93)	1.4 (1.19, 1.78)
Gut fractional compartment volume	VGutC	0.049 (0.041, 0.057)	0.048 (0.042, 0.055)	1.11 (1.07, 1.14)	1.11 (1.08, 1.14)
Liver fractional compartment volume	VLivC	0.054 (0.038, 0.071)	0.047 (0.037, 0.06)	1.22 (1.12, 1.29)	1.23 (1.17, 1.3)
Rapidly perfused fractional compartment volume	VRapC	0.1 (0.087, 0.11)	0.099 (0.09, 0.11)	1.08 (1.05, 1.11)	1.09 (1.06, 1.11)
Fractional volume of respiratory lumen	VRespLumC	0.0047 (0.004, 0.0053)	0.0047 (0.0041, 0.0052)	1.09 (1.06, 1.12)	1.09 (1.07, 1.12)
Fractional volume of respiratory tissue	VRespEffC	0.0007 (0.0006, 0.00079)	7e-04 (0.00062, 0.00078)	1.09 (1.06, 1.12)	1.1 (1.07, 1.12)
Kidney fractional compartment volume	VKidC	0.017 (0.015, 0.019)	0.017 (0.015, 0.019)	1.08 (1.05, 1.11)	1.09 (1.06, 1.11)
Blood fractional compartment volume	VBldC	0.049 (0.042, 0.056)	0.048 (0.043, 0.054)	1.1 (1.06, 1.13)	1.1 (1.08, 1.13)

Table 3-37. Prior and posterior uncertainty and variability in mouse PBPK model parameters (continued)

Parameter description	PBPK parameter	Prior population median: median (2.5%, 97.5%)	Posterior population median: median (2.5%, 97.5%)	Prior population GSD: median (2.5%, 97.5%)	Posterior population GSD: median (2.5%, 97.5%)
Slowly perfused fractional compartment volume	VSlwC	0.55 (0.5, 0.59)	0.54 (0.51, 0.57)	1.05 (1.04, 1.07)	1.05 (1.04, 1.07)
Plasma fractional compartment volume	VPlasC	0.026 (0.016, 0.036)	0.022 (0.016, 0.029)	1.24 (1.15, 1.35)	1.27 (1.19, 1.36)
TCA body fractional compartment volume [not incl. blood+liver]	VBodC	0.79 (0.77, 0.8)	0.79 (0.78, 0.81)	1.01 (1.01, 1.02)	1.01 (1.01, 1.02)
TCOH/G body fractional compartment volume [not incl. liver]	VBodTCOHC	0.84 (0.82, 0.85)	0.84 (0.83, 0.85)	1.01 (1.01, 1.02)	1.01 (1.01, 1.02)
TCE blood:air partition coefficient	PB	15 (10, 23)	14 (11, 17)	1.22 (1.12, 1.42)	1.44 (1.28, 1.53)
TCE fat:blood partition coefficient	PFat	36 (21, 62)	36 (26, 49)	1.26 (1.14, 1.52)	1.32 (1.16, 1.56)
TCE gut:blood partition coefficient	PGut	1.9 (0.89, 3.8)	1.5 (0.94, 2.6)	1.36 (1.2, 1.75)	1.36 (1.2, 1.79)
TCE liver:blood partition coefficient	PLiv	1.7 (0.89, 3.5)	2.2 (1.3, 3.3)	1.37 (1.2, 1.75)	1.39 (1.21, 1.84)
TCE rapidly perfused:blood partition coefficient	PRap	1.8 (0.98, 3.7)	1.8 (1.1, 3)	1.37 (1.2, 1.76)	1.37 (1.2, 1.77)
TCE respiratory tissue:air partition coefficient	PResp	2.7 (1.2, 5)	2.5 (1.5, 4.2)	1.36 (1.19, 1.78)	1.37 (1.19, 1.74)
TCE kidney:blood partition coefficient	PKid	2.2 (0.96, 4.6)	2.6 (1.7, 4)	1.36 (1.2, 1.77)	1.51 (1.25, 1.88)
TCE slowly perfused:blood partition coefficient	PSlw	2.4 (1.2, 4.9)	2.2 (1.4, 3.5)	1.38 (1.2, 1.78)	1.39 (1.21, 1.8)
TCA blood:plasma concentration ratio	TCAPlas	0.76 (0.4, 16)	1.1 (0.75, 1.8)	1.21 (1.09, 1.58)	1.23 (1.1, 1.73)
Free TCA body:blood plasma partition coefficient	PBodTCA	0.77 (0.27, 17)	0.87 (0.59, 1.5)	1.41 (1.23, 1.8)	1.39 (1.24, 1.9)
Free TCA liver:blood plasma partition coefficient	PLivTCA	1.1 (0.36, 21)	1.1 (0.64, 1.9)	1.41 (1.23, 1.8)	1.4 (1.24, 1.87)
Protein:TCA dissociation constant (μmole/L)	kDissoc	100 (13, 790)	130 (24, 520)	2.44 (1.73, 5.42)	2.64 (1.75, 5.45)

Table 3-37. Prior and posterior uncertainty and variability in mouse PBPK model parameters (continued)

Parameter description	PBPK parameter	Prior population median: median (2.5%, 97.5%)	Posterior population median: median (2.5%, 97.5%)	Prior population GSD: median (2.5%, 97.5%)	Posterior population GSD: median (2.5%, 97.5%)
Maximum binding concentration (μmole/L)	B _{MAX}	87 (9.6, 790)	140 (28, 690)	2.72 (1.92, 5.78)	2.88 (1.93, 5.89)
TCOH body:blood partition coefficient	PBodTCOH	1.1 (0.61, 2.1)	0.89 (0.65, 1.3)	1.29 (1.16, 1.66)	1.31 (1.17, 1.61)
TCOH liver:body partition coefficient	PLivTCOH	1.3 (0.73, 2.3)	1.9 (1.2, 2.6)	1.3 (1.16, 1.61)	1.35 (1.18, 1.68)
TCOG body:blood partition coefficient	PBodTCOG	0.95 (0.016, 77)	0.48 (0.18, 1.1)	1.36 (1.19, 2.05)	1.41 (1.22, 2.19)
TCOG liver:body partition coefficient	PLivTCOG	1.3 (0.019, 92)	1.3 (0.64, 2.6)	1.36 (1.18, 2.13)	1.56 (1.28, 2.52)
DCVG effective volume of distribution	VDCVG	0.033 (0.0015, 15)	0.027 (0.0016, 4.1)	1.28 (1.08, 1.97)	1.31 (1.1, 2.19)
TCE stomach absorption coefficient (/hr)	kAS	1.7 (0.0049, 450)	1.7 (0.37, 13)	4.74 (2.29, 23.4)	4.28 (2.39, 13.4)
TCE stomach-duodenum transfer coefficient (/hr)	kTSD	1.4 (0.043, 51)	4.5 (0.51, 26)	3.84 (2.09, 10.6)	4.79 (2.53, 10.9)
TCE duodenum absorption coefficient (/hr)	kAD	1.2 (0.0024, 200)	0.27 (0.067, 1.6)	4.33 (2.14, 26)	4.17 (2.34, 14.4)
TCA stomach absorption coefficient (/hr)	kASTCA	0.63 (0.0027, 240)	4 (0.2, 74)	4.26 (2.27, 23.4)	5.15 (2.56, 22)
V _{MAX} for hepatic TCE oxidation (mg/hr)	V _{MAX}	3.9 (1.4, 15)	2.5 (1.6, 4.2)	2.02 (1.56, 2.85)	1.86 (1.59, 2.47)
K _M for hepatic TCE oxidation (mg/L)	K _M	34 (1.6, 620)	2.7 (1.4, 8)	1.25 (1.15, 1.61)	2.08 (1.48, 3.49)
Fraction of hepatic TCE oxidation not to TCA+TCOH	FracOther	0.43 (0.0018, 1)	0.023 (0.0037, 0.15)	1.23 (1, 2.13)	1.49 (1.25, 2.83)
Fraction of hepatic TCE oxidation to TCA	FracTCA	0.086 (0.00022, 0.66)	0.13 (0.084, 0.21)	1.48 (1.12, 2.56)	1.4 (1.21, 1.96)
V _{MAX} for hepatic TCE GSH conjugation (mg/hr)	V _{MAX} DCVG	3.7 (0.0071, 2,800)	0.6 (0.01, 480)	1.55 (1.33, 2.52)	1.61 (1.37, 2.91)
K _M for hepatic TCE GSH conjugation (mg/L)	K _M DCVG	250 (0.0029, 6,500,000)	2200 (0.17, 2,300,000)	1.81 (1.47, 3.62)	1.93 (1.49, 3.68)

Table 3-37. Prior and posterior uncertainty and variability in mouse PBPK model parameters (continued)

Parameter description	PBPK parameter	Prior population median: median (2.5%, 97.5%)	Posterior population median: median (2.5%, 97.5%)	Prior population GSD: median (2.5%, 97.5%)	Posterior population GSD: median (2.5%, 97.5%)
V _{MAX} for renal TCE GSH conjugation (mg/hr)	V _{MAX} KidDCVG	0.34 (0.00051, 180)	0.027 (0.0012, 13)	1.49 (1.26, 2.49)	1.54 (1.28, 2.72)
K _M for renal TCE GSH conjugation (mg/L)	K _M KidDCVG	150 (0.0053, 6,200,000)	160 (0.078, 280,000)	1.79 (1.43, 3.45)	1.91 (1.5, 3.91)
V _{MAX} for tracheo-bronchial TCE oxidation (mg/hr)	V _{MAX} Clara	0.24 (0.03, 3.9)	0.42 (0.1, 1.5)	2.32 (1.74, 3.66)	4.13 (2.27, 6.79)
K _M for tracheo-bronchial TCE oxidation (mg/L)	K _M Clara	1.5 (0.0018, 630)	0.011 (0.0024, 0.09)	1.47 (1.25, 2.58)	1.63 (1.28, 5.02)
Fraction of respiratory metabolism to systemic circ.	FracLungSys	0.34 (0.0016, 1)	0.78 (0.18, 0.99)	1.24 (1, 2.1)	1.11 (1, 1.72)
V _{MAX} for hepatic TCOH→TCA (mg/hr)	V _{MAX} TCOH	0.064 (0.000014, 380)	0.12 (0.048, 0.28)	1.5 (1.24, 2.61)	1.6 (1.28, 2.92)
K _M for hepatic TCOH→TCA (mg/L)	K _M TCOH	1.4 (0.00018, 5,300)	0.92 (0.26, 2.7)	1.48 (1.24, 2.41)	1.49 (1.26, 2.4)
V _{MAX} for hepatic TCOH→TCOG (mg/hr)	V _{MAX} Gluc	0.11 (0.000013, 310)	4.6 (1.9, 16)	1.48 (1.26, 2.53)	1.47 (1.26, 2.14)
K _M for hepatic TCOH→TCOG (mg/L)	K _M Gluc	1.8 (0.0018, 610)	30 (5.3, 130)	1.48 (1.25, 2.48)	1.8 (1.3, 4.72)
Rate constant for hepatic TCOH→other (/hr)	kMetTCOH	0.19 (0.000039, 1,400)	8.8 (1.9, 23)	1.47 (1.25, 2.36)	1.54 (1.26, 2.92)
Rate constant for TCA plasma→urine (/hr)	kUrnTCA	32 (0.38, 1700)	3.2 (1.2, 7.1)	1.57 (1.34, 2.61)	1.84 (1.44, 2.94)
Rate constant for hepatic TCA→other (/hr)	kMetTCA	0.12 (0.0004, 130)	1.5 (0.63, 2.9)	1.48 (1.25, 2.32)	1.51 (1.26, 2.27)
Rate constant for TCOG liver→bile (/hr)	kBile	0.3 (0.0004, 160)	2.4 (0.74, 8.4)	1.48 (1.24, 2.29)	1.51 (1.26, 2.39)
Lumped rate constant for TCOG bile→TCOH liver (/hr)	kEHR	0.21 (0.00036, 150)	0.039 (0.0026, 0.11)	1.47 (1.23, 2.29)	1.53 (1.28, 2.94)
Rate constant for TCOG→urine (/hr)	kUrnTCOG	1 (0.00015, 6,200)	12 (2.6, 77)	1.71 (1.4, 3.13)	3.44 (1.89, 9.49)
Rate constant for hepatic DCVG→DCVC (/hr)	kDCVG	0.24 (0.0004, 160)	0.81 (0.0033, 46)	1.48 (1.25, 2.39)	1.52 (1.25, 2.5)

Table 3-37. Prior and posterior uncertainty and variability in mouse PBPK model parameters (continued)

Parameter description	PBPK parameter	Prior population median: median (2.5%, 97.5%)	Posterior population median: median (2.5%, 97.5%)	Prior population GSD: median (2.5%, 97.5%)	Posterior population GSD: median (2.5%, 97.5%)
Lumped rate constant for DCVC→urinary NAcDCVC (/hr)	kNAT	0.29 (0.0004, 160)	0.37 (0.0021, 34)	1.5 (1.25, 2.49)	1.53 (1.25, 2.77)
Rate constant for DCVC bioactivation (/hr)	kKidBioact	0.18 (0.0004, 150)	0.23 (0.0024, 33)	1.48 (1.25, 2.51)	1.53 (1.25, 3.03)

Table 3-38. Prior and posterior uncertainty and variability in rat PBPK model parameters

Parameter description	PBPK parameter	Prior population median: median (2.5%, 97.5%)	Posterior population median: median (2.5%, 97.5%)	Prior population GSD: median (2.5%, 97.5%)	Posterior population GSD: median (2.5%, 97.5%)
Cardiac output (L/hr)	QC	5.3 (4.2, 6.9)	6.1 (5.2, 7.4)	1.12 (1.07, 1.28)	1.26 (1.12, 1.36)
Alveolar ventilation (L/hr)	QP	10 (5.1, 18)	7.5 (5.8, 10)	1.32 (1.18, 1.71)	1.52 (1.33, 1.84)
Scaled fat blood flow	QFatC	0.071 (0.032, 0.11)	0.081 (0.06, 0.1)	1.66 (1.21, 2.02)	1.5 (1.3, 1.86)
Scaled gut blood flow	QGutC	0.15 (0.12, 0.18)	0.17 (0.15, 0.19)	1.15 (1.09, 1.19)	1.13 (1.08, 1.18)
Scaled liver blood flow	QLivC	0.021 (0.017, 0.026)	0.022 (0.018, 0.025)	1.15 (1.09, 1.2)	1.15 (1.1, 1.19)
Scaled slowly perfused blood flow	QSlwC	0.33 (0.21, 0.46)	0.31 (0.23, 0.4)	1.31 (1.15, 1.4)	1.32 (1.22, 1.41)
Scaled rapidly perfused blood flow	QRapC	0.28 (0.15, 0.42)	0.28 (0.18, 0.36)	1.38 (0.0777, 1.72)	1.42 (0.0856, 1.75)
Scaled kidney blood flow	QKidC	0.14 (0.12, 0.16)	0.14 (0.12, 0.16)	1.11 (1.07, 1.14)	1.11 (1.08, 1.14)
Respiratory lumen:tissue diffusive clearance rate (L/hr)	DResp	9.9 (0.48, 85)	21 (9.5, 46)	1.41 (1.26, 1.77)	1.59 (1.41, 1.9)
Fat fractional compartment volume	VFatC	0.069 (0.031, 0.11)	0.069 (0.046, 0.091)	1.61 (1.2, 1.93)	1.59 (1.34, 1.88)
Gut fractional compartment volume	VGutC	0.032 (0.027, 0.037)	0.032 (0.028, 0.036)	1.11 (1.07, 1.14)	1.11 (1.08, 1.14)
Liver fractional compartment volume	VLivC	0.034 (0.026, 0.042)	0.033 (0.028, 0.039)	1.16 (1.09, 1.21)	1.17 (1.12, 1.21)
Rapidly perfused fractional compartment volume	VRapC	0.087 (0.076, 0.1)	0.088 (0.079, 0.097)	1.1 (1.06, 1.13)	1.1 (1.07, 1.13)
Fractional volume of respiratory lumen	VRespLumC	0.0046 (0.0037, 0.0057)	0.0047 (0.0039, 0.0055)	1.16 (1.1, 1.21)	1.16 (1.11, 1.21)
Fractional volume of respiratory tissue	VRespEffC	0.0005 (0.00039, 0.00061)	5e-04 (0.00041, 0.00058)	1.16 (1.09, 1.21)	1.16 (1.11, 1.2)
Kidney fractional compartment volume	VKidC	0.0069 (0.0056, 0.0082)	0.007 (0.006, 0.008)	1.13 (1.08, 1.17)	1.13 (1.09, 1.17)

Table 3-38. Prior and posterior uncertainty and variability in rat PBPK model parameters (continued)

Parameter description	PBPK parameter	Prior population median: median (2.5%, 97.5%)	Posterior population median: median (2.5%, 97.5%)	Prior population GSD: median (2.5%, 97.5%)	Posterior population GSD: median (2.5%, 97.5%)
Blood fractional compartment volume	VBldC	0.073 (0.063, 0.085)	0.074 (0.066, 0.082)	1.1 (1.06, 1.13)	1.1 (1.07, 1.13)
Slowly perfused fractional compartment volume	VSlwC	0.6 (0.55, 0.63)	0.6 (0.57, 0.62)	1.05 (1.04, 1.06)	1.05 (1.04, 1.06)
Plasma fractional compartment volume	VPlasC	0.039 (0.025, 0.054)	0.04 (0.032, 0.049)	1.24 (1.15, 1.35)	1.22 (1.16, 1.33)
TCA body fractional compartment volume [not incl. blood+liver]	VBodC	0.79 (0.78, 0.81)	0.79 (0.78, 0.8)	1.01 (1.01, 1.01)	1.01 (1.01, 1.01)
TCOH/G body fractional compartment volume [not incl. liver]	VBodTCOHC	0.87 (0.86, 0.87)	0.87 (0.86, 0.87)	1.01 (1, 1.01)	1.01 (1, 1.01)
TCE blood:air partition coefficient	PB	22 (14, 33)	19 (16, 24)	1.26 (1.19, 1.35)	1.3 (1.22, 1.38)
TCE fat:blood partition coefficient	PFat	27 (16, 46)	31 (24, 42)	1.32 (1.22, 1.44)	1.32 (1.23, 1.43)
TCE gut:blood partition coefficient	PGut	1.3 (0.69, 3)	1.1 (0.79, 1.7)	1.36 (1.21, 1.79)	1.36 (1.2, 1.68)
TCE liver:blood partition coefficient	PLiv	1.5 (1.2, 1.9)	1.6 (1.3, 1.8)	1.15 (1.11, 1.2)	1.15 (1.11, 1.2)
TCE rapidly perfused:blood partition coefficient	PRap	1.3 (0.66, 2.7)	1.3 (0.82, 2.1)	1.35 (1.18, 1.82)	1.37 (1.2, 1.76)
TCE respiratory tissue:air partition coefficient	PResp	0.97 (0.48, 2.1)	1 (0.62, 1.6)	1.37 (1.19, 1.77)	1.36 (1.19, 1.78)
TCE kidney:blood partition coefficient	PKid	1.3 (0.77, 2.2)	1.2 (0.9, 1.7)	1.31 (1.19, 1.5)	1.3 (1.2, 1.45)
TCE slowly perfused:blood partition coefficient	PSlw	0.57 (0.35, 0.97)	0.73 (0.54, 0.97)	1.32 (1.23, 1.43)	1.33 (1.25, 1.46)
TCA blood:plasma concentration ratio	TCAPlas	0.78 (0.6, 0.96)	0.78 (0.71, 0.86)	1.12 (1.06, 1.22)	1.11 (1.07, 1.17)
Free TCA body:blood plasma partition coefficient	PBodTCA	0.7 (0.18, 2.2)	0.76 (0.46, 1.3)	1.72 (1.39, 2.81)	1.65 (1.4, 2.19)
Free TCA liver:blood plasma partition coefficient	PLivTCA	0.84 (0.25, 3.3)	1.1 (0.61, 2.1)	1.71 (1.39, 2.78)	1.66 (1.38, 2.37)

Table 3-38. Prior and posterior uncertainty and variability in rat PBPK model parameters (continued)

Parameter description	PBPK parameter	Prior population median: median (2.5%, 97.5%)	Posterior population median: median (2.5%, 97.5%)	Prior population GSD: median (2.5%, 97.5%)	Posterior population GSD: median (2.5%, 97.5%)
Protein:TCA dissociation constant ($\mu\text{mole/L}$)	kDissoc	270 (95, 790)	280 (140, 530)	1.62 (1.31, 2.43)	1.6 (1.31, 2.31)
Maximum binding concentration ($\mu\text{mole/L}$)	B _{MAX}	320 (80, 1300)	320 (130, 750)	1.89 (1.5, 2.64)	1.84 (1.49, 2.57)
TCOH body:blood partition coefficient	PBodTCOH	1 (0.33, 4)	1.1 (0.51, 2.1)	1.71 (1.37, 2.69)	1.76 (1.38, 2.45)
TCOH liver:body partition coefficient	PLivTCOH	1.3 (0.39, 4.5)	1.2 (0.59, 2.8)	1.71 (1.37, 2.8)	1.78 (1.37, 2.75)
TCOG body:blood partition coefficient	PBodTCOG	0.48 (0.021, 14)	1.6 (0.091, 16)	1.39 (1.2, 1.97)	1.42 (1.21, 2.52)
TCOG liver:body partition coefficient	PLivTCOG	1.3 (0.078, 39)	10 (2.7, 41)	1.4 (1.2, 2.14)	1.42 (1.21, 2.3)
DCVG effective volume of distribution	VDCVG	0.27 (0.27, 0.27)	0.27 (0.27, 0.27)	1 (1, 1)	1 (1, 1)
TCE stomach absorption coefficient (/hr)	kAS	0.73 (0.0044, 400)	2.5 (0.32, 19)	4.16 (2.21, 20)	9.3 (4.07, 31.1)
TCE stomach-duodenum transfer coefficient (/hr)	kTSD	1.4 (0.04, 45)	3.2 (0.31, 19)	3.92 (2.13, 10.4)	5.54 (2.77, 10.7)
TCE duodenum absorption coefficient (/hr)	kAD	0.96 (0.0023, 260)	0.17 (0.038, 1)	4.17 (2.15, 20.8)	4.07 (2.51, 11.9)
TCA stomach absorption coefficient (/hr)	kASTCA	0.83 (0.0024, 240)	1.4 (0.13, 13)	4.15 (2.2, 18.7)	4.21 (2.4, 11.4)
V _{MAX} for hepatic TCE oxidation (mg/hr)	V _{MAX}	5.8 (2, 19)	5.3 (3.9, 7.7)	1.97 (1.54, 2.92)	1.69 (1.47, 2.15)
K _M for hepatic TCE oxidation (mg/L)	K _M	18 (1.9, 240)	0.74 (0.54, 1.4)	2.76 (1.89, 6.46)	1.84 (1.51, 2.7)
Fraction of hepatic TCE oxidation not to TCA+TCOH	FracOther	0.027 (0.0018, 0.59)	0.29 (0.047, 0.56)	1.42 (1.15, 2.33)	2.15 (1.32, 5.06)
Fraction of hepatic TCE oxidation to TCA	FracTCA	0.2 (0.027, 0.76)	0.046 (0.023, 0.087)	1.35 (1.11, 2.14)	1.84 (1.36, 2.8)
V _{MAX} for hepatic TCE GSH conjugation (mg/hr)	V _{MAX} DCVG	2 (0.015, 1,100)	5.8 (0.16, 340)	1.52 (1.3, 2.67)	1.57 (1.32, 2.93)
K _M for hepatic TCE GSH conjugation (mg/L)	K _M DCVG	1,500 (1.2, 1,800,000)	6300 (120, 720,000)	1.83 (1.45, 3.15)	1.88 (1.48, 3.49)

Table 3-38. Prior and posterior uncertainty and variability in rat PBPK model parameters (continued)

Parameter description	PBPK parameter	Prior population median: median (2.5%, 97.5%)	Posterior population median: median (2.5%, 97.5%)	Prior population GSD: median (2.5%, 97.5%)	Posterior population GSD: median (2.5%, 97.5%)
V _{MAX} for renal TCE GSH conjugation (mg/hr)	V _{MAX} KidDCVG	0.038 (0.00027, 13)	0.0024 (0.0005, 0.014)	1.52 (1.3, 2.81)	1.56 (1.29, 2.72)
K _M for renal TCE GSH conjugation (mg/L)	K _M KidDCVG	470 (0.47, 530,000)	0.25 (0.038, 2.2)	1.84 (1.47, 4.27)	1.93 (1.49, 3.57)
V _{MAX} for tracheo-bronchial TCE oxidation (mg/hr)	V _{MAX} Clara	0.2 (0.0077, 2.4)	0.17 (0.042, 0.69)	2.26 (1.71, 3.3)	4.35 (1.99, 6.7)
K _M for tracheo-bronchial TCE oxidation (mg/L)	K _M Clara	0.016 (0.0014, 0.58)	0.025 (0.005, 0.15)	1.47 (1.26, 2.39)	1.65 (1.28, 10.5)
Fraction of respiratory metabolism to systemic circ.	FracLungSys	0.82 (0.027, 1)	0.73 (0.06, 0.98)	1.09 (1, 1.71)	1.13 (1.01, 1.86)
V _{MAX} for hepatic TCOH→TCA (mg/hr)	V _{MAX} TCOH	0.75 (0.037, 20)	0.71 (0.27, 2.2)	1.51 (1.25, 2.64)	1.68 (1.3, 3.23)
K _M for hepatic TCOH→TCA (mg/L)	K _M TCOH	1 (0.029, 23)	19 (3.6, 94)	1.52 (1.26, 2.7)	1.72 (1.26, 3.93)
V _{MAX} for hepatic TCOH→TCOG (mg/hr)	V _{MAX} Gluc	27 (0.83, 620)	11 (4.1, 32)	1.5 (1.25, 2.59)	2.3 (1.41, 5.19)
K _M for hepatic TCOH→TCOG (mg/L)	K _M Gluc	31 (1, 570)	6.3 (1.2, 20)	1.5 (1.25, 2.74)	2.04 (1.3, 8.4)
Rate constant for hepatic TCOH→other (/hr)	kMetTCOH	4.2 (0.17, 150)	3 (0.57, 15)	1.49 (1.27, 2.67)	1.72 (1.3, 8.31)
Rate constant for TCA plasma→urine (/hr)	kUrnTCA	1.9 (0.21, 47)	0.92 (0.51, 1.7)	1.56 (1.33, 2.81)	1.58 (1.36, 2.25)
Rate constant for hepatic TCA→other (/hr)	kMetTCA	0.76 (0.037, 19)	0.47 (0.17, 1.2)	1.5 (1.26, 2.74)	1.52 (1.27, 2.45)
Rate constant for TCOG liver→bile (/hr)	kBile	1.4 (0.052, 31)	14 (2.7, 39)	1.5 (1.25, 2.8)	1.63 (1.29, 4.1)
Lumped rate constant for TCOG bile→TCOH liver (/hr)	kEHR	0.013 (0.00055, 0.64)	1.7 (0.34, 7.4)	1.5 (1.25, 2.49)	1.67 (1.26, 5.91)
Rate constant for TCOG→urine (/hr)	kUrnTCOG	11 (0.063, 1,000)	12 (0.45, 370)	1.74 (1.42, 2.99)	1.86 (1.43, 3.54)
Rate constant for hepatic DCVG→DCVC (/hr)	kDCVG	30,000 (30,000, 30,000)	30,000 (30,000, 30,000)	1 (1, 1)	1 (1, 1)

Table 3-38. Prior and posterior uncertainty and variability in rat PBPK model parameters (continued)

Parameter description	PBPK parameter	Prior population median: median (2.5%, 97.5%)	Posterior population median: median (2.5%, 97.5%)	Prior population GSD: median (2.5%, 97.5%)	Posterior population GSD: median (2.5%, 97.5%)
Lumped rate constant for DCVC→urinary NAcDCVC (/hr)	kNAT	0.15 (0.00024, 84)	0.0029 (0.00066, 0.015)	1.49 (1.24, 2.8)	1.54 (1.26, 2.45)
Rate constant for DCVC bioactivation (/hr)	kKidBioact	0.12 (0.00023, 83)	0.0092 (0.0012, 0.043)	1.48 (1.24, 2.68)	1.52 (1.25, 2.5)

Table 3-39. Prior and posterior uncertainty and variability in human PBPK model parameters

Parameter description	PBPK parameter	Prior population median: median (2.5%, 97.5%)	Posterior population median: median (2.5%, 97.5%)	Prior population GSD: median (2.5%, 97.5%)	Posterior population GSD: median (2.5%, 97.5%)
Cardiac output (L/hr)	QC	390 (280, 560)	330 (280, 390)	1.17 (1.1, 1.39)	1.39 (1.26, 1.54)
Alveolar ventilation (L/hr)	QP	380 (220, 640)	440 (360, 530)	1.27 (1.17, 1.52)	1.58 (1.44, 1.73)
Scaled fat blood flow	QFatC	0.051 (0.021, 0.078)	0.043 (0.033, 0.055)	1.64 (1.23, 2)	1.92 (1.72, 2.09)
Scaled gut blood flow	QGutC	0.19 (0.15, 0.23)	0.16 (0.14, 0.18)	1.16 (1.1, 1.21)	1.16 (1.12, 1.2)
Scaled liver blood flow	QLivC	0.063 (0.029, 0.099)	0.039 (0.026, 0.055)	1.62 (1.22, 1.92)	1.8 (1.62, 1.98)
Scaled slowly perfused blood flow	QSlwC	0.22 (0.13, 0.3)	0.17 (0.14, 0.21)	1.34 (1.18, 1.45)	1.39 (1.31, 1.46)
Scaled rapidly perfused blood flow	QRapC	0.29 (0.18, 0.4)	0.39 (0.34, 0.43)	1.31 (1.14, 1.57)	1.22 (1.16, 1.3)
Scaled kidney blood flow	QKidC	0.19 (0.16, 0.22)	0.19 (0.18, 0.21)	1.1 (1.07, 1.13)	1.1 (1.07, 1.12)
Respiratory lumen:tissue diffusive clearance rate (L/hr)	DResp	560 (44, 3300)	270 (130, 470)	1.37 (1.25, 1.61)	1.71 (1.52, 2.35)
Fat fractional compartment volume	VFatC	0.19 (0.088, 0.31)	0.16 (0.12, 0.21)	1.66 (1.23, 1.93)	1.65 (1.4, 1.9)
Gut fractional compartment volume	VGutC	0.02 (0.018, 0.022)	0.02 (0.019, 0.021)	1.07 (1.04, 1.08)	1.06 (1.05, 1.08)
Liver fractional compartment volume	VLivC	0.026 (0.018, 0.032)	0.026 (0.022, 0.03)	1.21 (1.12, 1.28)	1.2 (1.13, 1.26)
Rapidly perfused fractional compartment volume	VRapC	0.087 (0.079, 0.096)	0.088 (0.083, 0.093)	1.07 (1.05, 1.09)	1.06 (1.05, 1.08)
Fractional volume of respiratory lumen	VRespLumC	0.0024 (0.0018, 0.003)	0.0024 (0.0021, 0.0027)	1.18 (1.1, 1.23)	1.17 (1.12, 1.22)
Fractional volume of respiratory tissue	VRespEffC	0.00018 (0.00014, 0.00022)	0.00018 (0.00015, 0.00021)	1.18 (1.1, 1.24)	1.17 (1.13, 1.23)
Kidney fractional compartment volume	VKidC	0.0043 (0.0034, 0.0052)	0.0043 (0.0038, 0.0048)	1.15 (1.09, 1.19)	1.14 (1.1, 1.19)

Table 3-39. Prior and posterior uncertainty and variability in human PBPK model parameters (continued)

Parameter description	PBPK parameter	Prior population median: median (2.5%, 97.5%)	Posterior population median: median (2.5%, 97.5%)	Prior population GSD: median (2.5%, 97.5%)	Posterior population GSD: median (2.5%, 97.5%)
Blood fractional compartment volume	VBldC	0.077 (0.066, 0.088)	0.078 (0.072, 0.084)	1.1 (1.06, 1.13)	1.1 (1.07, 1.13)
Slowly perfused fractional compartment volume	VSlwC	0.45 (0.33, 0.55)	0.48 (0.43, 0.52)	1.18 (1.1, 1.24)	1.16 (1.12, 1.22)
Plasma fractional compartment volume	VPlasC	0.044 (0.037, 0.051)	0.044 (0.04, 0.048)	1.11 (1.08, 1.14)	1.11 (1.08, 1.14)
TCA body fractional compartment volume [not incl. blood+liver]	VBodC	0.75 (0.74, 0.77)	0.75 (0.74, 0.76)	1.01 (1.01, 1.01)	1.01 (1.01, 1.01)
TCOH/G body fractional compartment volume [not incl. liver]	VBodTCOHC	0.83 (0.82, 0.84)	0.83 (0.83, 0.83)	1.01 (1, 1.01)	1.01 (1, 1.01)
TCE blood:air partition coefficient	PB	9.6 (6.5, 13)	9.2 (8.2, 10)	1.18 (1.13, 1.26)	1.21 (1.16, 1.28)
TCE fat:blood partition coefficient	PFat	68 (46, 98)	57 (49, 66)	1.18 (1.11, 1.33)	1.18 (1.11, 1.3)
TCE gut:blood partition coefficient	PGut	2.6 (1.3, 5.3)	2.9 (1.9, 4.1)	1.37 (1.2, 1.78)	1.41 (1.21, 1.77)
TCE liver:blood partition coefficient	PLiv	4 (1.9, 8.5)	4.1 (2.7, 5.9)	1.37 (1.22, 1.81)	1.33 (1.19, 1.6)
TCE rapidly perfused:blood partition coefficient	PRap	2.6 (1.2, 5.7)	2.4 (1.8, 3.2)	1.37 (1.21, 1.78)	1.5 (1.25, 1.87)
TCE respiratory tissue:air partition coefficient	PResp	1.3 (0.65, 2.7)	1.3 (0.9, 1.9)	1.36 (1.19, 1.81)	1.32 (1.2, 1.56)
TCE kidney:blood partition coefficient	PKid	1.6 (1.1, 2.3)	1.6 (1.3, 1.9)	1.17 (1.1, 1.33)	1.15 (1.09, 1.25)
TCE slowly perfused:blood partition coefficient	PSlw	2.1 (1.2, 3.5)	2.3 (1.9, 2.8)	1.28 (1.14, 1.53)	1.51 (1.36, 1.66)
TCA blood:plasma concentration ratio	TCAPlas	0.78 (0.55, 15)	0.65 (0.6, 0.77)	1.08 (1.03, 1.53)	1.52 (1.23, 2.03)
Free TCA body:blood plasma partition coefficient	PBodTCA	0.45 (0.19, 8.1)	0.44 (0.33, 0.55)	1.36 (1.19, 1.75)	1.67 (1.38, 2.2)
Free TCA liver:blood plasma partition coefficient	PLivTCA	0.59 (0.24, 10)	0.55 (0.39, 0.77)	1.36 (1.18, 1.76)	1.65 (1.37, 2.16)
Protein:TCA dissociation constant (μmole/L)	kDissoc	180 (160, 200)	180 (170, 190)	1.05 (1.03, 1.09)	1.04 (1.03, 1.07)

Table 3-39. Prior and posterior uncertainty and variability in human PBPK model parameters (continued)

Parameter description	PBPK parameter	Prior population median: median (2.5%, 97.5%)	Posterior population median: median (2.5%, 97.5%)	Prior population GSD: median (2.5%, 97.5%)	Posterior population GSD: median (2.5%, 97.5%)
Maximum binding concentration ($\mu\text{mole/L}$)	B_{MAX}	830 (600, 1100)	740 (630, 880)	1.17 (1.1, 1.3)	1.16 (1.1, 1.28)
TCOH body:blood partition coefficient	PBodTCOH	0.89 (0.51, 1.7)	1.5 (1.3, 1.7)	1.29 (1.16, 1.64)	1.34 (1.25, 1.47)
TCOH liver:body partition coefficient	PLivTCOH	0.58 (0.32, 1.1)	0.63 (0.45, 0.87)	1.29 (1.16, 1.65)	1.29 (1.17, 1.5)
TCOG body:blood partition coefficient	PBodTCOG	0.67 (0.036, 16)	0.72 (0.3, 1.8)	1.38 (1.2, 2.42)	7.83 (4.86, 12.6)
TCOG liver:body partition coefficient	PLivTCOG	1.8 (0.11, 28)	3.1 (0.87, 8.1)	1.38 (1.19, 2.04)	4.94 (2.73, 8.58)
DCVG effective volume of distribution	VDCVG	73 (5.2, 36000)	6.1 (5.4, 7.3)	1.27 (1.08, 1.95)	1.1 (1.07, 1.16)
TCE stomach absorption coefficient (/hr)	kAS	1.4 (1.4, 1.4)	1.4 (1.4, 1.4)	1 (1, 1)	1 (1, 1)
TCE stomach-duodenum transfer coefficient (/hr)	kTSD	1.4 (1.4, 1.4)	1.4 (1.4, 1.4)	1 (1, 1)	1 (1, 1)
TCE duodenum absorption coefficient (/hr)	kAD	0.75 (0.75, 0.75)	0.75 (0.75, 0.75)	1 (1, 1)	1 (1, 1)
TCA stomach absorption coefficient (/hr)	kASTCA	0.58 (0.0022, 210)	3 (0.061, 180)	4.26 (2.13, 17.6)	5.16 (2.57, 22.3)
TCOH stomach absorption coefficient (/hr)	kASTCOH	0.49 (0.0024, 210)	7.6 (0.11, 150)	4.19 (2.22, 21.5)	5.02 (2.44, 18.5)
V_{MAX} for hepatic TCE oxidation (mg/hr)	V_{MAX}	430 (130, 1500)	190 (130, 290)	1.98 (1.69, 2.31)	2.02 (1.77, 2.38)
K_{M} for hepatic TCE oxidation (mg/L)	K_{M}	3.7 (0.22, 63)	0.18 (0.078, 0.4)	2.74 (2.1, 5.62)	4.02 (2.9, 5.64)
Fraction of hepatic TCE oxidation not to TCA+TCOH	FracOther	0.12 (0.0066, 0.7)	0.11 (0.024, 0.23)	1.4 (1.11, 2.38)	2.71 (1.37, 5.33)
Fraction of hepatic TCE oxidation to TCA	FracTCA	0.19 (0.036, 0.56)	0.035 (0.024, 0.05)	2.55 (1.51, 3.96)	2.25 (1.89, 2.87)
V_{MAX} for hepatic TCE GSH conjugation (mg/hr)	$V_{\text{MAX}}\text{DCVG}$	100 (0.0057, 690,000)	340 (110, 1,100)	1.91 (1.55, 3.76)	6.18 (3.35, 11.3)
K_{M} for hepatic TCE GSH conjugation (mg/L)	$K_{\text{M}}\text{DCVG}$	3.1 (0.21, 42)	3.6 (1.2, 11)	1.52 (1.26, 2.91)	4.2 (2.48, 8.01)
V_{MAX} for renal TCE GSH conjugation (mg/hr)	$V_{\text{MAX}}\text{KidDCVG}$	220 (0.028, 6,700,000)	2.1 (0.17, 9.3)	1.86 (1.51, 3.33)	4.02 (1.57, 33.9)

Table 3-39. Prior and posterior uncertainty and variability in human PBPK model parameters (continued)

Parameter description	PBPK parameter	Prior population median: median (2.5%, 97.5%)	Posterior population median: median (2.5%, 97.5%)	Prior population GSD: median (2.5%, 97.5%)	Posterior population GSD: median (2.5%, 97.5%)
K _M for renal TCE GSH conjugation (mg/L)	K _M KidDCVG	2.7 (0.14, 41)	0.76 (0.29, 5.8)	1.5 (1.27, 2.56)	1.49 (1.27, 2.32)
V _{MAX} for tracheo-bronchial TCE oxidation (mg/hr)	V _{MAX} Clara	25 (1, 260)	18 (3.8, 41)	2.25 (1.85, 3.25)	2.9 (2.12, 6.49)
K _M for tracheo-bronchial TCE oxidation (mg/L)	K _M Clara	0.019 (0.0017, 0.5)	0.31 (0.057, 1.4)	1.48 (1.25, 2.39)	10.8 (1.99, 37.6)
Fraction of respiratory metabolism to systemic circ.	FracLungSys	0.75 (0.051, 0.99)	0.96 (0.86, 0.99)	1.12 (1, 1.75)	1.02 (1, 1.1)
V _{MAX} for hepatic TCOH→TCA (mg/hr)	V _{MAX} TCOH	42 (0.77, 2,200)	9.2 (5.5, 20)	1.83 (1.46, 3.43)	3.15 (2.3, 5.44)
K _M for hepatic TCOH→TCA (mg/L)	K _M TCOH	5 (0.23, 81)	2.2 (1.3, 4.5)	1.49 (1.25, 2.57)	2.58 (1.75, 4.5)
V _{MAX} for hepatic TCOH→TCOG (mg/hr)	V _{MAX} Gluc	720 (12, 50,000)	900 (340, 2,000)	1.83 (1.48, 3.5)	2.29 (1.84, 4.57)
K _M for hepatic TCOH→TCOG (mg/L)	K _M Gluc	10 (0.53, 190)	130 (47, 290)	1.5 (1.25, 2.6)	1.58 (1.26, 3.69)
Rate constant for hepatic TCOH→other (/hr)	kMetTCOH	0.83 (0.035, 10)	0.25 (0.042, 0.7)	1.5 (1.26, 3)	5.13 (2.72, 16.7)
Rate constant for TCA plasma→urine (/hr)	kUrnTCA	0.26 (0.038, 4)	0.11 (0.083, 0.15)	1.48 (1.29, 2.29)	1.86 (1.58, 2.28)
Rate constant for hepatic TCA→other (/hr)	kMetTCA	0.19 (0.01, 2.6)	0.096 (0.038, 0.19)	1.48 (1.26, 2.57)	2.52 (1.79, 4.34)
Rate constant for TCOG liver→bile (/hr)	kBile	1.2 (0.059, 16)	2.5 (1.1, 6.9)	1.47 (1.25, 2.75)	1.56 (1.27, 3.21)
Lumped rate constant for TCOG bile→TCOH liver (/hr)	kEHR	0.074 (0.004, 1.4)	0.053 (0.033, 0.087)	1.52 (1.26, 2.64)	1.72 (1.35, 2.51)
Rate constant for TCOG→urine (/hr)	kUrnTCOG	2.9 (0.061, 260)	2.4 (0.83, 7)	1.75 (1.4, 3.31)	18.7 (11.6, 31.8)
Rate constant for hepatic DCVG→DCVC (/hr)	kDCVG	0.044 (0.000063, 22)	2.5 (1.9, 3.4)	1.48 (1.25, 2.83)	1.51 (1.3, 1.86)
Lumped rate constant for DCVC→urinary NAcDCVC (/hr)	kNAT	0.00085 (0.000055, 0.041)	0.0001 (0.000047, 0.0007)	1.51 (1.25, 2.34)	1.47 (1.24, 2.48)
Rate constant for DCVC bioactivation (/hr)	kKidBioact	0.0022 (0.000095, 0.079)	0.023 (0.0062, 0.061)	1.51 (1.25, 2.57)	1.52 (1.25, 2.69)

Table 3-40. CI widths (ratio of 97.5–2.5% estimates) and fold-shift in median estimate for the PBPK model population median parameters, sorted in order of decreasing CI width^a

Mouse				Rat				Human			
PBPK parameter	Width of CI on population median		Fold-shift in population median	PBPK parameter	Width of CI on population median		Fold-shift in population median	PBPK parameter	Width of CI on population median		Fold-shift in population median
	Prior	Posterior			Prior	Posterior			Prior	Posterior	
K _M DCVG	2,230,000,000	13,400,000	×8.8	K _M DCVG	1,500,000	5,800	×4.29	kASTCA	94,300	3,040	×5.18
K _M KidDCVG	1,170,000,000	3,540,000	×1.05	V _{MAX} DCVG	71,100	2,130	×2.86	kASTCOH	85,900	1,420	×15.6
V _{MAX} DCVG	400,000	46,200	÷6.18	kUrnTCOG	16,700	822	×1.04	V _{MAX} -KidDCVG	236,000,000	55.1	÷105
V _{MAX} KidDCVG	357,000	11,000	÷12.8	PBodTCOG	666	172	×3.43	K _M Clara	289	23.9	×16.2
kASTCA	89,300	374	×6.3	kASTCA	98,200	95.7	×1.69	K _M KidDCVG	287	20	÷3.48
kTSD	1,190	51.1	×3.26	kTSD	1,130	61.8	×2.29	kMetTCOH	289	16.6	÷3.28
kEHR	412,000	42.1	÷5.43	kAS	91,000	60.2	×3.41	kNAT	756	15.1	÷8.14
FracOther	567	39.5	÷18.5	K _M KidDCVG	1,130,000	58.6	÷1880	V _{MAX} Clara	255	10.6	÷1.41
K _M Clara	351,000	37.5	÷134	kKidBioact	366,000	35.6	÷13.3	kKidBioact	833	9.91	×10.5
kAS	91,900	35.9	×1	K _M Clara	406	29.9	×1.53	V _{MAX} DCVG	122,000,000	9.78	×3.29
kUrnTCOG	4,050,000	29.9	×11.8	V _{MAX} KidDCVG	48,500	27.5	÷15.6	FracOther	106	9.75	÷1.09
B _{MAX}	81.8	24.4	×1.66	kMetTCOH	891	26.4	÷1.41	PLivTCOG	253	9.32	×1.77
K _M Gluc	344,000	24.3	×16.3	kAD	115,000	26.3	÷5.53	K _M DCVG	198	9.13	×1.18
kAD	84,900	23.8	÷4.53	K _M TCOH	781	26	×18.7	kUrnTCOG	4,290	8.5	÷1.19
kDissoc	60.3	21.8	×1.33	kNAT	351,000	22.7	÷50.2	kBile	274	6.54	×2.01
V _{MAX} Clara	131	15	×1.75	kEHR	1,160	21.9	×134	K _M Gluc	365	6.07	×13.4
kMetTCOH	35,500,000	12.1	×47.4	K _M Gluc	562	17.1	÷4.98	PBodTCOG	454	5.85	×1.08
kBile	390,000	11.3	×8.23	V _{MAX} Clara	305	16.5	÷1.21	V _{MAX} Gluc	4,330	5.71	×1.25
K _M TCOH	29,600,000	10.5	÷1.47	FracLungSys	36.7	16.3	÷1.12	K _M	288	5.1	÷20.5
V _{MAX} Gluc	23,600,000	8.28	×41.1	PLivTCOG	501	14.8	×8.07	kMetTCA	248	4.89	÷1.94

Table 3-40. CI widths (ratio of 97.5–2.5% estimates) and fold-shift in median estimate for the PBPK model population median parameters, sorted in order of decreasing CI width^a (continued)

Mouse				Rat				Human			
PBPK parameter	Width of CI on population median		Fold-shift in population median	PBPK parameter	Width of CI on population median		Fold-shift in population median	PBPK parameter	Width of CI on population median		Fold-shift in population median
	Prior	Posterior			Prior	Posterior			Prior	Posterior	
PBodTCOG	4,770	6.27	÷1.95	kBile	588	14.8	× 9.67	DResp	74.3	3.71	÷2.06
V _{MAX} TCOH	27,100,000	5.78	×1.8	FracOther	331	11.9	× 10.7	V _{MAX} TCOH	2,900	3.62	÷ 4.56
K _M	386	5.76	÷ 12.5	V _{MAX} TCOH	550	8.25	÷1.06	K _M TCOH	359	3.48	÷2.33
kUrnTCA	4,540	5.76	÷ 10.2	V _{MAX} Gluc	740	7.79	÷2.4	kEHR	339	2.62	÷1.39
FracLungSys	608	5.55	×2.27	kMetTCA	507	6.93	÷1.61	V _{MAX}	11.5	2.27	÷2.33
kMetTCA	316,000	4.59	× 12	B _{MAX}	16.2	5.79	×1	PResp	4.1	2.16	÷1.01
PLivTCOG	4,860	3.99	×1.04	DResp	180	4.81	×2.12	PLiv	4.44	2.14	×1.02
DResp	475,000	3.64	× 147	PLivTCOH	11.5	4.7	÷1.09	QLivC	3.46	2.11	÷1.62
PLivTCA	58.3	2.88	×1	PBodTCOH	12.1	4.03	×1.03	PGut	4.21	2.1	×1.11
PResp	4	2.85	÷1.07	kDissoc	8.38	3.85	×1.04	FracTCA	15.5	2.06	÷ 5.37
PRap	3.78	2.79	÷1.03	FracTCA	28.1	3.85	÷ 4.27	PLivTCA	42.6	1.98	÷1.07
PGut	4.33	2.77	÷1.25	PLivTCA	13.3	3.49	×1.37	PLivTCOH	3.52	1.93	×1.08
V _{MAX}	10.7	2.67	÷1.58	kUrnTCA	219	3.28	÷2	kDCVG	344,000	1.8	× 55.7
PBodTCA	62.6	2.55	×1.14	PBodTCA	12	2.8	×1.09	kUrnTCA	105	1.79	÷2.32
PSlw	4.04	2.54	÷1.06	PResp	4.32	2.6	×1.04	VFatC	3.49	1.76	÷1.21
PLiv	3.87	2.5	×1.26	K _M	123	2.56	÷ 24	PRap	4.66	1.74	÷1.09
FracTCA	3,060	2.49	×1.49	PRap	4.01	2.53	÷1.01	QFatC	3.7	1.7	÷1.19
TCAPlas	40.6	2.38	×1.46	PGut	4.35	2.16	÷1.17	PBodTCA	42.9	1.7	÷1.04
PKid	4.78	2.37	×1.2	V _{MAX}	9.5	1.98	÷1.11	PSlw	2.9	1.5	×1.11
QFatC	3.62	2.26	×1.02	QRapC	2.77	1.97	÷1	PKid	2.05	1.49	÷1.01
PLivTCOH	3.19	2.13	×1.48	VFatC	3.58	1.96	÷1	QP	2.97	1.48	×1.16
PBodTCOH	3.41	2.01	÷1.27	PKid	2.89	1.85	÷1.11	QSlwC	2.25	1.48	÷1.26
QKidC	2.39	1.91	÷1.01	QP	3.59	1.79	÷1.38	QC	2.04	1.39	÷1.19
PFat	3.01	1.89	÷1.01	PSlw	2.76	1.79	×1.28	B _{MAX}	1.92	1.38	÷1.12
QSlwC	2.04	1.88	÷1.02	PFat	2.91	1.77	×1.16	VLivC	1.79	1.36	×1.01
VPlasC	2.18	1.87	÷1.17	QSlwC	2.19	1.69	÷1.06	PFat	2.13	1.34	÷1.2
VFatC	3.49	1.83	×1.25	QFatC	3.47	1.66	×1.14	VDCVG	6,820	1.34	÷ 12
QP	2.75	1.82	÷1.02	VPlasC	2.17	1.55	×1.03	VRespEffC	1.66	1.33	÷1.02
VLivC	1.85	1.6	÷1.16	PB	2.37	1.51	÷1.15	PBodTCOH	3.32	1.32	×1.68

Table 3-40. CI widths (ratio of 97.5–2.5% estimates) and fold-shift in median estimate for the PBPK model population median parameters, sorted in order of decreasing CI width^a (continued)

Mouse				Rat				Human			
PBPK parameter	Width of CI on population median		Fold-shift in population median	PBPK parameter	Width of CI on population median		Fold-shift in population median	PBPK parameter	Width of CI on population median		Fold-shift in population median
	Prior	Posterior			Prior	Posterior			Prior	Posterior	
QC	2.1	1.59	×1.2	QC	1.64	1.43	×1.15	VRespLumC	1.65	1.31	÷1
PB	2.3	1.54	÷1.07	VRespEffC	1.56	1.43	÷1	TCAPlas	26.9	1.29	÷1.21
QLivC	1.55	1.42	×1.02	VRespLumC	1.56	1.41	×1	VKidC	1.54	1.28	÷1.01
QRapC	1.51	1.41	÷1.03	VLivC	1.57	1.4	÷1.05	PB	2.04	1.28	÷1.04
VGutC	1.38	1.3	÷1.01	PLiv	1.67	1.37	×1.05	QRapC	2.22	1.25	×1.34
VBldC	1.34	1.27	÷1.02	QLivC	1.53	1.34	×1.04	QGutC	1.59	1.23	÷1.19
VRespLumC	1.32	1.26	÷1.01	VKidC	1.47	1.33	×1.01	VSlwC	1.66	1.21	×1.07
VRespEffC	1.31	1.26	÷1	QKidC	1.39	1.28	×1	VPlasC	1.39	1.2	×1.01
QGutC	1.52	1.24	×1.15	VGutC	1.38	1.28	÷1.01	QKidC	1.36	1.17	÷1
VKidC	1.29	1.24	÷1	VBldC	1.34	1.25	×1.01	VBldC	1.34	1.17	×1.02
VRapC	1.3	1.23	÷1.01	VRapC	1.34	1.23	×1	FracLungSys	19.4	1.14	×1.29
VSlwC	1.19	1.11	÷1.01	QGutC	1.53	1.22	×1.14	VRapC	1.22	1.12	×1
VBodC	1.05	1.03	×1.01	TCAPlas	1.6	1.21	÷1.01	kDissoc	1.23	1.12	÷1.01
VBodTCOHC	1.04	1.03	×1.01	VSlwC	1.15	1.09	×1	VGutC	1.22	1.11	×1.01
				VBodC	1.04	1.03	×1	VBodC	1.04	1.02	÷1
				VBodTCOHC	1.02	1.01	×1	VBodTCOHC	1.02	1.01	÷1

^aShifts in the median estimate greater than threefold are in bold to denote larger shifts between the prior and posterior distributions

However, for some parameters, the posterior distributions in the population medians had CIs >100-fold. In mice, the absorption parameter for TCA still had posterior CI of 400-fold, reflecting the fact that the absorption rate is poorly estimated from the few available studies with TCA dosing. In addition, mouse metabolism parameters for GSH conjugation have posterior CIs >10,000-fold, reflecting the lack of any direct data on GSH conjugation in mice. In rats, two parameters related to TCOH and TCOG had CIs between 100- and 1,000-fold, reflecting the poor identifiability of these parameters given the available data. In humans, only the oral absorption parameters for TCA and TCOH had CIs >100-fold, reflecting the fact that the absorption rate is poorly estimated from the few available studies with TCOH and TCA dosing.

In terms of general consistency between prior and posterior distributions, in most cases, the central estimate of the population median shifted by less than threefold. In almost all of the cases that the shift was greater (see bold entries in Table 3-40), the prior distribution had a wide distribution, with CI greater (sometimes substantially greater) than 100-fold. The only exception was the fraction of TCE oxidation directly producing TCA, which shifted by fourfold in rats and fivefold in mice, with prior CIs of 28- and 16-fold, respectively. These shifts are still relatively modest in comparison to the prior CI, and moreover, the posterior CI is quite narrow (fourfold in rats, twofold in humans), suggesting that the parameter is well identified by the in vivo data.

In addition, there were only a few cases in which the interquartile regions of the prior and posterior distributions did not overlap. In most of these cases, including the diffusion rate from respiratory lumen to tissue, the K_M values for renal TCE GSH conjugation and respiratory TCE oxidation, and several metabolite kinetic parameters, the prior distributions themselves were noninformative. For a noninformative prior, the lack of overlap would only be an issue if the posterior distributions were affected by the truncation limit, which was not the case. The only other parameter for which there was a lack of interquartile overlap between the prior and posterior distribution was the K_M for hepatic TCE oxidation in mice and in rats, though the prior and posterior 95% CIs did overlap within each species. As discussed Section 3.3, there is some uncertainty in the extrapolation of in vitro K_M values to in vivo values (within the same species). In addition, in mice, it has been known for some time that K_M values appear to be discordant among different studies ([Greenberg et al., 1999](#); [Abbas and Fisher, 1997](#); [Fisher et al., 1991](#)).

In terms of estimates of population variability, for the vast majority of parameters, the posterior estimate of the population GSD was either twofold or less, indicating modest variability. In some cases, while the posterior population GSD was greater than twofold, it was similar to the prior estimate of the population GSD, indicating limited additional informative data on variability. This was the case for oral absorption parameters, which are expected to be highly variable because the current model lumps parameters for different oral dosing vehicles together, and a relatively wide prior distribution was given. In addition, in some cases, this was due to in vitro data showing a higher degree of variability. Examples of this include TCA plasma binding parameters in the mouse, and the V_{MAX} for hepatic oxidation and the fraction of

oxidation to TCA in humans. In a few other cases, the in vivo data appeared to indicate greater than twofold variability between subjects, and these are discussed in more detail below.

In the mouse, the two parameters for which this is the case are the V_{MAX} for respiratory tract oxidation and the urinary excretion rate for TCOG. In the first case, the variability is driven by the need for a higher respiratory tract V_{MAX} for males in the Fisher et al. (1991) study as compared to other studies. In the second case, it is driven by the relatively low estimate of urinary excretion of TCOG in the Abbas and Fisher (1997), Abbas et al. (1997), and Greenberg et al. (1999) studies as compared with the relatively high estimate in Green and Prout (1985) and Prout et al. (1985).

In the rat, the two parameters for which the in vivo data suggest greater than twofold variability are the fraction of oxidation not producing TCA or TCOH, and the V_{MAX} for respiratory tract oxidation. In the first case, this is driven by three studies that appeared to require greater (Bernauer et al., 1996; Kimmerle and Eben, 1973b) or lower (Hissink et al., 2002) estimates for this parameter as compared with the other studies. Nonetheless, the degree of variability is not much greater than twofold, with a central estimate population GSD of 2.15-fold. In the case of the V_{MAX} for respiratory tract oxidation, two studies appeared to require higher (Fisher et al., 1989) or lower (Simmons et al., 2002) values for this parameter as compared with the other studies.

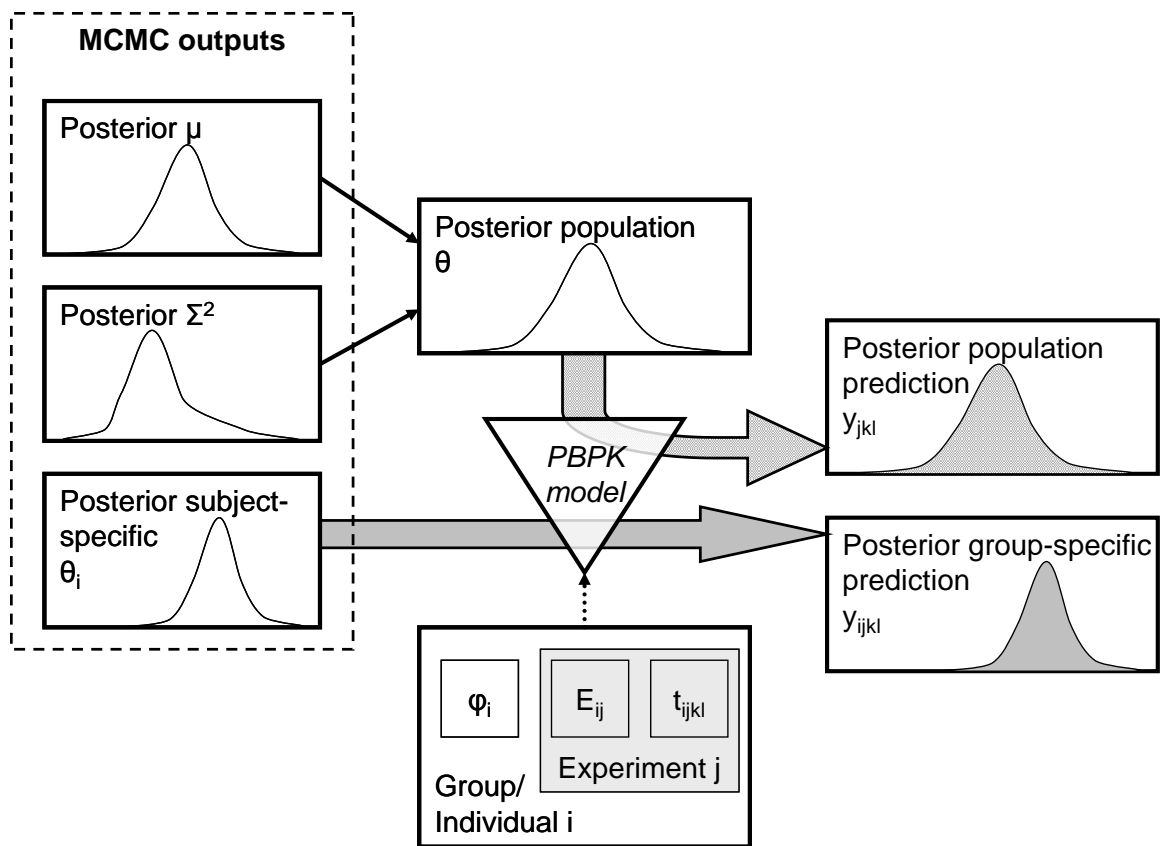
In humans, as would be expected, more parameters appeared to exhibit greater than twofold variability. In terms of distribution, the partition coefficients for TCOG had rather large posterior estimates for the population GSD of eightfold for the body and fivefold for the liver. In terms of the body, a few of the subjects in Fisher et al. (1998) and all of the subjects in Monster et al. (1976) appeared to require much higher partition coefficients for TCOG. For the liver, the variability did not have a discernable trend across studies. In addition, almost all of the metabolism and clearance parameters had posterior estimates for population variability of greater than a twofold GSD. The largest of these was the urinary excretion rate for TCOG, with a GSD of 19-fold. In this case, the variability was driven by individuals in the Chiu et al. (2007) 1 ppm study, who were predicted to have much lower rate of urinary excretion as compared to that estimated in the other, higher exposure studies.

In sum, the Bayesian analysis of the updated PBPK model and data exhibited no major inconsistencies in prior and posterior parameter distributions. The most significant issue in terms of population central estimates was the K_M for hepatic oxidative metabolism, for which the posterior estimates were low compared to, albeit somewhat uncertain, in vitro estimates, and it could be argued that a wider prior distribution would have been better. However, the central estimates were not at or near the truncation boundary, so it is unlikely that wider priors would change the results substantially. In terms of population variability, in rodents, the estimates of variability were generally modest, which is consistent with more homogeneous and controlled experimental subjects and conditions, whereas the estimates of human population variability

were greater—particularly for metabolism and clearance. Overall, there were no indications based on this evaluation of prior and posterior distributions either that prior distributions were overly restrictive or that model specification errors led to pathological parameter estimates.

3.5.6.3. Comparison of Model Predictions With Data

Comparisons of model predictions and data for each species are discussed in the subsections below. First, as an overall summary, for each species and each output measurement, the data and predictions generated from a random sample of the MCMC chain are scatter-plotted to show the general degree of consistency between data and predictions. Next, as with the Hack et al. (2006) model, the sampled subject-specific parameters were used to generate predictions for comparison to the calibration data (see Figure 3-8). Thus, the predictions for a particular data set are conditioned on the posterior parameter distributions for same data set. Because these parameters were “optimized” for each experiment, these subject-specific predictions should be accurate by design—and, on the whole, were so. In addition, the “residual-error” estimate for each measurement (see Table 3-41) provides some quantitative measure of the degree to which there were deviations due to intrastudy variability and model misspecification, including any difficulties fitting multiple dose levels in the same study using the same model parameters.



Two sets of posterior predictions were generated: population predictions (diagonal hashing) and subject-specific predictions (vertical hashing). (Same as Figure A-2 in Appendix A)

Figure 3-8. Schematic of how posterior predictions were generated for comparison with experimental data.

Table 3-41. Estimates of the residual-error

Measurement abbreviation	Measurement description	GSD for "residual" error (median estimate)		
		Mouse	Rat	Human
RetDose	Retained TCE dose (mg)	-	-	1.13
CAIvPPM	TCE concentration in alveolar air (ppm)	-	-	1.44~1.83
CIInhPPM	TCE concentration in closed-chamber (ppm)	1.18	1.11~1.12	-
CMixExh	TCE concentration in mixed exhaled air (mg/L)	-	1.5	-
CArt	TCE concentration in arterial blood (mg/L)	-	1.17~1.52	-
CVen	TCE concentration in venous blood (mg/L)	2.68	1.22~4.46	1.62~2.95
CBldMix	TCE concentration in mixed arterial and venous blood (mg/L)	1.61	1.5	-
CFat	TCE concentration in fat (mg/L)	2.49	1.85~2.66	-
CGut	TCE concentration in gut (mg/L)	-	1.86	-
CKid	TCE concentration in kidney (mg/L)	2.23	1.47	-
CLiv	TCE concentration in liver (mg/L)	1.71	1.67~1.78	-
CMus	TCE concentration in muscle (mg/L)	-	1.65	-
AExhpost	Amount of TCE exhaled postexposure (mg)	1.23	1.12~1.17	-

Table 3-41. Estimates of the residual-error (continued)

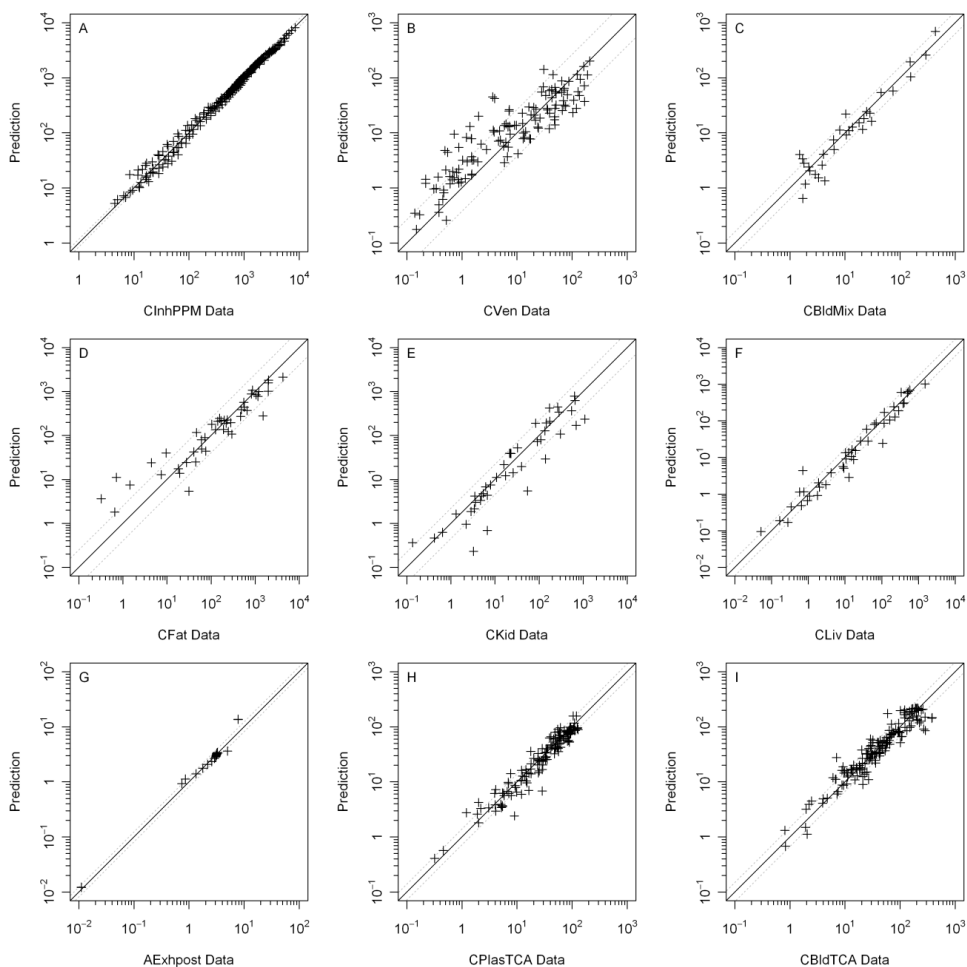
Measurement abbreviation	Measurement description	GSD for "residual" error (median estimate) ^a		
		Mouse	Rat	Human
CPlasTCA	TCA concentration in plasma (mg/L)	1.40	1.13~1.21	1.12~1.17
CBldTCA	TCA concentration in blood (mg/L)	1.49	1.13~1.59	1.12~1.49
CLivTCA	TCA concentration in liver (mg/L)	1.34	1.67	-
AUrnTCA	Cumulative amount of TCA excreted in urine (mg)	1.34	1.18~1.95	1.11~1.54
AUrnTCA_collect	Cumulative amount of TCA collected in urine (noncontinuous sampling) (mg)	-	-	2~2.79
CTCOH	Free TCOH concentration in blood (mg/L)	1.54	1.14~1.64	1.14~ 2.1
CLivTCOH	Free TCOH concentration in liver (mg/L)	1.59	-	-
TotCTCOH	Total TCOH concentration in blood (mg/L)	1.85	1.49	1.2~1.69
ABileTCOG	Cumulative amount of bound TCOH excreted in bile (mg)	-	2.13	-
CTCOG	Bound TCOH concentration in blood	-	2.76	-
CTCOGTCOH	Bound TCOH concentration in blood in free TCOH equivalents	1.49	-	-
CLivTCOGTCOH	Bound TCOH concentration in liver in free TCOH equivalents (mg/L)	1.63	-	-
AUrnTCOGTCOH	Cumulative amount of total TCOH excreted in urine (mg)	1.26	1.12~ 2.27	1.11~1.13
AUrnTCOGTCOH_collect	Cumulative amount of total TCOH collected in urine (noncontinuous sampling) (mg)	-	-	1.3~1.63
AUrnTCTotMole	Cumulative amount of TCA+total TCOH excreted in urine (mmol)	-	1.12~1.54	-
CDCVGmol	DCVG concentration in blood (mmol/L)	-	-	1.53
AUrnNDCVC	Cumulative amount of NAcDCVC excreted in urine (mg)	-	1.17	1.17

^aValues higher than twofold are in bold.

Next, only samples of the population parameters (means and variances) were used, and new subjects were sampled from appropriate distribution using these population means and variances (see Figure 3-8). That is, the predictions were only conditioned on the population-level parameters distributions, representing an “average” over all of the data sets, and not on the specific predictions for that data set. These “new” subjects then represent the predicted population distribution, incorporating variability in the population as well as uncertainty in the population means and variances. Because of the limited amount of mouse data, all available data for that species were utilized for calibration, and there were no data available for “out-of-sample” evaluation (often referred to as “validation data,” but this term is not used here due to ambiguities as to its definition). In rats, several studies that contained primarily blood TCE data, which were abundant, were used for out-of-sample evaluation. In humans, there were substantial individual and aggregated (mean of individuals in a study) data that were available for out-of-sample evaluation, as computational intensity limited the number of individuals who could be used in the MCMC-based calibration.

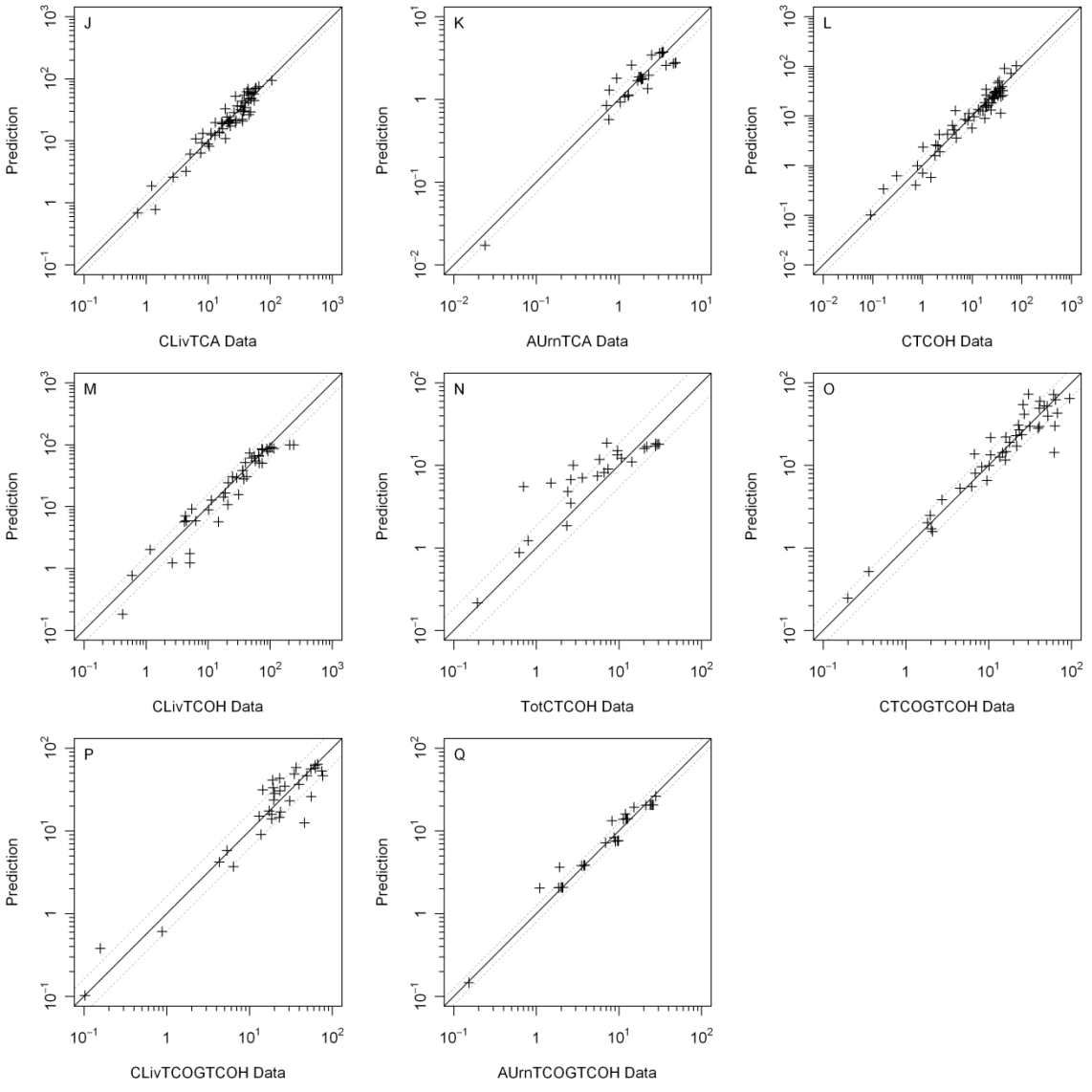
3.5.6.3.1. Mouse model and data

Each panel of Figure 3-9 shows a scatter plot of the calibration data and a random posterior prediction for each of the measured endpoint. The endpoint abbreviations are listed in Table 3-41, as are the implied GSDs for the “residual” errors, which include intrastudy variability, interindividual variability, and measurement and model errors. The residual-error GSDs are also shown as grey dotted lines in Figure 3-9. Table 3-42 provides an evaluation of the predictions of the mouse model for each data set, with figures showing individual time-course data and predictions in Appendix A.



Each panel shows results for a different measurement. The solid line represents prediction = data, and the grey dotted lines show prediction = data \times GSD_{err} and data \div GSD_{err}, where GSD_{err} is the median estimate of the residual-error GSD shown in Table 3-41.

Figure 3-9. Comparison of mouse data and PBPK model predictions from a random posterior sample.



Each panel shows results for a different measurement. The solid line represents prediction = data, and the grey dotted lines show prediction = data × GSD_{err} and data ÷ GSD_{err} , where GSD_{err} is the median estimate of the residual-error GSD shown in Table 3-41.

Figure 3-9 (continued). Comparison of mouse data and PBPK model predictions from a random posterior sample.

Table 3-42. Summary comparison of updated PBPK model predictions and in vivo data in mice

Study	Exposure(s)	Discussion
Abbas and Fisher (1997)	TCE gavage (corn oil)	Generally, model predictions were quite good, especially with respect to tissue concentrations of TCE, TCA, and TCOH. There were some discrepancies in TCA and TCOG urinary excretion and TCA and TCOG concentrations in blood due to the requirement (unlike in Hack et al., 2006) that all experiments in the same study utilize the same parameters. Thus, for instance, TCOG urinary excretion was accurately predicted at 300 mg/kg, underpredicted at 600 mg/kg, overpredicted at 1,200 mg/kg, and underpredicted again at 2,000 mg/kg, suggesting significant intraexperimental variability (not addressed in the model). Population predictions were quite good, with the almost all of the data within the 95% CI of the predictions, and most within the interquartile region.
Abbas et al. (1997)	TCOH, TCA i.v.	Both subject-specific and population predictions were quite good. Urinary excretion, which was overpredicted by the Hack et al. (2006) model, was accurately predicted due to the allowance of additional “untracked” clearance. In the case of population predictions, almost all of the data were within the 95% CI of the predictions, and most within the interquartile region.
Fisher and Allen (1993)	TCE gavage (corn oil)	Both subject-specific and population predictions were quite good. Some discrepancies in the time-course of TCE blood concentrations were evidence across doses in the subject-specific predictions, but not in the population predictions, suggesting significant intrasubject variability (not addressed in the model).
Fisher et al. (1991)	TCE inhalation	Blood TCE levels during and following inhalation exposures were still overpredicted at the higher doses. However, there was the stringent requirement (absent in Hack et al., 2006) that the model utilize the same parameters for all doses and in both the closed and open-chamber experiments. Moreover, the Hack et al. (2006) model required significant differences in the parameters for the different closed-chamber experiments, while predictions here were accurate utilizing the same parameters across different initial concentrations. These conclusions were the same for subject-specific and population predictions (e.g., TCE blood levels remained overpredicted in the later case).
Green and Prout (1985)	TCE gavage (corn oil)	Both subject-specific and population predictions were adequate, though the data collection was sparse. In the case of population predictions, almost all of the data were within the 95% CI of the predictions, and about half within the interquartile region.
Greenberg et al. (1999)	TCE inhalation	Model predictions were quite good across a wide variety of measures that included tissue concentrations of TCE, TCA, and TCOH. However, as with the Hack et al. (2006) predictions, TCE blood levels were overpredicted by up to twofold. Population predictions were quite good, with the exception of TCE blood levels. Almost all of the other data was within the 95% CI of the predictions, and most within the interquartile region.
Larson and Bull (1992a)	TCE gavage (aqueous)	Both subject-specific and population predictions were quite good, though the data collection was somewhat sparse. In the case of population predictions, all of the data were within the 95% CI of the predictions.
Larson and Bull (1992b)	TCA gavage (aqueous)	Both subject-specific and population predictions were quite good. In the case of population predictions, most of the data were within the interquartile region.
Merdink et al. (1998)	TCE i.v.	Both subject-specific and population predictions were quite good, though the data collection was somewhat sparse. In the case of population predictions, all of the data were within the 95% CI of the predictions.

Table 3-42. Summary comparison of updated PBPK model predictions and in vivo data in mice (continued)

Study	Exposure(s)	Discussion
Prout et al. (1985)	TCE gavage (corn oil)	Both subject-specific and population predictions were adequate, though there was substantial scatter in the data due to the use of single animals at each data point.
Templin et al. (1993)	TCE gavage (aqueous)	Both subject-specific and population predictions were quite good. With respect to population predictions, almost all of the other data was within the 95% CI of the predictions, and most within the interquartile region.

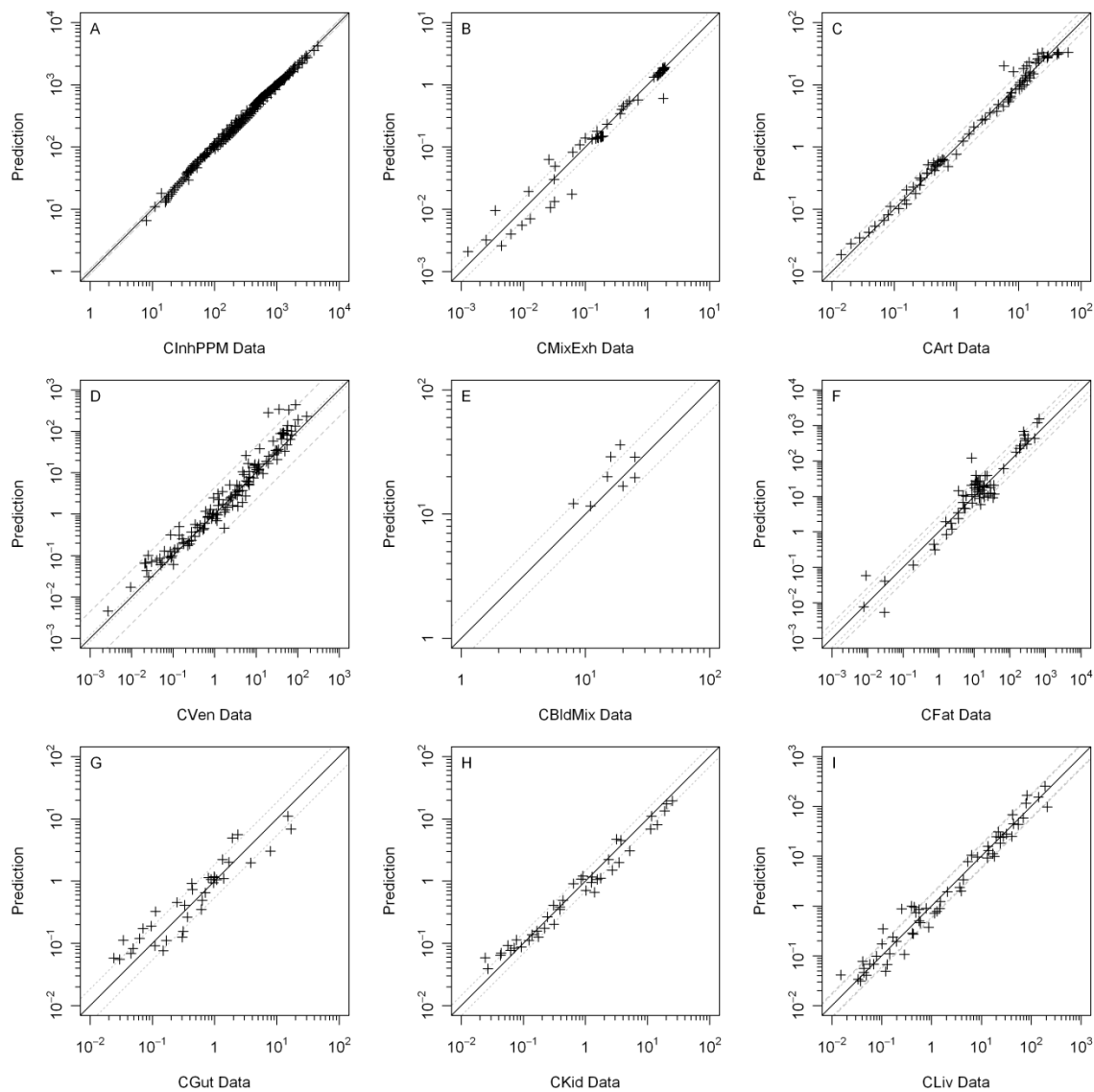
In terms of total metabolism, closed-chamber data (see Figure 3-9, panel A) were fit accurately with the updated model, with a small residual-error GSD of 1.18. While the previous analyses of Hack et al. (2006) allowed for each chamber experiment to be fit with different parameters, the current analysis made the more restrictive assumption that all experiments in a single study utilize the same parameters. Furthermore, the accuracy of closed-chamber predictions did not require the very high values for cardiac output that were used by Fisher et al. (1991), confirming the suggestion (discussed in Appendix A) that additional respiratory metabolism would resolve this discrepancy. The accurate model means that uncertainty with respect to possible wash-in/wash-out, respiratory metabolism, and extrahepatic metabolism could be well characterized. For instance, the absence of in vivo data on GSH metabolism in mice means that this pathway remains relatively uncertain; however, the current model should be reliable for estimating lower and upper bounds on the GSH pathway flux.

In terms of the parent compound TCE (see Figure 3-9, panels B-G), the parent PBPK model (for TCE) appears to now be robust, with the exception of the remaining overprediction of TCE in blood following inhalation exposure. As expected, the venous-blood TCE concentration had the largest residual-error, with a GSD of 2.7, reflecting largely the difficulty in fitting TCE blood levels following inhalation exposure. In addition, the fat and kidney TCE concentrations also are somewhat uncertain, with a GSD for the residual-error of 2.5 and 2.2, respectively. These tissues were only measured in two studies, Abbas and Fisher (1997) and Greenberg et al. (1999), and the residual-error reflects the difficulties in simultaneously fitting the model to the different dose levels with the same parameters. Residual-error GSDs for other TCE measurements were less than twofold. Thus, most of the problems previously encountered with the Abbas and Fisher (1997) gavage data were solved by allowing absorption from both the stomach and duodenal compartments. Notably, the addition of possible wash-in/wash-out, respiratory metabolism, and extrahepatic metabolism (i.e., kidney GSH conjugation) was insufficient to remove the long-standing discrepancy of PBPK models overpredicting TCE blood levels from mouse inhalation exposures, suggesting another source of model or experimental error is the cause. However, the availability of tissue concentration levels of TCE somewhat ameliorates this limitation.

In terms of TCA and TCOH, the overall mass balance and metabolic disposition to these metabolites also appeared to be robust, as urinary excretion following dosing with TCE, TCOH, and TCA could be modeled accurately (see Figure 3-9, panels K and Q). The residual GSDs for the urinary excretions are small: 1.34 for TCA and 1.26 for total TCOH. In addition, the blood and tissue concentrations were also accurately predicted (see Figure 3-9, panels H-J, L-P). All of the residual GSDs were less than twofold, with those for TCA measurements <1.5-fold. This improvement over the Hack et al. (2006) model was likely due in part to the addition of nonurinary clearance (“untracked” metabolism) of TCA and TCOH. Also, the addition of a liver compartment for TCOH and TCOG, so that first-pass metabolism could be properly accounted for, was essential for accurate simulation of the metabolite pharmacokinetics both from intravenous (i.v.) dosing of TCOH and from exposure to TCE.

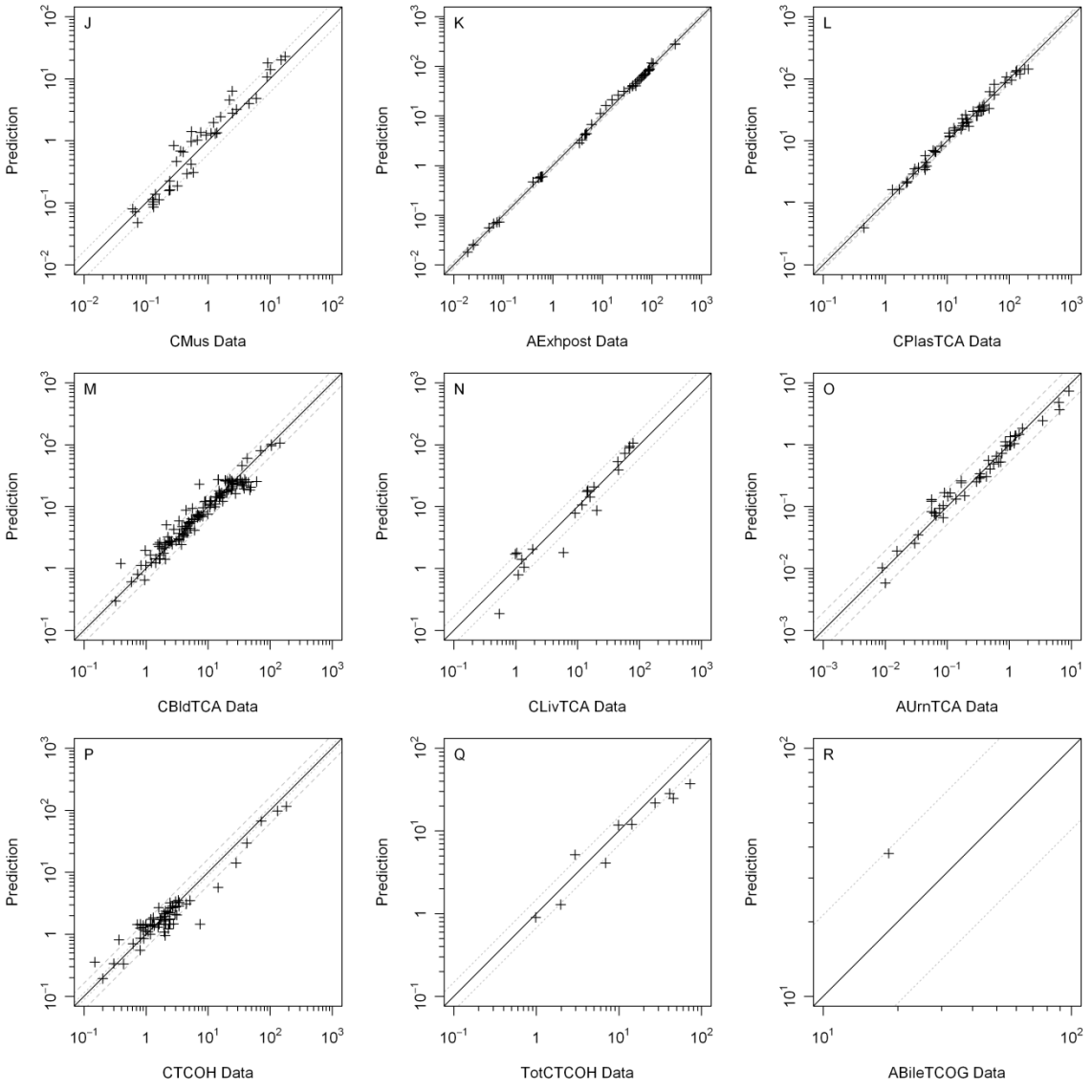
3.5.6.3.2. Rat model and data

Each panel of Figure 3-10 shows a scatter plot of the calibration data and a random posterior prediction for each of the measured endpoint. The endpoint abbreviations are listed in Table 3-41, as are the implied GSDs for the “residual” errors, which include intrastudy variability, interindividual variability, and measurement and model errors. The residual-error GSDs are also shown as grey dashed or dotted lines in Figure 3-10. A summary evaluation of the predictions of the rat model as compared to the data are provided in Tables 3-43 and 3-44, with figures showing individual time-course data and predictions in Appendix A.



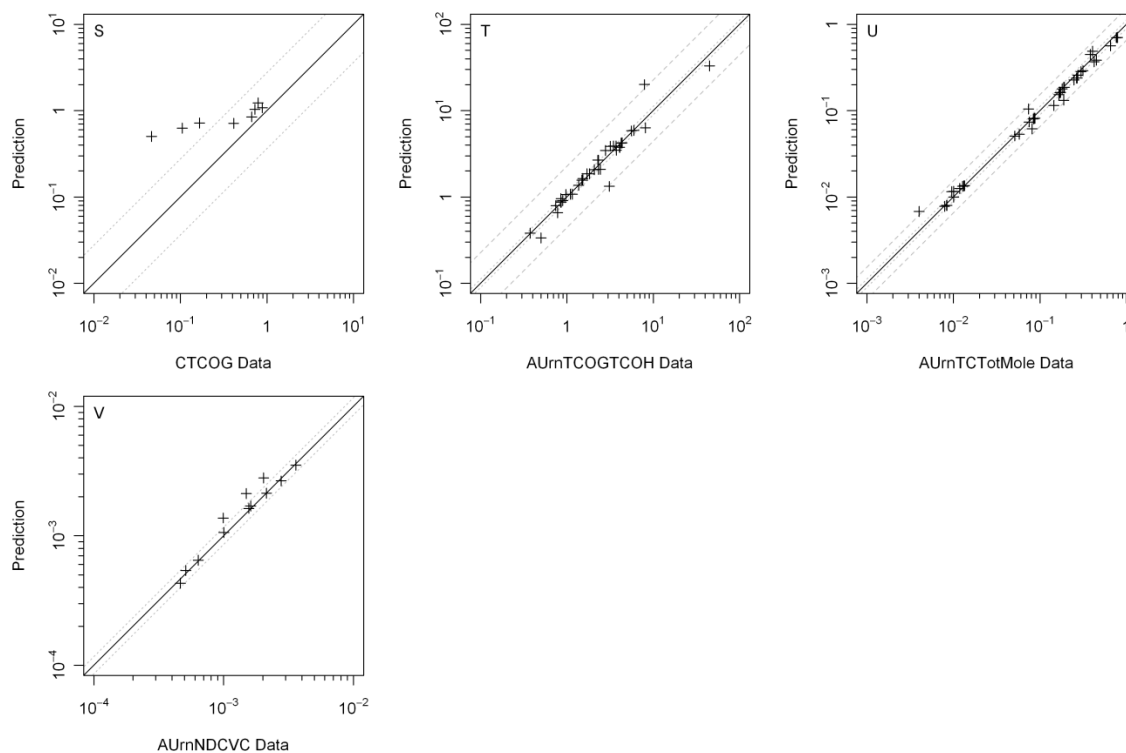
Each panel shows results for a different measurement. The solid line represents prediction = data, and the grey lines show prediction = data × GSD_{err} and data ÷ GSD_{err}, where GSD_{err} is the lowest (dotted) and highest (dashed) median estimate of the residual-error GSD shown in Table 3-41.

Figure 3-10. Comparison of rat data and PBPK model predictions from a random posterior sample.



Each panel shows results for a different measurement. The solid line represents prediction=data, and the grey lines show prediction = data \times GSD_{err} and data \div GSD_{err}, where GSD_{err} is the lowest (dotted) and highest (dashed) median estimate of the residual-error GSD shown in Table 3-41.

Figure 3-10 (continued). Comparison of rat data and PBPK model predictions from a random posterior sample.



Each panel shows results for a different measurement. The solid line represents prediction = data, and the grey lines show prediction = data \times GSD_{err} and data \div GSD_{err}, where GSD_{err} is the lowest (dotted) and highest (dashed) median estimate of the residual-error GSD shown in Table 3-41.

Figure 3-10 (continued). Comparison of rat data and PBPK model predictions from a random posterior sample.

Table 3-43. Summary comparison of updated PBPK model predictions and in vivo data used for “calibration” in rats

Study	Exposure(s)	Discussion
Bernauer et al. (1996)	TCE inhalation	Posterior fits to these data were adequate, especially with the requirement that all predictions for dose levels utilize the same PBPK model parameters. Predictions of TCOG and TCA urinary excretion was relatively accurate, though the time-course of TCA excretion seemed to proceed more slowly with increasing dose, an aspect not captured in the model. Importantly, unlike the Hack et al. (2006) results, the time-course of NAcDCVC excretion was quite well simulated, with the excretion rate remaining nonnegligible at the last time point (48 hrs). It is likely that the addition of the DCVC submodel between TCE and DCVC, along with prior distributions that accurately reflected the lack of reliable, independent (e.g., in vitro) data on bioactivation, allowed for the better fit.
Dallas et al. (1991)	TCE inhalation	These data, consisting of arterial blood and exhaled breath concentrations of TCE, were accurately predicted by the model using both subject-specific and population-sampled parameters. In the case of population predictions, most of the data were within the 95% CI of the predictions.
Fisher et al. (1989)	TCE inhalation	These data, consisting of closed-chamber TCE concentrations, were accurately simulated by the model using both subject-specific and population-sampled parameters. In the case of population predictions, most of the data were within the 95% CI of the predictions.
Fisher et al. (1991)	TCE inhalation	These data, consisting of TCE blood, and TCA blood and urine time-courses, were accurately simulated by the model using both subject-specific and population-sampled parameters. In the case of population predictions, most of the data were within the 95% CI of the predictions.

Table 3-43. Summary comparison of updated PBPK model predictions and in vivo data used for “calibration” in rats (continued)

Study	Exposure(s)	Discussion
Green and Prout (1985)	TCE gavage (corn oil) TCA i.v. TCA gavage (aqueous)	For TCE treatment, these data, consisting of one time point each in urine for TCA, TCA +TCOG, and TCOG, were accurately simulated by both subject-specific and population predictions. For TCA i.v. treatment, the single datum of urinary TCA+TCOG at 24 hrs was at the lower 95% CI in the subject-specific simulations, but accurately predicted with the population-sampled parameters, suggesting intrastudy variability is adequately accounted for by population variability. For TCA gavage treatment, the single datum of urinary TCA+TCOG at 24 hrs was accurately simulated by both subject-specific and population predictions.
Hissink et al. (2002)	TCE gavage (corn oil) TCE i.v.	These data, consisting of TCE blood, and TCA+TCOG urinary excretion time-courses, were accurately simulated by the model using subject-specific parameters. In the case of population predictions, TCA+TCOH urinary excretion appeared to be somewhat underpredicted.
Kaneko et al. (1994)	TCE inhalation	These data, consisting of TCE blood and TCA and TCOG urinary excretion time-courses, were accurately predicted by the model using both subject-specific and population-sampled parameters. In the case of population predictions, TCA+TCOH urinary excretion appeared to be somewhat underpredicted, However, all of the data were within the 95% CI of the predictions.

Table 3-43. Summary comparison of updated PBPK model predictions and in vivo data used for “calibration” in rats (continued)

Study	Exposure(s)	Discussion
Keys et al. (2003)	TCE inhalation, gavage (aqueous), i.a.	These data, consisting of TCE blood, gut, kidney, liver, muscle, and fat concentration time-courses, were accurately predicted by the model using both subject-specific and population-sampled parameters. In the case of population predictions, most of the data were within the 95% CI of the predictions.
Kimmerle and Eben (1973b)	TCE inhalation	Some inaccuracies were noted in subject-specific predictions, particularly with TCA and TCOG urinary excretion, TCE exhalation postexposure, and TCE venous blood concentrations. In the case of TCA excretion, the rate was underpredicted at the lowest dose (49 mg/kg) and overpredicted at 330 ppm. In terms of TCOG urinary excretion, the rate was overpredicted at 175 ppm and underpredicted at 330 ppm. Similarly for TCE exhaled postexposure, there was some overprediction at 175 ppm and some underprediction at 300 ppm. Finally, venous blood concentrations were overpredicted at 3,000 ppm. However, for population predictions, most of the data were within the 95% confidence region.
Larson and Bull (1992b)	TCA gavage (aqueous)	These data, consisting of TCA plasma time-courses, were accurately predicted by the model using both subject-specific and population-sampled parameters. In the case of population predictions, all of the data were within the 95% CI of the predictions.
Larson and Bull (1992a)	TCE gavage (aqueous)	These data, consisting of TCE, TCA, and TCOH in blood, were accurately predicted by the model using both subject-specific and population-sampled parameters. In the case of population predictions, all of the data were within the 95% CI of the predictions.
Lee et al. (2000a; Lee et al., 2000b)	TCE i.v., p.v.	These data, consisting of TCE concentration time course in mixed arterial and venous blood and liver, were predicted using both the subject specific and population predictions. In both cases, most of the data were within the 95% CI of the predictions.
Merdink et al. (1999)	TCOH i.v.	TCOH blood concentrations were accurately predicted using subject-specific parameters. However, population-based parameters seemed to lead to some underprediction, though most of the data were within the 95% CI of the predictions.
Prout et al. (1985)	TCE gavage (corn oil)	Most of these data were accurately predicted using both subject-specific and population-sampled parameters. However, at the highest two doses (1,000 and 2,000 mg/kg), there were some discrepancies in the (very sparsely collected) urinary excretion measurements. In particular, using subject-specific parameters, TCA+TCOH urinary excretion was underpredicted at 1,000 mg/kg and overpredicted at 2,000 mg/kg. Using population-sampled parameters, this excretion was underpredicted in both cases, though not entirely outside of the 95% CI.
Simmons et al. (2002)	TCE inhalation	Most of these data were accurately predicted using both subject-specific and population-sampled parameters. In the open-chamber experiments, there was some scatter in the data that did not seem to be accounted for in the model. The closed-chamber data were accurately fit.

Table 3-43. Summary comparison of updated PBPK model predictions and in vivo data used for “calibration” in rats (continued)

Study	Exposure(s)	Discussion
Stenner et al. (1997)	TCE intraduodenal TCOH i.v. TCOH i.v., bile-cannulated	These data, consisting of TCA and TCOH in blood and TCA and TCOG in urine, were generally accurately predicted by the model using both subject-specific and population-sampled parameters. However, using subject-specific parameters, the amount of TCOG in urine was overpredicted for 100 TCOH mg/kg i.v. dosing, though total TCOH in blood was accurately simulated. In addition, in bile-cannulated rats, the TCOG excretions at 5 and 20 mg/kg i.v. were underpredicted, while the amount at 100 mg/kg was accurately predicted. On the other hand, in the case of population predictions, all of the data were within the 95% CI of the predictions, and mostly within the interquartile region, even for TCOG urinary excretion. This suggests that intrastudy variability may be a source of the poor fit in using the subject-specific parameters.
Templin et al. (1995b)	TCE oral (aqueous)	These data, consisting of TCE, TCA, and TCOH in blood, were accurately predicted by the model using both subject-specific and population-sampled parameters. In the case of population predictions, all of the data were within the 95% CI of the predictions.
Yu et al. (2000)	TCA i.v.	These data, consisting of TCA in blood, liver, plasma, and urine, were generally accurately predicted by the model using both subject-specific and population-sampled parameters. The only notable discrepancy was at the highest dose of 50 mg/kg, in which the rate of urinary excretion from 0 to 6 hrs appeared to more rapid than the model predicted. However, all of the data were within the 95% CI of the predictions based on population-sampled parameters.

Table 3-44. Summary comparison of updated PBPK model predictions and in vivo data used for “out-of-sample” evaluation in rats

Study	Exposure(s)	Discussion
Andersen et al. (1987a)	TCE inhalation	These closed-chamber data were well within the 95% CI of the predictions based on population-sampled parameters.
Bruckner et al. unpublished	TCE inhalation	These data on TCE in blood, liver, kidney, fat, muscle, gut, and venous blood were generally accurately predicted based on population-sampled parameters. The only notable exception was TCE in the kidney during the exposure period at the 500 ppm level, which was somewhat underpredicted (though levels postexposure were accurately predicted).
Fisher et al. (1991)	TCE inhalation	These data on TCE in blood were well within the 95% CI of the predictions based on population-sampled parameters.
Jakobson et al. (1986)	TCE inhalation	These data on TCE in arterial blood were well within the 95% CI of the predictions based on population-sampled parameters.
Lee et al. (1996)	TCE i.a., i.v., p.v., gavage	Except at some very early time-points (<0.5 hr), these data on TCE in blood were well within the 95% CI of the predictions based on population-sampled parameters.
Lee et al. (2000a; 2000b)	TCE gavage	These data on TCE in blood were well within the 95% CI of the predictions based on population-sampled parameters.

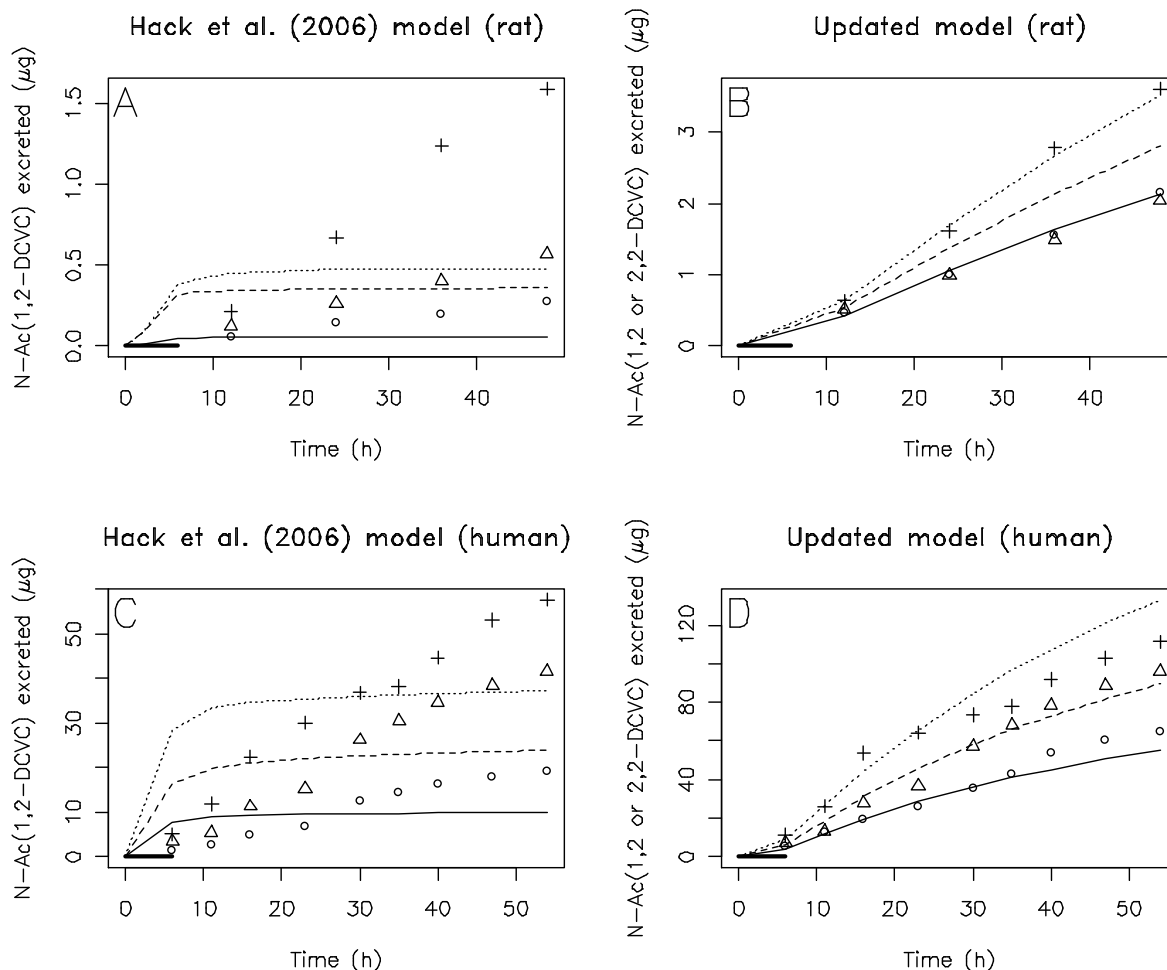
Similar to previous analyses (Hack et al., 2006), the TCE submodel for the rat appears to be robust, accurately predicting blood and tissue concentrations (see Figure 3-10, panels A-K), with residual-error GSDs generally less than twofold. The only exceptions are the predictions of

venous blood from Kimmerle and Eben ([1973b](#)), which have residual-error GSDs greater than fourfold, and the predictions of fat concentrations from Simmons et al. ([2002](#)); with residual-error GSD of 2.7-fold. For Kimmerle and Eben ([1973b](#)), the inaccuracy was primarily at the 3,000-ppm exposure, which might reflect other factors related to the high exposure. For Simmons et al. ([2002](#)), the high residual-error appears to reflect scatter due to intrastudy variability. Unlike in the mouse, some data consisting of TCE blood and tissue concentrations were used for “out-of-sample evaluation” (sometimes loosely termed “validation”). These data were generally well simulated (see Table 3-44); most of the data were within the 95% CI of posterior predictions. This provides additional confidence in the predictions for the parent compound.

In terms of TCA and TCOH, as with the mouse, the overall mass balance and metabolic disposition to these metabolites also appeared to be robust: urinary excretion following dosing with TCE, TCOH, and TCA could be modeled accurately (see Figure 3-10 panels O, T, and U), with the residual-errors also indicating good predictions in most cases. Residual-error for these measurements was larger for Green and Prout ([1985](#)), Prout et al. ([1985](#)), and Stenner et al. ([1997](#)), ranging from a GSD of 1.8 to 2.3, reflecting largely intrastudy variability. Residual-errors for the other studies had GSDs of 1.1–1.5. This improvement over the Hack et al. ([2006](#)) model was likely due in part to the addition of nonurinary clearance (“untracked” metabolism) of TCA and TCOH. In addition, adding a liver compartment for TCOH and TCOG, so that first-pass metabolism could be properly accounted for, was essential for accurate simulation of the metabolite pharmacokinetics both from i.v. dosing of TCOH and from TCE exposure. Blood and plasma concentrations of TCA and free or total TCOH were also fairly well simulated (see Figure 3-10, panels L, M, P, Q, and S), with GSDs for the residual-error of 1.1–1.6. A bit more discrepancy (residual-error GSD of 1.7) was evident with TCA liver concentrations (see Figure 3-10, panel N). However, TCA liver concentrations were only available in one study ([Yu et al., 2000](#)), and the data show a change in the ratio of liver to blood concentrations at the last time point, which may be the source of the added residual-error. Predictions of biliary excretion of TCOG in bile-cannulated rats (see Figure 3-10, panel R), from Green and Prout ([1985](#)), and TCOG in blood (see Figure 3-10, panel S), from Stenner et al. ([1997](#)), were less accurate, with residual-error GSDs >2. However, the biliary excretion data consisted of a single measurement, and the amount of free TCOH in the same experiment from Stenner et al. ([1997](#)) was accurately predicted.

In terms of total metabolism, as with the mouse, closed-chamber data (see Figure 3-10, panel A) were fit accurately with the updated model (residual-error GSD of about 1.1). In addition, the data on NAcDCVC urinary excretion was well predicted (see Figure 3-10, panel V), with residual-error GSD of 1.18. In particular, the fact that excretion was still ongoing at the end of the experiment was accurately predicted (see Figure 3-11, panels A and B). Thus, there is greater confidence in the estimate of the flux through the GSH pathway than there was from the

Hack et al. (2006) model. However, the overall flux is still estimated indirectly, and there remains some ambiguity as to the relative contributions of respiratory wash-in/wash-out, respiratory metabolism, extrahepatic metabolism, DCVC bioactivation vs. *N*-acetylation, and oxidation in the liver producing something other than TCOH or TCA. Therefore, there remains a large range of possible values for the flux through the GSH conjugation and other indirectly estimated pathways that are nonetheless consistent with all of the available in vivo data. The use of noninformative priors for the metabolism parameters for which there were no in vitro data means that a fuller characterization of the uncertainty in these various metabolic pathways could be achieved. Thus, the model should be reliable for estimating lower and upper bounds on several of these pathways.



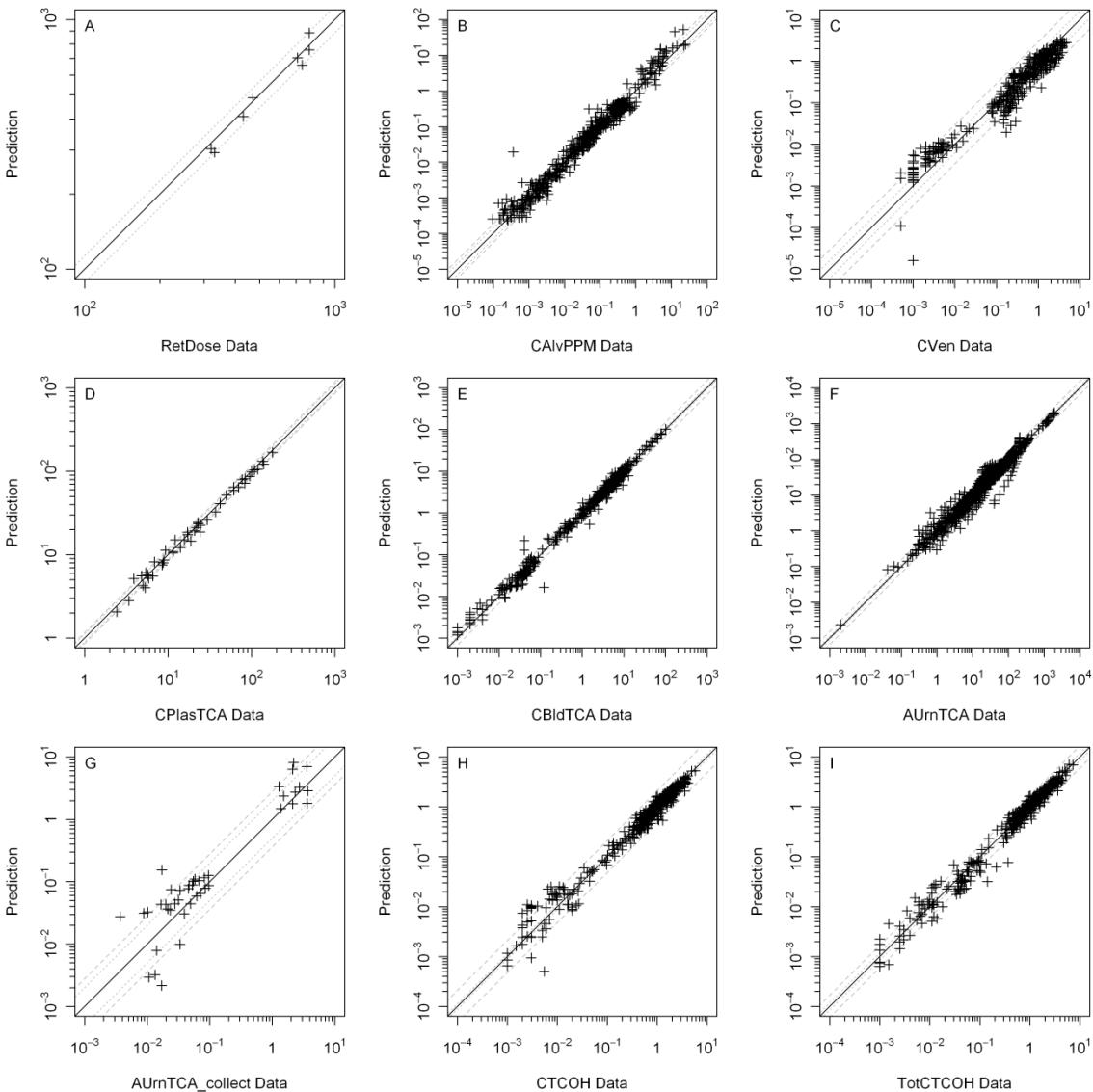
Data are from Bernauer et al. (1996) for (A and B) rats or (C and D) humans exposed for 6 hour to 40 (○), 80 (△), or 160 (+) ppm in air (thick horizontal line denotes the exposure period). Predictions from Hack et al. (2006) and the corresponding data (A and C) are only for the 1,2 isomer, whereas those from the updated model (B and D) are for both isomers combined. Parameter values used for each prediction are a random sample from the subject-specific parameters from the rat and human MCMC chains (the last iteration of the first chain was used in each case). Note that in the Hack et al. (2006) model, each dose group had different model parameters, whereas in the updated model, all dose groups are required to have the same model parameters. See files linked to Appendix A for comparisons with the full distribution of predictions.

Figure 3-11. Comparison of urinary excretion data for NAcDCVC and predictions from the Hack et al. (2006) and the updated PBPK models.

3.5.6.3.3. Human model and data

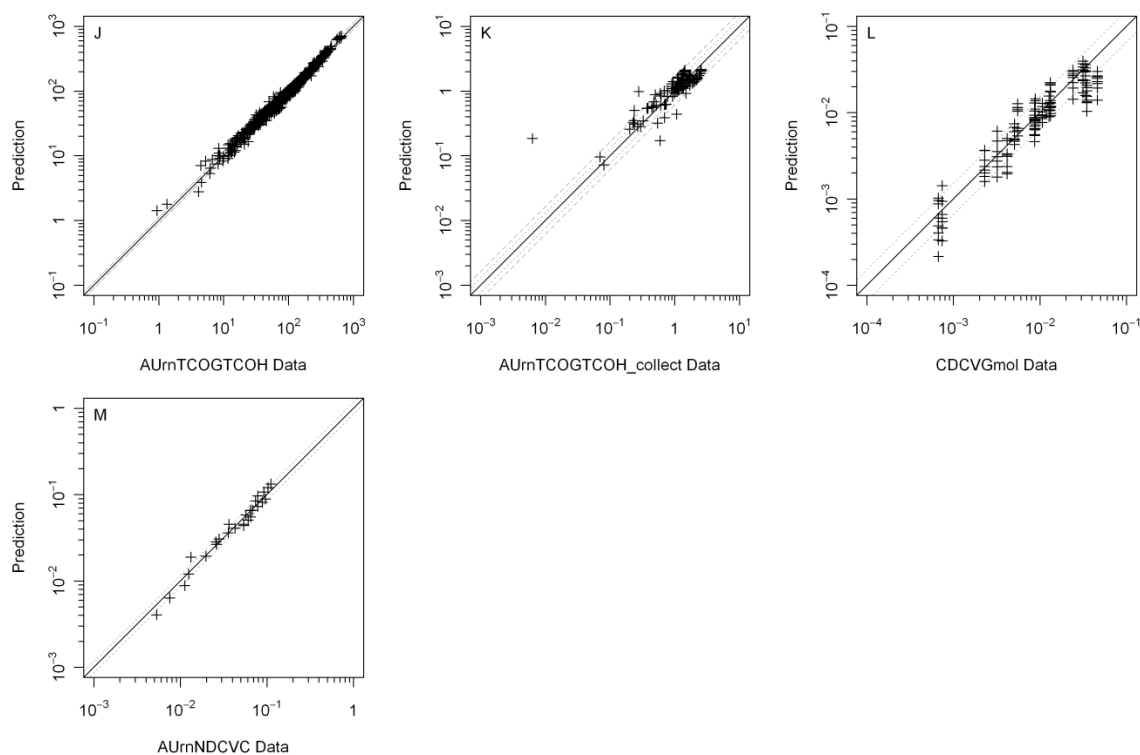
Each panel of Figure 3-12 shows a scatter plot of the calibration data and a random posterior prediction for each of the measured endpoint. The endpoint abbreviations are listed in Table 3-41, as are the implied GSDs for the “residual” errors, which include intrastudy

variability, interindividual variability, and measurement and model errors. The residual-error GSDs are also shown as grey dashed or dotted lines in Figure 3-12. Table 3-45–3-46 provide a summary evaluation of the predictions of the model as compared to the human data, with figures showing individual time-course data and predictions in Appendix A.



Each panel shows results for a different measurement. The solid line represents prediction = data, and the grey lines show prediction = data × GSD_{err} and data ÷ GSD_{err}, where GSD_{err} is the lowest (dotted) and highest (dashed) median estimate of the residual-error GSD shown in Table 3-41.

Figure 3-12. Comparison of human data and PBPK model predictions from a random posterior sample.



Each panel shows results for a different measurement. The solid line represents prediction = data, and the grey lines show prediction = data \times GSD_{err} and data \div GSD_{err} , where GSD_{err} is the lowest (dotted) and highest (dashed) median estimate of the residual-error GSD shown in Table 3-41.

Figure 3-12 (continued). Comparison of rat data and PBPK model predictions from a random posterior sample.

Table 3-45. Summary comparison of updated PBPK model predictions and in vivo data used for “calibration” in humans

Reference	Exposure(s)	Discussion
Bernauer et al. (1996)	TCE inhalation	These data, consisting of TCA, TCOG and NAcDCVC excreted in urine, were accurately predicted by the model using both individual-specific and population-sampled parameters. The posterior NAcDCVC predictions were an important improvement over the predictions of Hack et al. (2006), which predicted much more rapid excretion than observed. The fit improvement is probably a result of the addition of the DCVG submodel between TCE and DCVC, along with the broader priors on DCVC excretion and bioactivation. Interestingly, in terms of population predictions, the NAcDCVC excretion data from this study were on the low end, though still within the 95% CI.

Table 3-45. Summary comparison of updated PBPK model predictions and in vivo data used for “calibration” in humans (continued)

Reference	Exposure(s)	Discussion
Chiu et al. (2007)	TCE inhalation	<p>Overall, posterior predictions were quite accurate across most of the individuals and exposure occasions. TCE alveolar breath concentrations were well simulated for both individual-specific and population-generated simulations, though there was substantial scatter (intraoccasion variability). However, TCE blood concentrations were consistently overpredicted in most of the experiments, both using individual-specific and population-generated parameters. This was not unexpected, as Chiu et al. (2007) noted the TCE blood measurements to be lower by about twofold relative to previously published studies. As discussed in Chiu et al. (2007) wash-in/wash-out and extrahepatic (including respiratory) metabolism were not expected to be able to account for the difference, and indeed all of these processes were added to the current model without substantially improving the discrepancy. With respect to metabolite data, TCA and total TCOH in blood were relatively accurately predicted. There was individual experimental variability observed for both TCA and TCOH in blood at 6 hrs (end of exposure). The population-generated simulations overpredicted TCA in blood, while they were accurate in predicting blood TCOH. Predictions of free TCOH in blood also showed overprediction for individual experiments, with variability at the end of exposure timepoint. However, TCOH fits were improved for the population-generated simulations. TCA and TCOG urinary excretion was generally well simulated, with simulations slightly under- or overpredicting the individual experimental data in some cases.</p>
Fisher et al. (1998)	TCE inhalation	<p>The majority of the predictions for these data were quite accurate. Interestingly, in contrast to the predictions for Chiu et al. (2007), TCE blood levels were somewhat underpredicted in a few cases, both from using individual-specific and population-generated predictions. These two results together suggest some unaccounted-for study-to-study variance, though interindividual variability cannot be discounted as the data from Chiu et al. (2007) were from individuals in the Netherlands and that from Fisher et al. (1998) were from individuals in the United States. As reported by Fisher et al. (1998), TCE in alveolar air was somewhat overpredicted in several cases; however, the discrepancies seemed smaller than originally reported for the Fisher et al. model.</p>
Fisher et al. (1998) (continued)	TCE inhalation (continued)	<p>With respect to metabolite data, TCOH and TCA in blood and TCOG and TCA in urine were generally well predicted, though data for some individuals appeared to exhibit inter- and/or intraoccasion variability. For example, in one case in which the same individual (female) was exposed to both 50 and 100 ppm, the TCOH blood data was overpredicted at the higher one exposure. In addition, in one individual, initial individual-specific simulations for TCA in urine were underpredicted but shifted to overpredictions towards the end of the simulations. The population-generated results overpredicted TCA in urine for the same individual. Given the results from Chiu et al. (2007), interoccasion variability is likely to be the cause, though some dose-related effect cannot be ruled out.</p> <p>Finally, DCVG data was well predicted in light of the high variability in the data and availability of only grouped data or data from multiple individuals who cannot be matched to the appropriate TCE and oxidative metabolite data set. In all cases, the basic shape (plateau and then sharp decline) and order of magnitude of the time-course were well predicted, Furthermore, the range of the data was well-captured by the 95% CI of the population-generated predictions.</p>
Kimmerle and Eben (1973a)	TCE inhalation	<p>These data were well fit by the model, using either individual-specific or population-generated parameters.</p>

Table 3-45. Summary comparison of updated PBPK model predictions and in vivo data used for “calibration” in humans (continued)

Reference	Exposure(s)	Discussion
Monster et al. (1976)	TCE inhalation	The data simulated in this case were exhaled alveolar TCE, TCE in venous blood, TCA in blood, TCA in urine, and TCOG in urine. Both using individual-specific and population-generated simulations, all fits are within the 95% CI. The one exception was the retained dose for a male exposed to 65 ppm, which was outside the 95% CI for the population-generated results.
Muller et al. (1974)	TCA, TCOH oral	The data measured after oral TCA was timecourse TCA measured in plasma and urine. Individual-specific predictions were accurate, but both data sets were overpredicted in the population-generated simulations. The data measured after oral TCOH were timecourse TCOH in blood, TCOG in urine, TCA in plasma, and TCA in urine. Individual-specific predictions were accurate, but the population-generated simulations overpredicted TCOH in blood and TCOG in urine. The population-based TCA predictions were accurate. These results indicate that “unusual” parameter values were necessary in the individual-specific simulations to give accurate predictions.
Paykoc et al. (1945)	TCA i.v.	These data were well fit by the model, using either individual-specific or population-generated parameters.

Table 3-46. Summary comparison of updated PBPK model predictions and in vivo data used for “out-of-sample” evaluation in humans

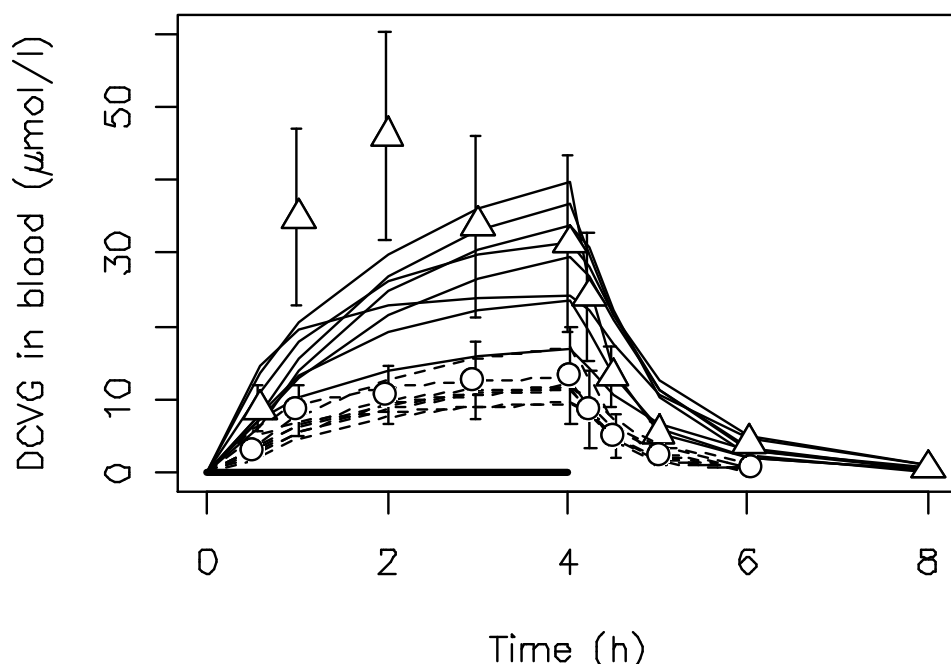
Reference	Exposure(s)	Discussion
Bartonicek (1962)	TCE inhalation	While these data were mostly within the 95% CI of the predictions, they tended to be at the high end for all of the individuals in the study.
Bloemen et al. (2001)	TCE inhalation	These data were all well within the 95% CI of the predictions.
Fernandez et al. (1977)	TCE inhalation	These data were all well within the 95% CI of the predictions.
Lapare et al. (1995)	TCE inhalation	These data were all well within the 95% CI of the predictions.
Monster et al. (1979a)	TCE inhalation	These data were all well within the 95% CI of the predictions.
Muller et al. (1975; 1974)	TCE inhalation	Except for TCE in alveolar air, which was overpredicted during exposure, these data were all well within the 95% CI of the predictions.
Sato et al. (1977)	TCE inhalation	These data were all well within the 95% CI of the predictions.
Stewart et al. (1970)	TCE inhalation	These data were all well within the 95% CI of the predictions.
Triebig et al. (1976)	TCE inhalation	Except for TCE in alveolar air, these data were all well within the 95% CI of the predictions.

With respect to the TCE submodel, retained dose, blood, and exhaled air measurements (see Figure 3-12, panels A-C) appeared more robust than previously found from the Hack et al. (2006) model. TCE blood concentrations from most studies were well predicted, with residual-error GSD in most studies of less than twofold. However, those from Chiu et al. (2007) were consistently overpredicted (i.e., data <0.1 mg/L in Figure 3-12, panel C), with residual-error GSD of almost threefold, and a few of those from Fisher et al. (1989) were consistently underpredicted. Alveolar breath concentrations and retained dose of TCE were well predicted (residual-error GSD <1.5-fold) from all studies except Fisher et al. (1998), which had a residual-error GSD of 1.8-fold. However, the discrepancy in alveolar breath appeared smaller than that originally reported by Fisher et al. (1998) for their PBPK model. In addition, the majority of the “out-of-sample” evaluation data consisted of TCE in blood or breath, and were generally well predicted (see Table 3-46), lending confidence to the model predictions for the parent compound.

In terms of TCA and TCOH, as with the mouse and rat, the overall mass balance and metabolic disposition to these metabolites also appeared to be robust, as urinary excretion following TCE exposure could be modeled accurately (see Figure 3-12, panels F, G, J, and K). In most cases, the residual-error GSD was less than twofold. However, TCA urinary data from Chiu et al. (2007) (panel G in Figure 3-12) indicated greater interoccasion variability, reflected in the residual-error GSD of 2.8. In this study, the same individual exposed to the same concentration on different occasions sometimes had substantial differences in urinary excretion. In addition, many TCA urine measurements in this study were saturated, and had to be omitted, and the fact that the remaining data were sparse and possibly censored may have contributed to the greater intrastudy variability. Blood and plasma concentrations of TCA and free TCOH (see Figure 3-12, panels D, E, and H) were fairly well simulated, with GSD for the residual-error of 1.1–1.4, though total TCOH in blood (see Figure 3-12, panel I) had slightly greater residual-error with GSD of about 1.6. This partially reflects the “sharper” peak concentrations of total TCOH in the Chiu et al. (2007) data relative to the model predictions. In addition, TCA and TCOH blood and urine data were available from several studies for “out-of-sample” evaluation and were generally well predicted by the model (see Table 3-46), lending further confidence to the model predictions for these metabolites.

In terms of total metabolism, no closed-chamber data exist in humans, but, as discussed above, alveolar breath concentrations and retained dose (see Figure 3-12, panels A and B) were generally well simulated, suggesting that total metabolism may be fairly robust. In addition, as with the rat, the data on NAcDCVC urinary excretion was well predicted (see Figure 3-11, Figure 3-12 panel M), with residual-error GSD of 1.12). In particular, the model accurately predicted the fact that excretion was still ongoing at the end of the experiment (48 hours after the end of exposure). Thus, there is greater confidence in the estimate of the flux through this part of the GSH pathway than there was from the Hack et al. (2006) model, in which excretion was completed within the first few hours after exposure (see Figure 3-11, panels C and D).

If only urinary NAcDCVC data were available, as is the case for the rat, the overall GSH conjugation flux would still be estimated indirectly, and there would remain some ambiguity as to the relative contributions of respiratory wash-in/wash-out, respiratory metabolism, extrahepatic metabolism, DCVC bioactivation vs. *N*-acetylation, and oxidation in the liver producing something other than TCOH or TCA. However, unlike in the rat, the blood DCVG data, while highly variable, nonetheless provide substantial constraints (at least a strong lower bound) on the flux of GSH conjugation, and is well fit by the model (see Figure 3-12, panel L, and Figure 3-13). Importantly, the high residual-error GSD for blood DCVG reflects the fact that only grouped or unmatched individual data were available, so in this case, the residual-error includes interindividual variability, which is not included in the other residual-error estimates. However, as discussed above in Section 3.3.3.2.1, there are uncertainties as to the accuracy of analytical method used by Lash et al. ([1999b](#)) in the measurement of DCVG in blood. Because these data are so determinative of the overall GSH conjugation flux, these analytical uncertainties are important to consider in the overall evaluation of the PBPK model predictions (see below, Section 3.5.7).



Data are mean concentrations for males (Δ) and females (\circ) reported in Lash et al. (1999b) for humans exposed for 4 hours to 100 ppm TCE in air (thick horizontal line denotes the exposure period). Data for oxidative metabolites from the same individuals were reported in Fisher et al. (1998) but could not be matched with the individual DCVG data (Lash 2007, personal communication). The vertical error bars are SEs of the mean as reported in Lash et al. (1999b) ($n = 8$, so SD is 80.5-fold larger). Lines are PBPK model predictions for individual male (solid) and female (dashed) subjects. Parameter values used for each prediction are a random sample from the individual-specific parameters from the human MCMC chains (the last iteration of the 1st chain was used). See files linked to Appendix A for comparisons with the full distribution of predictions.

Figure 3-13. Comparison of DCVG concentrations in human blood and predictions from the updated model.

For the other indirectly estimated pathways, there remain a large range of possible values that are nonetheless consistent with all of the available in vivo data. The use of noninformative priors for the metabolism parameters for which there were no in vitro data means that a fuller characterization of the uncertainty in these various metabolic pathways could be achieved. Thus, as with the rat, the model should be reliable for estimating lower and upper bounds on several of these pathways.

3.5.6.4. Sensitivity Analysis With Respect to Calibration Data

To assess the informativeness of the calibration data to the parameters, local sensitivity analysis is performed with respect to the calibration data points. For each scaling parameter, the

central difference is used to estimate the partial derivatives by centering on the sample mean of its estimated population mean, and then increasing and decreasing by 5%. The relative change in the model output $f(\theta)$ is used to estimate a local sensitivity coefficient (SC) as follows:

$$SC = 10 \times \{f(\theta_+) - f(\theta_-)\} / [\frac{1}{2} \times \{f(\theta_+) + f(\theta_-)\}]$$

Here, $f(\theta)$ is one of the model predictions of the calibration data, θ_{\pm} is the maximum likelihood estimate (MLE) or baseline value of $\pm 5\%$. For log-transformed parameters, 0.05 was added or subtracted from the baseline value, whereas for untransformed parameters, the baseline value was multiplied by 1.05 or 0.95. The resulting values of SC are binned into five categories according to their sensitivity coefficient: negligible ($|SC| \leq 0.01$) very low ($0.01 < |SC| \leq 0.1$), low ($0.1 < |SC| \leq 0.5$), medium ($0.5 < |SC| \leq 1.0$), and high ($|SC| > 1.0$).

Note that local sensitivity analyses as typically performed in deterministic PBPK modeling can only inform the “primary” effects of parameter uncertainties (i.e., the direct change on the quantity of interest due to change in a parameter). They cannot address the *propagation* of uncertainties, such as those that can arise due to parameter correlations in the parameter fitting process. Those can only be addressed in a global sensitivity analysis, which is left for future research.

The results of local sensitivity analyses are shown in Figures 3-14–3-16. For each parameter, the number of data points (out of the entire calibration set) that have sensitivity coefficients in the various categories are shown graphically. As summarized in Table 3-47, most of the parameters have at least some calibration data to which they are at least moderately sensitive ($|SC| > 0.5$). Across species, the cardiac output (lnQCC), ventilation-perfusion ratio (lnVPRC), blood-air partition coefficient (lnPBC), V_{MAX} for oxidation (ln $V_{MAX}C$), and $V_{Liv}C$ are consistently among the most sensitive parameters, with $>10\%$ of the calibration data exhibiting $|SC| > 0.5$ to these parameters. Note that the reason the liver volume is sensitive is that it is used to scale the capacity or clearance rate for oxidation.

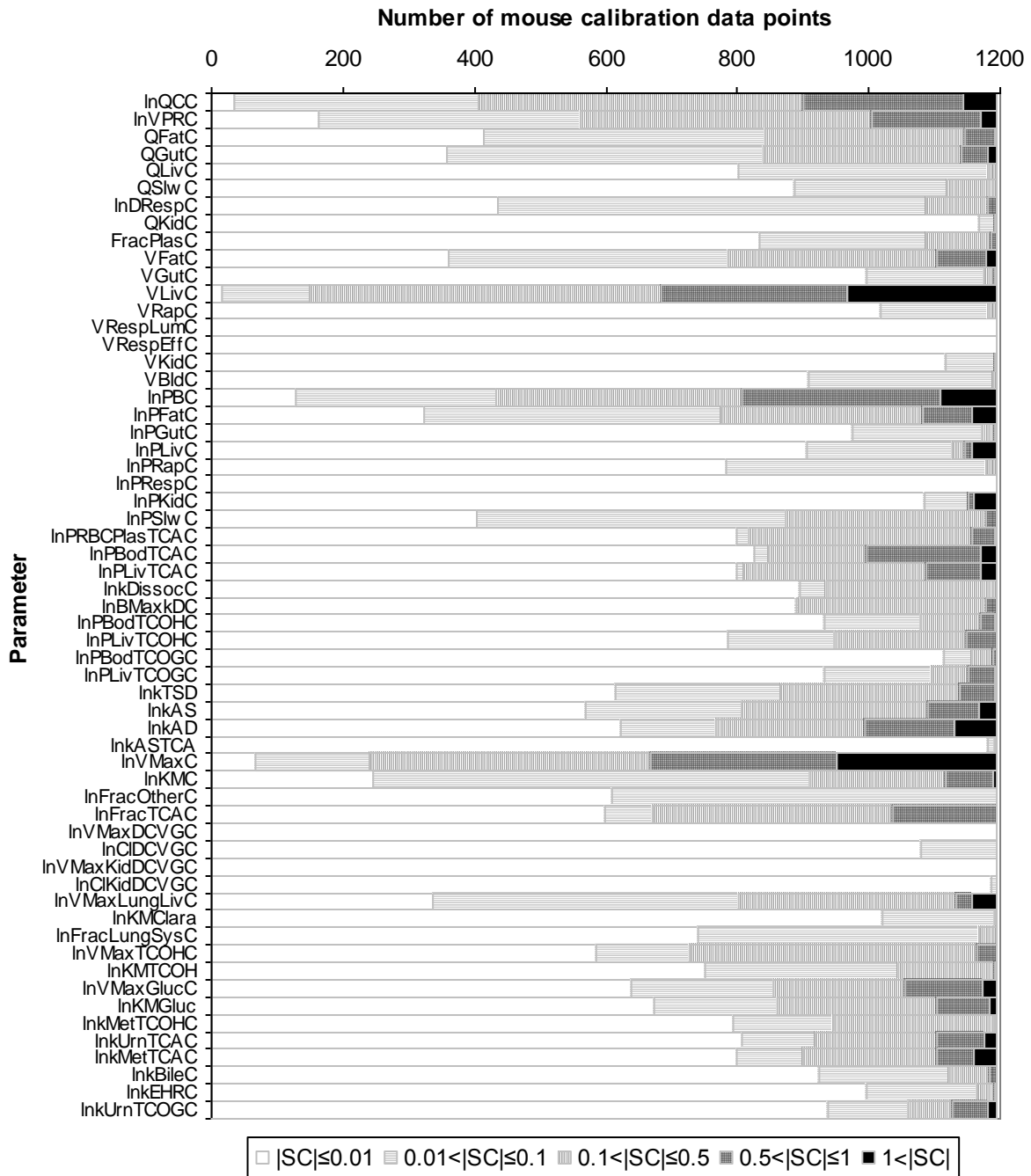


Figure 3-14. Sensitivity analysis results: Number of mouse calibration data points with SC in various categories for each scaling parameter.

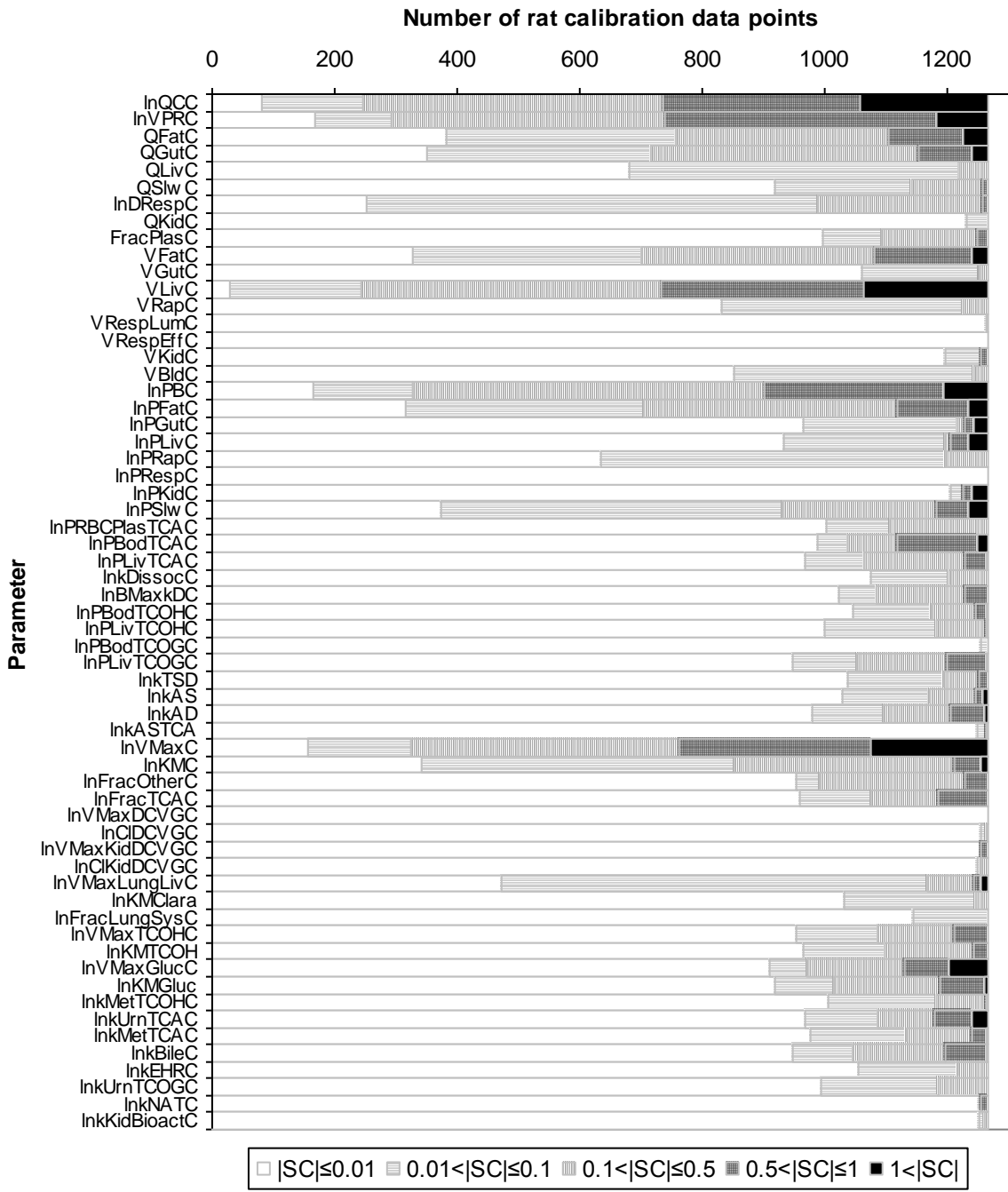


Figure 3-15. Sensitivity analysis results: Number of rat calibration data points with SC in various categories for each scaling parameter.

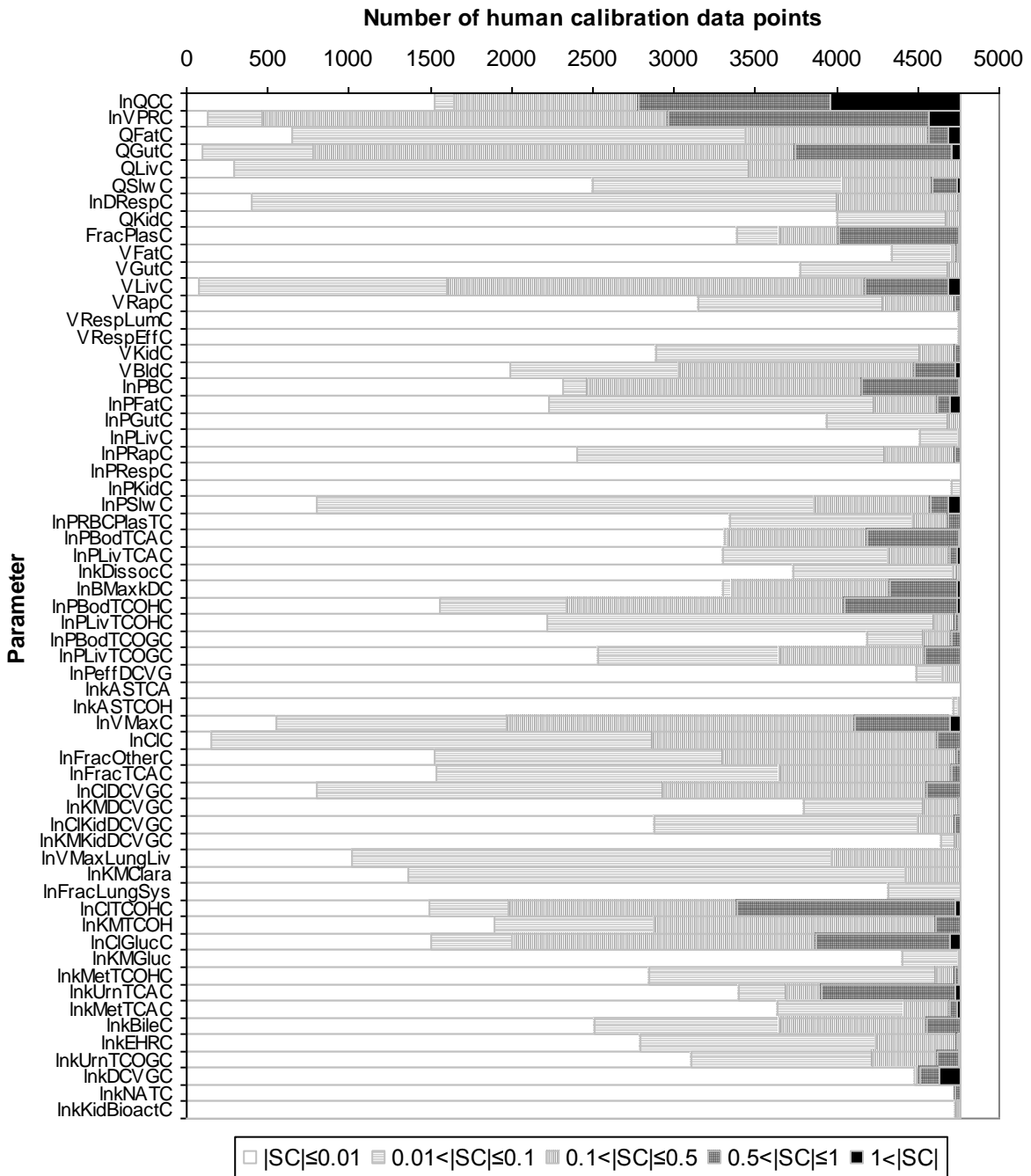


Figure 3-16. Sensitivity analysis results: Number of human calibration data points with SC in various categories for each scaling parameter.

Table 3-47. Summary of scaling parameters ordered by fraction of calibration data of moderate or high sensitivity

Mouse		Rat		Human	
Parameter ^a	Fraction with SC >0.5	Parameter ^a	Fraction with SC >0.5	Parameter ^a	Fraction with SC >0.5
lnV _{MAX} C	0.4405	VLivC	0.4213	lnQCC	0.4159
VLivC	0.428	lnQCC	0.4182	lnVPRC	0.3777
lnPBC	0.3233	lnVPRC	0.4158	lnCITCOHC	0.2871
lnQCC	0.2454	lnV _{MAX} C	0.3984	QGutC	0.2137
lnkAD	0.1675	lnPBC	0.2893	lnCIGlucC	0.186
lnPBodTCAC	0.1642	VFatC	0.1455	lnkUrnTCAC	0.1789
lnVPRC	0.1575	QFatC	0.1273	FracPlasC	0.1553
lnFracTCAC	0.1323	lnPBodTCAC	0.1162	lnPBodTCOHC	0.1486
lnV _{MAX} GlucC	0.1147	lnPFatC	0.1154	lnV _{MAX} C	0.1358
lnPFatC	0.093	lnV _{MAX} GlucC	0.1083	lnPBC	0.1269
lnPLivTCAC	0.0896	QGutC	0.0885	VLivC	0.1225
lnkAS	0.0863	lnkUrnTCAC	0.0696	lnPBodTCAC	0.12
VFatC	0.0762	lnPSlwC	0.0664	lnBMaxkDC	0.0897
lnKMGluc	0.0762	lnFracTCAC	0.064	VBldC	0.0586
lnkMetTCAC	0.0762	lnKMGluc	0.0625	lnkDCVGC	0.0515
lnkUrnTCAC	0.0754	lnkBileC	0.0538	lnPLivTCOGC	0.0446
lnKMC	0.0653	lnPLivTCOGC	0.0514	lnCIDCVGC	0.0435
lnkUrnTCOGC	0.0544	lnPLivC	0.0482	lnkBileC	0.0422
lnV _{MAX} LungLivC	0.0511	lnkAD	0.0474	QFatC	0.0401
lnkTSD	0.0469	lnKMC	0.0427	lnPSlwC	0.0372
QGutC	0.0452	lnV _{MAX} TCOHC	0.0427	QSlwC	0.0345
QFatC	0.0402	lnPKidC	0.0324	lnKMTCOH	0.0305
lnPLivC	0.0402	lnPGutC	0.03	lnPFatC	0.0292
lnPLivTCOHC	0.0377	lnFracOtherC	0.03	lnCIC	0.0288
lnPKidC	0.0352	lnPLivTCAC	0.0292	lnkUrnTCOGC	0.0282
lnPLivTCOGC	0.0352	lnBMaxkDC	0.0285	lnPRBCPlasTCAC	0.0147
lnPRBCPlasTCAC	0.031	lnkMetTCAC	0.0213	lnPLivTCAC	0.0135
lnV _{MAX} TCOHC	0.0235	lnV _{MAX} LungLivC	0.0182	lnkMetTCAC	0.013
lnPBodTCOHC	0.0201	lnKMTCOH	0.0182	lnFracTCAC	0.0103
lnPSlwC	0.0134	lnkAS	0.0158	lnPBodTCOGC	0.0095
lnBMaxkDC	0.0134	lnPBodTCOHC	0.015	VRapC	0.0063
lnDRespC	0.0109	FracPlasC	0.0126	VKidC	0.0057
lnkBileC	0.0084	lnkTSD	0.0103	lnCICidDCVGC	0.0057
FracPlasC	0.0059	VKidC	0.0095	lnkNATC	0.0057
lnPBodTCOGC	0.005	lnV _{MAX} KidDCVGC	0.0095	lnPRapC	0.005
VGutC	0.0025	lnkNATC	0.0095	lnPLivTCOHC	0.005
lnPGutC	0.0025	lnDRespC	0.0063	lnkMetTCOHC	0.005
lnKMTCOH	0.0017	QSlwC	0.0055	lnFracOtherC	0.0046
lnkMetTCOHC	0.0017	lnPLivTCOHC	0.0016	VFatC	0.0036
lnkEHRC	0.0017	lnkASTCA	0.0016	lnkEHRC	0.0036
QKidC	0.0008	lnkMetTCOHC	0.0016	lnDRespC	0.0011
VKidC	0.0008	VGutC	0.0008	lnKMDCVGC	0.0011
		lnPRBCPlasTCAC	0.0008	lnkKidBioactC	0.0002
		lnkUrnTCOGC	0.0008		

^aParameters not shown have no data with |SC| > 0.5.

For scaling parameters for which all of the calibration data are negligibly sensitive ($|\text{SC}| < 0.01$), it is important that they either have informative prior data or are unimportant for dose-metric predictions. For mice, these parameters are the volumes of the respiratory lumen and tissue (V_{RespLumC} , V_{RespEffC}), the partition coefficient for the respiratory tissue (lnPRespC), and the V_{MAX} values for GSH conjugation in the liver and kidney. For the respiratory tract parameters, there are prior data to identify the parameters. Moreover, none of the dose-metric predictions are sensitive to these parameters (see Section 3.5.7.2, below). For GSH conjugation, it should be noted that for the clearance in the liver and lung ($V_{\text{MAX}}/K_{\text{M}}$), some data are available with sensitivity $0.01 < |\text{SC}| < 0.1$. The data are not at all informative as to the maximum capacity for GSH conjugation.

For rats, all of the scaling parameters have at least one calibration data point with $|\text{SC}| > 0.01$. However, for the volumes of the respiratory lumen and tissue (V_{RespLumC} , V_{RespEffC}), the partition coefficient for the respiratory tissue (lnPRespC), and the V_{MAX} values for GSH conjugation in the liver, these consist of only one or two data points. As with mice, there are prior data to help identify the respiratory tract parameters. Moreover, none of the dose-metric predictions are sensitive to the respiratory tract parameters (see Section 3.5.7.2, below). The data are not very informative as to maximum capacity for GSH conjugation in the liver. However, there are some data that have low or moderate informativeness ($0.1 < |\text{SC}| < 1$) as to the maximum capacity for GSH conjugation in the kidney, and clearance via GSH conjugation ($V_{\text{MAX}}/K_{\text{M}}$) in the liver and kidney, which have much greater impact on the dose-metric predictions than the maximum capacity in the liver (see Section 3.5.7.2, below).

For humans, all of the scaling parameters have at least one calibration data point with $|\text{SC}| > 0.01$. However, for the volumes of the respiratory lumen and tissue (V_{RespLumC} , V_{RespEffC}), the partition coefficient for the respiratory tissue (lnPRespC), and the oral absorption rate for TCA, these consist of only one or two data points. As with mice and rats, there are prior data to help identify the respiratory tract parameters. Moreover, none of the dose-metric predictions are sensitive to the respiratory or TCA oral absorption parameters (see Section 3.5.7.2, below).

Therefore, the local sensitivity analysis with respect to calibration data confirms that most of the scaling parameters are informed by at least some of the calibration data. In addition, the parameters for which the calibration data have very little or negligible sensitivity are either informed by prior data or have little impact on dose-metric predictions.

3.5.6.5. Summary Evaluation of Updated PBPK Model

Overall, the updated PBPK model, utilizing parameters consistent with the available physiological and in vitro data from published literature, provides reasonable fits to an extremely large database of in vivo pharmacokinetic data in mice, rats, and humans. Posterior parameter distributions were obtained by MCMC sampling using a hierarchical Bayesian population

statistical model and a large fraction of this in vivo database. Convergence of the MCMC samples for model parameters was good for mice, and adequate for rats and humans. Evaluation of posterior parameter distributions suggests reasonable results in light of prior expectations and the nature of the available calibration data. In addition, in rats and humans, the model produced predictions that are consistent with in vivo data from many studies not used for calibration (insufficient studies were available in mice for such “out of sample” evaluation). Finally, the local sensitivity analysis with respect to calibration data confirms that most of the scaling parameters are informed by at least some of the calibration data, and those that were not either were informed by prior data or would not have great impact on dose-metric predictions.

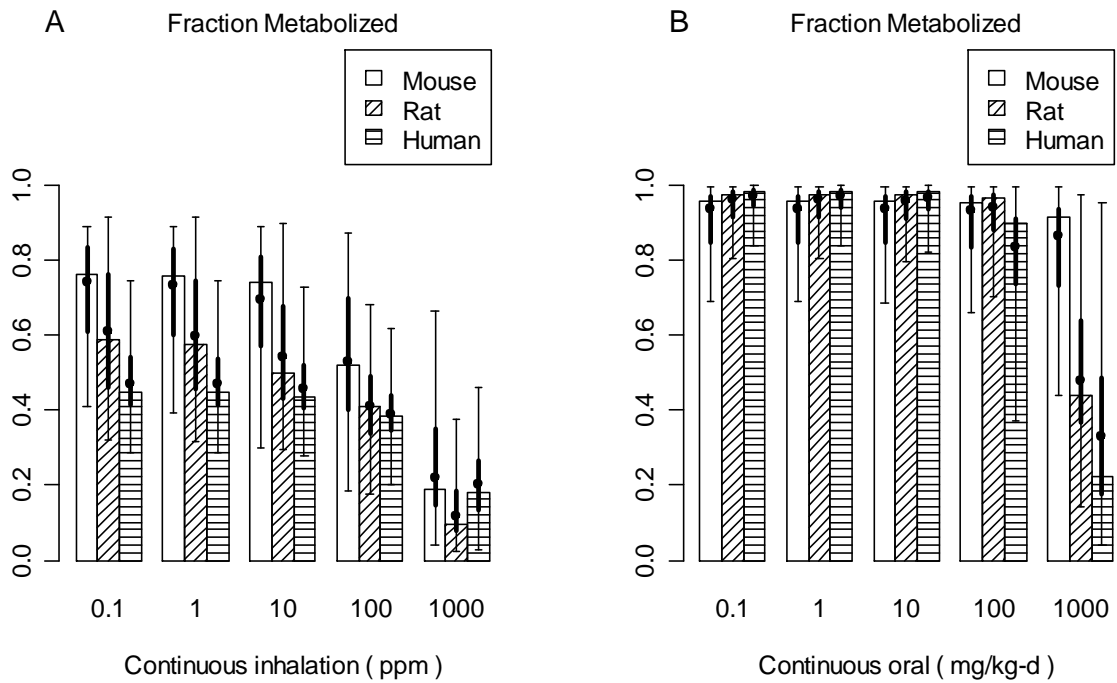
3.5.7. PBPK Model Dose-Metric Predictions

3.5.7.1. Characterization of Uncertainty and Variability

Since it is desirable to characterize the contributions from both uncertainty in population parameters and variability within the population, the following procedure is adopted. First, 500 sets of population parameters (i.e., population mean and variance for each parameter) are extracted from the posterior MCMC samples—these represent the uncertainty in the population parameters. To minimize autocorrelation, they were obtained by “thinning” the chains to the appropriate degree. From each of these sets of population parameters, 100 subject-specific parameters were generated by Monte Carlo—each of these represents the population variability, given a *particular* set of population parameters. Thus, a total of 50,000 subjects, representing 100 (variability) each for 500 different populations (uncertainty), were generated.

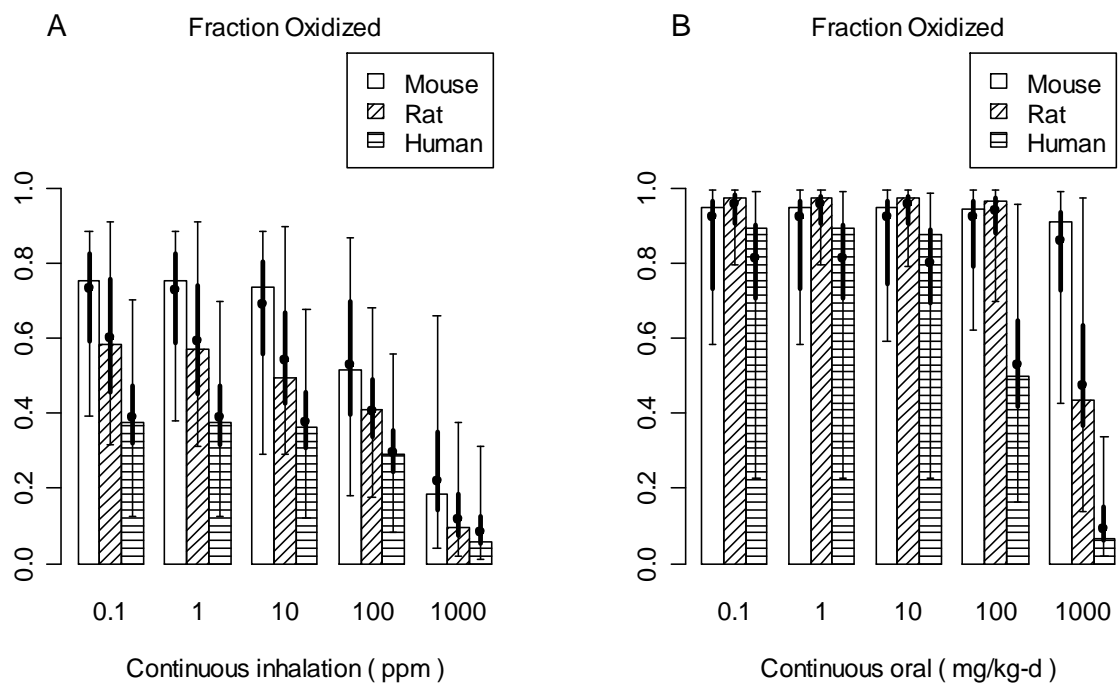
Each set was run for a variety of generic exposure scenarios. The combined distribution of all 50,000 individuals reflects both uncertainty and variability (i.e., the case in which one is trying to predict the dosimetry for a single random subject). In addition, for each dose-metric, the mean predicted internal dose was calculated from each of the 500 sets of 100 individuals, resulting in a distribution for the uncertainty in the population mean. Comparing the combined uncertainty and variability distribution with the uncertainty distribution in the population mean gives a sense of how much of the overall variation is due to uncertainty vs. variability.

Figures 3-17–3-25 show the results of these simulations for a number of representative dose-metrics across species continuously exposed via inhalation or orally. For display purposes, dose-metrics have been scaled by total intake (resulting in a predicted “fraction” metabolized) or exposure level (resulting in an internal dose per ppm for inhalation or per mg/kg-day for oral exposures). In these figures, the thin error bars represent the 95% CI for overall uncertainty and variability, and the thick error bars represent the 95% CI for the uncertainty in the population mean. The interpretation of these figures is that if the thick error bars are much smaller (or greater) than the thin error bars, then variability (or uncertainty) contributes the most to overall uncertainty and variability.



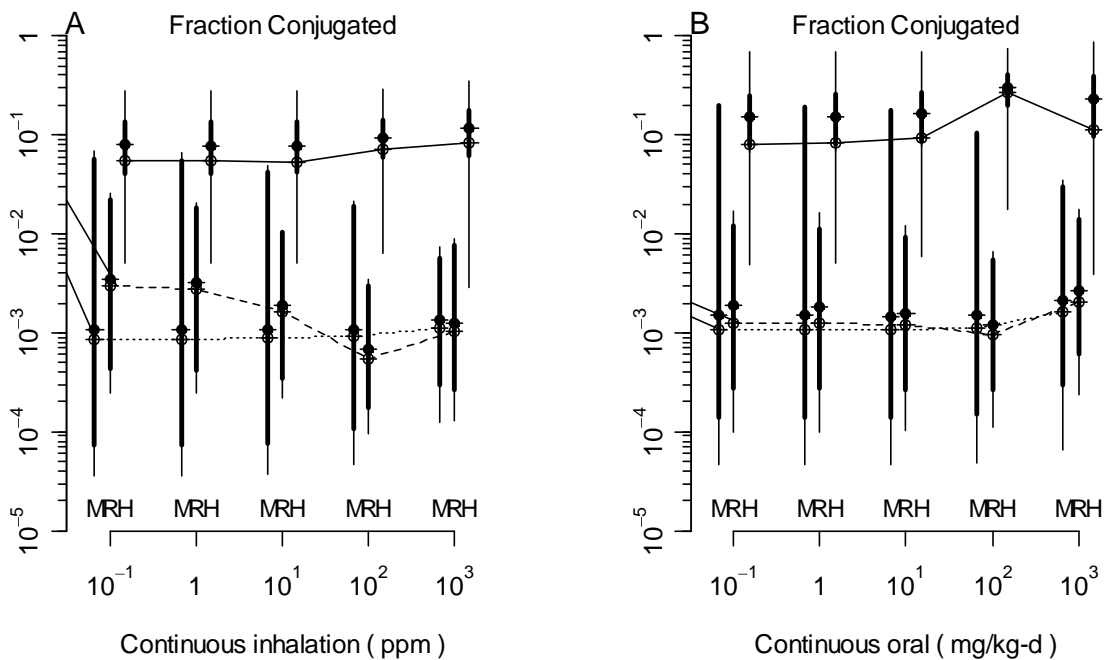
Bars and thin error bars represent the median estimate and 95% CI for a random subject, and reflect combined uncertainty and variability. Circles and thick error bars represent the median estimate and 95% CI for the population mean, and reflect uncertainty only.

Figure 3-17. PBPK model predictions for the fraction of intake that is metabolized under continuous inhalation (A) and oral (B) exposure conditions in mice (white), rats (diagonal hashing), and humans (horizontal hashing).



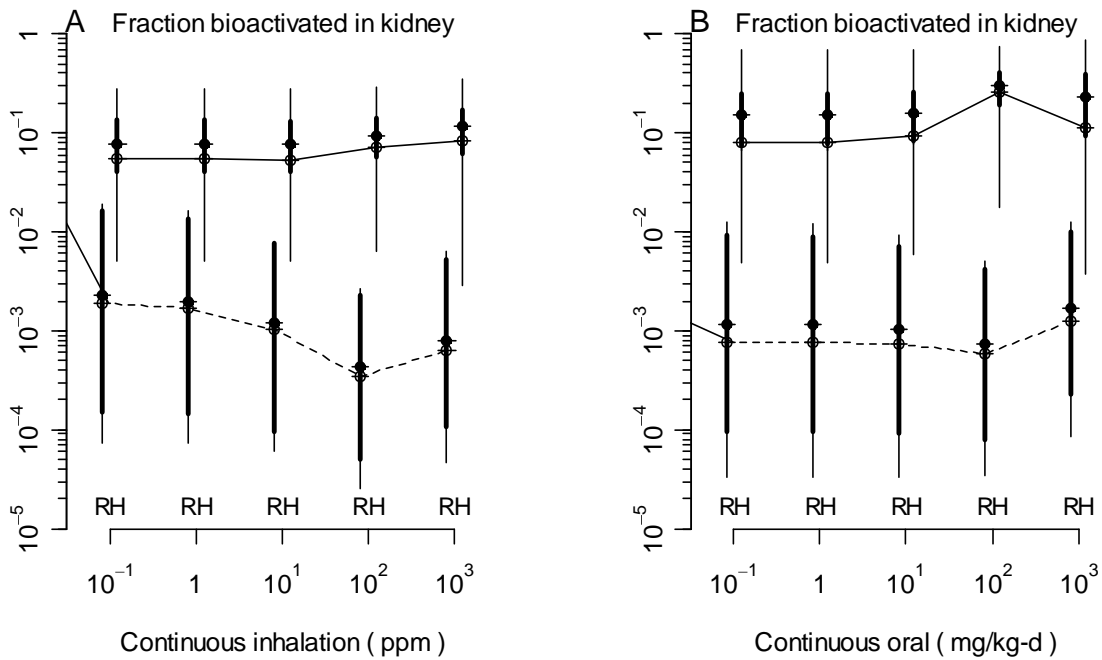
Bars and thin error bars represent the median estimate and 95% CI for a random subject, and reflect combined uncertainty and variability. Circles and thick error bars represent the median estimate and 95% CI for the population mean, and reflect uncertainty only.

Figure 3-18. PBPK model predictions for the fraction of intake that is metabolized by oxidation (in the liver and lung) under continuous inhalation (A) and oral (B) exposure conditions in mice (white), rats (diagonal hashing), and humans (horizontal hashing).



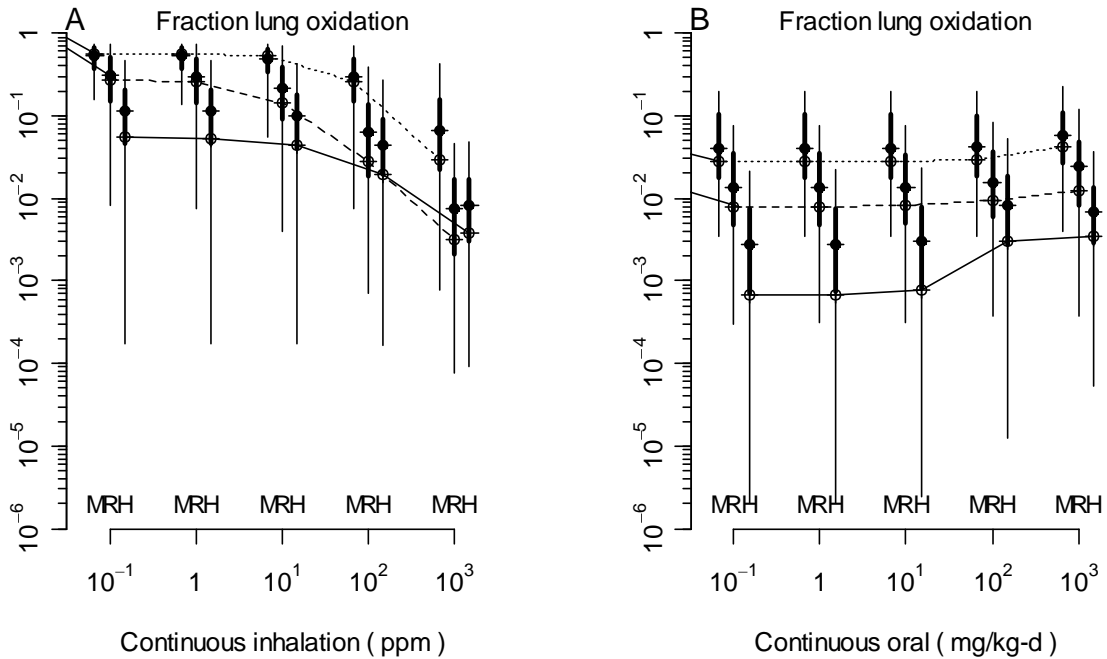
X-values are slightly offset for clarity. Open circles (connected by lines) and thin error bars represent the median estimate and 95% CI for a random subject, and reflect combined uncertainty and variability. Filled circles and thick error bars represent the median estimate and 95% CI for the population mean, and reflect uncertainty only.

Figure 3-19. PBPK model predictions for the fraction of intake that is metabolized by GSH conjugation (in the liver and kidney) under continuous inhalation (A) and oral (B) exposure conditions in mice (dotted line), rats (dashed line), and humans (solid line).



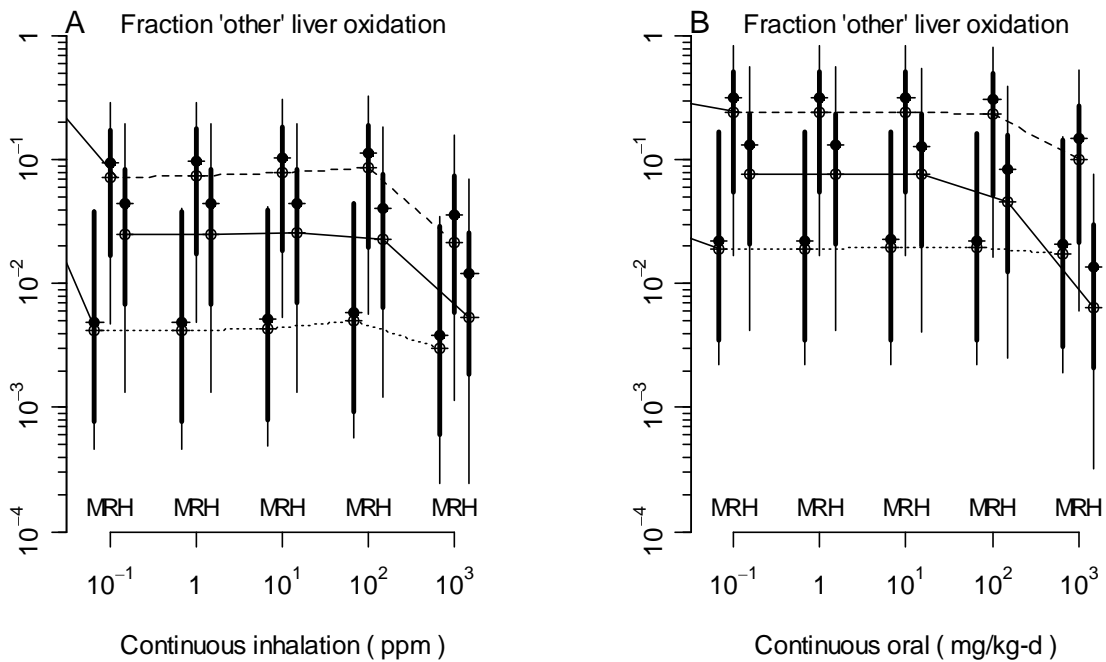
X-values are slightly offset for clarity. Open circles (connected by lines) and thin error bars represent the median estimate and 95% CI for a random subject, and reflect combined uncertainty and variability. Filled circles and thick error bars represent the median estimate and 95% CI for the population mean, and reflect uncertainty only.

Figure 3-20. PBPK model predictions for the fraction of intake that is bioactivated DCVC in the kidney under continuous inhalation (A) and oral (B) exposure conditions in rats (dashed line) and humans (solid line).



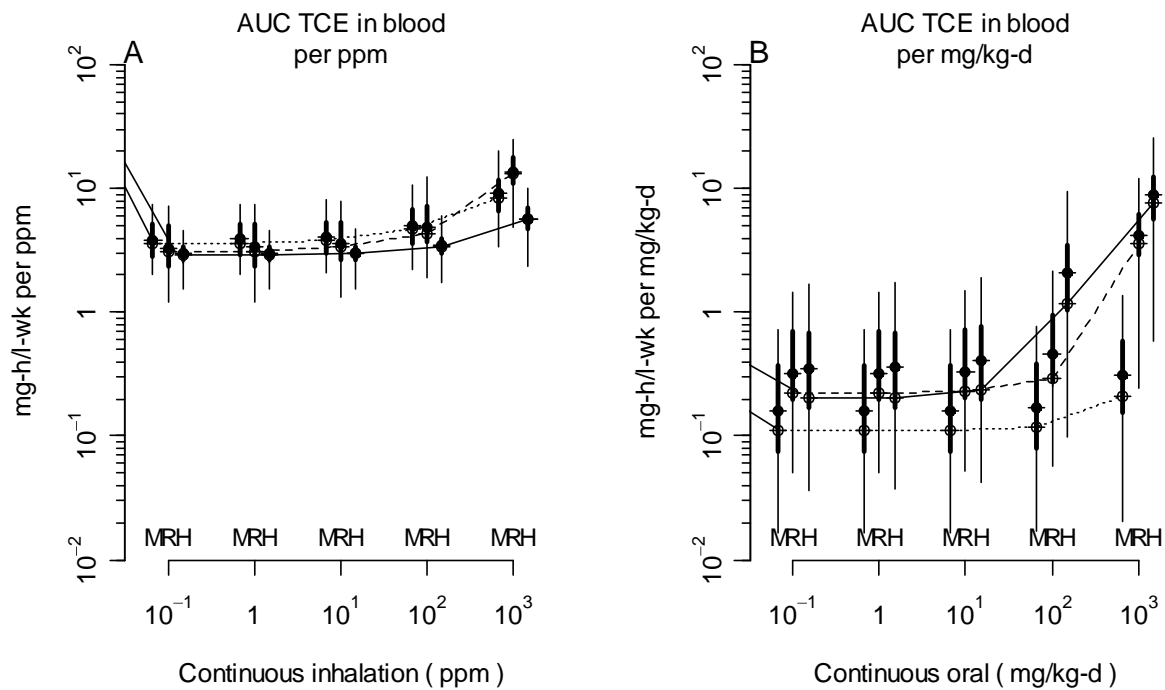
X-values are slightly offset for clarity. Open circles (connected by lines) and thin error bars represent the median estimate and 95% CI for a random subject, and reflect combined uncertainty and variability. Filled circles and thick error bars represent the median estimate and 95% CI for the population mean, and reflect uncertainty only.

Figure 3-21. PBPK model predictions for fraction of intake that is oxidized in the respiratory tract under continuous inhalation (A) and oral (B) exposure conditions in mice (dotted line), rats (dashed line), and humans (solid line).



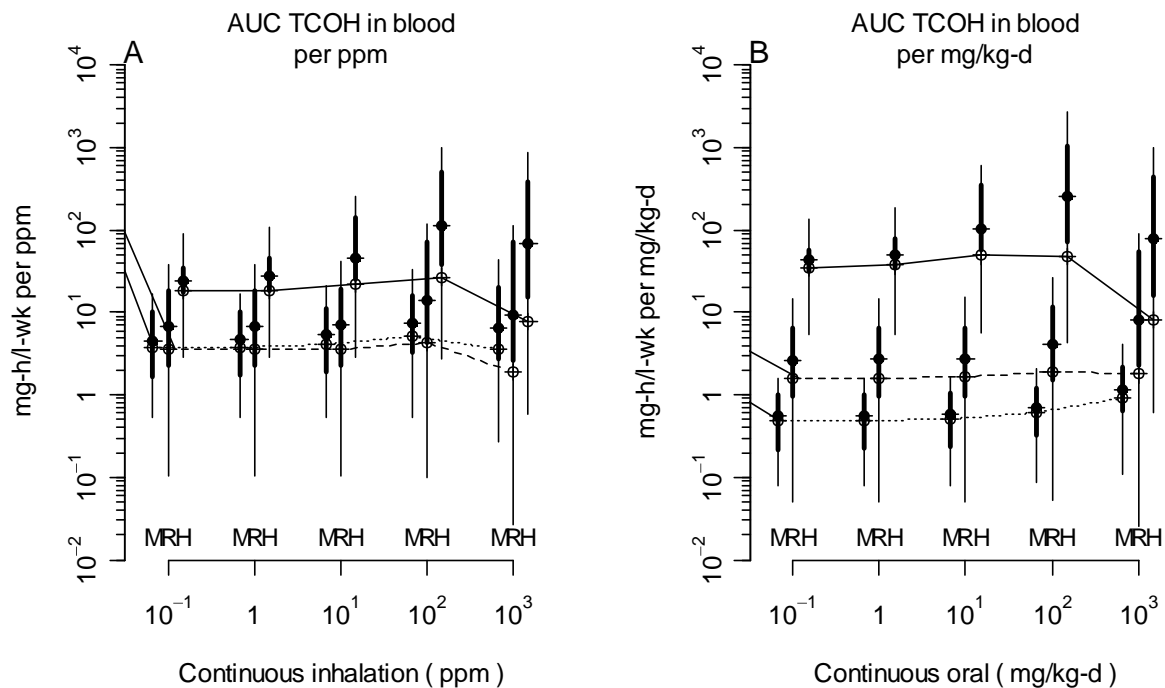
X-values are slightly offset for clarity. Open circles (connected by lines) and thin error bars represent the median estimate and 95% CI for a random subject, and reflect combined uncertainty and variability. Filled circles and thick error bars represent the median estimate and 95% CI for the population mean, and reflect uncertainty only.

Figure 3-22. PBPK model predictions for the fraction of intake that is “untracked” oxidation of TCE in the liver under continuous inhalation (A) and oral (B) exposure conditions in mice (dotted line), rats (dashed line), and humans (solid line).



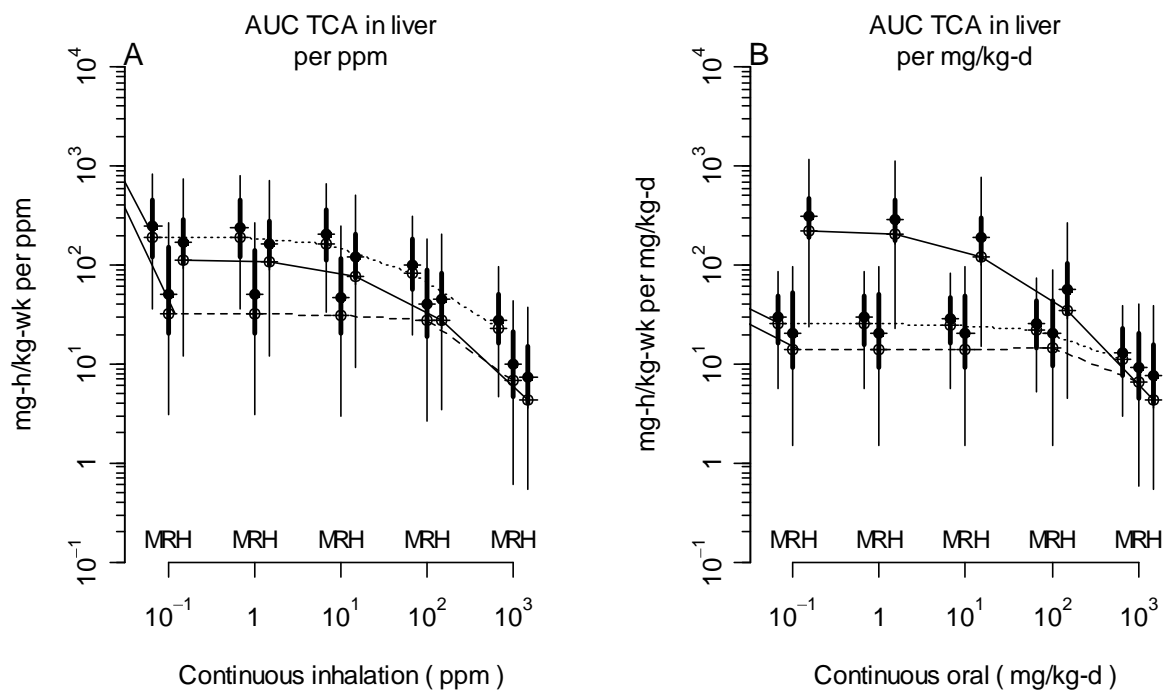
X-values are slightly offset for clarity. Open circles (connected by lines) and thin error bars represent the median estimate and 95% CI for a random subject, and reflect combined uncertainty and variability. Filled circles and thick error bars represent the median estimate and 95% CI for the population mean, and reflect uncertainty only.

Figure 3-23. PBPK model predictions for the weekly AUC of TCE in venous blood (mg-hour/L-week) per unit exposure (ppm or mg/kg-day) under continuous inhalation (A) and oral (B) exposure conditions in mice (dotted line), rats (dashed line), and humans (solid line).



X-values are slightly offset for clarity. Open circles (connected by lines) and thin error bars represent the median estimate and 95% CI for a random subject, and reflect combined uncertainty and variability. Filled circles and thick error bars represent the median estimate and 95% CI for the population mean, and reflect uncertainty only.

Figure 3-24. PBPK model predictions for the weekly AUC of TCOH in blood (mg-hour/L-week) per unit exposure (ppm or mg/kg-day) under continuous inhalation (A) and oral (B) exposure conditions in mice (dotted line), rats (dashed line), and humans (solid line).



X-values are slightly offset for clarity. Open circles (connected by lines) and thin error bars represent the median estimate and 95% CI for a random subject, and reflect combined uncertainty and variability. Filled circles and thick error bars represent the median estimate and 95% CI for the population mean, and reflect uncertainty only.

Figure 3-25. PBPK model predictions for the weekly AUC of TCA in the liver (mg-hour/L-week) per unit exposure (ppm or mg/kg-day) under continuous inhalation (A) and oral (B) exposure conditions in mice (dotted line), rats (dashed line), and humans (solid line).

For application to human health risk assessment, the uncertainty in and variability among rodent internal dose estimates both contribute to uncertainty in human risk estimates. Therefore, it is appropriate to combine uncertainty and variability when applying rodent dose-metric predictions to quantitative risk assessment. The median and 95% CI for each dose-metric at some representative exposures in rodents are given in Tables 3-48 and 3-49, and the CI in these tables includes both uncertainty in the population mean and variance as well as variability in the population. On the other hand, for use in predicting human risk, it is often necessary to separate, to the extent possible, interindividual variability from uncertainty, and this disaggregation is summarized in Table 3-50.

3.5.7.2. Local Sensitivity Analysis With Respect to Dose-Metric Predictions

To assess the parameter sensitivity of dose-metric predictions, a local sensitivity analysis is performed. The representative exposure scenarios in Tables 3-48–3-50 are used, but with

metabolic flux dose-metrics converted to “fraction of intake” (i.e., amount metabolized through a pathway divided by total dose). Each parameter is centered on the sample mean of its estimated population mean, and then increased and decreased by 5%. The relative change in the model output $f(\theta)$ is used to estimate a local SC as follows:

$$SC = 10 \times \{f(\theta_+) - f(\theta_-)\} / [\frac{1}{2} \times \{f(\theta_+) + f(\theta_-)\}]$$

Here, $f(\theta)$ is one of dose-metric predictions, θ_{\pm} is the MLE or baseline value of $\pm 5\%$. For log-transformed parameters, 0.05 was added or subtracted from the baseline value, whereas for untransformed parameters, the baseline value was multiplied by 1.05 or 0.95.

Note that local sensitivity analyses as typically performed in deterministic PBPK modeling can only inform the “primary” effects of parameter uncertainties (i.e., the direct change on the quantity of interest due to change in a parameter). They cannot address the *propagation* of uncertainties through an analysis, such as those that can arise due to parameter correlations in the parameter fitting process. Those can only be addressed in a global sensitivity analysis, which is left for future research.

The results of local sensitivity analyses are shown in Figures 3-26–3-31. As expected, each dose-metric is sensitive to a only a small fraction of the scaling parameters. Many of these are well-specified a priori, either due to their being physiological parameters or partition coefficients that can be measured in vitro. The remaining sensitive parameters are generally related to metabolism or clearance.

Table 3-48. Posterior predictions for representative internal doses: mouse^a

Dose-metric	Posterior predictions for mouse dose-metrics: median (2.5%, 97.5%)				Units
	100 ppm, 7 hr/d, 5 d/wk	600 ppm, 7 hr/d, 5 d/wk	300 mg/kg-d, 5 d/wk	1,000 mg/kg-d, 5 d/wk	
ABioactDCVCBW34	0.304 (0.000534, 12.4)	2.35 (0.00603, 37)	0.676 (0.00193, 18.4)	2.81 (0.0086, 42.4)	mg/wk-kg ^{3/4}
ABioactDCVCKid	43.7 (0.0774, 1780)	336 (0.801, 5,240)	96.8 (0.281, 2,550)	393 (1.23, 6,170)	mg/wk-kg tissue
AMetGSHBW34	0.684 (0.0307, 17.6)	5.15 (0.285, 44.9)	1.66 (0.0718, 24.5)	6.37 (0.567, 49.4)	mg/wk-kg ^{3/4}
AMetLiv1BW34	170 (61.2, 403)	878 (342, 2,030)	400 (125, 610)	874 (233, 1,960)	mg/wk-kg ^{3/4}
AMetLivOtherBW34	3.81 (0.372, 38.4)	20 (1.86, 192)	8.38 (0.773, 80.1)	20 (1.55, 202)	mg/wk-kg ^{3/4}
AMetLivOtherLiv	196 (19, 2,070)	1,030 (96.5, 10,100)	437 (39.5, 4,180)	1,020 (82.1, 10,400)	mg/wk-kg tissue
AMetLngBW34	187 (7.75, 692)	263 (10.9, 2,240)	38.5 (3.49, 147)	127 (8.59, 484)	mg/wk-kg ^{3/4}
AMetLngResp	638,000 (26,500, 2,510,000)	918,000 (36,800, 7,980,000)	134,000 (12,500, 514,000)	433,000 (30,200, 1,690,000)	mg/wk-kg tissue
AUCBld	96.9 (45, 211)	822 (356, 2,040)	110 (6.95, 411)	592 (56, 1,910)	mg-hr/L-wk
AUCCTCOH	87.9 (9.9, 590)	480 (42.1, 4,140)	132 (14.4, 670)	389 (34, 2,600)	mg-hr/L-wk
AUCLivTCA	1,880 (444, 7,190)	5,070 (1,310, 18,600)	2,260 (520, 8,750)	4,660 (939, 18,900)	mg-hr/L-wk
TotMetabBW34	377 (140, 917)	1,260 (475, 3,480)	472 (165, 617)	1,110 (303, 2,010)	mg/wk-kg ^{3/4}
TotOxMetabBW34	375 (139, 916)	1,250 (451, 3,450)	465 (161, 616)	1,100 (294, 2,010)	mg/wk-kg ^{3/4}
TotTCAInBW	272 (88.9, 734)	729 (267, 1,950)	334 (106, 875)	694 (185, 1,910)	mg/wk-kg

^aMouse body weight is assumed to be 0.03 kg. Predictions are weekly averages over 10 weeks of the specified exposure protocol. CI reflects both uncertainties in population parameters (mean, variance) as well as population variability.

Table 3-49. Posterior predictions for representative internal doses: rat^a

Dose-metric	Posterior predictions for rat dose-metrics: median (2.5%,97.5%)				Units
	100 ppm, 7 hr/d, 5 d/wk	600 ppm, 7 hr/d, 5 d/wk	300 mg/kg-d, 5 d/wk	1,000 mg/kg-d, 5 d/wk	
ABioactDCVCBW34	0.341 (0.0306, 2.71)	2.3 (0.175, 22.6)	2.15 (0.17, 20.2)	8.89 (0.711, 84.1)	mg/wk-kg ^{3/4}
ABioactDCVCKid	67.8 (6.03, 513)	450 (35.4, 4,350)	420 (31.6, 3,890)	1,720 (134, 15,800)	mg/wk-kg tissue
AMetGSHBW34	0.331 (0.0626, 2.16)	2.27 (0.315, 19.3)	2.13 (0.293, 16)	8.84 (1.35, 69.3)	mg/wk-kg ^{3/4}
AMetLiv1BW34	176 (81.1, 344)	623 (271, 1,270)	539 (176, 1,060)	951 (273, 2,780)	mg/wk-kg ^{3/4}
AMetLivOtherBW34	45.5 (2.52, 203)	160 (7.84, 749)	134 (6.83, 659)	238 (11.3, 1390)	mg/wk-kg ^{3/4}
AMetLivOtherLiv	1,870 (92.1, 8,670)	6,660 (313, 31,200)	5,490 (280, 27,400)	9,900 (492, 59,600)	mg/wk-kg tissue
AMetLngBW34	15 (0.529, 173)	24.5 (0.819, 227)	15.1 (0.527, 115)	32.1 (1.01, 311)	mg/wk-kg ^{3/4}
AMetLngResp	41,900 (1,460, 496,000)	67,900 (2,350, 677,000)	40,800 (1,500, 325,000)	85,700 (2,660, 877,000)	mg/wk-kg tissue
AUCCBld	86.7 (39.2, 242)	1,160 (349, 2,450)	670 (47.8, 1,850)	3,340 (828, 8,430)	mg-hr/L-wk
AUCCTCOH	83.6 (1.94, 1,560)	446 (6, 10,900)	304 (4.71, 7,590)	685 (8.14, 32,500)	mg-hr/L-wk
AUCLivTCA	587 (53.7, 4,740)	2,030 (186, 13,400)	1,730 (124, 11,800)	3,130 (200, 21,000)	mg-hr/L-wk
TotMetabBW34	206 (103, 414)	682 (288, 1,430)	572 (199, 1,080)	1,030 (302, 2,920)	mg/wk-kg ^{3/4}
TotOxMetabBW34	206 (103, 414)	677 (285, 1,430)	568 (191, 1,080)	1,010 (286, 2,910)	mg/wk-kg ^{3/4}
TotTCAInBW	31.7 (3.92, 174)	110 (13.8, 490)	90.1 (10.4, 417)	164 (17.3, 800)	mg/wk-kg

^aRat body weight is assumed to be 0.3 kg. Predictions are weekly averages over 10 weeks of the specified exposure protocol. CI reflects both uncertainties in population parameters (mean, variance) as well as population variability.

Table 3-50. Posterior predictions for representative internal doses: human^a

Dose-metric	Posterior predictions for human dose-metrics: 2.5% population: median (2.5%, 97.5%) 50% population: median (2.5%, 97.5%) 97.5% population: median (2.5%, 97.5%)			
	Female 0.001 ppm continuous	Male 0.001 ppm continuous	Female 0.001 mg/kg-d continuous	Male 0.001 mg/kg-d continuous
ABioactDCVCBW34	0.000256 (6.97×10^{-5} , 0.000872)	0.000254 (6.94×10^{-5} , 0.000879)	0.000197 (6.13×10^{-5} , 0.000502)	0.0002 (6.24×10^{-5} , 0.000505)
	0.00203 (0.00087, 0.00408)	0.00202 (0.000859, 0.00413)	0.00262 (0.0012, 0.00539)	0.00271 (0.00125, 0.00559)
	0.0119 (0.00713, 0.0177)	0.012 (0.00699, 0.0182)	0.021 (0.0118, 0.0266)	0.022 (0.0124, 0.0277)
ABioactDCVCKid	0.02 (0.00549, 0.0709)	0.0207 (0.00558, 0.0743)	0.0152 (0.0048, 0.0384)	0.016 (0.00493, 0.0407)
	0.16 (0.0671, 0.324)	0.163 (0.0679, 0.342)	0.207 (0.0957, 0.43)	0.22 (0.102, 0.459)
	0.95 (0.56, 1.45)	0.979 (0.563, 1.51)	1.68 (0.956, 2.26)	1.81 (1.03, 2.43)
AMetGSHBW34	0.000159 (4.38×10^{-5} , 0.000539)	0.000157 (4.37×10^{-5} , 0.00054)	0.000121 (3.82×10^{-5} , 0.000316)	0.000123 (3.82×10^{-5} , 0.000323)
	0.00126 (0.000536, 0.00253)	0.00125 (0.000528, 0.00254)	0.00161 (0.000748, 0.00331)	0.00167 (0.000777, 0.00343)
	0.00736 (0.00442, 0.011)	0.00736 (0.00434, 0.0112)	0.013 (0.00725, 0.0164)	0.0136 (0.00759, 0.0171)
AMetLiv1BW34	0.00161 (0.000619, 0.00303)	0.00157 (0.000608, 0.00292)	0.00465 (0.00169, 0.0107)	0.00498 (0.00184, 0.0112)
	0.00637 (0.00501, 0.00799)	0.00619 (0.00484, 0.00779)	0.0172 (0.0153, 0.0183)	0.018 (0.0161, 0.0191)
	0.0157 (0.0118, 0.0206)	0.0152 (0.0115, 0.02)	0.0192 (0.019, 0.0193)	0.02 (0.0198, 0.0201)
AMetLivOtherBW34	4.98×10^{-5} (8.59×10^{-6} , 0.000222)	4.87×10^{-5} (8.33×10^{-6} , 0.000214)	0.000143 (2.35×10^{-5} , 0.000681)	0.00015 (2.49×10^{-5} , 0.000713)
	0.000671 (0.000134, 0.00159)	0.000652 (0.000129, 0.00153)	0.00166 (0.00035, 0.00365)	0.00173 (0.000365, 0.00382)
	0.00507 (0.00055, 0.00905)	0.00491 (0.000531, 0.00885)	0.00993 (0.00109, 0.0153)	0.0103 (0.00113, 0.0159)
AMetLivOtherLiv	0.000748 (0.000138, 0.00335)	0.00065 (0.000119, 0.00288)	0.00214 (0.000354, 0.00979)	0.00197 (0.00033, 0.00907)
	0.0104 (0.00225, 0.0237)	0.00898 (0.00193, 0.0203)	0.0253 (0.00564, 0.0543)	0.0234 (0.00526, 0.0503)
	0.0805 (0.00871, 0.147)	0.0691 (0.00751, 0.127)	0.157 (0.0188, 0.251)	0.146 (0.0173, 0.232)
AMetLngBW34	6.9×10^{-6} (6.13×10^{-7} , 7.99×10^{-5})	7.25×10^{-6} (6.44×10^{-7} , 8.39×10^{-5})	7.54×10^{-8} (6.59×10^{-9} , 7.85×10^{-7})	7.05×10^{-8} (6.1×10^{-9} , 7.25×10^{-7})
	0.00122 (0.000309, 0.0032)	0.00127 (0.000325, 0.00329)	1.51×10^{-5} (3.44×10^{-6} , 4.6×10^{-5})	1.39×10^{-5} (3.21×10^{-6} , 4.24×10^{-5})
	0.0123 (0.00563, 0.0197)	0.0124 (0.00582, 0.0199)	0.000396 (0.000104, 0.00097)	0.000366 (9.54×10^{-5} , 0.000906)

Table 3-50. Posterior predictions for representative internal doses: human^a (continued)

Dose-metric	Posterior predictions for human dose-metrics: 2.5% population: median (2.5%, 97.5%) 50% population: median (2.5%, 97.5%) 97.5% population: median (2.5%, 97.5%)			
	Female 0.001 ppm continuous	Male 0.001 ppm continuous	Female 0.001 mg/kg-d continuous	Male 0.001 mg/kg-d continuous
AMetLngResp	0.0144 (0.00116, 0.155)	0.0146 (0.00118, 0.157)	0.00015 (1.27 × 10 ⁻⁵ , 0.00153)	0.000134 (1.15 × 10 ⁻⁵ , 0.00137)
	2.44 (0.613, 6.71)	2.44 (0.621, 6.65)	0.0313 (0.00725, 0.0963)	0.0279 (0.00644, 0.086)
	25.8 (12.4, 42.3)	25.3 (12.2, 41.2)	0.813 (0.216, 2.13)	0.716 (0.189, 1.9)
AUCCBld	0.00151 (0.00122, 0.00186)	0.00158 (0.00127, 0.00191)	4.33 × 10 ⁻⁵ (3.3 × 10 ⁻⁵ , 6.23 × 10 ⁻⁵)	3.84 × 10 ⁻⁵ (2.89 × 10 ⁻⁵ , 5.61 × 10 ⁻⁵)
	0.00285 (0.00252, 0.00315)	0.00295 (0.00262, 0.00326)	0.000229 (0.000122, 0.000436)	0.000204 (0.000109, 0.000391)
	0.00444 (0.00404, 0.00496)	0.00456 (0.00416, 0.00507)	0.00167 (0.000766, 0.00324)	0.00153 (0.000693, 0.00303)
AUCCTCOH	0.00313 (0.00135, 0.00547)	0.00305 (0.00134, 0.00532)	0.00584 (0.00205, 0.0122)	0.00615 (0.00213, 0.0127)
	0.0181 (0.0135, 0.0241)	0.0179 (0.0133, 0.0238)	0.0333 (0.025, 0.0423)	0.035 (0.0264, 0.0445)
	0.082 (0.0586, 0.118)	0.0812 (0.0585, 0.117)	0.115 (0.0872, 0.163)	0.122 (0.0919, 0.172)
AUCLivTCA	0.0152 (0.00668, 0.0284)	0.0137 (0.00598, 0.0258)	0.029 (0.0116, 0.0524)	0.0279 (0.0114, 0.0501)
	0.126 (0.0784, 0.194)	0.114 (0.0704, 0.177)	0.227 (0.138, 0.343)	0.219 (0.133, 0.33)
	0.754 (0.441, 1.38)	0.699 (0.408, 1.3)	1.11 (0.661, 1.87)	1.09 (0.64, 1.88)
TotMetabBW34	0.0049 (0.00383, 0.00595)	0.00482 (0.0038, 0.00585)	0.0163 (0.0136, 0.0181)	0.0173 (0.0147, 0.019)
	0.0107 (0.00893, 0.0129)	0.0105 (0.00877, 0.0127)	0.0191 (0.0188, 0.0193)	0.0199 (0.0196, 0.0201)
	0.0246 (0.0185, 0.0326)	0.0244 (0.0183, 0.0324)	0.0194 (0.0194, 0.0194)	0.0202 (0.0202, 0.0202)
TotOxMetabBW34	0.00273 (0.00143, 0.00422)	0.00269 (0.00143, 0.00415)	0.0049 (0.00183, 0.0108)	0.00516 (0.00194, 0.0114)
	0.00871 (0.0069, 0.0111)	0.00857 (0.00675, 0.011)	0.0173 (0.0154, 0.0183)	0.018 (0.0161, 0.0191)
	0.0224 (0.0158, 0.0309)	0.0222 (0.0155, 0.0308)	0.0192 (0.019, 0.0193)	0.02 (0.0198, 0.0201)

Table 3-50. Posterior predictions for representative internal doses: human^a (continued)

Dose-metric	Posterior predictions for human dose-metrics: 2.5% population: median (2.5%, 97.5%) 50% population: median (2.5%, 97.5%) 97.5% population: median (2.5%, 97.5%)			
	Female 0.001 ppm continuous	Male 0.001 ppm continuous	Female 0.001 mg/kg-d continuous	Male 0.001 mg/kg-d continuous
TotTCAInBW	0.000259 (0.000121, 0.000422)	0.000246 (0.000114, 0.000397)	0.000501 (0.000189, 0.000882)	0.000506 (0.000192, 0.00089)
	0.00154 (0.00114, 0.00202)	0.00146 (0.00109, 0.00193)	0.00286 (0.00222, 0.00357)	0.00289 (0.00222, 0.0036)
	0.00525 (0.00399, 0.00745)	0.00499 (0.0038, 0.0071)	0.00659 (0.00579, 0.00724)	0.00662 (0.00581, 0.00726)

^aHuman body weight is assumed to be 70 kg for males, 60 kg for females. Predictions are weekly averages over 100 weeks of continuous exposure (dose-metric units same as previous tables). Each row represents a different population percentile (2.5, 50, and 97.5%), and the CI in each entry reflects uncertainty in population parameters (mean, variance).

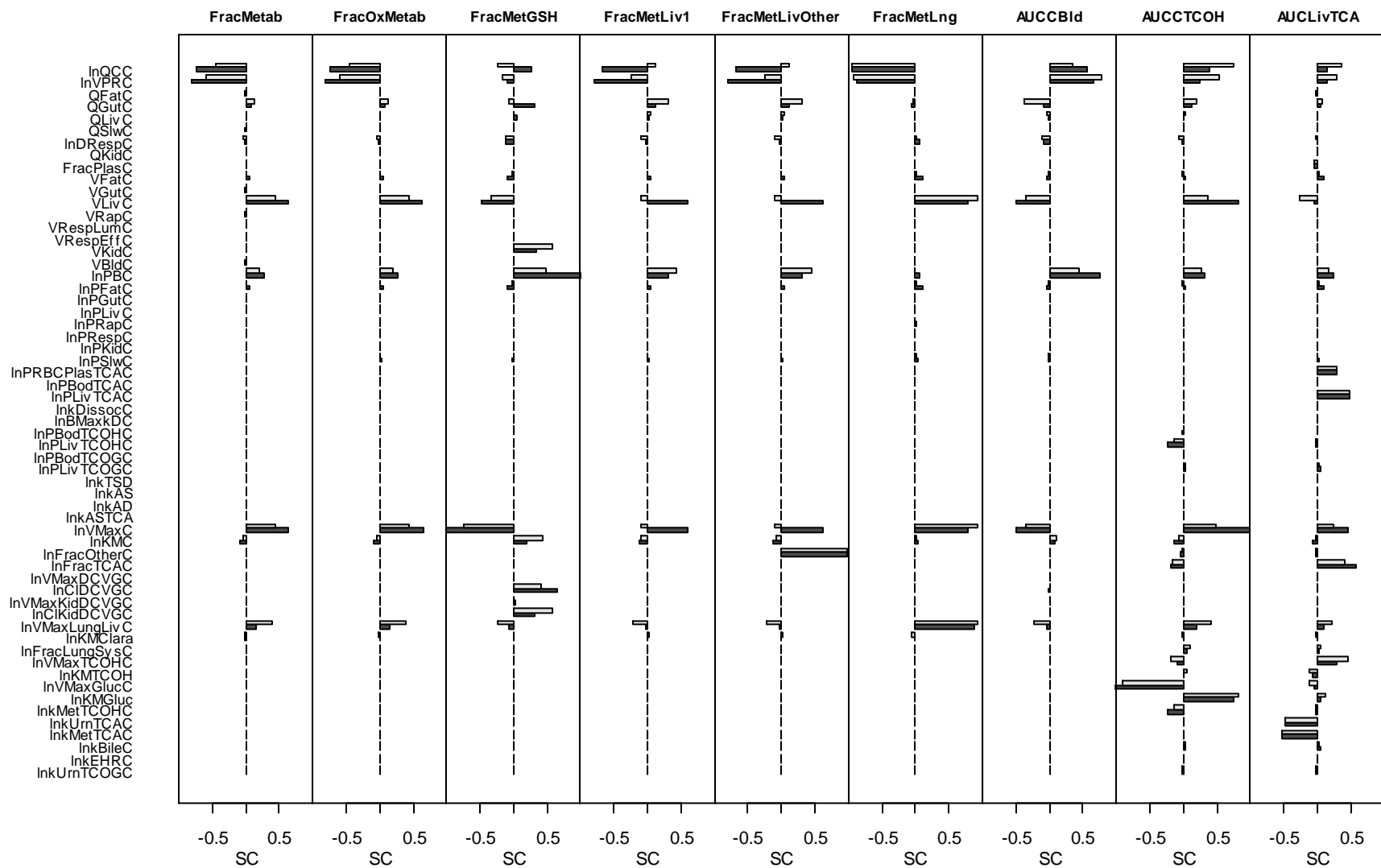


Figure 3-26. Sensitivity analysis results: SC for mouse scaling parameters with respect to dose-metrics following 100 ppm (light bars) and 600 ppm (dark bars), 7 hours/day, 5 days/week inhalation exposures.

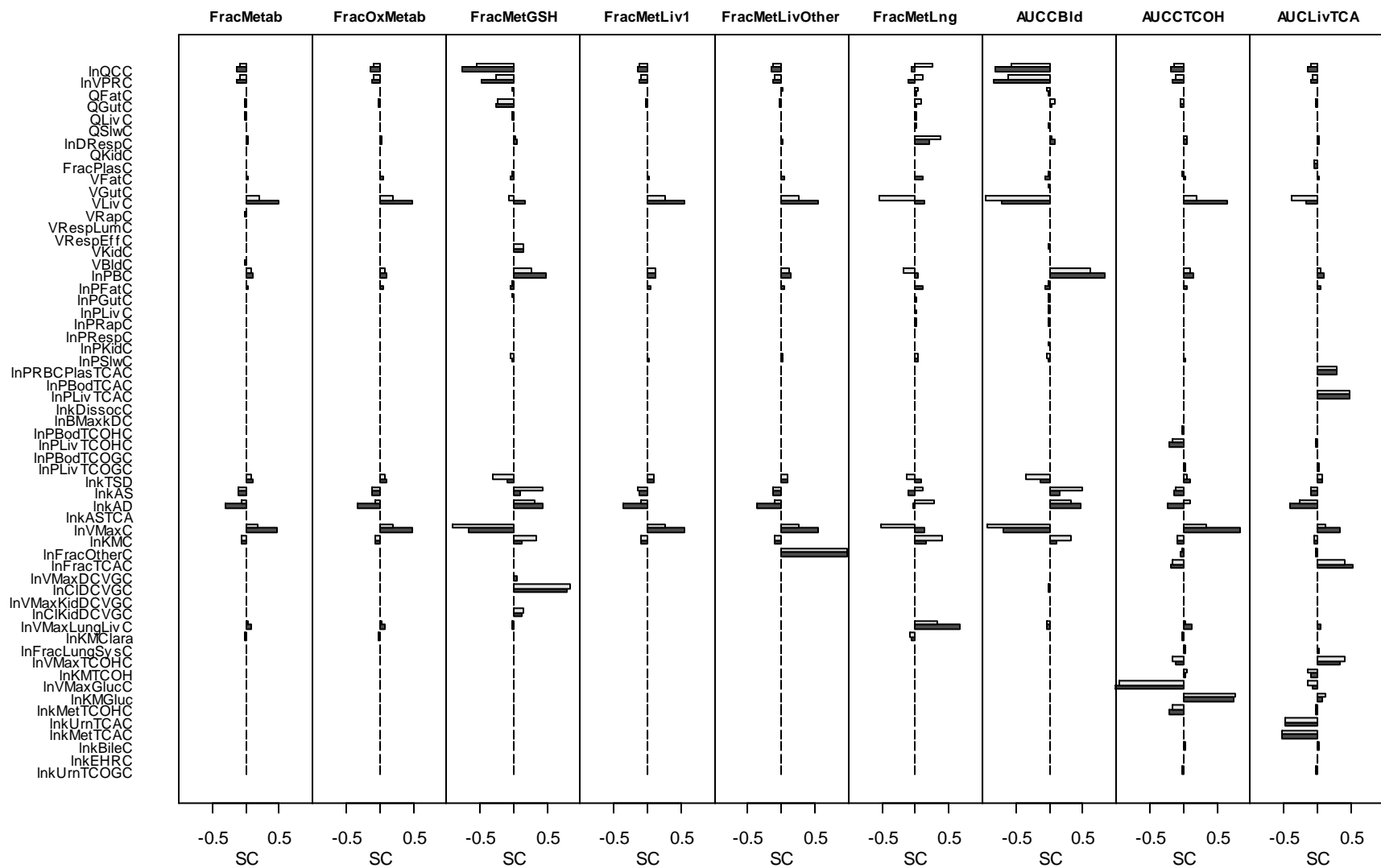


Figure 3-27. Sensitivity analysis results: SC for mouse scaling parameters with respect to dose-metrics following 300 mg/kg-day (light bars) and 1,000 mg/kg-day (dark bars), 5 days/week gavage exposures.

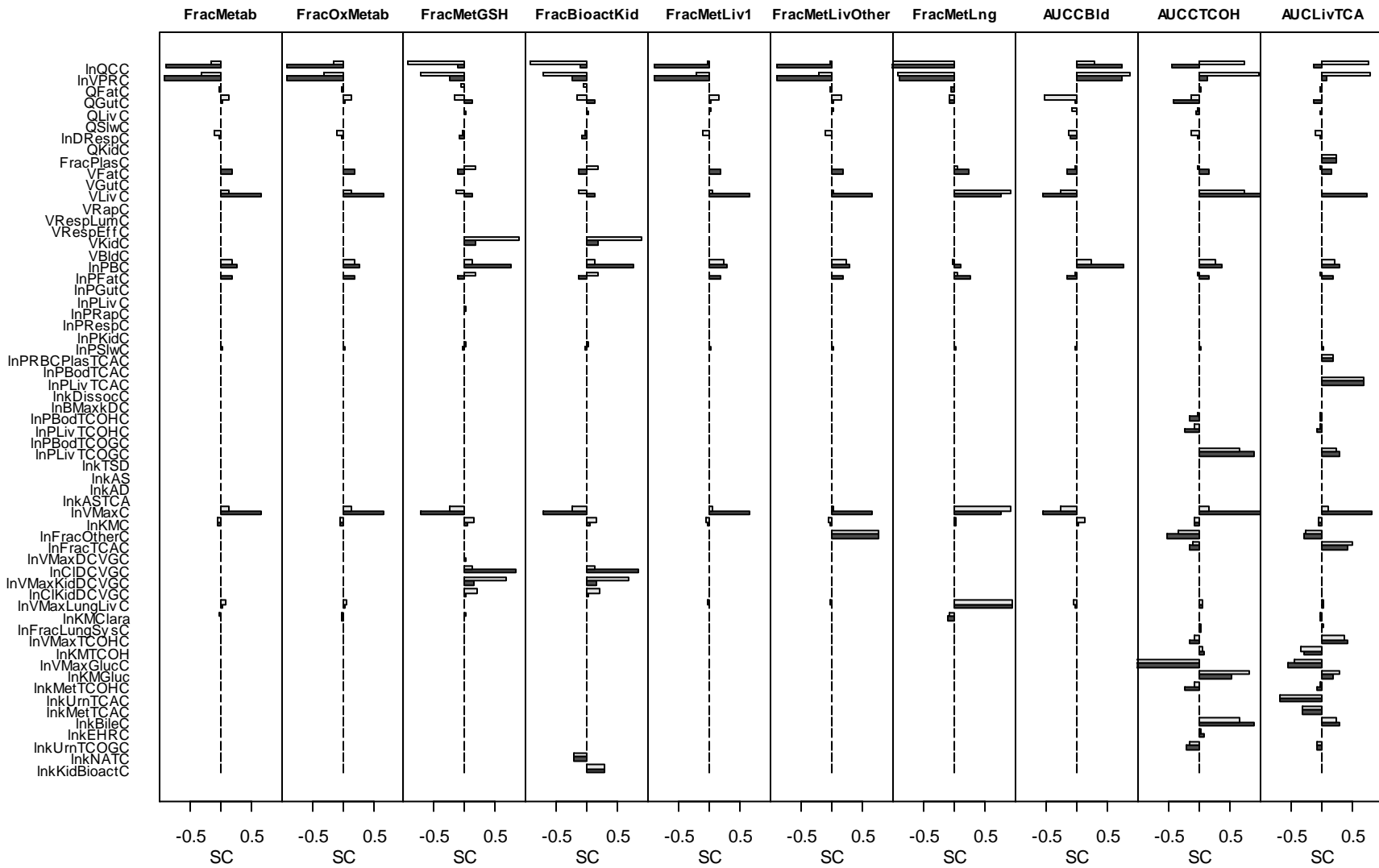


Figure 3-28. Sensitivity analysis results: SC for rat scaling parameters with respect to dose-metrics following 100 ppm (light bars) and 600 ppm (dark bars), 7 hours/day, 5 days/week inhalation exposures.

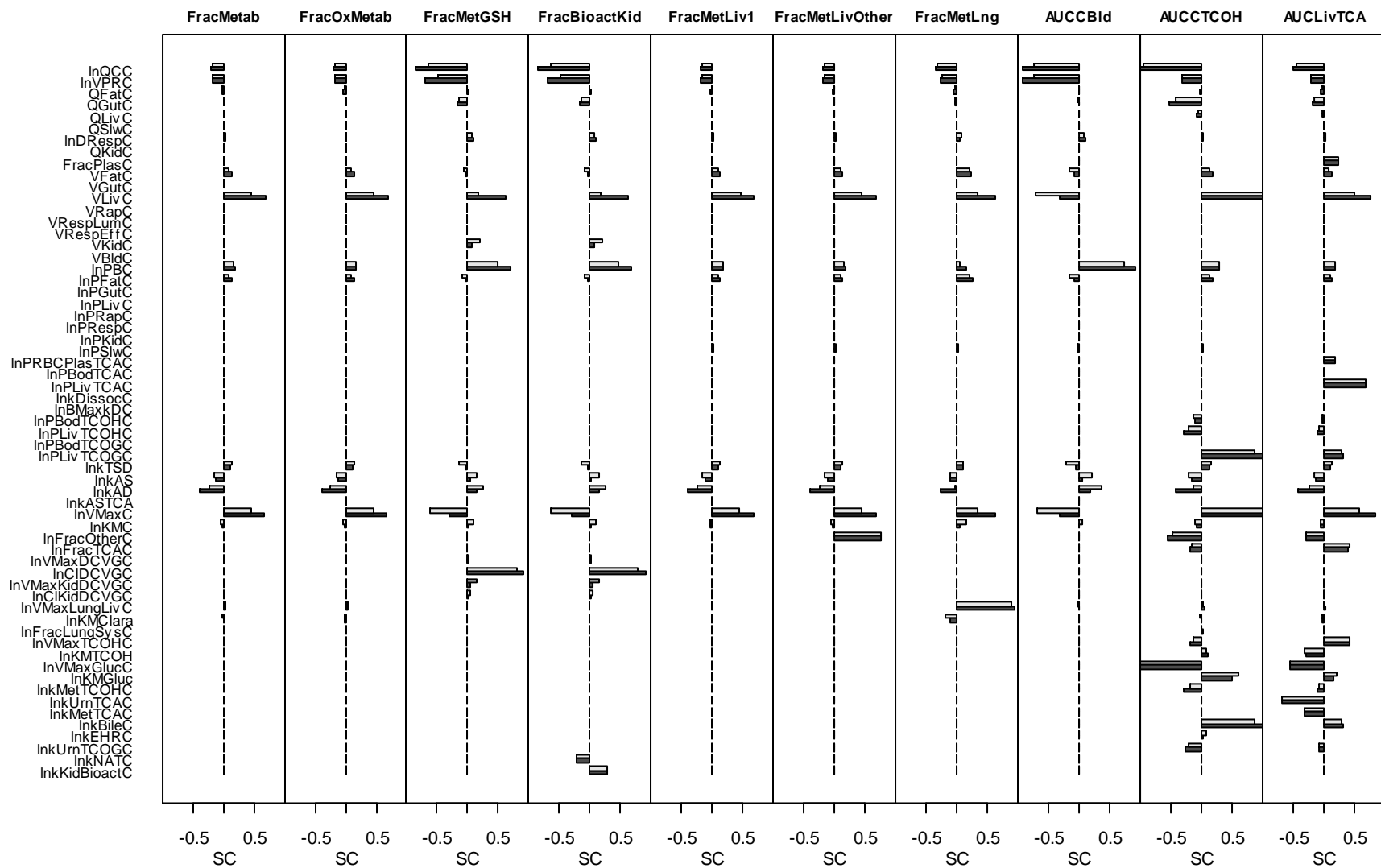


Figure 3-29. Sensitivity analysis results: SC for rat scaling parameters with respect to dose-metrics following 300 mg/kg-day (light bars) and 1,000 mg/kg-day (dark bars), 5 days/week gavage exposures.

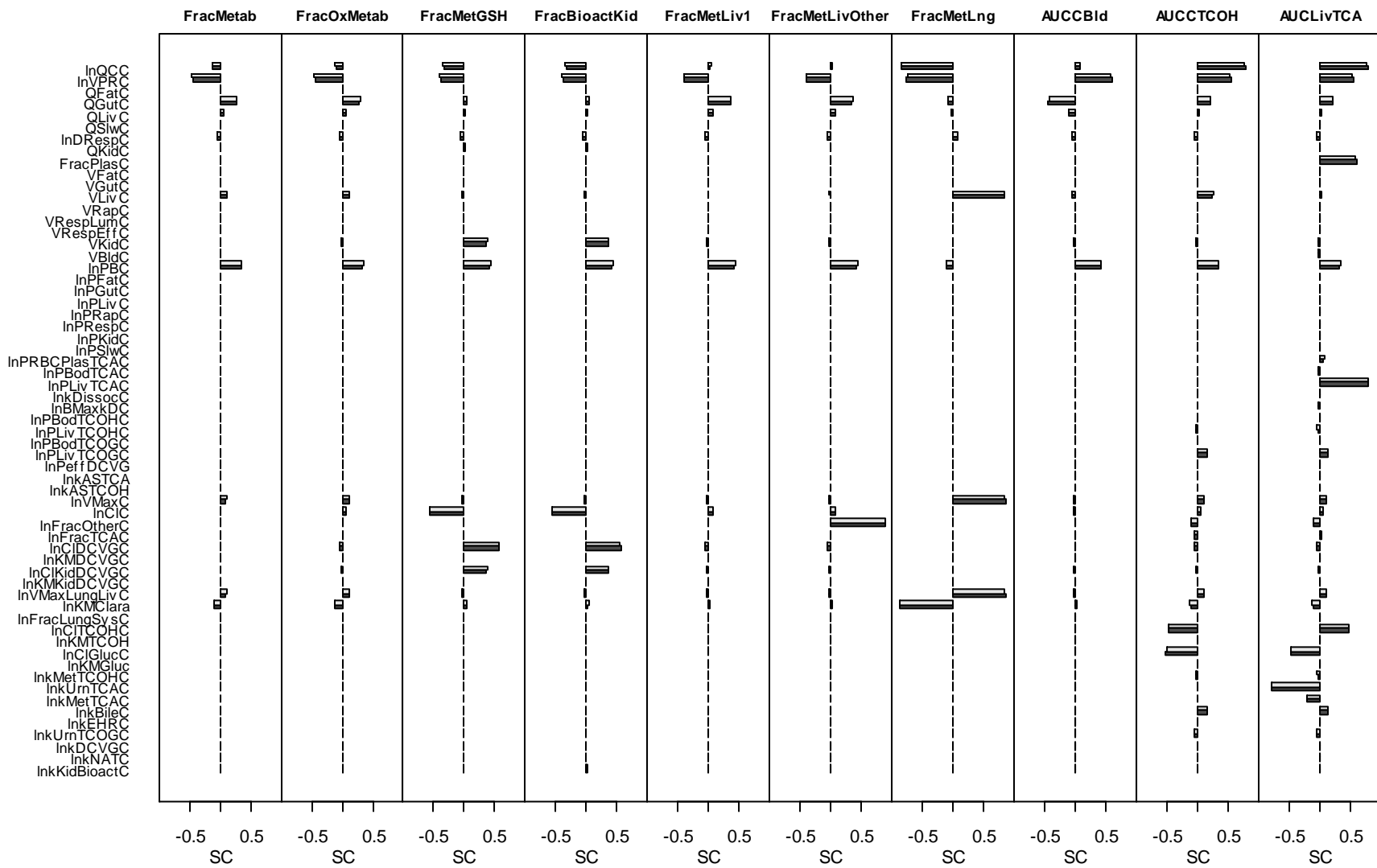


Figure 3-30. Sensitivity analysis results: SC for female (light bars) and male (dark bars) human scaling parameters with respect to dose-metrics following 0.001 ppm continuous inhalation exposures.

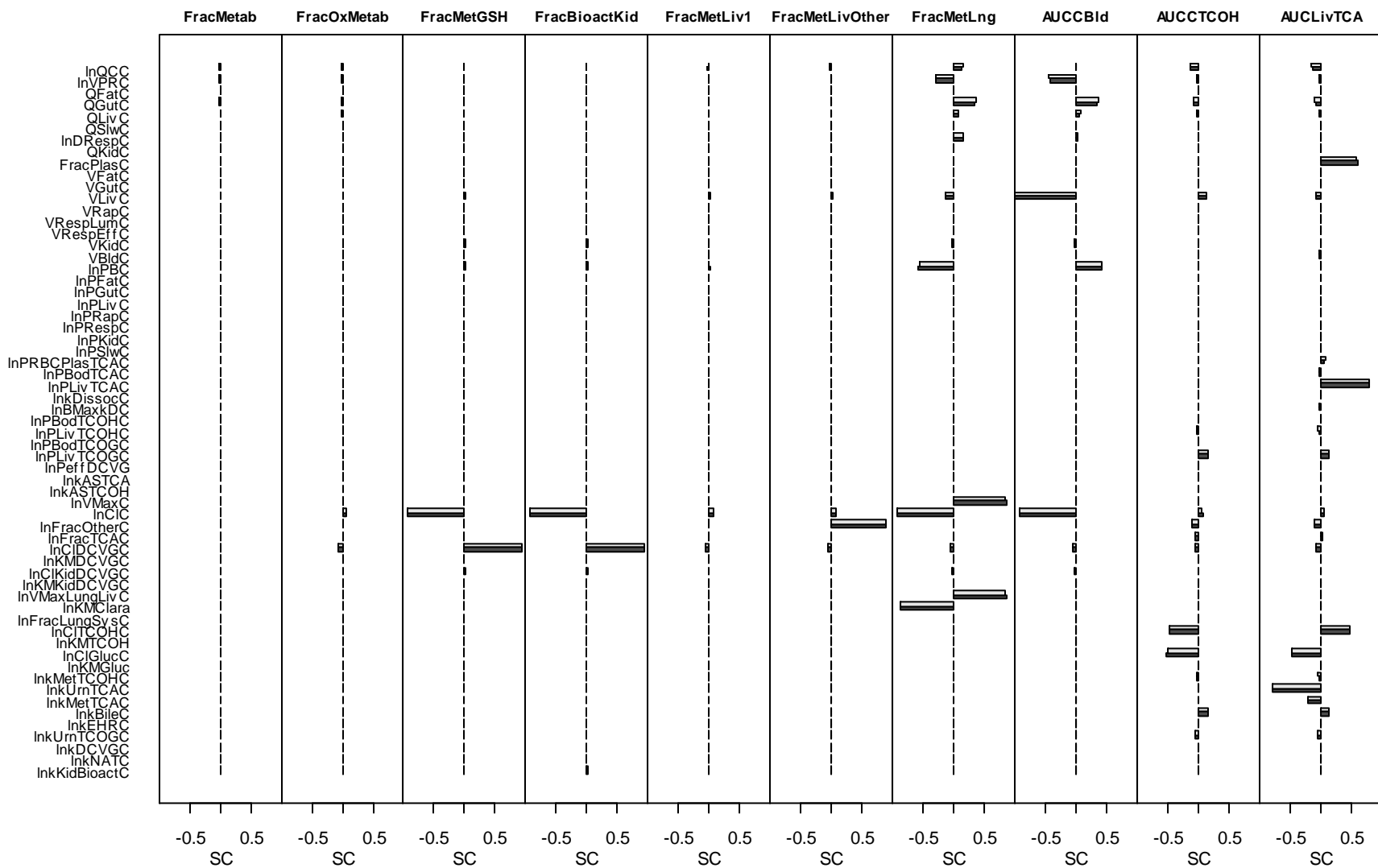


Figure 3-31. Sensitivity analysis results: SC for female (light bars) and male (dark bars) human scaling parameters with respect to dose-metrics following 0.001 mg/kg-day continuous oral exposures.

3.5.7.3. Implications for the Population Pharmacokinetics of TCE

3.5.7.3.1. Results

The overall uncertainty and variability in key toxicokinetic predictions, as a function of dose and species, is shown in Figures 3-17–3-25. As expected, TCE that is inhaled or ingested is substantially metabolized in all species, predominantly by oxidation (see Figures 3-17–3-18). At higher exposures, metabolism becomes saturated and the fraction metabolized declines. Mice, on average, have a greater capacity to oxidize TCE than rats or humans, and this is reflected in the predictions at the two highest levels for each route. The uncertainty in the predictions for the population means for total and oxidative metabolism is relatively modest; therefore, the wide CI for combined uncertainty and variability largely reflects intersubject variability. Of particular note is the high variability in oxidative metabolism at low doses in humans, with the 95% CIs spanning 0.1–0.7 for inhalation and 0.2–1.0 for ingestion.

Predictions of GSH conjugation and renal bioactivation of DCVC are highly uncertain in rodents, spanning >1,000-fold in mice and 100-fold in rats (see Figures 3-19–3-20). In both mice and rats, the uncertainty in the population mean virtually overlaps with the combined uncertainty and variability. The uncertainty in mice reflects the lack of GSH-conjugate specific data in that species, and is, therefore, based on overall mass balance only. The somewhat smaller uncertainty in rats reflects the fact that, in addition to overall mass balance, urinary NAcDCVC excretion data are available in that species. However, while the lower bound of GSH conjugation is informed by NAcDCVC excretion data, the upper bound for GSH conjugation and the amount of DCVC bioactivation are still indirectly estimated from data on other clearance pathways. In humans, however, overall GSH conjugation is strongly constrained by the blood concentrations of DCVG from Lash et al. ([1999b](#)), with 95% CIs on the population mean spanning only about threefold. DCVC bioactivation is still indirectly estimated, derived from the difference between overall GSH conjugation flux and NAcDCVC excretion data from Bernauer et al. ([1996](#)). However, substantial variability is predicted (reflecting variability in the measurements of Lash et al., ([1999b](#)), since the error bars for the population mean are substantially smaller than those for overall uncertainty and variability. Of particular note is the prediction of 1 or 2 orders of magnitude more GSH conjugation and DCVC bioactivation, on average, in humans than in rats, although importantly, the 95% CIs for the predicted population means do overlap. However, as discussed above in Section 3.3.3.2.1, there are uncertainties as to the accuracy of analytical method used by Lash et al. ([1999b](#)) in the measurement of DCVG in blood. Because these data are so influential, the analytical uncertainties contribute substantially to the overall uncertainty in the estimates of the overall GSH conjugation flux, and may be greater than the statistical uncertainties calculated using the model.

Predictions for respiratory tract oxidative metabolism were, as expected, greatest in mice, followed by rats and then humans (see Figure 3-21). In addition, due to the “presystemic” nature of the respiratory tract metabolism model as well as the hepatic first-pass effect, substantially

more metabolism was predicted from inhalation exposures as compared to oral exposures. Interestingly, the population means appeared to be fairly well constrained despite the lack of direct data, suggesting that overall mass balance is an important constraint for the presystemic respiratory tract metabolism modeled here.

Some constraints were also placed on “other” hepatic oxidation (i.e., through a pathway that does not result in chloral formation and subsequent formation of TCA and TCOH, see Figure 3-22). The 95% CI for overall uncertainty and variability spanned about 100-fold, a large fraction of that due to uncertainty in the population mean. Interestingly, a higher rate per kg tissue was predicted for rats than for mice or humans, although importantly, the 95% CIs for the population means overlap among all three species.

The AUC of TCE in blood (see Figure 3-23) showed the expected nonlinear behavior with increasing dose, with the nonlinearity more pronounced with oral exposure, as would be expected by hepatic first-pass. Notably, the predicted AUC of TCE in blood from inhalation exposures corresponds closely with cross-species ppm-equivalence, as is assumed for Category 3 gases for which the blood:air partition coefficient in laboratory animals is greater than that in humans (U.S. EPA, 1994b). For low oral exposures (≤ 1 mg/kg-day), cross-species mg/kg-day equivalence appears to be fairly accurate (within twofold), implying the usual assumption of mg/kg^{3/4}-day equivalence would be somewhat less accurate, at least for humans. Interestingly, the AUC of TCOH in blood (see Figure 3-24) was relatively constant with dose, reflecting the parallel saturation of both TCE oxidation and TCOH glucuronidation. In fact, in humans, the mean AUC for TCOH in blood increases up to 100 ppm or 100 mg/kg-day, due to saturation of TCOH glucuronidation, before decreasing at 1,000 ppm or 1,000 mg/kg-day, due to saturation of TCE oxidation.

The predictions for the AUC for TCA in the liver showed some interesting features (see Figure 3-25). The predictions for all three species were within an order of magnitude of each other, with a relatively modest uncertainty in the population mean (reflecting the substantial amount of data on TCA). The shape of the curves, however, differs substantially, with humans showing saturation at much lower doses than rodents, especially for oral exposures. In fact, the ratio between the liver TCA AUC and the rate of TCA production, although differing between species, is relatively constant as a function of dose within species (not shown). Therefore, the shape of the curves largely reflect saturation in the production of TCA from TCOH, *not* in the oxidation of TCE itself, for which saturation is predicted at higher doses, particularly via the oral route (see Figure 3-18). In addition, while for the same exposure (ppm or mg/kg-day TCE), more TCA (on a mg/kg-day basis) is produced in mice relative to rats and humans, humans and rats have longer TCA half-lives even though plasma protein binding of TCA is, on average, greater.

3.5.7.3.2. Discussion

This analysis substantially informs four of the major areas of pharmacokinetic uncertainty previously identified in numerous reports ([reviewed in Chiu et al., 2006b](#)): GSH conjugation pathway, respiratory tract metabolism, alternative pathways of TCE oxidation including DCA formation, and the impact of plasma binding on TCA kinetics, particularly in the liver. In addition, the analysis helps identify data that have the potential to further reduce the uncertainties in TCE toxicokinetics and risk assessment.

With respect to the first, previous estimates of the degree of TCE GSH conjugation and subsequent bioactivation of DCVC in humans were based on urinary excretion data alone ([Bernauer et al., 1996](#); [Birmer et al., 1993](#)). For instance, Bloemen et al. (2001) concluded that due to the low yield of identified urinary metabolites through this pathway (<0.05% as compared to 20–30% in urinary metabolites of TCE oxidation), GSH conjugation of TCE is likely of minor importance. However, as noted by Lash et al. (2000a; 2000b), urinary excretion is a poor quantitative marker of flux through the GSH pathway because it only accounts for the portion detoxified, and not the portion bioactivated ([a limitation acknowledged by Bloemen et al., 2001](#)).

A reexamination of the available in vitro data on GSH conjugation by Chiu et al. (2006b) suggested that the difference in flux between TCE oxidation and GSH conjugation may not be as large as suggested by urinary excretion data. For example, the formation rate of DCVG from TCE in freshly isolated hepatocytes was similar in order of magnitude to the rate measured for oxidative metabolites ([Lash et al., 1999a](#); [Lipscomb et al., 1998b](#)). A closer examination of the only other available human in vivo data on GSH conjugation, the DCVG blood levels reported in Lash et al. (1999b), also suggests a substantially greater flux through this pathway than inferred from urinary data. In particular, the peak DCVG blood levels reported in this study were comparable on a molar basis to peak blood levels of TCOH, the major oxidative metabolite, in the same subjects, as previously reported by Fisher et al. (1998). A lower bound estimate of the GSH conjugation flux can be derived as follows. The reported mean peak blood DCVG concentrations of 46 μM in males exposed to 100 ppm TCE for 4 hours ([Lash et al., 1999b](#)), multiplied by a typical blood volume of 5 L ([ICRP, 2003](#)), yields a peak amount of DCVG in blood of 0.23 mmoles. In comparison, the retained dose from 100 ppm exposure for 4 hours is 4.4 mmol, assuming retention of about 50% ([Monster et al., 1976](#)) and minute-volume of 9 L/minute ([ICRP, 2003](#)). Thus, in these subjects, about 5% of the retained dose is present in blood as DCVG at the time of peak blood concentration. This is a strong lower bound on the total fraction of retained TCE undergoing GSH conjugation because DCVG clearance is ongoing at the time of peak concentration, and DCVG may be distributed to tissues other than blood. It should be reiterated that only grouped DCVG blood data were available for PBPK model-based analysis; however, this should only result in an underestimation of the degree of *variation* in GSH conjugation. Finally, this hypothesis of a significant flux through the human GSH conjugation pathway is consistent with the limited available total recovery data in humans in

which only 60–70% of the TCE dose is recovered as TCE in breath and excreted urinary metabolites ([reviewed in Chiu et al., 2007](#)).

Thus, there is already substantial qualitative and semi-quantitative evidence to suggest a substantially greater flux through the GSH conjugation pathway than previously estimated based on urinary excretion data alone. The scientific utility of applying a combination of PBPK modeling and Bayesian statistical methods to this question comes from being able to systematically integrate these different types of data—in vitro and in vivo, direct (blood DCVG) and indirect (total recovery, urinary excretion)—and quantitatively assess their consistency and implications. For example, the in vitro data discussed above on GSH conjugation were used for developing prior distributions for GSH conjugation rates, and were not used in previous PBPK models for TCE. Then, both the direct and indirect in vivo data were used to the extent possible either in the Bayesian calibration or model evaluation steps.

However, this evidence—both qualitative and quantitative—is highly dependent on the reliability of the human DCVG measurements, both in vitro and in vivo, from Lash et al. ([1999a](#); [1999b](#)). In vitro, Green et al. ([1997a](#)) reported much lower rates of DCVG formation in humans using a different analytical method. Similarly, the rates of in vitro DCVG formation in rats have uneven consistency among studies. In male rat liver cytosol, Green et al. ([1997a](#)) reported a rate of 0.54 pmol/minute-mg, consistent with the <2 pmol/minute-mg reported by Dekant et al. ([1990](#)), but much less than the 121 pmol/minute-mg reported by Lash et al. ([1999a](#)). However, in microsomes, Green et al. ([1997a](#)) reported no enzymatic formation, whereas Dekant et al. ([1990](#)) reported a higher rate (i.e., 2 pmol/minute-mg) and Lash et al. ([1999a](#)) reported a much higher rate (i.e., 171 pmol/minute-mg). Differing results in humans may be attributable to true interindividual variation (especially since GSTs are known to be polymorphic). However, this may be less plausible for rats, suggesting that significant uncertainties remain in the quantitative estimation of GSH conjugation flux.

Several other aspects of the predictions related to GSH conjugation of TCE are worthy of note. Predictions for rats and mice remain more uncertain due to their having less direct toxicokinetic data, but are better constrained by total recovery studies. For instance, the total recovery of 60-70% of dose in exhaled breath and oxidative metabolites in human studies is substantially less than the >90% reported in rodent studies ([also noted by Goeptar et al., 1995](#)). In addition, it has been suggested that “saturation” of the oxidative pathway for volatiles in general, and TCE in particular, may lead to marked increases in flux through the GSH conjugation pathway ([Slikker et al., 2004a, b](#); [Goeptar et al., 1995](#)), but the PBPK model predicts only a modest, at most ~twofold, change in flux. This is because there is evidence that both pathways are saturable in the liver for this substrate at similar exposures and because GSH conjugation also occurs in the kidney. Therefore, the available data are not consistent with toxicokinetics alone causing substantially nonlinearities in TCE kidney toxicity or cancer, or in any other effects associated with GSH conjugation of TCE.

Finally, the present analysis suggests a number of areas where additional data can further reduce uncertainty in and better characterize the TCE GSH conjugation pathway. The Bayesian analysis predicts a relatively low distribution volume for DCVG in humans, a hypothesis that could be tested experimentally. In addition, *in vivo* measurements of DCVG in blood via a different, validated analytical method, in humans with known exposures to TCE, would be highly influential in either corroborating the DCVG blood levels reported in Lash et al. (1999b) or providing evidence that those reported DCVG blood levels are too high due to analytical issues. Moreover, it would be useful in such studies to be able to match individuals with respect to toxicokinetic data on oxidative and GSH conjugation metabolites so as to better characterize variability. A consistent picture as to which GST isozymes are involved in TCE GSH conjugation, along with data on variability in isozyme polymorphisms and activity levels, can further inform the extent of human variability. In rodents, more direct data on GSH metabolites, such as reliably-determined DCVG blood concentrations, preferably coupled with simultaneous data on oxidative metabolites, would greatly enhance the assessment of GSH conjugation flux in laboratory animals. Given the large apparent variability in humans, data on interstrain variability in rodents may also be useful.

With respect to oxidative metabolism, as expected, the liver is the major site of oxidative metabolism in all three species, especially after oral exposure, where >85% of total metabolism is oxidation in the liver in all three species. However, after inhalation exposure, the model predicts a greater proportion of metabolism via the respiratory tract than previous models for TCE. This is primarily because previous models for TCE respiratory tract metabolism (Hack et al., 2006; Clewell et al., 2000) were essentially flow-limited—i.e., the amount of respiratory tract metabolism (particularly in mice) was determined primarily by the (relatively small) blood flow to the tracheobronchial region. However, the respiratory tract structure used in the present model is more biologically plausible, is more consistent with that of other volatile organics metabolized in the respiratory tract (e.g., styrene), and leads to a substantially better fit to closed-chamber data in mice.

Consistent with the qualitative suggestions from *in vitro* data, the analysis here predicts that mice have a greater rate of respiratory tract oxidative metabolism as compared to rats and humans. However, the predicted difference of about 50-fold on average between mice and humans is not as great as the 600-fold suggested by previous reports (NRC, 2006; Green, 2000; Green et al., 1997b). The suggested factor of 600-fold was based on multiplying the Green et al. (1997b) data on TCE oxidation in lung microsomes from rats vs. mice (23-fold lower) by a factor for the total CYP content of human lung compared to rat lung (27-fold lower) (incorrectly cited as being from Raunio et al., 1998; Wheeler and Guenther, 1990). However, because of the isozyme-specificity of TCE oxidation, and the differing proportions of different isozymes across species, total CYP content may not be the best measure of interspecies differences in TCE respiratory tract oxidative metabolism. Wheeler et al. (1992) reported that CYP2E1 content of

human lung microsomes is about 10-fold lower than that of human liver microsomes. Given that Green et al. ([1997b](#)) report that TCE oxidation by human liver microsomes is about threefold lower than that in mouse lung microsomes, this suggests that the mouse-to-human comparison TCE oxidation in lung microsomes would be about 30-fold. Moreover, the predicted amount of metabolism corresponds to about the detection limit reported by Green et al. ([1997b](#)) in their experiments with human lung microsomes, suggesting overall consistency in the various results. Therefore, the 50-fold factor predicted by our analysis is biologically plausible given the available in vitro data. More direct in vivo measures of respiratory tract metabolism would be especially beneficial to reduce its uncertainty as well as better characterize its human variability.

TCA dosimetry is another uncertainty that was addressed in this analysis. In particular, the predicted interspecies differences in liver TCA AUC are modest, with a range of about 10-fold across species, due to the combined effects of interspecies differences in the yield of TCA from TCE, plasma protein binding, and elimination half-life. This result is in contrast to previous analyses that did not include TCA protein binding ([Clewell et al., 2000](#); [Fisher, 2000](#)), which predicted significantly more than an order of magnitude difference in TCA AUC across species. In addition, in order to be consistent with available data, the model requires some metabolism or other clearance of TCA in addition to urinary excretion. That urinary excretion does not represent 100% of TCA clearance is evident empirically, as urinary recovery after TCA dosing is not complete even in rodents ([Yu et al., 2000](#); [Abbas et al., 1997](#)). Additional investigation into possible mechanisms, including metabolism to DCA or enterohepatic recirculation with fecal excretion, would be beneficial to provide a stronger biological basis for this empirical finding.

With respect to “untracked” oxidative metabolism, this pathway appears to be a relatively small contribution to total oxidative metabolism. While it is tempting to use this pathway as a surrogate for DCA production through from the TCE epoxide ([Cai and Guengerich, 1999](#)), one should be reminded that DCA may be formed through multiple pathways (see Section 3.3). Therefore, this pathway at best represents a lower bound on DCA production. In addition, better quantitative markers of oxidative metabolism through the TCE epoxide pathway (e.g., dichloroacetyl lysine protein adducts, as reported in [e.g., dichloroacetyl lysine protein adducts, as reported in Forkert et al. ([2006](#))] are needed in order to more confidently characterize its flux.

In a situation such as TCE in which there is large database of studies coupled with complex toxicokinetics, the Bayesian approach provides a systematic method of simultaneously estimating model parameters and characterizing their uncertainty and variability. While such an approach is not necessarily needed for all applications, such as route-to-route extrapolation ([Chiu and White, 2006](#)), as discussed in Barton et al. ([2007](#)), characterization of uncertainty and variability is increasingly recognized as important for risk assessment while representing a continuing challenge for both PBPK modelers and users. If there is sufficient reason to characterize uncertainty and variability in a highly transparent and objective manner, there is no

reason why our approach could not be applied to other chemicals. However, such an endeavor is clearly not trivial, though the high level of effort for TCE is partially due to the complexity of its metabolism and the extent of its toxicokinetic database.

It is notable that, with experience, the methodology for the Bayesian approach to PBPK modeling of TCE has evolved significantly from that of Bois (2000b, a), to Hack et al. (2006), to the present analysis. Part of this evolution has been a more refined specification of the problem being addressed, showing the importance of “problem formulation” in risk assessment applications of PBPK modeling. The particular hierarchical population model for each species was specified based on the intended use of the model predictions, so that relevant data can be selected for analysis (e.g., excluding most grouped human data in favor of individual human data) and data can be appropriately grouped (e.g., in rodent data, grouping by sex and strain within a particular study). Thus, the predictions from the population model in rodents are the “average” for a particular “lot” of rodents of a particular species, strain, and sex. This is in contrast to the Hack et al. (2006) model, in which each dose group was treated as a separate subject. As discussed above, this previous population model structure led to the unlikely result that different dose groups within a closed-chamber study had significantly different V_{MAX} values. In humans, however, interindividual variability is of interest, and furthermore, substantial individual data are available in humans. Hack et al. (2006) mixed individual- and group-level data, depending on the availability from the published study, but this approach likely underestimates population variability due to group means being treated as individuals. In addition, in some studies, the same individual was exposed more than once, and in Hack et al. (2006), these were treated as different “individuals.” In this case, actual interindividual variability may be either over- or underestimated, depending on the degree of interoccasion variability. While it is technically feasible to include interoccasion variability, it would have added substantially to the computational burden and reduced parameter identifiability. In addition, a primary interest for this risk assessment is chronic exposure, so the predictions from the population model in humans are the “average” across different occasions for a particular individual (adult).

The second aspect of this evolution is the drive towards increased objectivity and transparency. For instance, available information, or the lack thereof, is formally codified and explicit either in prior distributions or in the data used to generate posterior distributions, and not both. Methods at minimizing subjectivity (and hence improving reproducibility) in parameter estimation include: (1) clear separation between the in vitro or physiologic data used to develop prior distributions and the in vivo data used to generate posterior distributions; (2) use of noninformative distributions, first updated using a probabilistic model of interspecies-scaling that allows for prediction error, for parameters lacking in prior information; and (3) use of a more comprehensive database of physiologic data, in vitro measurements, and in vivo data for parameter calibration or for out-of-sample evaluation (“validation”). These measures increase

the confidence that the approach employed also provides adequate characterization of the uncertainty in metabolic pathways for which available data was sparse or relatively indirect, such as GSH conjugation in rodents and respiratory tract metabolism. Moreover, this approach yields more confident insights into what additional data can reduce these uncertainties than approaches that rely on more subjective methods.

3.5.7.4. Key Limitations and Potential Implications of Violating Key Assumptions

Like all analyses, this one has a number of limitations and opportunities for refinement, both biological and statistical. Of course, the modeling results are highly dependent on the assumed PBPK model structure. However, most of the elements of the model structure are well established for volatile, lipophilic chemicals such as TCE, and, thus, these assumptions are unlikely to introduce much bias or inaccuracy. In terms of the statistical model, a key assumption is the choice of prior and population distributions—particularly the choice of unimodal distributions for population variability. While reasonable as a first approximation, especially without data to suggest otherwise, this assumption may introduce inaccuracies in the predictions of population variability. For example, if there were an underlying bimodal distribution, then fitting using a unimodal population distribution would lead to a high estimate for the variance, and potentially overestimate the degree of population variability. In some cases in the human model where larger population variance distributions are estimated, this may be the underlying cause. However, only in the case of GSH conjugation in humans do the larger estimates of population variability impact the dose-metric predictions used in the dose-response assessment, so the impact of this assumption is limited for this assessment.

In addition, certain sources of variability, such as between-animal variability in rodents and between-occasion variability in humans were not included in the hierarchical model, but were aggregated with other sources of variability in a “residual” error term. Based on the posterior predictions, it does not appear that this assumption has introduced significant bias in the estimates because the residuals between predictions and data do not overall appear systematically high or low. However, this could be verified by addressing between-animal variability in rodents [requiring a more rigorous treatment of aggregated data, e.g., Chiu and Bois (2007)] and incorporation of interoccasion variability in humans (e.g., Bernillon and Bois, 2000).

Some key potential refinements are as follows. First would be the inclusion of a CH submodel, so that pharmacokinetic data, such as that recently published by Merdink et al. (2008), could be incorporated. In addition, the current analysis is still dependent on a model structure substantially informed by deterministic analyses that test alternative model structures (Evans et al., 2009), as probabilistic methods for discrimination or selection among complex, nonlinear models such as that for TCE toxicokinetics have not yet been widely accepted. Therefore, additional refinement of the respiratory tract model may be possible, though more direct in vivo data would likely be necessary to strongly discriminating among models. In terms of validation,

application of more sophisticated methods such as cross-validation, may be useful in further assessing the robustness of the modeling. Finally, additional model changes that may be of utility to risk assessment, such as development of models for different lifestages (including childhood and pregnancy), would likely require additional in vivo or in vitro data, particularly as to metabolism, to ensure model identifiability.

3.5.7.5. Overall Evaluation of PBPK Model-Based Internal Dose Predictions

The utility of the PBPK model developed here for making predictions of internal dose can be evaluated based on four different components: (1) the degree to which the simulations have converged to the true posterior distribution; (2) the degree of overall uncertainty and variability; (3) for humans, the degree of uncertainty in the population; and (4) the degree to which the model predictions are consistent with in vivo data that are informative to a particular dose-metric. Table 3-51 summarizes these considerations for each dose-metric prediction. Note that this evaluation does not consider in any way the extent to which a dose-metric may be the appropriate choice for a particular toxic endpoint.

Table 3-51. Degree of variance in dose-metric predictions due to incomplete convergence (columns 2–4), combined uncertainty and population variability (columns 5–7), uncertainty in particular human population percentiles (columns 8–10), model fits to in vivo data (column 11); the GSD is a “fold-change” from the central tendency

Dose-metric abbreviation	Convergence: <i>R</i> for generic scenarios			GSD for combined uncertainty and variability			GSD for uncertainty in human population percentiles			Comments regarding model fits to in vivo data
	Mouse	Rat	Human	Mouse	Rat	Human	1~5%	25~75%	95~99%	
ABioactDCVCBW34, ABioactDCVCKid	–	≤1.016	≤1.015	–	≤3.92	≤3.77	≤2.08	≤1.64	≤1.30	Good fits to urinary NAcDCVC and blood DCVG.
AMetGSHBW34	≤1.011	≤1.024	≤1.015	≤9.09	≤3.28	≤3.73	≤2.08	≤1.64	≤1.29	Good fits to urinary NAcDCVC and blood DCVG.
AMetLiv1BW34	≤1.000	≤1.003	≤1.004	≤2.02	≤1.84	≤1.97	≤1.82	≤1.16	≤1.16	Good fits to oxidative metabolites.
AMetLivOtherBW34, AMetLivOtherLiv	≤1.004	≤1.151	≤1.012	≤3.65	≤3.36	≤3.97	≤2.63	≤1.92	≤2.05	No direct in vivo data.
AMetLngBW34, AMetLngResp	≤1.001	≤1.003	≤1.002	≤4.65	≤4.91	≤10.4	≤4.02	≤2.34	≤1.83	No direct in vivo data, but good fits to closed-chamber.
AUCBld	≤1.001	≤1.004	≤1.005	≤3.04	≤3.16	≤3.32	≤1.20	≤1.43	≤1.49	Generally good fits, but poor fit to a few mouse and human studies.
AUCCTCOH	≤1.001	≤1.029	≤1.002	≤3.35	≤8.78	≤5.84	≤1.73	≤1.20	≤1.23	Good fits across all three species.
AUCLivTCA	≤1.000	≤1.005	≤1.002	≤2.29	≤3.18	≤2.90	≤1.65	≤1.30	≤1.40	Good fits to rodent data.
TotMetabBW34	≤1.001	≤1.004	≤1.004	≤1.92	≤1.82	≤1.81	≤1.13	≤1.12	≤1.18	Good fits to closed-chamber.
TotOxMetabBW34	≤1.001	≤1.003	≤1.004	≤1.94	≤1.85	≤1.96	≤1.77	≤1.15	≤1.20	Good fits to closed-chamber and oxidative metabolites.
TotTCAInBW	≤1.002	≤1.002	≤1.001	≤1.96	≤2.69	≤2.30	≤1.68	≤1.19	≤1.19	Good fits to TCA data.

Overall, the least uncertain dose-metrics are the fluxes of total metabolism (TotMetabBW34), total oxidative metabolism (TotOxMetabBW34), and hepatic oxidation (AMetLiv1BW34). These all have excellent posterior convergence (R diagnostic ≤ 1.01), relatively low uncertainty and variability (GSD < 2), and relatively low uncertainty in human population variability (GSD for population percentiles < 2). In addition, the PBPK model predictions compare well with the available in vivo pharmacokinetic data.

Predictions for TCE in blood (AUCCBld) are somewhat more uncertain. Although convergence was excellent across species ($R \leq 1.01$), overall uncertainty and variability was about threefold. In humans, the uncertainty in human population variability was relatively low (GSD for population percentiles < 1.5). TCE blood level predictions were somewhat high in comparison to the Chiu et al. (2007) study at 1 ppm, though the predictions were better for most of the other studies at higher exposure levels. In mice, TCE blood levels were somewhat overpredicted in open-chamber inhalation studies. In both mice and rats, there were some cases in which fits were inconsistent across dose groups if the same parameters were used across dose groups, indicating unaccounted-for dose-related effects or intrastudy variability. However, in both rats and humans, TCE blood (humans and rats) and tissue (rats only) concentrations from studies not used for calibration (i.e., saved for “out-of-sample” evaluation/“validation”) were well simulated, adding confidence to the parent compound dose-metric predictions.

For the TCA dose-metric predictions (TotTCAInBW, AUCLivTCA) convergence in all three species was excellent ($R \leq 1.01$). Overall uncertainty and variability was intermediate between dose-metrics for metabolism and that for TCE in blood, with GSDs of about two to threefold. Uncertainty in human population percentiles was relatively low (GSD of 1.2–1.7). While liver TCA levels were generally well fit, the data was relatively sparse. Plasma and blood TCA levels were generally well fit, though in mice, there were again some cases in which fits were inconsistent across dose groups if the same parameters were used across dose groups, indicating unaccounted-for dose-related effects or intrastudy variability. In humans, the accurate predictions for, TCA blood and urine concentrations from studies used for “out of sample” evaluation lends further confidence to dose-metrics involving TCA.

The evaluation of TCOH in blood followed a similar pattern. Convergence in all three species was good, though the rat model had slightly worse convergence ($R \sim 1.03$) than the mouse and humans ($R \leq 1.01$). In mice, overall uncertainty and variability was slightly more than for TCE in blood. There was much higher overall uncertainty and variability in the rat predictions (GSD of almost 9), which likely reflects true interstudy variability. The population-generated predictions for TCOH and TCOG in blood and urine were quite wide, with some in vivo data at both the upper and lower ends of the range of predictions. In humans, the overall uncertainty and variability was intermediate between mice and rats (GSD = 5.8). As with the rats, this likely reflects true population heterogeneity, as the uncertainty in human population percentiles was relatively low (GSD of around 1.2~1.7-fold). For all three species, fits to in vivo

data are generally good. In mice, however, there were again some cases in which fits were inconsistent across dose groups if the same parameters were used across dose groups, indicating unaccounted-for, dose-related effects or intrastudy variability. In humans, the accurate predictions for TCOH blood and urine concentrations from studies used for “out of sample” evaluation lends further confidence to those dose-metrics involving TCOH.

GSH metabolism dose-metrics (ABioactDCVCBW34, ABioactDCVCKid, AMetGSHBW34) had the greatest overall uncertainty in mice but was fairly well characterized in rats and humans. In mice, there were no in vivo data informing this pathway except for the indirect constraint of overall mass balance. So although convergence was adequate ($R < 1.02$), the uncertainty/variability was very large, with a GSD of ninefold for the overall flux (the amount of bioactivation was not characterized because there are no data constraining downstream GSH pathways). For rats, there were additional constraints from (well-fit) urinary NAcDCVC data, which reduced the overall uncertainty and variability substantially (GSD less than fourfold). In humans, in addition to urinary NAcDCVC data, DCVG blood concentration data was available, though only at the group level. These data, both of which were well fit, in addition to the greater amount of in vitro metabolism data, allowed for the flux through the GSH pathway and the rate of DCVC bioactivation to be fairly well constrained, with overall uncertainty and variability having GSD less than fourfold, and uncertainty in population percentiles no more than about twofold. However, these predictions may need to be interpreted with caution, given potential analytical issues with quantifying DCVG either in vitro or in vivo (see Section 3.3.3.2). Thus, the substantial inconsistencies across studies and methods in the quantification of DCVG following TCE exposure suggest lower confidence in the accuracy of these predictions.

The final two dose-metrics, respiratory metabolism (AMetLngBW34, AMetLngResp) and “other” oxidative metabolism (AMetLivOtherBW34, AMetLivOtherLiv), also lacked direct in vivo data and were predicted largely on the basis of mass balance and physiological constraints. Respiratory metabolism had good convergence ($R < 1.01$), helped by the availability of closed-chamber data in rodents. In rats and mice, overall uncertainty and variability was rather uncertain (GSD of 4~5-fold), but the overall uncertainty and variability was much greater in humans, with a GSD of about 10-fold. This largely reflects the significant variability across individuals as well as substantial uncertainty in the low population percentiles (GSD of fourfold). However, the middle (i.e., “typical” individuals) and upper percentiles (i.e., the individuals at highest risk) are fairly well constrained with a GSD of around twofold. For the “other” oxidative metabolism dose-metric, convergence was good in mice and humans ($R < 1.02$), but less than ideal in rats ($R \sim 1.15$). In rodents, the overall uncertainty and variability were moderate, with a GSD around 3.5-fold, slightly higher than that for TCE in blood. The overall uncertainty and variability in this metric in humans had a GSD of about fourfold, slightly higher than for GSH

conjugation metrics. However, uncertainty in the middle and upper population percentiles had GSDs of only about twofold, similar to that for respiratory metabolism.

Overall, as shown in Table 3-51, the updated PBPK model appears to be most reliable for the fluxes of total, oxidative, and hepatic oxidative metabolism. In addition, dose-metrics related to blood levels of TCE and oxidative metabolites, TCOH and TCA, had only modest uncertainty. In the case of TCE in blood, for some data sets, model predictions overpredicted the *in vivo* data, and, in the case of TCOH in rats, substantial interstudy variability was evident. For GSH metabolism, dose-metric predictions for rats and humans had only slightly greater uncertainty than the TCE and metabolism metrics. Predictions for mice were much more uncertain, reflecting the lack of GSD-specific *in vivo* data. Finally, for “other” oxidative metabolism and respiratory oxidative metabolism, predictions also had somewhat more uncertainty than the TCE and metabolism metrics, though uncertainty in middle and upper human population percentiles was modest.